Peak Sidelobe Level Distribution Computation for Ad Hoc Arrays using Extreme Value Theory

Peak Sidelobe Level Distribution Computation for Ad Hoc Arrays using Extreme Value Theory

A dissertation presented

by

Siddhartha Krishnamurthy

to

The School of Engineering and Applied Science

in partial fulfillment of the requirements

for the degree of

Doctor of Philosophy

in the subject of

Engineering Sciences

Harvard University

Cambridge, Massachusetts

November 2013

Dissertation Advisor:
Professor Vahid Tarokh

Author:
Siddhartha Krishnamurthy

Peak Sidelobe Level Distribution Computation for Ad Hoc Arrays using Extreme Value Theory

Abstract

Extreme Value Theory (EVT) is used to analyze the peak sidelobe level distribution for array element positions with arbitrary probability distributions. Computations are discussed in the context of linear antenna arrays using electromagnetic energy. The results also apply to planar arrays of random elements that can be transformed into linear arrays.

Before EVT is introduced, the number of times a beampattern crosses a certain level in an upward direction is considered. For this upward-crossing method, the evaluation of the probability of exceeding a given peak sidelobe is investigated as a function of the antenna array spatial position variance in the asymptotic limit of a large number of array elements.

For sparse arrays with small number of elements, Gaussian approximations to the beampattern distribution at a particular angle introduce inaccuracies to the probability calculations. EVT is applied without making these Gaussian approximations. A bound is given for how close using a certain number of beampattern samples will get to the true peak sidelobe level of a random array. It is shown that the peak sidelobe level distribution converges to a Gumbel distribution in the limit of a large number of beampattern samples when the number of elements is larger than ten. It is also shown that being in the domain of attraction of the Gumbel distribution occurs under weak convergence as the number of elements increases. An expression for the beampattern distribution at a particular angle is given for any number of array elements, and simulations show that it is in the domain of attraction of the Weibull

distribution.

This work was sponsored by the United States Air Force under United States Air Force Contract FA8721-05-C-0002. Opinions, interpretations, conclusions, and recommendations are those of the authors and are not necessarily endorsed by the United States Government.

Table of Contents

List of Tables

List of Figures

Acknowledgments

I would like to thank MIT Lincoln Laboratory, the Lincoln Scholars Program at MIT Lincoln Laboratory, and Harvard University for the privilege to conduct this research.

My gratitude goes to my Harvard University advisor, Dr. Vahid Tarokh, and my advisors at MIT Lincoln Laboratory, Dr. Christ Richmond and Dr. Dan Bliss, who is now professor at Arizona State University, School of Electrical, Computer, and Energy Engineering, for their encouragement, patience, and knowledge as I completed my education. I thank them for introducing me to the problem of calculating beampattern distributions when array element positions are randomly distributed. My research would not have progressed so far without their guidance.

Thanks also goes to PhD defense and qualifier committee member Dr. Roger Brockett and qualifier committee member Dr. H.T. Kung for their guidance and research feedback.

During the early stages of my PhD program, Dr. Tom Kirchhausen at Harvard Medical School and Dr. Bob Galejs at MIT Lincoln Laboratory were invaluable mentors. They provided opportunities that continued to help me throughout my research.

Many thanks go to my group leaders at MIT Lincoln Laboratory, who gave me the opportunity to pursue graduate studies at Harvard University through the Lincoln Scholars program. My group leaders are Dr. Bob Atkins, Dr. Justin Brooke, Dr. Marc Viera, Dr. Kevin Cohen, Dr. Greg Lyons, and Dr. Chris Cherry. Their insights and suggestions during the course of my studies strengthened my research.

I received much support from other personnel at MIT Lincoln Laboratory, without whose help completing my graduate studies would have become more difficult. My thanks go to all the staff of Group 107, Advanced Capabilities and Systems, MIT Lincoln Laboratory, who supported me in the group while I pursued my education. Marybeth Hopkins, Debi Corcoran, Dori Hayes, and Felicia Gauthier were instrumental in navigating me through

the administrative portion of being a student at Harvard University while being funded through the MIT Lincoln Scholars program. The LL Grid Team helped with diagnosing and solving computing issues that occurred during the many simulations required for this research. Thanks also to MIT Lincoln Laboratory technical staff Dr. Adam Margetts, Dr. Swaroop Appadwedulla, and Jonathan Williams, who is now at Autoliv, for their input during my research progress.

It was an honor to be supported by the MIT Lincoln Scholars program while pursuing my graduate education at Harvard University. I thank the entire Lincoln Scholars committee including Dr. William Keicher, Dr. Mark Weber, and Ken Estabrook for this opportunity.

Kathleen Maase at Harvard University was terrific in steering me through administrative processes throughout my graduate education. I will never forget her kindness.

The staff at the School of Engineering and Applied Science at Harvard University were also helpful and a pleasure to work with.

The students and researchers at Harvard University gave me a fantastic education experience. Thank you to Harvard University researchers Dr. Hyoseok Yi and Dr. Emanuele Cocucci for their help, great feedback on my research, and for patiently answering my questions. I enjoyed working with students Shuo Song and Hossein Azari as we helped each other through our graduate studies.

Before I joined Harvard University, many mentors and advisors encouraged my pursuit of research and a graduate education. At NASA Langley Research Center, I thank Dr. Erik Saether, Dr. Edward Glaessgen, Dr. Robert Singeterry, Paul Brewster, Ronnie Gillian, and Dr. Olaf Storaasli, who is now at USEC, for introducing me to technical work outside of the classroom. Dr. Mark Jones of Virginia Tech gave me the privilege to conduct undergraduate research at the Configurable Computing Laboratory. I also thank him for his career and education guidance. Thank you also to late Dr. Jin Au Kong and late Dr. David Staelin at MIT who were kind enough to meet with me before I was a graduate student, and who

showed me a path towards obtaining a PhD.

I would not have been able to succeed in my studies without the love, patience, and encouragement of my father, Dr. T. Krishnamurthy, mother, Kamala Krishnamurthy, brother, Karthik Krishnamurthy, and wife, Aarthi Balasubramaniam. My achievements exist because of their care and belief in me. My parents' guidance provided me my first exposure to technical work at NASA Langley. They were there to help me during the troubles and triumphs throughout my education and work. To my wife, thank you so much for your patience and support as I completed this thesis and my PhD defense.

To my family

Introduction

The way arrays of elements, such as antenna arrays, radiate energy into space is dependent on the spatial distribution of their elements. Usually, the positions and phases at each element is known, and the topography of the radiation can be determined. However, there are applications and conditions where the positions and phases are not known or not known precisely. The positions and phases are described by a probability distribution. Consequently, quantities in the topography of the radiation, or radiation pattern, surrounding an array of elements can also be described by probability distributions.

One such quantity is the beampattern, which is the normalized radiation pattern in the power domain. The main beam is the location of maximum beampattern intensity. Sidelobes are peaks in the beampattern outside of the main beam. Chapter 1 discusses the beampattern and sidelobes in more detail. Chapter 2 then explains the beampattern for linear arrays.

Researchers have long been interested in the peak sidelobe level distribution, which is the distribution of the maximum sidelobe value. Early investigations into this probability distribution was motivated by the need for high resolution and full-scanning capability in space applications. Other applications, which are detailed in Chapter 3, include analysis of communication and target detection systems where antenna arrays with unknown or random element positions can interfere with performance or form the system under analysis. The peak sidelobe level distribution can also help design antenna arrays since elements spaced unequally apart can obtain a narrow main beam but avoid grating lobes. The narrow main

beams become important where direction finding is important, and so the peak sidelobe level distribution is also needed for angle estimation.that radiate and receive electromagnetic energy.

Methods used to calculate the peak sidelobe level distribution were to sample the beampattern at equally spaced intervals and to use the number of times the beampattern crosses a certain level in an upward direction. In Chapter 4, we investigate these methods of calculating the peak sidelobe level distribution and make the following contributions:

- A closed form expression for the peak sidelobe level distributions is determined in terms of the element position distribution for beampatterns with angle-independent statistics given an arbitrary antenna location probability density. The conditions in which this closed form expression can be found from angle-independent statistics are discussed.

- The limit of peak sidelobe level distributions as the aperture and number of nodes increases is investigated.

When using the sample and upcrossing methods in previous research, the quadrature components of the antenna array factor were approximated as Gaussian random variables. However, these Gaussian approximations cause the beampattern probability distribution calculations for arrays with a small number of elements to become inaccurate, especially for sparse arrays. In Chapter 5, we attempt to calculate the peak sidelobe level distribution without making the Gaussian approximations by using Extreme Value Theory (EVT). With the EVT approach in this thesis, samples of the beampattern are taken, and we give a bound to how close the EVT peak sidelobe level distribution gets to the true distribution. An expression for the beampattern distribution at a particular angle is given. It is shown that with a large number of elements, the beampattern distribution is in the domain of attraction of the EVT Gumbel distribution. We also show that the domain of attraction of the Gumbel distribution occurs under weak convergence as the number of elements is increased. When

the number of elements is less than ten, the calculations become non-trivial, and simulations show that the beampattern distributions are in the domain of attraction of the Weibull distribution. We calculate the EVT distribution parameters from the number of samples taken of the beampattern. Tables are given to determine the number of samples for different number of elements and element position variances.

The peak sidelobe level probability distribution computations are done for arrays with independent and identically distributed (iid) element positions. The work is motivated by antenna arrays utilizing electromagnetic energy, but the computations may be applied to any array system whose power output is a function of the sum of phase differences in its elements. We concentrate on analyzing the peak sidelobe level for linear arrays. This work also applies to planar arrays whose element position distributions allow a transformation of the beampattern equation to make it similar to linear arrays.

Chapter 6 shows how calculating the peak sidelobe level distribution using EVT can be applied to radar where the equation for the beampattern introduces correlated random variables.

Chapter 1

Antenna Radiation Pattern and Sidelobes

1.1 Antenna Introduction

The IEEE definition of an antenna in Ref. [2] is the part of a transmitting or receiving system that radiates or receives electromagnetic energy. The spatial distribution of the electromagnetic energy around an antenna forms its radiation or antenna pattern. An individual antenna's radiation pattern is the same whether it is transmitting or receiving energy, a property known as the reciprocity of antennas. Antennas do not need an external power source to operate. If an antenna is powered, it is done to operate associated electronics such as low-noise amplifiers.

Transducers used in sonar may also be called antennas. Analysis of the radiation pattern of these acoustic sensors is similar to that of antennas using electromagnetic energy. In this thesis, we will discuss the radiation pattern using the IEEE definition of antenna, but the computations can be applied to acoustic antenna radiation patterns.

Antennas are mostly used in the radio wave and microwave portions of the electromagnetic

spectrum, which include frequencies below 300 GHz. For the infrared, visible, and higher frequency portions of the spectrum, other methods of transmission and reception such as lasers, lenses, and photodetectors are used [3]. There has been research in using optical antennas [4]. An example is nantenna development for the infrared frequency region [5]. The material properties of these optical antennas are investigated in much of the research, but a discussion of the state-of-the art of this technology is beyond the scope of this thesis. The equations in this thesis may be used with any wavelength in the electromagnetic spectrum.

Many different types of antennas exist. Each has performance properties that make them desirable to certain situations. When the operating frequency is relatively narrow, antennas such as dipoles and microstrip patches may be used. Conical or planar spiral antennas can be used when a wide range of operating frequencies is desired. When size constraints relative to the operating wavelength are issues, then helical or rhombic antennas may be used. In aperture antennas such as the horn and reflector, the size of the physical aperture or opening over which the electric and magnetic fields are distributed defines the antenna radiation properties. Aperture antennas may be useful in applications where the antenna needs to be flush with a surface.

In this thesis, we are concerned with antenna arrays, which are interconnected antennas arranged in space. Antenna arrays combine power from many antennas to improve signal strength. Their radiation pattern can be electronically steered. The ability to manipulate the radiation pattern with the positions or phase centers of each array element allows spatial signal processing.

There are several metrics to measure antenna performance. The ones usually used are:

- Voltage standing wave ratio (VSWR)
- Polarization
- Radiation patterns

- Directivity and gain
- Sidelobe levels.

VSWR and polarization will be explained here briefly. It is the last item, sidelobe levels, which is the focus in this thesis. A discussion of radiation patterns, directivity, and gain is needed to understand sidelobe levels.

1.1.1 VSWR

VSWR characterizes the mismatch between antenna and transmission line impedances. Antennas are connected to the rest of the transmitting or receiving system through a transmission line. Both the antenna and transmission line have complex impedances made up of their electrical resistance and reactance. If the impedance of the antenna does not match the impedance of the transmission line, then energy will be lost between the antenna and the rest of the transmitter or receiver. The frequency bandwidth of an antenna may be specified using the frequencies where VSWR $< 2.0 : 1$ [6].

1.1.2 Polarization

Polarization describes the orientation of a radiated wave's electric field as it propagates in time. The orientations are taken with respect to the Earth's surface. An example is horizontal polarization where the electrical field oscillates right and left in time. Another orientation is left-hand elliptical polarization where the electric field direction and magnitude oscillates clockwise as it propagates to the observer. Maximum energy transfer between a transmit and a receive antenna will occur when both antennas have the same polarization.

1.2 Coordinate System Specification

Before radiation pattern is discussed, we will define the coordinate system used. Fig. 1.1 shows the orientations of the cartesian (x, y, z) and spherical (r, ϕ, θ) coordinates. The unit vectors for the cartesian and spherical directions are orthogonal. The relationships among the coordinates are:

$$\begin{aligned} x &= r\cos(\theta) \\ y &= r\sin(\theta)\cos(\phi) \\ z &= r\sin(\theta)\sin(\phi) \end{aligned}$$

and the unit vectors for the spherical coordinate system are:

$$\begin{aligned} \hat{\mathbf{r}} &= \cos(\theta)\hat{\mathbf{x}} + \cos(\phi)\sin(\theta)\hat{\mathbf{y}} + \sin(\theta)\sin(\phi)\hat{\mathbf{z}} \\ \hat{\theta} &= -\sin(\theta)\hat{\mathbf{x}} + \cos(\theta)\cos(\phi)\hat{\mathbf{y}} + \cos(\theta)\sin(\phi)\hat{\mathbf{z}} \\ \hat{\phi} &= -\sin(\phi)\hat{\mathbf{y}} + \cos(\phi)\hat{\mathbf{z}} \end{aligned}$$

where $\hat{\mathbf{x}}$, $\hat{\mathbf{y}}$, and $\hat{\mathbf{z}}$ are the unit vectors for the x, y, and z cartesian coordinate directions, respectively.

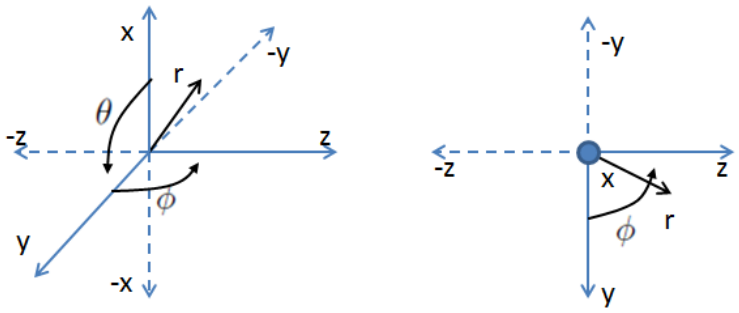

Figure 1.1: *Cartesian (x, y, z) and spherical (r, ϕ, θ) coordinate system definition*

1.3 Radiation Pattern

The radiation pattern shows how electromagnetic energy is transmitted or received in angle around an antenna. Electromagnetic wave propagation around an antenna can be divided into three regions: reactive near field, radiating near field, and the far field. When radiation pattern is mentioned, it typically refers to a quantity from electromagnetic wave propagation in the far-field.

Electric and magnetic fields produced or reached by an antenna form the transmitted or received electromagnetic energy. Let there be a small antenna, or dipole, of length $\triangle x$ oriented in the $\hat{\mathbf{x}}$ direction and centered at the origin with current I. For the dipole, $\triangle x << \lambda$ where λ is the operating wavelength. The antenna is shown in Fig. 1.2.

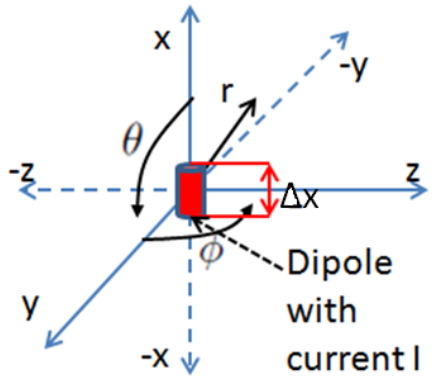

Figure 1.2: *Dipole antenna of length $\triangle x$ with current I*

The electric field at some point a distance $r = \sqrt{x^2 + y^2 + z^2}$ from the antenna is given in phasor notation with time dependence not being shown by

$$\begin{aligned} \mathbf{E}(r,\theta,\phi) &= \frac{I\Delta x\eta\cos(\theta)e^{-j\beta r}(\beta r - j)}{4\pi\beta r^3}\hat{\mathbf{r}} \\ &\quad + \frac{I\Delta x\eta\sin(\theta)e^{-j\beta r}\left(j\beta^2 r^2 + 2\beta r - 2j\right)}{4\pi\beta r^3}\hat{\theta} \end{aligned} \tag{1.1}$$

where β is the wave number corresponding to wavelength λ, or

$$\beta = \frac{2\pi}{\lambda},$$

and η is the intrinsic impedance of the medium. The magnetic field is given by

$$\mathbf{H}(r,\theta,\phi) = \left(\frac{I\triangle x \sin(\theta) e^{-j\beta r}}{4\pi r^2} + \frac{j\beta I \triangle x \sin(\theta) e^{-j\beta r}}{4\pi r}\right)\hat{\phi}. \tag{1.2}$$

Derivations of Eqs. (1.1) and (1.2) from Maxwell's equations can be found in Ref. [7]. Ref. [7] also gives in more detail the follwing discussion in calculating and interpreting the time-average power density.

The reactive near field is close to the antenna. Here, $r << \lambda$. From Eqs. (1.1) and (1.2), the electric and magnetic field vectors may be approximated by

$$\begin{aligned}\mathbf{E}(r,\theta,\phi) \approx & -\frac{jI\triangle x \eta \cos(\theta) e^{-j\beta r}}{4\pi\beta r^3}\hat{\mathbf{r}} \\ & -\frac{jI\triangle x \eta \sin(\theta) e^{-j\beta r}}{2\pi\beta r^3}\hat{\theta}\end{aligned} \tag{1.3}$$

and

$$\mathbf{H}(r,\theta,\phi) \approx \frac{I\triangle x \sin(\theta) e^{-j\beta r}}{4\pi r^2}\hat{\phi}. \tag{1.4}$$

The power flow density, or Poynting vector, is given by

$$\mathbf{S}(r,\theta,\phi) = \frac{1}{2}\mathbf{E}(r,\theta,\phi) \times \mathbf{H}^*(r,\theta,\phi). \tag{1.5}$$

In Eq. (1.5), the Poynting vector is the time-average power density. Using Eqs. (1.3) and (1.4), we have

$$\begin{aligned}\mathbf{S}(r,\theta,\phi) \approx & -\frac{jI^2\triangle x^2 \eta \sin^2(\theta)}{16\pi^2\beta r^5}\hat{\mathbf{r}} \\ & +\frac{jI^2\triangle x^2 \eta \sin(\theta)\cos(\theta)}{32\pi^2\beta r^5}\hat{\theta}.\end{aligned}$$

We see that the time-average power density vector contains only imaginary parts. The imaginary parts indicate reactive energy and the presence of standing waves. The propagating real radial power is not as dominant.

As r increases, the radiating near field is reached, and the electric and magnetic field vectors can be approximated by

$$\begin{aligned}\mathbf{E}(r,\theta,\phi) &\approx \frac{I\triangle x\eta\cos(\theta)e^{-j\beta r}}{4\pi r^2}\hat{\mathbf{r}} \\ &\quad + \left(\frac{I\triangle x\eta\sin(\theta)e^{-j\beta r}}{2\pi r^2} + \frac{j\beta I\triangle x\eta\sin(\theta)e^{-j\beta r}}{4\pi r}\right)\hat{\theta}\end{aligned}$$

and

$$\mathbf{H}(r,\theta,\phi) \approx \frac{j\beta I\triangle x\sin(\theta)e^{-j\beta r}}{4\pi r}\hat{\phi}$$

giving a time-average power density vector approximated by:

$$\mathbf{S}(r,\theta,\phi) \approx \frac{\beta I^2\triangle x^2\eta\sin^2(\theta)(\beta r-2j)}{32\pi^2 r^3}\hat{\mathbf{r}} + \frac{j\beta I^2\triangle x^2\eta\sin(\theta)\cos(\theta)}{32\pi^2 r^3}\hat{\theta}$$

In the radiating near field, the real part of the radial component of the time-average power density becomes more dominant, but there is still some reactive energy. The real part indicates the propagating energy. The boundary between the reactive near field and the radiating near field may be taken as:

$$r = 0.62\sqrt{\frac{\triangle x^3}{\lambda}}.[6]$$

As r increases beyond

$$r = \frac{2\triangle x^2}{\lambda}, [6]$$

the far-field region is reached. Here, the electric and magnetic field vectors may be approximated by

$$\begin{aligned}\mathbf{E}(r,\theta,\phi) &\approx \frac{j\beta I\triangle x\eta\sin(\theta)e^{-j\beta r}}{4\pi r}\hat{\theta} \\ \mathbf{H}(r,\theta,\phi) &\approx \frac{j\beta I\triangle x\sin(\theta)e^{-j\beta r}}{4\pi r}\hat{\phi}.\end{aligned}$$

In the far-field, the relationship between the electric and magnetic field vectors can be stated

as

$$\mathbf{H}(r,\theta,\phi) = \frac{1}{\eta}\hat{\mathbf{r}} \times \mathbf{E}(r,\theta,\phi).$$

The time-average power density is approximated by:

$$\begin{aligned} \mathbf{S}(r,\theta,\phi) &= \tfrac{1}{2}\mathbf{E}(r,\theta,\phi) \times \mathbf{H}^*(r,\theta,\phi) \\ &\approx \tfrac{1}{2}\mathbf{E}(r,\theta,\phi) \times \left(\tfrac{1}{\eta}\hat{\mathbf{r}} \times \mathbf{E}(r,\theta,\phi)\right)^* \\ &\approx \tfrac{1}{2\eta}\left(|E_\theta(r,\theta,\phi)|^2 + |E_\phi(r,\theta,\phi)|^2\right)\hat{\mathbf{r}} \\ &\approx \tfrac{\beta^2 I^2 \triangle x^2 \eta \sin^2(\theta)}{32\pi^2 r^2}\hat{\mathbf{r}}. \end{aligned} \tag{1.6}$$

$E_\theta(r,\theta,\phi)$ and $E_\phi(r,\theta,\phi)$ represent the components of the electric field vector in the $\hat{\theta}$ and $\hat{\phi}$ directions, respectively. The radial portion of the electric field is zero in the far-field. In the far-field, only the real part, representing the propagating energy, of the time-average power density is dominant.

1.3.1 Field Pattern

The radiation pattern is generally discussed in the context of the far-field. When the quantity measured by the radiation pattern is a component of the electric field vector, the radiation pattern may be called the field pattern [2]. If we assume that the electric field vector has only the $E_\theta(r,\theta,\phi)$ component or the $E_\phi(r,\theta,\phi)$ component, the field pattern is normalized and is given by

$$F_i(r,\theta,\phi) = \frac{\mathbf{E}_i(r,\theta,\phi)}{\mathbf{E}_i(r,\theta_{max},\phi_{max})}$$

where $i = \theta$ or $i = \phi$ depending on whether the measured electric field vector is in the $\hat{\theta}$ or $\hat{\phi}$ direction, respectively. In the far-field, the electric field vector will not have a radial component. Also,

$$\{\theta_{max},\phi_{max}\} = \arg\max_{\theta,\phi} |\mathbf{E}_i(r,\theta,\phi)|.$$

For all values of ϕ the field pattern for the dipole is

$$F_\theta(r, \theta, \phi) = \sin(\theta) \equiv F(\theta, \phi).$$

The normalization of the electric field causes the field pattern to become a function of angle and not the radial distance from the antenna. Therefore, the field pattern remains the same at all far-field distances from the antenna.

1.3.2 Beampattern in Power Domain

In addition to the field pattern, the radiation pattern may be quantified as the power pattern. The power pattern may be considered as a normalized time-average power density component. It is given by

$$P(r, \theta, \phi) = \frac{\mathbf{S}_r(r, \theta, \phi)}{\mathbf{S}_r(r, \theta_{max}, \phi_{max})} \tag{1.7}$$

where $\mathbf{S}_r(r, \theta, \phi)$ is the component of the time-average power density vector in the radial direction and

$$\{\theta_{max}, \phi_{max}\} = \arg\max_{\theta,\phi} |\mathbf{S}_r(r, \theta, \phi)|. \tag{1.8}$$

The power pattern for the dipole is

$$P(r, \theta, \phi) = \sin^2(\theta) \equiv P(\theta, \phi).$$

From Eqs. (1.6), (1.7), and (1.8), the power pattern may also be expressed as

$$\begin{aligned} P(\theta, \phi) &= \frac{\frac{1}{2\eta}\left(|E_\theta(r, \theta, \phi)|^2 + |E_\phi(r, \theta, \phi)|^2\right)}{\frac{1}{2\eta}\left(|E_\theta(r, \theta_{max}, \phi_{max})|^2 + |E_\phi(r, \theta_{max}, \phi_{max})|^2\right)} \\ &= \frac{\left(|E_\theta(r, \theta, \phi)|^2 + |E_\phi(r, \theta, \phi)|^2\right)}{\left(|E_\theta(r, \theta_{max}, \phi_{max})|^2 + |E_\phi(r, \theta_{max}, \phi_{max})|^2\right)} \\ &= |F(\theta, \phi)|^2. \end{aligned}$$

The power pattern may also be called the beampattern in the power domain, and it will be referred to as the beampattern for the remaining of the thesis.

1.3.3 Plane Wave Approximation of Far-Field Radiation

The radially propagating electromagnetic energy can be approximated by plane waves in the far-field. We briefly state the far-field magnetic and electric fields of the dipole with space and time dependency as

$$\mathbf{E}(r,\theta,\phi,t) \approx -\frac{\beta^2 I \triangle x}{4\pi\epsilon r}\sin(\theta)\cos(\beta r-\omega t)\hat{\theta} \tag{1.9}$$

$$\mathbf{H}(r,\theta,\phi,t) \approx -\frac{\omega\beta I \triangle x}{4\pi r}\sin(\theta)\cos(\beta r-\omega t)\hat{\phi} \tag{1.10}$$

where t is time, ω is the operating angular frequency, and ϵ is the permittivity of the propagating medium. The power density or Poynting vector is

$$\begin{aligned}\mathbf{S}(r,\theta,\phi,t) &= \mathbf{E}(r,\theta,\phi,t)\times\mathbf{H}(r,\theta,\phi,t)\\ &\approx \tfrac{\omega\beta^3}{\epsilon}\left(\tfrac{I\triangle x}{4\pi r}\right)^2\sin^2(\theta)\cos^2(\beta r-\omega t)\hat{\mathbf{r}}.\end{aligned} \tag{1.11}$$

Derivations of Eqs. (1.9), (1.10), and (1.11) can be found in Ref. [8]. For any value of θ, if we plot the magnitude of Eq. (1.11) from $r = 0$ to the far-field region along with time, then the magnitude will be constant in ϕ. As seen in Fig. 1.3, for any value of θ, the electromagnetic energy intensity countours are circular near the antenna, but can be approximated as plane waves in the far-field region.

1.3.4 Reciprocity of Antennas

The radiation pattern or beampattern of an antenna is the same whether the antenna is transmitting or receiving electromagnetic energy. This property of antennas is called reciprocity. Proof of reciprocity will not be discussed in this thesis. A discussion of reciprocity may be found in other texts such as Ref. [7].

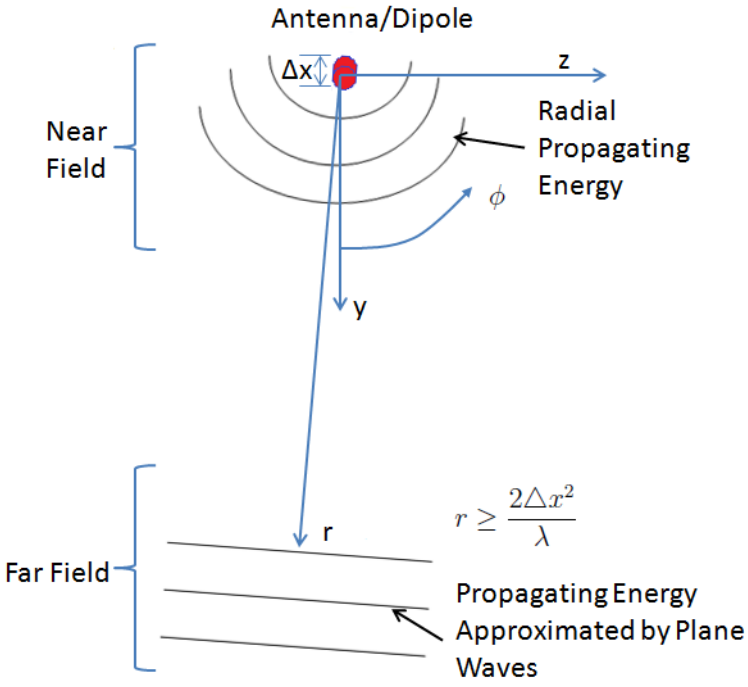

Figure 1.3: *Radial propagating electromagnetic energy from dipole antenna to far-field where it can be approximated as a plane wave. θ can be any value.*

1.4 Directivity and Gain

The directivity of an antenna is defined as the ratio of the radiation intensity in a given direction from the antenna to the radiation intensity averaged over all directions [2]. The radiation intensity in a given direction is defined as

$$R(\theta, \phi) \equiv \mathbf{S}_r(r, \theta, \phi) r^2. \tag{1.12}$$

We can restate Eq. (1.12) as

$$R(\theta, \phi) = \mathbf{S}_r(r, \theta_{max}, \phi_{\max}) r^2 \cdot P(\theta, \phi)$$

where θ_{max} and ϕ_{max} are from Eq. (1.8). The average radiation intensity per steradian is given by

$$\begin{aligned} R_{ave} &= \frac{1}{4\pi}\int_0^{2\pi}\int_0^{\pi} R(\theta,\phi)\sin(\theta)d\theta d\phi \\ &= \frac{1}{4\pi}\int_0^{2\pi}\int_0^{\pi} \mathbf{S}_r(r,\theta_{max},\phi_{\max})r^2\cdot P(\theta,\phi)\sin(\theta)d\theta d\phi \\ &= \frac{\mathbf{S}_r(r,\theta_{max},\phi_{\max})r^2}{4\pi}\int_0^{2\pi}\int_0^{\pi} P(\theta,\phi)\sin(\theta)d\theta d\phi \end{aligned}$$

Now, the directivity in a given direction is

$$\begin{aligned} D(\theta,\phi) &\equiv \frac{R(\theta,\phi)}{R_{ave}} \\ &= \frac{\mathbf{S}_r(r,\theta_{max},\phi_{\max})r^2\cdot P(\theta,\phi)}{\frac{\mathbf{S}_r(r,\theta_{max},\phi_{\max})r^2}{4\pi}\int_0^{2\pi}\int_0^{\pi} P(\theta,\phi)\sin(\theta)d\theta d\phi} \\ &= 4\pi\frac{P(\theta,\phi)}{\int_0^{2\pi}\int_0^{\pi} P(\theta,\phi)\sin(\theta)d\theta d\phi}. \end{aligned} \tag{1.13}$$

The gain of antenna is given by

$$G(\theta,\phi) = e_r D(\theta,\phi),\ 0 \le e_r \le 1 \tag{1.14}$$

where e_r represents losses in the antenna. The losses could come from the VSWR ratio and mismatch in polarization.

The direction of maximum gain is the direction of the main beam of the antenna. For the

dipole, the gain is given by

$$\begin{aligned} G(\theta,\phi) &= e_r D(\theta,\phi) \\ &= e_r \cdot 4\pi \frac{P(\theta,\phi)}{\int_0^{2\pi}\int_0^{\pi} P(\theta,\phi)\sin(\theta)d\theta d\phi} \\ &= e_r \cdot 4\pi \frac{\sin^2(\theta)}{\int_0^{2\pi}\int_0^{\pi} \sin^3(\theta)d\theta d\phi} \\ &= e_r \cdot 4\pi \frac{\sin^2(\theta)}{\frac{8\pi}{3}} \\ &= \frac{3}{2}\sin^2(\theta)e_r. \end{aligned}$$

The direction of maximum gain occurs when $\theta = \frac{\pi}{2}$ and ϕ can be any value. Therefore, the main beam direction for the dipole antenna is the entire y, z plane. The maximum gain direction is the same as the direction of maximum radiation pattern value.

1.5 Sidelobes

Other antennas will have different radiation patterns, and therefore, different gain values. For example, the horn aperture antenna with dimensions L_x and L_y has the power pattern

$$P(\theta,\phi) = \frac{16\sin^2\left(\frac{\beta L_x \sin(\theta)\cos(\phi)}{2}\right)\sin^2\left(\frac{\beta L_y \sin(\theta)\sin(\phi)}{2}\right)}{\beta^2 L_x^2 L_y^2 \sin^4(\theta)\cos^2(\phi)\sin^2(\phi)}$$

for large L_x and L_y. For a uniform line source of length L with current directed in the $\hat{\mathbf{x}}$ direction, the power pattern is

$$P(\theta,\phi) = \sin^2(\theta)\frac{\sin^2\left(\frac{\beta L}{2}\cos(\theta)\right)}{\frac{\beta^2 L^2}{4}\cos^2(\theta)}.$$

Fig. 1.4 shows the power pattern in dB scale. The direction of maximum gain is at $\theta = \frac{\pi}{2}$, and it is the direction of the main beam. A definition of how wide the main beam is may vary. The width of the main beam is sometimes taken with respect to where the beampattern

is greater than half its maximum value. The width of the main beam can also be defined as the angular length between the first beampattern null locations around the main beam direction. The main beam may also be referred to as the main lobe.

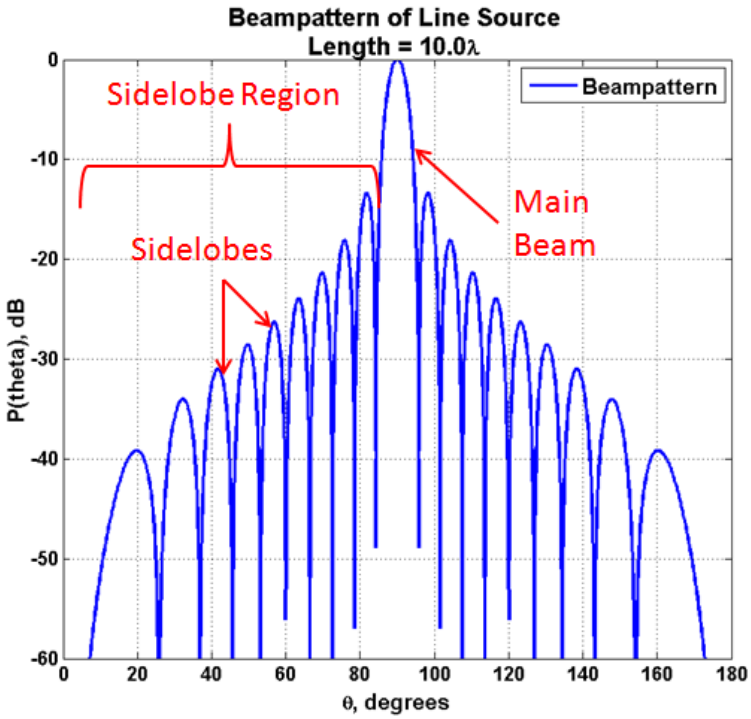

Figure 1.4: *Beampattern of line source showing main lobe and sidelobes*

The area of the beampattern outside the definition of the main beam width is the sidelobe region. Local peaks of the beampattern in the sidelobe region are the sidelobes.

The maximum value of the beampattern in the sidelobe region is the peak sidelobe level. It may also be referred to as just the sidelobe level or the peak sidelobe. It is the peak sidelobe level that is of interest in this thesis.

Chapter 2

Linear Antenna Arrays

2.1 Linear Array of Dipoles

Returning to the dipole of length $\triangle x$ with current I in the $\hat{\mathbf{x}}$ direction, the electric field when $\theta = \frac{\pi}{2}$ is

$$\mathbf{E}\left(r, \frac{\pi}{2}, \phi\right) \approx \frac{j\beta I \triangle x \eta e^{-j\beta r}}{4\pi r}\hat{\theta}$$

giving a field pattern of

$$F\left(\frac{\pi}{2}, \phi\right) = 1.$$

An isotropic antenna has the same radiation intensity in all directions in a sphere around the antenna. Its radiation pattern is unity in in all directions, and therefore, its directivity is unity in all directions. A true isotropic antenna cannot exist because continuously non-zero tangent vectors cannot exist on a spherical surface [9].

Although the dipole does not have the same radiation pattern over a sphere that surrounds it, it does have a unity radiation pattern at all angles in the y, z plane. Therefore, it can be considered to have the same radiation pattern as an isotropic antenna when $\theta = \frac{\pi}{2}$ and only the y, z plane is considered.

Instead of one dipole, let there be a few dipole antennas each having length $\triangle x$ and current

I in the $\hat{\mathbf{x}}$ direction. Let z-coordinate positions of these dipole antennas vary. Fig. 2.1 shows four identical dipoles arranged linearly on the z-axis with different positions. Their positions are at z_1, z_2, z_3, and z_4. Position $z_2 = 0$ is the origin. All the dipoles have the same isotropic far-field radiation pattern in the y, z plane. In the far-field, the electromagnetic energy may be approximated by plane waves. The plane wave approximation allows the distance vectors from the dipoles to a far-field observation or measurement point to be approximately parallel. The differences in distance vector lengths are a function of the antenna positions on the z-axis and the angle ϕ to the observation or measurement point. The electric field at the observation point is a sum of the electric field contributions from each of the dipoles. It is given as

$$\mathbf{E}\left(r, \frac{\pi}{2}, \phi\right) \approx j\beta I \triangle x \eta \left(\frac{e^{-j\beta(r+z_1 \sin(\phi))}}{4\pi(r + z_1 \sin(\phi))} + \frac{e^{-j\beta r}}{4\pi r} + \frac{e^{-j\beta(r+z_3 \sin(\phi))}}{4\pi(r + z_3 \sin(\phi))} + \frac{e^{-j\beta(r+z_4 \sin(\phi))}}{4\pi(r + z_4 \sin(\phi))} \right) \hat{\theta}. \tag{2.1}$$

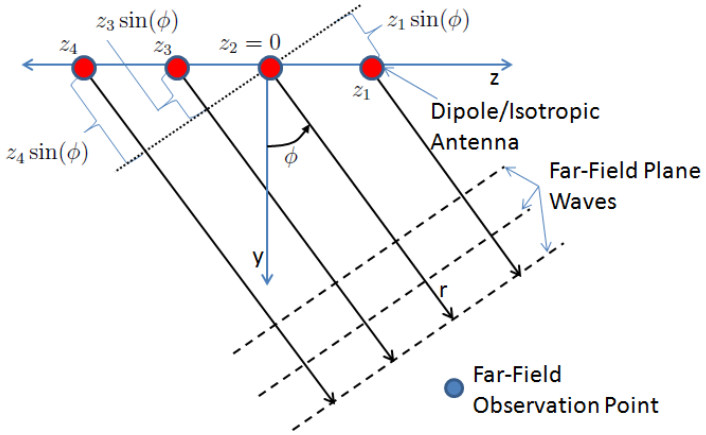

Figure 2.1: *Linear array of dipoles on z-axis. X-axis is out of page. Plane wave approximation of far-field radiation.*

The far-field observation point will be at a distance much greater than the maximum distance between any two dipoles which in this case gives the relation $r >> (z_1 - z_4)$. So, Eq.

(2.1) can be simplified to

$$\mathbf{E}\left(r, \frac{\pi}{2}, \phi\right) \approx \frac{j\beta I \triangle x \eta e^{-j\beta r}}{4\pi r}\left(e^{-j\beta z_1 \sin(\phi)} + 1 + e^{-j\beta z_3 \sin(\phi)} + e^{-j\beta z_4 \sin(\phi)}\right)\hat{\theta}. \tag{2.2}$$

Normalizing the $\hat{\theta}$ component of the electric field in Eq. (2.2) gives

$$\begin{aligned} F\left(r, \frac{\pi}{2}, \phi\right) &\approx \frac{\frac{j\beta I \triangle x \eta e^{-j\beta r}}{4\pi r}\left(e^{-j\beta z_1 \sin(\phi)} + 1 + e^{-j\beta z_3 \sin(\phi)} + e^{-j\beta z_4 \sin(\phi)}\right)}{\frac{j4\beta I \triangle x \eta e^{-j\beta r}}{4\pi r}} \\ &\approx \frac{\left(e^{-j\beta z_1 \sin(\phi)} + 1 + e^{-j\beta z_3 \sin(\phi)} + e^{-j\beta z_4 \sin(\phi)}\right)}{4} \\ &\approx \frac{1}{4}\sum_{k=1}^{4} e^{-j\beta z_k \sin(\phi)} \\ &\equiv F(\phi, \{z_1, z_2 = 0, z_3, z_4\}). \end{aligned} \tag{2.3}$$

Eq. (2.3) is the field pattern of the set of dipoles in Fig. 2.1.

The antenna setup in Fig. 2.1 is called a linear antenna array. Each isotropic antenna in the antenna array is referred to as an antenna element.

2.2 Antenna Array Steering

For the antenna array in Fig. 2.1, the dipole locations along the z-axis affected the phase of electric field from each antenna. The direction of maximum gain, or the direction when the field pattern in unity, is when $\phi = 0$. The main beam of the antenna array in the y, z plane will be directed towards $\phi = 0$. If we desire the main beam to point in a different direction, say at $\phi = \phi_0$, we can introduce a phase to each of the dipole's current by

$$I_k = Ie^{j\beta z_k \sin(\phi_0)},\ k = \{1, 2, 3, 4\}$$

where k represents the kth dipole. Now, the field pattern is

$$\begin{aligned} F(\phi, \phi_0, \{z_1, z_2 = 0, z_3, z_4\}) &= \frac{\frac{j\beta \triangle x \eta e^{-j\beta r}}{4\pi r} \sum_{k=1}^{4} I_k e^{-j\beta z_k \sin(\phi)}}{\frac{j\beta \triangle x \eta e^{-j\beta r}}{4\pi r} \sum_{k=1}^{4} I_k e^{-j\beta z_k \sin(\phi_0)}} \\ &= \frac{I \sum_{k=1}^{4} e^{j\beta z_k \sin(\phi_0)} e^{-j\beta z_k \sin(\phi)}}{I \sum_{k=1}^{4} e^{j\beta z_k \sin(\phi_0)} e^{-j\beta z_k \sin(\phi)}} \\ &= \frac{1}{4} \sum_{k=1}^{4} e^{-j\beta z_k (\sin(\phi) - \sin(\phi_0))}. \end{aligned}$$

Now, the main beam is steered towards angle ϕ_0. This steering can be accomplished mechanically or electronically. When electronic steering is done, the antenna array is called a phased array.

In addition to main beam steering, the currents in each antenna may be phase shifted by an arbitrary amount α_k with

$$I_k = I e^{j\beta z_k \sin(\phi_0)} e^{-j\beta \alpha_k},\ k = \{1, 2, 3, 4\}.$$

The field pattern now becomes

$$F(\phi, \phi_0, \{z_1, z_2 = 0, z_3, z_4\}, \{\alpha_1, \alpha_2, \alpha_3, \alpha_4\}) = \frac{1}{4} \sum_{k=1}^{4} e^{-j\beta (z_k (\sin(\phi) - \sin(\phi_0)) - \alpha_k)}.$$

For N isotropic antennas on a linear array with positions

$$\mathbf{z} = \{z_1, z_2, \ldots, z_N\}$$

and phase shifts

$$\alpha = \{\alpha_1, \alpha_2, \ldots, \alpha_N\},$$

the field pattern is

$$F(\phi, \phi_0, \mathbf{z}, \alpha) = \frac{1}{N} \sum_{k=1}^{N} e^{-j\beta (z_k (\sin(\phi) - \sin(\phi_0)) - \alpha_k)}. \tag{2.4}$$

This thesis focuses on changes in the positions of each antenna element and ignores

additional arbitrary phase shifts at each element.

2.3 Non-Isotropic Antenna Elements

Other types of antennas could replace the dipoles or isotropic antennas in the antenna array. The resulting field pattern will be the field pattern of the antenna array in Eq. 2.4 times the individual field pattern of the antenna element, assuming all antennas in the array have the same field pattern and are oriented in the same direction. Since the field pattern of the antenna array assuming isotropic elements is multiplied by the field pattern of an individual antenna, the field pattern in Eq. (2.4) is called the array factor.

If the radiation pattern of an array with a certain kind of antenna is needed, the radiation patterns from isotropic sources may be multiplied by the non-isotropic antenna radiation pattern after scaling antenna elements. In Fig. 2.2, the beampattern for an antenna array is shown after being multiplied by a non-isotropic element pattern. The portions of the array beampattern furthest from the main beam are lost after multiplication. If the element positions of the array are scaled, then the original beampattern levels can be preserved after multiplication with the non-isotropic element pattern.

2.4 Beampattern of Antenna Array with Arbitrary Number of Elements, N

We define

$$u = \sin(\phi) - \sin(\phi_0). \tag{2.5}$$

With the definition of u in Eq. (2.5), the main beam of the antenna array will always be directed at $u = 0$ no matter what the steering angle may be.

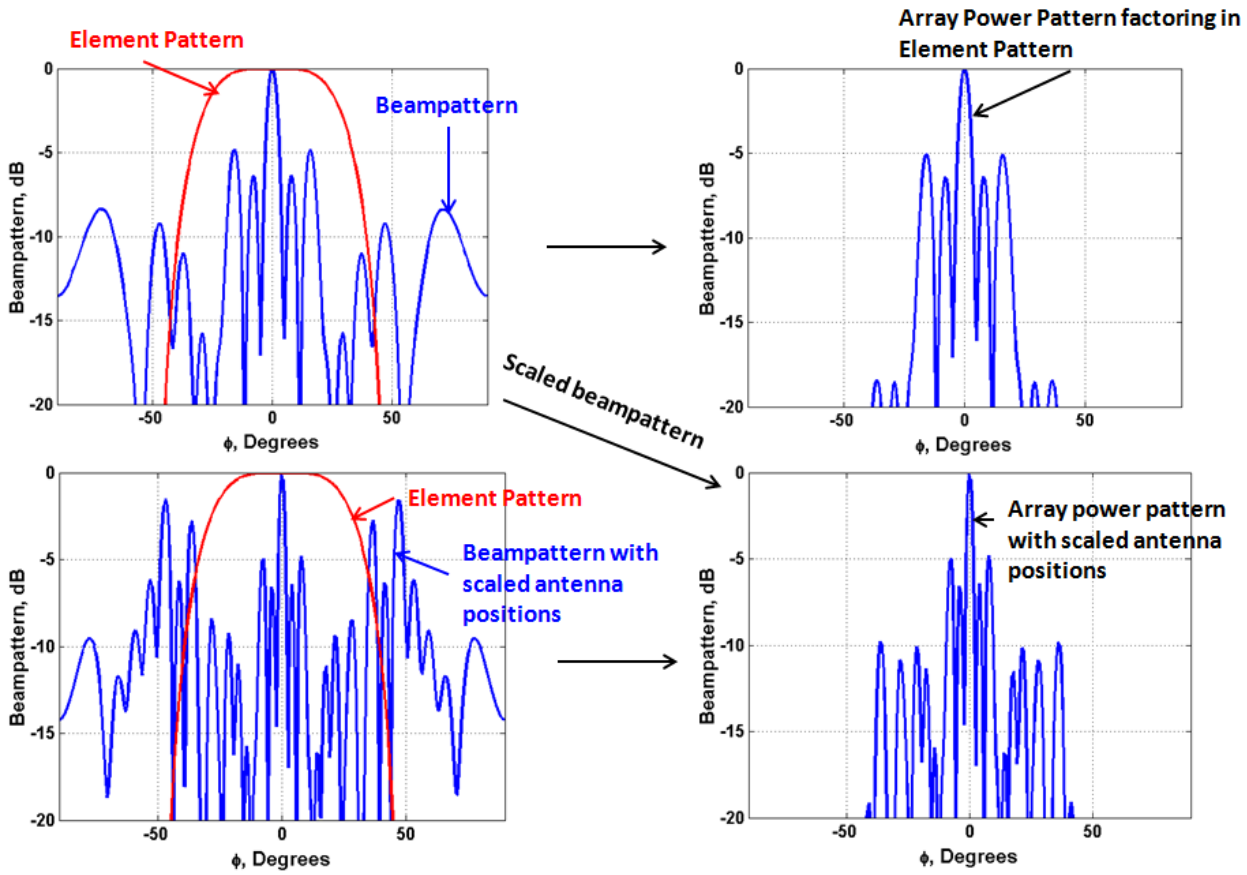

Figure 2.2: *The beampattern of an array with non-isotropic antenna radiation patterns may be analyzed after scaling the element positions*

The field pattern or array factor is now re-written as

$$F(u, \mathbf{z}) \equiv \frac{1}{N} \sum_{k=1}^{N} e^{-j\beta u z_k}. \tag{2.6}$$

We now introduce two terms:

$$X(u, \mathbf{z}) \equiv \frac{1}{\sqrt{N}} \sum_{k=1}^{N} \cos(z_k \beta u) \tag{2.7}$$

and

$$Y(u, \mathbf{z}) \equiv \frac{1}{\sqrt{N}} \sum_{k=1}^{N} \sin(z_k \beta u). \tag{2.8}$$

Eqs. (2.7) and (2.8) can be put into equation Eq. (2.6) to produce

$$F(u, \mathbf{z}) = \frac{1}{\sqrt{N}} \left(X(u, \mathbf{z}) - jY(u, \mathbf{z}) \right).$$

Eqs. (2.7) and (2.8) can be called the quadrature components of the array factor [10]. They form the real and imaginary parts of the array factor, respectively.

The beampattern of the antenna array can now be written as

$$\begin{aligned} P(u, \mathbf{z}) &= |F(u, \mathbf{z})|^2 \\ &= F(u, \mathbf{z}) F^*(u, \mathbf{z}) \\ &= \frac{1}{N}(X^2(u, \mathbf{z}) + Y^2(u, \mathbf{z})) \end{aligned} \tag{2.9}$$

2.4.1 Shifting Array Elements by Arbitrary Amount

In the far-field, shifting the antenna elements by an arbitrary amount will not change the beampattern. To see that the beampattern does not change, we introduce a shift of $z_\alpha > 0$ to all antennas on the linear array. The resulting beampattern is

$$\begin{aligned} P(u, \mathbf{z} + z_\alpha) &= F(u, \mathbf{z} + z_\alpha) F^*(u, \mathbf{z} + z_\alpha) \\ &= \frac{1}{N} \sum_{k=1}^{N} e^{-j\beta u(z_k + z_\alpha)} \frac{1}{N} \sum_{k=1}^{N} e^{j\beta u(z_k + z_\alpha)} \\ &= \frac{e^{-j\beta u z_\alpha}}{N} \sum_{k=1}^{N} e^{-j\beta u z_k} \frac{e^{j\beta u z_\alpha}}{N} \sum_{k=1}^{N} e^{j\beta u z_k} \\ &= \frac{1}{N} \sum_{k=1}^{N} e^{-j\beta u z_k} \frac{1}{N} \sum_{k=1}^{N} e^{j\beta u z_k} \\ &= F(u, \mathbf{z}) F^*(u, \mathbf{z}) \\ &= P(u, \mathbf{z}), \end{aligned}$$

and so the far-field beampattern is not affected by shifting antenna positions.

2.4.2 Changing Steering Angle

With the azimuth angle, ϕ, ranging from $-\pi$ to π,

$$u \in [-1, 1] - \sin(\phi_0).$$

Looking at the beampattern for a linear array in Fig. 2.3, it can be seen that it is reflected about $u = 0$ when the steering angle is $\phi_0 = 0$. When the steering angle is set to $\phi_0 = \pi/6$ so that $\sin(\phi_0) = 0.5$, u is now $u \in [-1.5, 0.5]$.

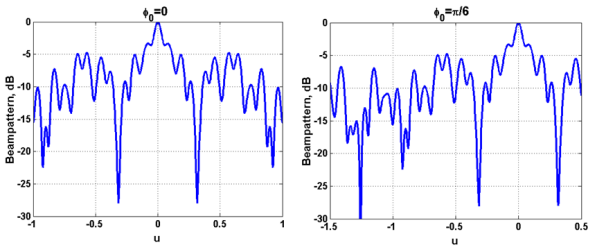

Figure 2.3: *Power domain beampattern of linear array in u, dB scale*

If we were to extend u so that $u \in [-1.5, 1.5]$ as seen in Fig. 2.4, then we see that the beampattern is still reflected about $u = 0$.

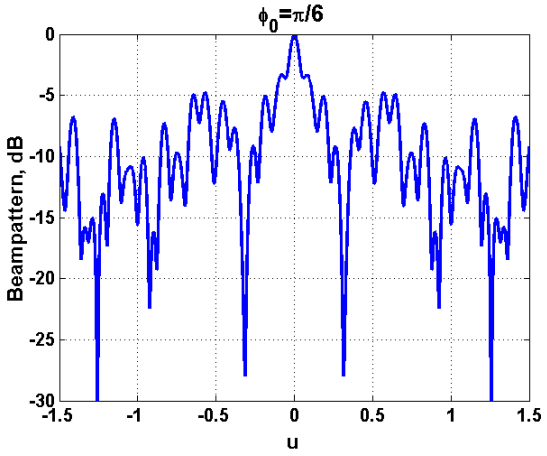

Figure 2.4: *Power domain beampattern of linear array in u with* $u \in [-1 - |\sin(\phi_0)|, 1 + |\sin(\phi_0)|]$, *dB scale*

Therefore, if we are interested in the peak sidelobe level or any quantity of the power domain beampattern, we can focus on

$$u \in [0, 1 + |\sin(\phi_0)|]$$

since the same values appear for $u \in [-1 - |\sin(\phi_0)|, 0]$.

Chapter 3

Problem of Random Positions in Antenna Array

3.1 Research Objectives

Let there be antenna elements distributed according to some arbitrary antenna position distribution as seen in Fig. 3.1. The resulting beampattern values at each angle outside the main beam direction will be randomly distributed. The peak sidelobe level will also be randomly distributed.

Our first goal is to compute the peak sidelobe level distribution and accomplish the following:

1. Express the peak sidelobe level distribution as a function of the antenna position distribution.

2. Evaluate the effects of antenna aperture on peak sidelobe level distribution.

3. Evaluate the peak sidelobe level distribution in the asymptotic limit of a large number of antennas.

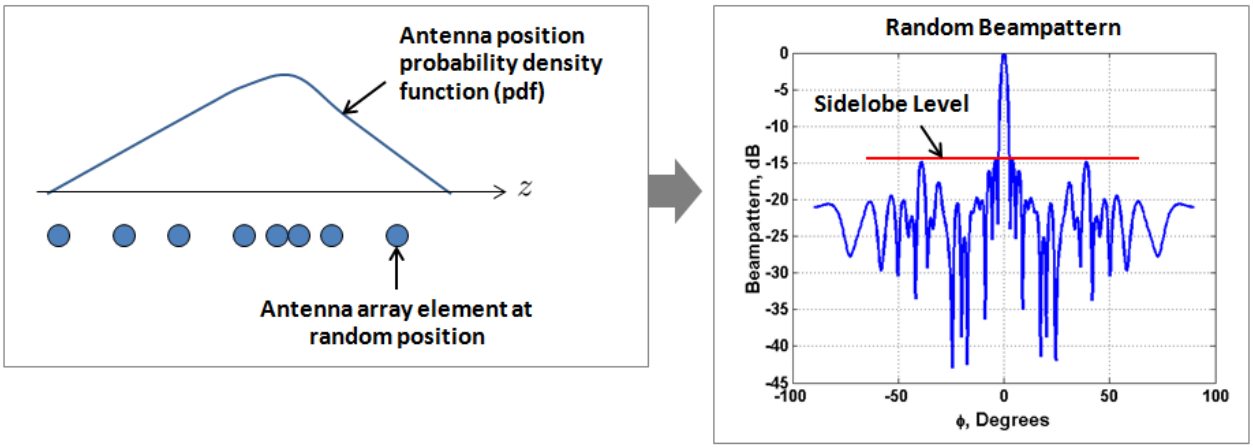

Figure 3.1: *Random antenna positions with arbitrary pdf producing random beampattern and random peak sidelobe level*

The methods used to calculate the sidelobe level distribution initially involved finding the expected number of upward crossings of the beampattern of a certain level. However, this approach involved making approximations of the beampatterns statistics that only worked well for very large antenna arrays. For a smaller number of antennas, another approach was needed.

Finding the peak sidelobe level distribution using Extreme Value Theory (EVT) can allow more accurate probability calculations for smaller antenna arrays. Our second goal will be to use EVT to calculate the peak sidelobe level distributions without making the approximations in the upward-crossing method thereby achieving more accurate results for smaller antenna arrays.

3.2 Planar Arrays Transformed into Linear Arrays

In the far-field, planar array antenna position distributions may be transformed into linear array position distributions. An example is given in Ref. [11] where a planar array with uniform distributed element positions is transformed into a linear arrangement of elements

that are semicircle distributed in position. In Ref. [11], N antenna elements have independent random radial positions $\mathbf{r} = \{r_1, r_2, \ldots, r_N\}$ and independent random azimuth position components $\psi = \{\psi_1, \psi_2, \ldots, \psi_N\}$. The distribution of each radial position is given by the probability density function (pdf) $f_{r_k}(r)$, and the distribution of each azimuth position is given by the pdf $f_{\psi_k}(\psi)$. The array factor for a planar array is given by

$$F(\phi, \mathbf{r}, \psi) = \frac{1}{N} \sum_{k=1}^{N} e^{-j\frac{4\pi}{\lambda} r_k \sin\left(\frac{\phi-\phi_0}{2}\right) \sin\left(\psi_k - \frac{\psi_0+\psi}{2}\right)} [11]. \tag{3.1}$$

Here, ϕ_0 is the array steering direction and ϕ is the measurement or observation direction. We let $\beta = \frac{4\pi}{\lambda}$ and $u = \sin\left(\frac{\phi-\phi_0}{2}\right)$. Eq. (3.1) will have the same form as the linear array factor in Eq. (2.6) if the planar array positions $\mathbf{r}$ and ψ are transformed into linear array positions $\mathbf{z} = \{z_1, z_2, \ldots, z_N\}$ by

$$\begin{aligned} z_k &= r_k \sin\left(\psi_k - \frac{\phi_0 + \phi}{2}\right) \\ &= r_k \sin(\tilde{\psi}_k) \end{aligned}$$

where

$$\tilde{\psi}_k = \psi_k - \frac{\phi_0 + \phi}{2}.$$

Fig. 3.2 illustrates this transformation.

The probability distribution of z_k can be found from the joint probability distribution of r_k and $\tilde{\psi}_k$. The probability distribution of $\tilde{\psi}_k$ can be found from that of ψ_k.

In order for probability computations for the planar array to proceed in the same manner as for the linear array, the probability distribution of each $z_k \in \mathbf{z}$ must be independent of observation direction ϕ and steering direction ϕ_0. The distribution of ψ_k must allow the distribution of $\tilde{\psi}_k$ to also be independent of ϕ and ϕ_0. One probability distribution that allows this independence is the uniform distribution. When considering planar arrays, the results in this thesis apply where the distribution of $\tilde{\psi}_k$ is made independent of the beampattern

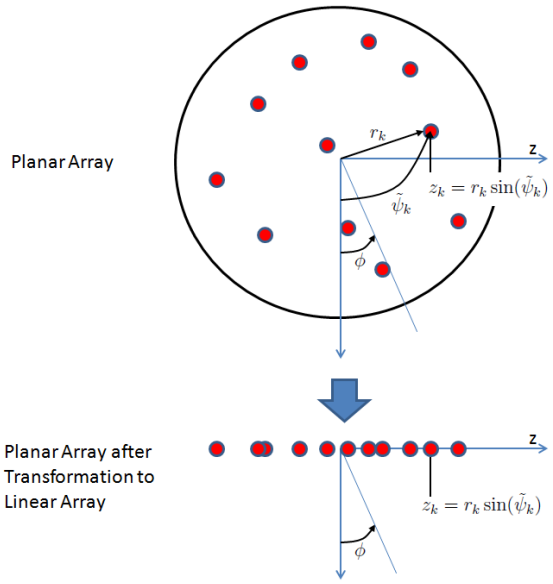

Figure 3.2: *Transformation of a planar array whose antenna element k has position coordinate $(r_k, \tilde{\psi}_k)$. Transformed linear position of element k is given by z_k.*

viewing angle, ϕ, and array steering direction ϕ_0.

We also note that for the planar array, $u \in [-1, 1]$ with the main beam at $u = 0$ regardless of what the steering angle, ϕ_0, is.

3.3 Defense Applications Involving Random Antenna Positions

The probability that the peak sidelobe of a random array instantiation exceeding some threshold has been of long interest, as seen in Refs. [12], [13], [14], [15], [16], [17], [18], [10], and [19]. Motivation for considering phased arrays with random element positions in this past research came from space exploration. There was a need for high resolution and full-scanning capability in radio astronomy, space communication, and long range radar.

National defense applications of arrays with random antenna positions also exist. An example is enemy jammers located along a coastline that affect aircraft communication. In

Fig. 3.3, a fighter aircraft over water in the far-field is trying to receive communication from another transmitting aircraft. Enemy jammers along the coast disrupt the communication. The coastline jammers can be considered to form a linear array. The positions and phases of the jammers are not known. The jammed aircraft tries to fly in the sidelobe region of the jammer array beampattern to minimize communication disruption. Without knowing the exact position and phases of the jammers, it is difficult to know how intense the jamming will be to the aircraft communication. The peak sidelobe level distribution calculations in this thesis can help analyze this scenario. How much the communication system's physical layer can overcome jamming at different distances from the coastline can be given as probabilities using the probability of peak sidelobe level when jammer locations are unknown.

In addition to analyzing aircraft communication performance against jamming, the aircraft's target detection capabilities can also be studied. The transmitting aircraft need not be friendly to the receiving aircraft. The receiving aircraft could be using radar and detecting the returned signal from the transmitting aircraft. Similarly to how communication system performance can be quantified with probabilities when jammer locations are unknown, the peak sidelobe level distribution can aid analysis of the radar performance against jamming.

Another defense application lies in unmanned aerial vehicles (UAVs) communicating, detecting, or targeting other aircraft. Instead of single aircraft, swarms of UAVs could provide more power in detecting or communicating with targets as seen in Fig. 3.4. Since the positions of the aircraft can constantly change, the peak sidelobe level distribution will be useful in analyzing the communication and detection performance of the UAV swarm. The calculations in this thesis may also be applied to uniform planar antenna arrays since the beampattern equation may be transformed to resemble a linear array. So, instead of linear arrangement, the UAV swarms may be arranged in a uniform planar geometry as seen in Fig. 3.5.

Soldiers out in the field or in a combat zone can have receivers and/or transmitters attached to them for communication or target detection. Analysis of the resulting beampattern and

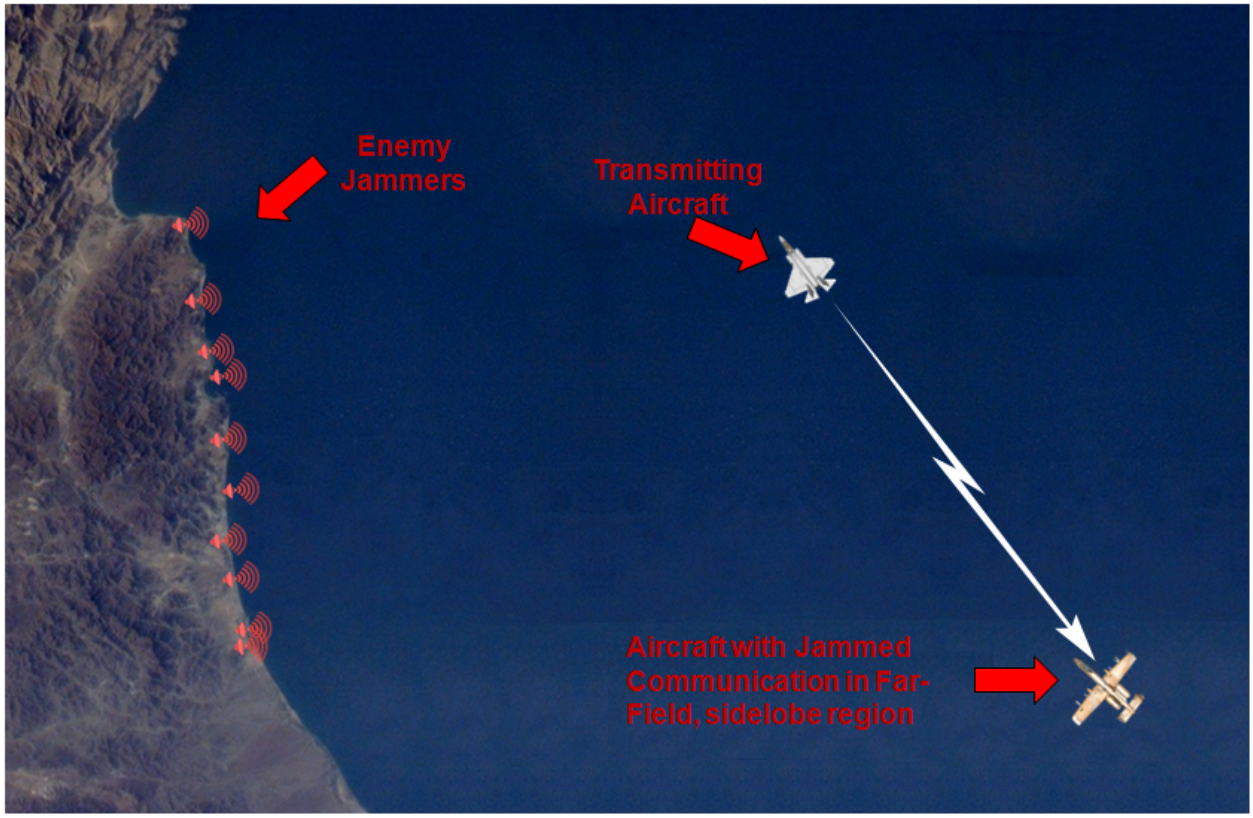

Figure 3.3: *Aircraft jamming scenario with linear array of jammers at unknown positions*

Figure 3.4: *UAV swarm in linear array arrangement communicating with or detecting target in far-field*

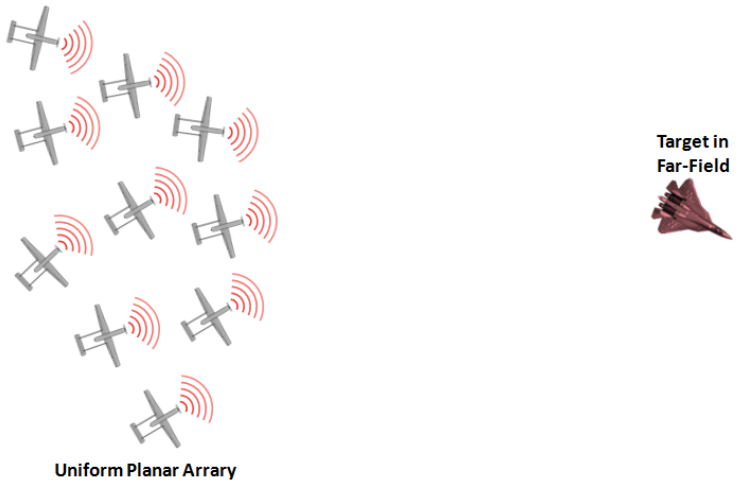

Figure 3.5: *UAV swarm in uniform planar array arrangement communicating with or detecting target in far-field*

peak sidelobe level will be similar to analysis for the UAV swarm.

3.4 Unequal Antenna Array Element Spacings

In addition to adding more power to an antenna array, additional UAVs and soldiers also increase the overall length of the array. This additional length leads to improved target resolution but also to higher sidelobe levels. It will now be shown that antennas spaced unequally apart in the case of random positions can reduce sidelobe levels compared to arrays of the same length and number of elements but that have equally spaced elements.

If array elements are evenly spaced, the array factor in Eq. (2.6) can be written as

$$F(u, \{0, d, 2d, \ldots, (N-1)d\}) = \frac{1}{N} \sum_{k=0}^{N-1} e^{-j\beta u \cdot d \cdot k}$$

where d is the distance between two elements in the array. Since only the far-field beampattern is being considered, the array does not have to be centered at position 0. Letting

$$\psi = \beta u \cdot d = \frac{2\pi}{\lambda} u \cdot d,$$

the array factor can be written as

$$F(\psi) = \frac{1}{N} \sum_{k=0}^{N-1} e^{-j\psi k}. \tag{3.2}$$

As u changes from -1 to 1, ψ changes from $-\frac{2\pi}{\lambda} \cdot d$ to $\frac{2\pi}{\lambda} \cdot d$. In the beampattern, lobes with the peak normalized power of 1 only occur at $\psi = 2\pi n$ where $n = 0, \pm 1, \pm 2, \ldots$. These lobes are called grating lobes. They are guaranteed to occur if $d \geq \lambda$. Looking at Fig. 3.6, we see grating lobes occuring in the beampattern for an antenna array with nine elements when the spacing is $d = \frac{5}{2\lambda}$.

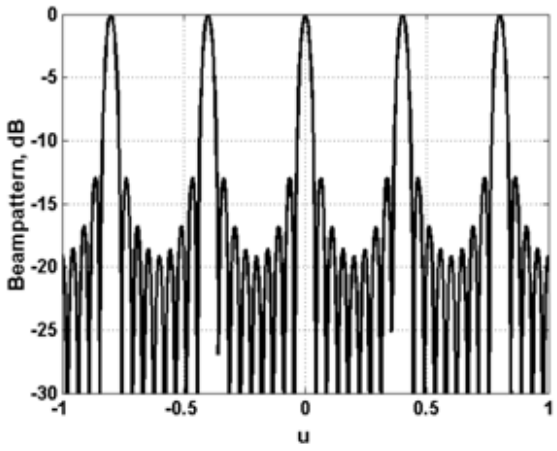

Figure 3.6: *Beampattern for antenna array with nine antenna elements spaced evenly at* $d = \frac{5}{2\lambda}$, *dB scale*

It is seen that $F(\psi + 2\pi) = F(\psi)$ making the array factor periodic with period 2π. When $d = \lambda$, this period is covered from $u = 0$ to $u = \pm 1$ so that ψ changes from $\psi = 0$ to $\psi = \pm 2\pi$. The main lobe will be at $u = 0$ and grating lobes will appear at $u = \pm 1$.

If $d < \lambda$, then ψ will never be a multiple of 2π and grating lobes will not occur except for the main beam at $u = 0$. However, the peak sidelobe level will still be relatively high when d is close to λ. The height of the sidelobes will be at their lowest when $\psi = \pm\pi$, which correspond to half a period of the array factor. When $d = \lambda/2$, $\psi = \pm\pi$ at $u = \pm 1$. The

height of the sidelobes will reduce from $u = 0$ to $u = \pm 1$ as seen in Fig. 3.7 for nine antenna elements spaced at half a wavelength apart.

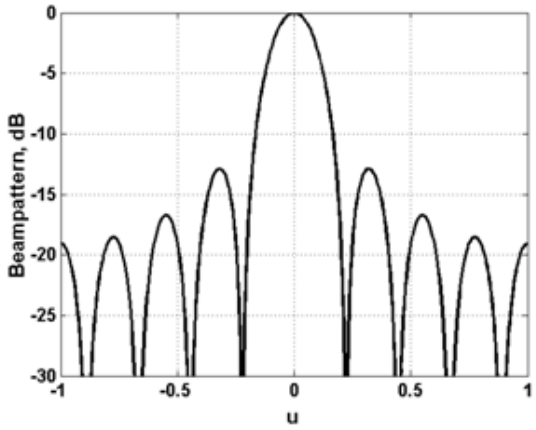

Figure 3.7: *Beampattern for antenna array with nine antenna elements spaced evenly at $d = \lambda/2$, dB scale*

Reducing the antenna element spacing further to $d < \lambda/2$ will not reduce the peak height of the sidelobes. It will only reduce the number of sidelobes in the sidelobe region as seen in Fig. 3.8 for $d = 3\lambda/10$. For $d < \lambda/2$, less than half the beampattern period is being reached at $u = \pm 1$.

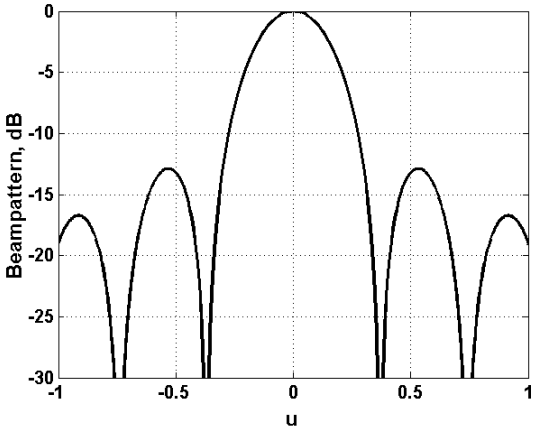

Figure 3.8: *Beampattern for antenna array with nine antenna elements spaced evenly at $d = 3\lambda/10$, dB scale*

Reducing d while keeping the number of antenna elements the same reduces the total length of the antenna array, or the difference between the maximum element position and the minimum element position. We refer to this difference as the antenna array aperture.

So, reducing the antenna array aperture is synonymous with zooming in to the beampattern around the main beam. This reduction in aperture also increases the width of the main beam regardless of which definition of the main beam width is being used. From the definitions of directivity and gain in Eqs. (1.13) and (1.14), narrow main beams have greater directivity and gain than wider main beams. This larger gain is useful in pointing more precisely to a target whether the antenna array is receiving or transmitting.

Reducing the peak height of sidelobes is also desirable in applications where transmitting or receiving from a particular direction is important. With a high sidelobe power value in a direction in the sidelobe region, energy in that direction can be mistaken as coming from the main lobe.

Since $d = \lambda/2$ will not give a higher peak sidelobe level than when $d < \lambda/2$ but still provide a narrower main beam, this spacing is often used with equally spaced antenna arrays. If one wishes to have a narrower main beam than the one given with $\lambda/2$ spacing, then the antenna aperture must increase using the following options:

1. Using the same number of antenna elements, increase the spacing between the elements to give a larger aperture. A narrower main beam will result at the expense of higher peak sidelobe levels. If the spacing is increased beyond a wavelength, grating lobes will occur.

2. Keeping the $\lambda/2$ spacing, increase the number of antenna elements. This option will result in a narrower main beam and lower peak sidelobe levels relative to the main beam. It will come at the expense of additional antenna elements.

3. A third option is keeping the number of antenna elements the same but use unequal

spacing between elements. This option will allow main beams to be as narrow as when $d > \lambda$ but can avoid grating lobes. In Fig. 3.9, nine antenna elements are spread over the same aperture as the evenly spaced antenna array of nine elements spaced $d = 5\lambda/2$ apart. The elements in this case have unequal spacing to give the beampattern in Fig. 3.9. A main beam as narrow as the $d = 5\lambda/2$ evenly spaced case is achieved but without grating lobes.

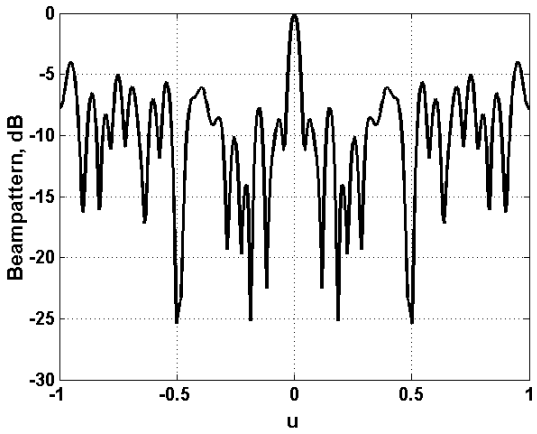

Figure 3.9: *Beampattern for antenna array with nine antenna elements unequally spaced between* $z = 0$ *and* $z = 20\lambda$*, dB scale*

The third option is most desirable in applications where narrow mean beams can be advantageous. However, the spacings between elements must be optimized so that as low a peak sidelobe level as possible is achieved while maintaining the narrow beam that comes with a large aperture.

A distribution of the peak sidelobe level can be useful to this optimization. The distribution will show the probability that N random antenna elements of some arbitrary position distribution and maximum possible aperture will achieve a certain peak sidelobe level.

In addition to avoiding grating lobes, Refs. [19] and [20] show that antenna arrays with random antenna element positions mitigate the effects of mutual coupling.

3.5 Application to Designing Unequally Spaced Antenna Arrays

The advantage of narrow main beams without grating lobes led to research in designing arrays with unequally spaced antenna elements. Another motivation was that sidelobes could be reduced with unequally spaced antenna elements without applying tapering to the antenna array illumination. Tapering would cause inefficiencies in antenna operation and make designing and building them more difficult [21].

Finding an optimal design proved difficult. Different methods to design arrays with unequally spaced elements were proposed such as the methods discussed in Refs. [21], [22], and [23]. Researchers came to the conclusion that there was probably no unique solution to low sidelobe levels [24]. It appeared unlikely that a simple optimization procedure could be devised for nonuniform arrays [25]. Ref. [26] stated that the methods proposed to design arrays with unequal spacings were not optimal, and that some were tedious and time-consuming for large arrays. In fact, a trial method to finding an array design with unequal spacings would produce results that were just as good as a systematic design method [26]. When using a trial method to designing unequally spaced arrays, knowing the distribution of the peak sidelobe level can help determine the parameters and array geometries that will most likely result in an acceptable array design even if the design is not optimal.

Despite not finding an optimal design, the design of thinned arrays with unequal element spacing continues to be of interest to researchers as evidenced by Refs. [27], [28], and [29]. Ref. [30] gave the interesting method of averaging beampatterns of unequally spaced antenna elements through frequency or spatial diversity to lower sidelobe levels. Knowing the peak sidelobe level distribution with different array parameters can help in designing algorithms and diversity methods. Ref. [31] showed that deterministic spiral arrays have comparable sidelobe and main beam characteristics to random planar arrays. The peak sidelobe level

distribution can be used to compare designs with random arrays.

3.6 Application to Angle Estimation to Target

For a variety of applications, including those where direction finding is important, antenna arrays with random element placement are employed to perform angle estimation. As shown in Fig. 3.10, the angle-estimation performance determines the threshold signal-to-noise ratio (SNR) point at which it deviates from the Cramér-Rao angle-estimation bound. SNR values greater than the threshold point are needed for accurate angle-estimations. Ref. [32] defines the SNR threshold point as where the second derivative of the angle-estimation performance peaks. However, this definition is arbitrary. In addition to the Cramér-Rao bound, it is also of interest to know how the angle-estimation performance compares with the tighter Weiss-Weinstein and Barankin bounds at low SNR [33] [34] [35].[1][1]

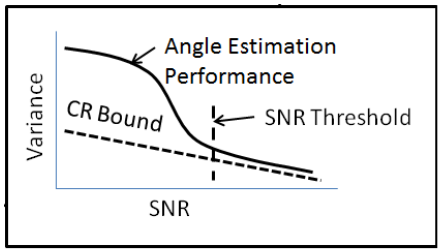

Figure 3.10: *Angle-Estimation Performance, taken from Ref. [1] ©2011 IEEE*

In Refs. [36], [37], and [38], the method of interval errors calculates the angle-estimation performance when there is low SNR. This performance is a function of the probability that the maximum-likelihood estimator of the target angle will misidentify a point within a sidelobe interval as the main lobe. It assumes the maximum peak sidelobe is above a certain beampattern level. The angle-estimation performance can be modified to include the

[1][1] ©2011 IEEE

peak sidelobe level distribution from this thesis. An expression for the peak sidelobe level distribution in terms of the antenna position distribution can help show more clearly how the angle-estimation performance is affected by random antenna element positions.

Chapter 4

Sidelobe Peak Distribution using Method of Upcrossings and Sampling Beampattern

4.1 Introduction

Portions of the content in this chapter has been published in Ref. [1].[1]

Sampling the beampattern is one method of determining the peak sidelobe level distribution as done by Refs. [13] and [17].

A more accurate approach uses the number of times a beampattern upward-crosses a certain level. Ref. [14] calculated the peak sidelobe level distribution by using this method but assumed beampattern upward-crossing locations were independent and Poisson distributed. Ref. [14] did not account for the beampattern being above a certain level at the beginning of the sidelobe region, but it has a small effect for arrays with many elements. Refs. [18] and [19] account for the initial beampattern level. They find the peak sidelobe level distribution

[1] [1] ©2011 IEEE

for linear arrays with uniformly distributed element locations by using the upward-crossing method. Ref. [18] also computes the peak sidelobe level distribution for cosine squared distributed element locations on linear arrays. Refs. [39], [11], and [40] used the upward-crossing method to determine upper bounds for maximum peak sidelobe distributions but not the peak sidelobe level distributions themselves.[2]

Both the sampling of the beampattern and the upcrossing method will be analyzed in this chapter. The antenna positions in both methods are independently and indentically distributed (iid).

We define the notation used for the sidelobe region as follows. Let $u = \pm u_s$, $u_s \geq 0$, be where the sidelobe region arbitrarily begins after the main beam. The sidelobe region, $\mathcal{S}$, is

$$\mathcal{S} \triangleq \{u | u_s \leq |u|\}.$$

Due to beampattern symmetry, a part of the sidelobe region is redundant. For linear arrays, the length non-redundant portion of the sidelobe region, $\mathcal{S}_{nr}$, is

$$\mu(\mathcal{S}_{nr}) = 1 + |\sin(\phi_0)| - u_s$$

where $\mu(X)$ is the measure of set X. For planar arrays, the length is

$$\mu(\mathcal{S}_{nr}) = 1 - u_s.$$

4.2 Quadrature Component Statistics

Let the antenna array element location distribution have probability density function (pdf) $f_{z_k}(z)$. Its characteristic function or Fourier Transform is

$$\hat{f}_{z_k}(u) \triangleq \int_{L_{\min}}^{L_{\max}} f_{z_k}(z) e^{-jz\beta u} dz \tag{4.1}$$

[2] [1] ©2011 IEEE

where $L_{\min}$ is the smallest possible value of position z_k, and $L_{\max}$ is the largest possible value. The maximum possible aperture for the antenna array is $L_{\max} - L_{\min}$.

In both the sampling and upcrossing methods of calculating the peak sidelobe level distribution in this chapter, the quadrature components $X(u, \mathbf{z})$ and $Y(u, \mathbf{z})$ in Eqs. (2.7) and (2.8) are assumed to have large enough N so that their distributions can be assumed Gaussian by the Central Limit Theorem.

The expected values or first moments of $X(u, \mathbf{z})$, $Y(u, \mathbf{z})$, $X'(u, \mathbf{z})$, and $Y'(u, \mathbf{z})$ at each u are given as follows. $E_{\mathbf{z}}[X]$ is the expectation of X over the joint distribution of the elements of $\mathbf{z}$. $E_{z_k}[X]$ is the expectation of X over the distribution of element $z_k \in \mathbf{z}$. $VAR(X)$ is the variance of X.

The expected value of $X(u, \mathbf{z})$ over $\mathbf{z}$,

$$\begin{aligned}
E_{\mathbf{z}}[X(u,\mathbf{z})] &\equiv m_{X,z}(u) \\
&= E_{\mathbf{z}}\left[\frac{1}{\sqrt{N}}\sum_{k=1}^{N}\cos(z_k\beta u)\right] \\
&= \sqrt{N}E_z\left[\cos(z\beta u)\right] \\
&= \sqrt{N}\int_{L_{\min}}^{L_{\max}} f_{z_k}(z)\cos(z\beta u)dz \\
&= \sqrt{N}\int_{L_{\min}}^{L_{\max}} f_{z_k}(z)\left(\frac{e^{jz\beta u}+e^{-jz\beta u}}{2}\right)dz \\
&= \sqrt{N}\left(\int_{L_{\min}}^{L_{\max}} f_{z_k}(z)\frac{e^{jz\beta u}}{2}dz + \int_{L_{\min}}^{L_{\max}} f_{z_k}(z)\frac{e^{-jz\beta u}}{2}dz\right) \\
&= \sqrt{N}\left(\frac{\hat{f}_{z_k}(-u)+\hat{f}_{z_k}(u)}{2}\right). \qquad (4.2)
\end{aligned}$$

The variance of $X(u, \mathbf{z})$ over $\mathbf{z}$ is

$$
\begin{aligned}
VAR(X(u,\mathbf{z})) &\equiv \sigma^2_{X,z}(u) \\
&= E_z\left[X^2(u,\mathbf{z})\right] - m^2_{X,z}(u) \\
&= E_z\left[\frac{1}{N}\sum_{k=1}^{N}\cos^2(z_k\beta u) + \frac{1}{N}\sum_{k=1}^{N}\cos(z_k\beta u)\sum_{\substack{l=1\\ l\neq k}}^{N}\cos(z_l\beta u)\right] \\
&\quad -N\left(\frac{\hat{f}_{z_k}(-u)}{2} + \frac{\hat{f}_{z_k}(u)}{2}\right)^2 \\
&= E_z\left[\frac{1}{N}\sum_{k=1}^{N}\cos^2(z_k\beta u)\right] + (N-1)\left(\frac{\hat{f}_{z_k}(-u)}{2} + \frac{\hat{f}_{z_k}(u)}{2}\right)^2 \\
&\quad -N\left(\frac{\hat{f}_{z_k}(-u)}{2} + \frac{\hat{f}_{z_k}(u)}{2}\right)^2 \\
&= E_z\left[\cos^2(z\beta u)\right] - \left(\frac{\hat{f}_{z_k}(-u)}{2} + \frac{\hat{f}_{z_k}(u)}{2}\right)^2 \\
&= \int_{L_{\min}}^{L_{\max}} f_{z_k}(z)\cos^2(z\beta u)dz - \left(\frac{\hat{f}_{z_k}(-u)}{2} + \frac{\hat{f}_{z_k}(u)}{2}\right)^2 \\
&= \int_{L_{\min}}^{L_{\max}} f_{z_k}(z)\left(\frac{1}{2} + \frac{\cos(2z\beta u)}{2}\right)dz - \left(\frac{\hat{f}_{z_k}(-u)}{2} + \frac{\hat{f}_{z_k}(u)}{2}\right)^2 \\
&= \int_{L_{\min}}^{L_{\max}} f_{z_k}(z)\frac{1}{2}dz + \int_{L_{\min}}^{L_{\max}} f_{z_k}(z)\frac{\cos(2z\beta u)}{2}dz - \left(\frac{\hat{f}_{z_k}(-u)}{2} + \frac{\hat{f}_{z_k}(u)}{2}\right)^2 \\
&= \frac{1}{2} + \int_{L_{\min}}^{L_{\max}} f_{z_k}(z)\frac{e^{j2z\beta u} + e^{-j2z\beta u}}{4}dz - \left(\frac{\hat{f}_{z_k}(-u)}{2} + \frac{\hat{f}_{z_k}(u)}{2}\right)^2 \\
&= \frac{1}{2} + \int_{L_{\min}}^{L_{\max}} f_{z_k}(z)\frac{e^{j2z\beta u}}{4}dz + \int_{L_{\min}}^{L_{\max}} f_{z_k}(z)\frac{e^{-j2z\beta u}}{4}dz \\
&\quad -\left(\frac{\hat{f}_{z_k}(-u)}{2} + \frac{\hat{f}_{z_k}(u)}{2}\right)^2 \\
&= \frac{1}{2} + \frac{\hat{f}_{z_k}(-2u)}{4} + \frac{\hat{f}_{z_k}(2u)}{4} - \left(\frac{\hat{f}_{z_k}(-u)}{2} + \frac{\hat{f}_{z_k}(u)}{2}\right)^2. \qquad (4.3)
\end{aligned}
$$

Continuing from Eq. (4.3),

$$\begin{aligned} VAR(X(u,\mathbf{z})) &= \frac{1}{2}+\frac{1}{2}\left(\frac{\hat{f}_{z_k}(-2u)}{2}+\frac{\hat{f}_{z_k}(2u)}{2}\right)-\left(\frac{\hat{f}_{z_k}(-u)}{2}+\frac{\hat{f}_{z_k}(u)}{2}\right)^2 \\ &= \frac{1}{2}+\frac{1}{2\sqrt{N}}\left(m_{X,z}(2u)\right)-\frac{m_{X_z}^2(u)}{N}. \end{aligned} \tag{4.4}$$

For $Y(u,\mathbf{z})$, the expected value over $\mathbf{z}$ is

$$\begin{aligned} E_{\mathbf{z}}[Y(u,\mathbf{z})] &\equiv m_{Y,z}(u) \\ &= E_z\left[\frac{1}{\sqrt{N}}\sum_{k=1}^{N}\sin(z_k\beta u)\right] \\ &= \sqrt{N}E_z\left[\sin(z\beta u)\right] \\ &= \sqrt{N}\int_{L_{\min}}^{L_{\max}} f_{z_k}(z)\sin(z\beta u)dz \\ &= \sqrt{N}\int_{L_{\min}}^{L_{\max}} f_{z_k}(z)\left(\frac{e^{jz\beta u}-e^{-jz\beta u}}{j2}\right)dz \\ &= \sqrt{N}\left(\int_{L_{\min}}^{L_{\max}} f_{z_k}(z)\frac{e^{jz\beta u}}{j2}dz-\int_{L_{\min}}^{L_{\max}} f_{z_k}(z)\frac{e^{-jz\beta u}}{j2}dz\right) \\ &= \sqrt{N}\left(\frac{\hat{f}_{z_k}(-u)-\hat{f}_{z_k}(u)}{j2}\right). \end{aligned} \tag{4.5}$$

Its variance over $\mathbf{z}$ is

$$
\begin{aligned}
VAR(Y(u,\mathbf{z})) &\equiv \sigma^2_{Y,z}(u) \\
&= E_z\left[Y^2(u,\mathbf{z}\right] - m^2_{Y,z}(u) \\
&= E_z\left[\frac{1}{N}\sum_{k=1}^{N}\sin^2(z_k\beta u) + \frac{1}{N}\sum_{k=1}^{N}\sin(z_k\beta u)\sum_{\substack{l=1\\ l\neq k}}^{N}\sin(z_l\beta u)\right] \\
&\quad -N\left(\frac{\hat{f}_{z_k}(-u)}{j2} - \frac{\hat{f}_{z_k}(u)}{j2}\right)^2 \\
&= E_z\left[\frac{1}{N}\sum_{k=1}^{N}\sin^2(z_k\beta u)\right] + (N-1)\left(\frac{\hat{f}_{z_k}(-u)}{j2} - \frac{\hat{f}_{z_k}(u)}{j2}\right)^2 \\
&\quad -N\left(\frac{\hat{f}_{z_k}(-u)}{j2} - \frac{\hat{f}_{z_k}(u)}{j2}\right)^2 \\
&= E_z\left[\sin^2(z\beta u)\right] - \left(\frac{\hat{f}_{z_k}(-u)}{j2} - \frac{\hat{f}_{z_k}(u)}{j2}\right)^2 \\
&= \int_{L_{\min}}^{L_{\max}} f_{z_k}(z)\sin^2(z\beta u)dz - \left(\frac{\hat{f}_{z_k}(-u)}{j2} - \frac{\hat{f}_{z_k}(u)}{j2}\right)^2 \\
&= \int_{L_{\min}}^{L_{\max}} f_{z_k}(z)\left(\frac{1}{2} - \frac{\cos(2z\beta u)}{2}\right)dz - \left(\frac{\hat{f}_{z_k}(-u)}{j2} - \frac{\hat{f}_{z_k}(u)}{j2}\right)^2 \\
&= \int_{L_{\min}}^{L_{\max}} f_{z_k}(z)\frac{1}{2}dz - \int_{L_{\min}}^{L_{\max}} f_{z_k}(z)\frac{\cos(2z\beta u)}{2}dz - \left(\frac{\hat{f}_{z_k}(-u)}{j2} - \frac{\hat{f}_{z_k}(u)}{j2}\right)^2 \\
&= \frac{1}{2} - \int_{L_{\min}}^{L_{\max}} f_{z_k}(z)\frac{e^{j2z\beta u} + e^{-j2z\beta u}}{4}dz - \left(\frac{\hat{f}_{z_k}(-u)}{j2} - \frac{\hat{f}_{z_k}(u)}{j2}\right)^2 \\
&= \frac{1}{2} - \int_{L_{\min}}^{L_{\max}} f_{z_k}(z)\frac{e^{j2z\beta u}}{4}dz - \int_{L_{\min}}^{L_{\max}} f_{z_k}(z)\frac{e^{-j2z\beta u}}{4}dz \\
&\quad - \left(\frac{\hat{f}_{z_k}(-u)}{j2} - \frac{\hat{f}_{z_k}(u)}{j2}\right)^2 \\
&= \frac{1}{2} - \left(\frac{\hat{f_{z_k}}(-2\beta u)}{4} + \frac{\hat{f_{z_k}}(2\beta u)}{4}\right) - \left(\frac{\hat{f}_{z_k}(-u)}{j2} - \frac{\hat{f}_{z_k}(u)}{j2}\right)^2. \qquad (4.6)
\end{aligned}
$$

Continuing from Eq. (4.6),

$$\begin{aligned} VAR(Y(u,\mathbf{z})) &= \frac{1}{2} - \frac{1}{2}\left(\frac{\hat{f_{z_k}}(-2\beta u)}{2} + \frac{\hat{f_{z_k}}(2\beta u)}{2}\right) - \left(\frac{\hat{f}_{z_k}(-u)}{j2} - \frac{\hat{f}_{z_k}(u)}{j2}\right)^2 \\ &= \frac{1}{2} - \frac{1}{2\sqrt{N}}\left(m_{X,z}(2u)\right) - \frac{m_{Y,z}^2(u)}{N}. \end{aligned} \tag{4.7}$$

The covariance between $X(u,\mathbf{z})$ and $Y(u,\mathbf{z})$ is

$$\begin{aligned} COV(X(u,\mathbf{z}),Y(u,\mathbf{z})) &\equiv \sigma_{XY,z}(u) \\ &= E_{\mathbf{z}}[X(u,\mathbf{z})Y(u,\mathbf{z})] - E_{\mathbf{z}}[X(u,\mathbf{z})]E_{\mathbf{z}}[Y(u,\mathbf{z})] \\ &= E_{\mathbf{z}}\left[\frac{1}{\sqrt{N}}\sum_{k=1}^{N}\cos\left(z_k\beta u_1\right)\frac{1}{\sqrt{N}}\sum_{l=1}^{N}\sin\left(z_l\beta u_1\right)\right] \\ &\quad -E_{\mathbf{z}}\left[\frac{1}{\sqrt{N}}\sum_{k=1}^{N}\cos\left(z_k\beta u_1\right)\right]E_{\mathbf{z}}\left[\frac{1}{\sqrt{N}}\sum_{l=1}^{N}\sin\left(z_l\beta u_1\right)\right] \\ &= \frac{1}{N}\sum_{k=1}^{N}E_{z_k}\left[\cos\left(z_k\beta u_1\right)\sin\left(z_k\beta u_1\right)\right] \\ &\quad +\frac{1}{N}\sum_{k=1}^{N}E_{z_k}\left[\cos\left(z_k\beta u_1\right)\right]\sum_{\substack{l=1\\l\neq i}}^{N}E_{z_k}\left[\sin\left(z_l\beta u_1\right)\right] \\ &\quad -\frac{1}{N}\sum_{k=1}^{N}E_{z_k}\left[\cos\left(z_k\beta u_1\right)\right]\sum_{l=1}^{N}E_{z_k}\left[\sin\left(z_l\beta u_1\right)\right] \\ &= E_{z_k}\left[\cos\left(z_k\beta u_1\right)\sin\left(z_k\beta u_1\right)\right] \\ &\quad +(N-1)E_{z_k}\left[\cos\left(z_k\beta u_1\right)\right]E_{z_k}\left[\sin\left(z_l\beta u_1\right)\right] \\ &\quad -NE_{z_k}\left[\cos\left(z_k\beta u_1\right)\right]E_{z_k}\left[\sin\left(z_l\beta u_1\right)\right] \\ &= E_{z_k}\left[\cos\left(z_k\beta u_1\right)\sin\left(z_k\beta u_1\right)\right] - E_{z_k}\left[\cos\left(z_k\beta u_1\right)\right]E_{z_k}\left[\sin\left(z_l\beta u_1\right)\right] \\ &= \frac{1}{2}E_{z_k}\left[\sin\left(z_k 2\beta u_1\right)\right] \\ &\quad -E_{z_k}\left[\cos\left(z_k\beta u_1\right)\right]E_{z_k}\left[\sin\left(z_l\beta u_1\right)\right] \end{aligned} \tag{4.8}$$

If antenna position pdf, $f_{z_k}(z)$ is an even function, or is symmetric about $z = 0$, then

$$\sigma_{XY,z}(u) = 0 \tag{4.9}$$

and

$$m_{Y,z}(u) = 0$$

since $f_{z_k}(z)\sin(z_k\beta u)$ is integrated, and the integral of an even function times an odd function is zero. If $\sigma_{XY,z}$ is zero, $X(u, \mathbf{z})$ and $Y(u, \mathbf{z})$ are uncorrelated, and if they are assumed to be approximately Gaussian, they are approximately independent.

The autocovariance between $X(u_1, \mathbf{z})$ and $X(u_2, \mathbf{z})$ where $u = u_1$ and $u = u_2$ are locations

of two different samples of the beampattern is

$$
\begin{aligned}
COV(X(u_1,\mathbf{z}),X(u_2,\mathbf{z})) &= E_{\mathbf{z}}[X(u_1,\mathbf{z})X(u_2,\mathbf{z})] - E_{\mathbf{z}}[X(u_1,\mathbf{z})]E_{\mathbf{z}}[X(u_2,\mathbf{z})] \\
&= E_{\mathbf{z}}\left[\frac{1}{\sqrt{N}}\sum_{k=1}^{N}\cos\left(z_k\beta u_1\right)\frac{1}{\sqrt{N}}\sum_{l=1}^{N}\cos\left(z_l\beta u_2\right)\right] \\
&\quad -E_{\mathbf{z}}\left[\frac{1}{\sqrt{N}}\sum_{k=1}^{N}\cos\left(z_k\beta u_1\right)\right]E_{\mathbf{z}}\left[\frac{1}{\sqrt{N}}\sum_{l=1}^{N}\cos\left(z_l\beta u_2\right)\right] \\
&= \frac{1}{N}\sum_{k=1}^{N}E_{z_k}\left[\cos\left(z_k\beta u_1\right)\cos\left(z_k\beta u_2\right)\right] \\
&\quad +\frac{1}{N}\sum_{k=1}^{N}E_{z_k}\left[\cos\left(z_k\beta u_1\right)\right]\sum_{\substack{l=1\\l\neq i}}^{N}E_{z_k}\left[\cos\left(z_l\beta u_2\right)\right] \\
&\quad -\frac{1}{N}\sum_{k=1}^{N}E_{z_k}\left[\cos\left(z_k\beta u_1\right)\right]\sum_{l=1}^{N}E_{z_k}\left[\cos\left(z_l\beta u_2\right)\right] \\
&= E_{z_k}\left[\cos\left(z_k\beta u_1\right)\cos\left(z_k\beta u_2\right)\right] \\
&\quad +(N-1)E_{z_k}\left[\cos\left(z_k\beta u_1\right)\right]E_{z_k}\left[\cos\left(z_l\beta u_2\right)\right] \\
&\quad -NE_{z_k}\left[\cos\left(z_k\beta u_1\right)\right]E_{z_k}\left[\cos\left(z_l\beta u_2\right)\right] \\
&= E_{z_k}\left[\cos\left(z_k\beta u_1\right)\cos\left(z_k\beta u_2\right)\right] - E_{z_k}\left[\cos\left(z_k\beta u_1\right)\right]E_{z_k}\left[\cos\left(z_l\beta u_2\right)\right] \\
&= \frac{1}{2}E_{z_k}\left[\cos\left(z_k\beta(u_1-u_2)\right)+\cos\left(z_k\beta(u_1+u_2)\right)\right] \\
&\quad -E_{z_k}\left[\cos\left(z_k\beta u_1\right)\right]E_{z_k}\left[\cos\left(z_l\beta u_2\right)\right] \qquad (4.10)
\end{aligned}
$$

The autocovariance between $Y(u_1, \mathbf{z})$ and $Y(u_2, \mathbf{z})$

$$\begin{aligned}
COV(Y(u_1,\mathbf{z}),Y(u_2,\mathbf{z})) &= E_{\mathbf{z}}[Y(u_1,\mathbf{z})Y(u_2,\mathbf{z})] - E_{\mathbf{z}}[Y(u_1,\mathbf{z})]E_{\mathbf{z}}[Y(u_2,\mathbf{z})] \\
&= E_{\mathbf{z}}\left[\frac{1}{\sqrt{N}}\sum_{k=1}^{N}\sin(z_k\beta u_1)\frac{1}{\sqrt{N}}\sum_{l=1}^{N}\sin(z_l\beta u_2)\right] \\
&\quad -E_{\mathbf{z}}\left[\frac{1}{\sqrt{N}}\sum_{k=1}^{N}\sin(z_k\beta u_1)\right]E_{\mathbf{z}}\left[\frac{1}{\sqrt{N}}\sum_{l=1}^{N}\sin(z_l\beta u_2)\right] \\
&= \frac{1}{N}\sum_{k=1}^{N}E_{z_k}[\sin(z_k\beta u_1)\sin(z_k\beta u_2)] \\
&\quad +\frac{1}{N}\sum_{k=1}^{N}E_{z_k}[\sin(z_k\beta u_1)]\sum_{\substack{l=1\\l\neq i}}^{N}E_{z_k}[\sin(z_l\beta u_2)] \\
&\quad -\frac{1}{N}\sum_{k=1}^{N}E_{z_k}[\sin(z_k\beta u_1)]\sum_{l=1}^{N}E_{z_k}[\sin(z_l\beta u_2)] \\
&= E_{z_k}[\sin(z_k\beta u_1)\sin(z_k\beta u_2)] \\
&\quad +(N-1)E_{z_k}[\sin(z_k\beta u_1)]E_{z_k}[\sin(z_l\beta u_2)] \\
&\quad -NE_{z_k}[\sin(z_k\beta u_1)]E_{z_k}[\sin(z_l\beta u_2)] \\
&= E_{z_k}[\sin(z_k\beta u_1)\sin(z_k\beta u_2)] - E_{z_k}[\sin(z_k\beta u_1)]E_{z_k}[\sin(z_l\beta u_2)] \\
&= \frac{1}{2}E_{z_k}[\cos(z_k\beta(u_1-u_2)) - \cos(z_k\beta(u_1+u_2))] \\
&\quad -E_{z_k}[\sin(z_k\beta u_1)]E_{z_k}[\sin(z_l\beta u_2)] \qquad (4.11)
\end{aligned}$$

4.3 Peak Sidelobe Distribution, Sample Method

Letting

$$L_{\max} = -L_{\min} = \frac{L}{2}$$

so that

$$L = L_{\max} - L_{\min},$$

Ref. [17] calculates the probability that $2L$ equally spaced samples of the beampattern are less than some threshold to calculate the peak sidelobe level distribution. In this method, only adjacent points in the beampattern are assumed to be correlated. $2L$ samples are considered because the beampattern can be thought of as a signal that is bandlimited to $[0, L]$. Since $\mathbf{z} \in [-L/2, L/2]^N$, the beampattern, $P(u, \mathbf{z})$, is like a signal having frequency components in $[-L, L]$. The sampling interval will need to $1/(2L)$. With with sidelobe region beginning at $u = u_s$ and the length of the sidelobe region being $\mu(\mathcal{S}_{nr})$, the number of samples taken in the sidelobe region will be $\lceil \mu(\mathcal{S}_{nr})2L \rceil$, where $\lceil \ldots \rceil$ indicates the ceiling operation.

Letting $P(u_1, \mathbf{z})$ and $P(u_2, \mathbf{z})$ be two sampled points of the beampattern at u_1 and u_2 such that $|u_1 - u_2| = 1/(2L)$, Ref. [17] gives the peak sidelobe level distribution as

$$\begin{aligned} \Pr(P(u, \mathbf{z}) < P_0 \forall u \in \mathcal{S}) &\approx \Pr[P(u_1, \mathbf{z}) \leq P_0] \\ &\quad \cdot \left[\frac{\Pr[P(u_1, \mathbf{z}) \leq P_0, P(u_2, \mathbf{z}) \leq P_0]}{\Pr[P(u_1, \mathbf{z})| \leq P_0]} \right]^{\lceil \mu(\mathcal{S}_{nr})2L \rceil - 1} \\ &\approx \left[\frac{\Pr[P(u_1, \mathbf{z}) \leq P_0, P(u_2, \mathbf{z}) \leq P_0]^{\lceil \mu(\mathcal{S}_{nr})2L \rceil - 1}}{\Pr[P(u_1, \mathbf{z})| \leq P_0]^{\lceil \mu(\mathcal{S}_{nr})2L \rceil - 2}} \right] \end{aligned} \tag{4.12}$$

The sample method used by Ref. [17] to find the sidelobe level distributions assumes the quadrature components of the array factor have zero mean and variance $1/2$ in the sidelobe region. Looking at the means and variances of $X(u, \mathbf{z})$ and $Y(u, \mathbf{z})$ in Eqs. (4.2), (4.4), (4.5), and (4.7), the means can be zero and the variances can be $1/2$ if

$$\sqrt{N} \cdot \hat{f}_{z_k}(u) = 0 \, \forall u \in \mathcal{S}.$$

With the assumption that $X(u, \mathbf{z})$ and $Y(u, \mathbf{z})$ are uncorrelated, approximately Gaussian, and using Eq. (2.9), the distribution of $X^2(u, \mathbf{z}) + Y^2(u, \mathbf{z})$ is approximately Rayleigh and is given by

$$\Pr(\sqrt{X^2(u, \mathbf{z}) + Y^2(u, \mathbf{z})} \leq \sqrt{NP_0}) \approx 1 - e^{-NP_0}$$

and

$$\begin{aligned}\Pr[P(u,\mathbf{z}) \leq P_0] &= \Pr(\sqrt{X^2(u,\mathbf{z}) + Y^2(u,\mathbf{z})} \leq \sqrt{NP_0}) \\ &\approx 1 - e^{-NP_0}. \end{aligned} \tag{4.13}$$

The peak sidelobe level distribution is now given by

$$\begin{aligned}&\Pr(P(u,\mathbf{z}) > P_0 \forall u \in \mathcal{S}) \approx 1 \\ &- \frac{[1 - e^{-NP_0}[1 - Q(\rho b, b) + Q(b, \rho b)]]^{\lceil \mu(\mathcal{S}_{\rm nr})2{\rm L} \rceil - 1}}{[1 - \exp(-NP_0)]^{\lceil \mu(\mathcal{S}_{\rm nr})2{\rm L} \rceil - 2}},\end{aligned} \tag{4.14}$$

where $\lceil \ldots \rceil$ indicates the ceiling operation, ρ is the correlation between adjacent points of the beampattern

$$b = \sqrt{\frac{2N}{1-\rho^2} P_0} \tag{4.15}$$

and

$$Q(x,y) = \int_y^\infty \exp\left(-\frac{x^2+t^2}{2}\right) I_0(xt) t \, dt. \tag{4.16}$$

$I_0(xt)$ is the zeroth order modified bessel function of the first kind. Ref. [17] gives ρ as

$$\rho = |Corr[F(u_1,\mathbf{z}), F^*(u_2,\mathbf{z})]| \tag{4.17}$$

where $F(u,\mathbf{z})$ is the array factor in Eq. (2.6). Letting $X(u,\mathbf{z}) \equiv X(u)$ and $Y(u,\mathbf{z}) \equiv Y(u)$,

the autocovariance of $F(u_1, \mathbf{z})$ and $F(u_2, \mathbf{z})$ is

$$\begin{aligned}
COV[F(u_1,\mathbf{z}), F^*(u_2,\mathbf{z})] &= E_{\mathbf{z}}[F(u_1,\mathbf{z})F^*(u_2,\mathbf{z})] - E_{\mathbf{z}}[F(u_1,\mathbf{z})]E_{\mathbf{z}}[F^*(u_2,\mathbf{z})] \\
&= \frac{1}{N}E_z[(X(u_1)+jY(u_1))(X(u_2)-jY(u_2))] \\
&\quad -\frac{1}{N}E_z[X(u_1)+jY(u_1)]E_z[X(u_2)-jY(u_2)] \\
&= \frac{1}{N}\,[E_z[X(u_1)X(u_2)] + jE_z[X(u_2)]E_z[Y(u_1)] \\
&\quad -jE_z[X(u_1)]E_z[Y(u_2)] + E_z[Y(u_1)Y(u_2)] \\
&\quad +jE_z[X(u_1)]E_z[Y(u_2)] - E_z[X(u_1)]E_z[X(u_2)] \\
&\quad -jE_z[Y(u_1)]E_z[X(u_2)] - E_z[Y(u_1)]E_z[Y(u_2)]] \\
&= \frac{1}{N}[E_z[X(u_1)X(u_2)] - E_z[X(u_1)]E_z[X(u_2)] \\
&\quad +E_z[Y(u_1)Y(u_2)] - E_z[Y(u_1)]E_z[Y(u_2)]] \\
&= \frac{1}{N}[COV[X(u_1),X(u_2)] + COV[Y(u_1),Y(u_2)]] \qquad (4.18)
\end{aligned}$$

Since $COV[F(u,\mathbf{z}), F^*(u,\mathbf{z})] = VAR[F(u,\mathbf{z})]$ where $VAR(X)$ is variance of X, we have

$$VAR[F(u,\mathbf{z})] = \frac{1}{N}[VAR[X(u)] + VAR[Y(u)]].$$

Using $VAR[X(u)] = VAR[Y(u)] = 1/2$, the correlation of $F(u_1,\mathbf{z})$ and $F(u_2,\mathbf{z})$ is given by

$$\begin{aligned}
Corr[F(u_1,\mathbf{z}), F^*(u_2,\mathbf{z})] &= \frac{COV[F(u_1,\mathbf{z}), F^*(u_2,\mathbf{z})]}{\sqrt{VAR[F(u_1,\mathbf{z})]}\sqrt{VAR[F(u_2,\mathbf{z})]}} \\
&= \frac{\frac{1}{N}[COV[X(u_1),X(u_2)] + COV[Y(u_1),Y(u_2)]]}{\frac{1}{N}\sqrt{VAR[X(u_1)] + VAR[Y(u_1)]}\sqrt{VAR[X(u_2)] + VAR[Y(u_2)]}} \\
&\approx COV[X(u_1),X(u_2)] + COV[Y(u_1),Y(u_2)]. \qquad (4.19)
\end{aligned}$$

$COV[X(u_1),X(u_2)]$ and $COV[Y(u_1),Y(u_2)]$ are given by Eqs. (4.10) and (4.11), respectively.

Sampling the beampattern to calculate the sidelobe level distribution fits closely to experimental observations as mentioned in Ref. [41] for large arrays, but it is not clear that having a sampling interval of $1/(2L)$ is sufficient. Ref. [10] gave some correction to this

approach by calculating the average difference between the largest of a set of samples and the approximate height of the lobe from which the sample is taken. Nevertheless, the Gaussian approximations and the $1/(2L)$ sampling interval introduce errors in the computations. Also, it is not clear what the sampling interval should be when the antenna positions are not bounded such as with a Gaussian positions distribution.

4.4 Peak Sidelobe Distribution, Upward-Crossing Method

4.4.1 Introduction of Upward-Crossing Method

Let there be some function $y(a_1, a_2, \ldots, a_n, x)$ where $a_1, a_2, \ldots, a_n$ are random variables with known distributions, and x is a deterministic variable. Let

$$\frac{dy(a_1, a_2, \ldots, a_n, x)}{dx} = y'(a_1, a_2, \ldots, a_n, x).$$

Let $\rho(y, y'; x)$ be the joint distribution of $y(a_1, a_2, \ldots, a_n, x)$ and $y'(a_1, a_2, \ldots, a_n, x)$. If $\rho(y, y'; x)$ is continuous for all y and y', and the integral

$$\int_0^\infty \rho(a\eta, \eta; x_1) d\eta$$

converges uniformly with respect to a in some interval $-a_1 \leq a \leq a_2$ where a_1 and a_2 are positive, then Ref. [42] gives the probability that $y(a_1, a_2, \ldots, a_n, x)$ will pass through zero in some interval $[x_1, x_1 + dx]$ with positive slope as

$$dx \int_0^\infty \eta\rho(0, \eta; x_1) d\eta. \tag{4.20}$$

Eq. (4.20) can be modified so that $y(a_1, a_2, \ldots, a_n, x)$ passes through some threshold y_0 with positive slope as

$$dx \int_0^\infty \eta\rho(y_0, \eta; x_1) d\eta.$$

The probability of passing through a positive slope, which can be called an upcrossing or upward-crossing, can be used to determine the probability that the maximum of a random function is greater or less than some threshold y_0. The maximum of $y(a_1, a_2, \ldots, a_n, x)$ must occur at some $x_{\max}$ such that $x_{\max} > x_0$ where $y(x_0) = y_0$ so that x_0 is the point of upcrossing of threshold y_0.

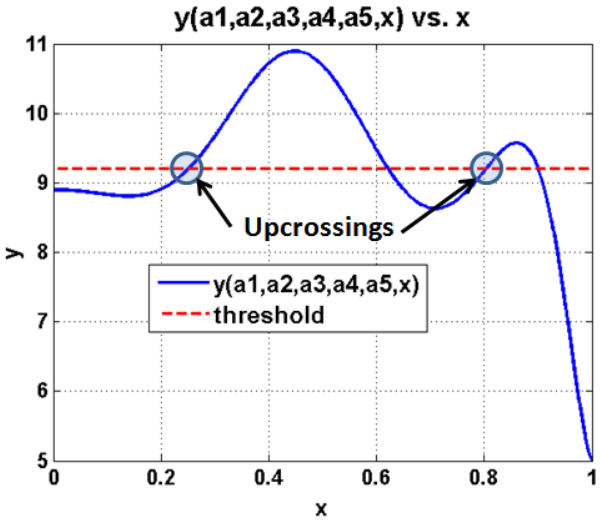

Figure 4.1: *Upcrossings of* $y(a_1, a_2, \ldots, a_5, x)$

If $\nu(y_0)$ is the number of times $y(a_1, a_2, \ldots, a_n, x)$ upward crosses y_0 over the interval $[x_a, x_b]$ where $x_a \leq x \leq x_b$, then,

$$\nu(y_0)dx = dx \int_0^\infty \eta\rho(y_0, \eta; x_1)d\eta$$

and

$$E[\nu(y_0)] = \int_{x_a}^{x_b} \nu(y_0)dx = \int_{x_a}^{x_b} dx_1 \int_0^\infty \eta\rho(y_0, \eta; x_1)d\eta. \tag{4.21}$$

By the Law of Large Numbers, Eq. (4.21) is the average number of upcrossings in the interval $[x_a, x_b]$. These results for upcrossings can be applied to determine the probability of the maximum of the beampattern exceeding some threshold.

Both Refs. [14] and [43] state that the number of exceedances or upcrossings can be

regarded as a point process. The points along the beampattern at which upcrossings occur are assumed to occur randomly and independently. With this assumption, let there be m different beampatterns, each formed by N iid distributed elements. Similarly to the approach in Ref. [18], divide each beampattern over angle into n equally spaced intervals. Choose n so that every interval in each of the m beampatterns has at most one upward crossing of some level P_0. The value n becomes the total number of upward crossings possible in each beampattern. Let $\nu_j(P_0))$ be the number of upward crossings in the sidelobe region of beampattern j of m beampatterns ($j = 1, 2, \ldots, m$). The probability that any interval in any of the m beampatterns has an upward crossing is given by

$$\frac{\sum_{j=1}^{m} \nu_j(P_0)}{mn}.$$

By the laws of large numbers

$$\lim_{m\to\infty} \frac{\sum_{j=1}^{m} \nu_j(P_0)}{mn} = \frac{E[\nu(P_0)]}{n}.$$

$E[\nu(P_0)]$ is the expected number of upward crossings. The probability that there are no upward crossings in the sidelobe region is given by

$$\prod_{i=1}^{n} \left(1 - \frac{E[\nu(P_0)]}{n}\right).$$

Increasing the number of bins gives $e^{-E[\nu(P_0)]}$. It can now be claimed that $e^{-E[\nu(P_0)]}$ is the probability that $\nu(P_0) = 0$ or the probability that there are no upcrossings of level P_0 by the beampattern. $\nu(P_0)$ is a Poisson distributed random variable with pmf

$$\Pr(\nu(P_0) = k) = \frac{E[\nu(P_0)]^k e^{-E[\nu(P_0)]}}{k!}. \tag{4.22}$$

4.4.2 Applying Method of Upward-Crossings to Beampattern

Using the upward-crossing method, the general complementary cumulative distribution function (CCDF) for the peak sidelobe level distribution is

$$\begin{aligned} &\Pr\{P(u|\mathbf{z}) \geq P_0 \,\forall\, u \in \mathcal{S}\} \\ &\approx 1 - \Pr\left\{P(|u| = u_s|, \mathbf{z}) \leq P_0\right\} e^{-E[\nu(P_0)]}, \end{aligned} \tag{4.23}$$

where $\nu(P_0)$ is the number of times the beampattern crosses the level P_0 in an upward direction in the sidelobe region. $E[\nu(P_0)]$ is the expected number of upward-crossings. Previous researchers implied Eq. (4.23) but did not explicitly state it [19][18]. The term $\Pr\left\{P(|u| = u_s|\mathbf{z}) \leq \mathrm{P}_0\right\}$ in Eq. (4.23) is the probability of the beampattern initially being below P_0. The term $e^{-E[\nu(P_0)]}$ is the probability that the Poisson distributed random variable $\nu(P_0)$ is zero. However, the points of upward-crossing have some correlation, and the Poisson distribution model is approximate. Since calculations closely match simulated experiments in Refs. [19] and [18], Eq. (4.23) will be accepted as the general equation for the peak sidelobe level CCDF.[3]

If the mean and variance of the array factor quadrature components, $X(u)$ and $Y(u)$, change considerably with angle in the sidelobe region, Eq. (4.23) must be evaluated using numerical methods as done in Refs. [11] and [39]. Since $X(u)$, $Y(u)$, and their derivatives are regarded as having approximately Gaussian distributions by the Central Limit Theorem, only their means, variances, and covariances were needed to calculate the peak sidelobe level distributions in Ref. [39].[4]

If the statistics can also be regarded as angle-independent, the peak sidelobe level distribution can be written in closed form. This paper contributes to the closed form

[3] [1] ©2011 IEEE

[4] [1] ©2011 IEEE

expression through the following discussion by stating it in terms of the antenna element position variance.[5]

As given in Eqs. (4.2) and (4.5), the means of $X(u, \mathbf{z})$ and $Y(u, \mathbf{z})$ over the element locations $\mathbf{z}$, $m_{X,z}(u)$ and $m_{Y,z}(u)$, respectively, are

$$m_{X,z}(u) = \sqrt{N}\left(\frac{\hat{f}_{z_k}(-u) + \hat{f}_{z_k}(u)}{2}\right) \tag{4.24}$$

$$m_{Y,z}(u) = \sqrt{N}\left(\frac{\hat{f}_{z_k}(-u) - \hat{f}_{z_k}(u)}{j2}\right). \tag{4.25}$$

The variances of $X(u, \mathbf{z})$ and $Y(u, \mathbf{z})$ over $\mathbf{z}$, $\sigma^2_{X,z}(u)$ and $\sigma^2_{Y,z}(u)$, respectively, as given by Eqs. (4.4) and (4.7) are

$$\sigma^2_{X,z}(u) = \frac{1}{2} + \frac{1}{2\sqrt{N}}\left(m_{X,z}(2u)\right) - \frac{m^2_{X_z}(u)}{N} \tag{4.26}$$

$$\sigma^2_{Y,z}(u) = \frac{1}{2} - \frac{1}{2\sqrt{N}}\left(m_{X,z}(2u)\right) - \frac{m^2_{Y,z}(u)}{N}. \tag{4.27}$$

As in the sampling beampattern case, if

$$\sqrt{N} \cdot \hat{f}_{z_k}(u) \approx 0 \, \forall u \in \mathcal{S}, \tag{4.28}$$

then,

$$\left.\begin{matrix} m_{X,z}(u) \\ m_{Y,z}(u) \end{matrix}\right\} \approx 0 \, \forall u \in \mathcal{S}$$

$$\left.\begin{matrix} \sigma^2_{X,z}(u) \\ \sigma^2_{Y,z}(u) \end{matrix}\right\} \approx \frac{1}{2} \, \forall u \in \mathcal{S}. \tag{4.29}$$

We continue with the assumption that $X(u, \mathbf{z})$ and $Y(u, \mathbf{z})$ are uncorrelated and approximately Gaussian. Now, the beampattern level at angle u_s is approximately Rayleigh distributed

[5] [1] ©2011 IEEE

giving

$$\Pr\{P(u_s, \mathbf{z}) \leq P_0\} \approx (1 - e^{-NP_0}). \tag{4.30}$$

We introduce the derivatives of the quadrature components with respect to u as

$$X'(u, \mathbf{z}) = -\frac{1}{\sqrt{N}} \sum_{k=1}^{N} z_k \beta \sin(z_k \beta u) \tag{4.31}$$

$$Y'(u, \mathbf{z}) = \frac{1}{\sqrt{N}} \sum_{k=1}^{N} z_k \beta \cos(z_k \beta u). \tag{4.32}$$

These quadrature component derivatives are also considered approximately Gaussian for large N by the Central Limit Theorem.

Let $\hat{f}'_{z_k}(u)$ be the first derivative with respect to u of the characteristic function in Eq. (4.1) so that

$$\begin{aligned}
\hat{f}'_{z_k}(u) &= \frac{d}{du}\hat{f}_{z_k}(u) \\
&= \frac{d}{du}\int_{B_0}^{B_1} f_{z_k}(z) e^{-j\beta z u} dz \\
&= \int_{B_0}^{B_1} f_{z_k}(z) \frac{d}{du} e^{-j\beta z u} dz \\
&= -\int_{B_0}^{B_1} j\beta z f_{z_k}(z) e^{-j\beta z u} dz.
\end{aligned}$$

The means of $X'(u,\mathbf{z})$ and $Y'(u,\mathbf{z})$ over $\mathbf{z}$, $m_{X',z}(u)$ and $m_{Y',z}(u)$, respectively, are

$$\begin{aligned}
m_{X',z}(u) &= E_{\mathbf{z}}\left[-\frac{1}{\sqrt{N}}\sum_{k=1}^{N}\beta z_k \sin(z_k\beta u)\right] \\
&= -\sqrt{N}\beta E_{z_k}\left[z_k \sin(z_k\beta u)\right] \\
&= -\sqrt{N}\beta \int_{B_0}^{B_1} f_{z_k}(z) z \sin(z\beta u) dz \\
&= -\sqrt{N}\beta \int_{B_0}^{B_1} f_{z_k}(z) z \left(\frac{e^{jz\beta u} - e^{-jz\beta u}}{j2}\right) dz \\
&= -\sqrt{N}\left(-j\int_{B_0}^{B_1} f_{z_k}(z)\beta z \frac{e^{jz\beta u}}{2} - \int_{B_0}^{B_1} f_{z_k}(z)\beta z \frac{e^{-jz\beta u}}{j2}\right) dz \\
&= -\sqrt{N}\left(\frac{\hat{f}'_{z_k}(-u) - \hat{f}'_{z_k}(u)}{2}\right) \qquad (4.33)
\end{aligned}$$

and

$$\begin{aligned}
m_{Y',z}(u) &= E_z\left[\frac{1}{\sqrt{N}}\sum_{k=1}^{N}\beta z_k \cos(z_k\beta u)\right] \\
&= \sqrt{N}\beta E_z\left[z\cos(z\beta u)\right] \\
&= \sqrt{N}\beta \int_{B_0}^{B_1} f_{z_k}(z) z \cos(z\beta u) dz \\
&= \sqrt{N}\beta \int_{B_0}^{B_1} f_{z_k}(z) z \left(\frac{e^{jz\beta u} + e^{-jz\beta u}}{2}\right) dz \\
&= \sqrt{N}\left(j\int_{B_0}^{B_1} f_{z_k}(z)\beta z \frac{e^{jz\beta u}}{j2} dz + j\int_{B_0}^{B_1} f_{z_k}(z)\beta z \frac{e^{-jz\beta u}}{2j}\right) dz \\
&= -\sqrt{N}\left(\frac{\hat{f}'_{z_k}(-u) + \hat{f}'_{z_k}(u)}{2j}\right). \qquad (4.34)
\end{aligned}$$

The covariance over $\mathbf{z}$ of $X(u,\mathbf{z})$ and $X'(u,\mathbf{z})$, $\sigma_{X,X',z}(u)$, and of $Y(u)$ and $Y'(u)$, $\sigma_{Y,Y',z}(u)$,

are

$$\begin{aligned}
\sigma_{XX',z} &= E_{z_k}\left[-\cos\left(z_k\beta u\right) z_k\beta \sin\left(z_k\beta u\right)\right] - \frac{m_X m_{X'}}{N} \\
&= \int_{B_0}^{B_1} f_{z_k}(z)\left(\frac{1}{4}j\beta z e^{-2j\beta uz}\left(-1+e^{4j\beta uz}\right)\right)dz - \frac{m_X m_{X'}}{N} \\
&= \int_{B_0}^{B_1} f_{z_k}(z)\left(-\frac{1}{8}2j\beta z e^{-2i\beta uz} - \frac{1}{8}2j\beta z e^{2i\beta uz}\right)dz - \frac{m_X m_{X'}}{N} \\
&= \left(\frac{\hat{f}'_{z_k}(2u) - \hat{f}'_{z_k}(-2u)}{4}\right) - \frac{m_{X,z}(u) m_{X',z}(u)}{N}
\end{aligned} \tag{4.35}$$

and

$$\begin{aligned}
\sigma_{YY',z} &= E_{z_k}\left[\sin\left(z_k\beta u\right) z_k\beta \cos\left(z_k\beta u\right)\right] - \frac{m_Y m_{Y'}}{N} \\
&= \left(\frac{\hat{f}'_{z_k}(-2u) - \hat{f}'_{z_k}(2u)}{4}\right) - \frac{m_{Y,z}(u) m_{Y',z}(u)}{N}.
\end{aligned} \tag{4.36}$$

Since $X(u,\mathbf{z})$ and $Y(u,\mathbf{z})$ are uncorrelated, the remaining covariance pairs, which are shown in Eq. (4.37), are zero.

$$\left.\begin{array}{l} \sigma_{XY,z}(u) \\ \sigma_{XY',z}(u) \\ \sigma_{X'Y,z}(u) \\ \sigma_{X'Y',z}(u) \end{array}\right\} = 0\,\forall u \in \mathcal{S} \tag{4.37}$$

If

$$\sqrt{N}\cdot \hat{f}'_{z_k}(u) \approx 0\,\forall u \in \mathcal{S}, \tag{4.38}$$

then

$$\left.\begin{array}{l} m_{X',z}(u) \\ m_{Y',z}(u) \\ \sigma_{XX',z}(u) \\ \sigma_{YY',z}(u) \end{array}\right\} \approx 0\,\forall u \in \mathcal{S} \tag{4.39}$$

However, the variances over $\mathbf{z}$ of $X'(u,\mathbf{z})$, $\sigma^2_{X',z}(u)$, and $Y'(u)$, $\sigma^2_{Y',z}(u)$, must also be shown

as angle-independent.

The second derivative of the characteristic function with respect to u is designated $\hat{f}''_{z_k}(u)$ so that

$$\begin{aligned}
\hat{f}''_{z_k}(u) &= -\frac{d}{du}\int_{B_0}^{B_1} j\beta z f_{z_k}(z) e^{-j\beta z u} dz \\
&= -\int_{B_0}^{B_1} j\beta z f_{z_k}(z) \frac{d}{du} e^{-j\beta z u} dz \\
&= -\int_{B_0}^{B_1} \beta^2 z^2 f_{z_k}(z) e^{-j\beta z u} dz.
\end{aligned}$$

The second moment of $X'(u, \mathbf{z})$ is

$$
\begin{aligned}
E_{\mathbf{z}}[X'^2(u,\mathbf{z})] &= E_{\mathbf{z}}\left[\left(-\frac{1}{\sqrt{N}}\sum_{k=1}^{N}\beta z_k \sin(z_k\beta u)\right)^2\right] \\
&= E_{z_k}\left[\frac{1}{N}\sum_{k=1}^{N}\beta^2 z_k^2\sin^2(z_k\beta u) + \frac{1}{N}\sum_{k=1}^{N}\beta z_k\sin(z_k\beta u)\sum_{\substack{l=1\\ l\neq k}}^{N}\beta z_l\sin(z_l\beta u)\right] \\
&= E_{z_k}\left[\beta^2 z_k^2\sin^2(z_k\beta u)\right] + (N-1)E_{z_k}[\beta z_k\sin(z_k\beta u)]^2 \\
&= \int_{B_0}^{B_1}\beta^2 f_{z_k}(z)z^2\sin^2(z\beta u)dz + (N-1)E_{z_k}[\beta z\sin(z\beta u)]^2 \\
&= \int_{B_0}^{B_1}\beta^2 f_{z_k}(z)z^2\left(\frac{1}{2}-\frac{\cos(2z\beta u)}{2}\right)dz + (N-1)E_{z_k}[\beta z_k\sin(z_k\beta u)]^2 \\
&= \int_{B_0}^{B_1}\frac{\beta^2}{2}f_{z_k}(z)z^2dz \\
&\quad -\int_{B_0}^{B_1}\frac{\beta^2}{2}f_{z_k}(z)z^2\cos(2z\beta u)dz + (N-1)E_{z_k}[\beta z_k\sin(z_k\beta u)]^2 \\
&= \frac{\beta^2 E_{z_k}[z_k^2]}{2} - \int_{B_0}^{B_1}\beta^2 f_{z_k}(z)z^2\frac{e^{j2z\beta u}+e^{-j2z\beta u}}{4}dz \\
&\quad +(N-1)E_{z_k}[\beta z_k\sin(z_k\beta u)]^2 \\
&= \frac{\beta^2 E_{z_k}[z_k^2]}{2} - \frac{1}{4}\left(\frac{-4\int_{B_0}^{B_1}\beta^2 f_{z_k}(z)z^2e^{j2z\beta u}}{-4} - \frac{4\int_{B_0}^{B_1}\beta^2 f_{z_k}(z)z^2e^{-j2z\beta u}dz}{4}\right) \\
&\quad +(N-1)E_{z_k}[\beta z_k\sin(z_k\beta u)]^2 \\
&= \frac{\beta^2 E_{z_k}[z_k^2]}{2} - \frac{1}{4}\left(\frac{\hat{f_{z_k}}''(-2\beta u)}{-4} - \frac{\hat{f_{z_k}}''(2\beta u)}{4}\right) + (N-1)E_{z_k}[\beta z_k\sin(z_k\beta u)]^2 \\
&= \frac{\beta^2 E_{z_k}[z_k^2]}{2} + \frac{1}{16}\left(\hat{f}''_{z_k}(2u) + \hat{f}''_{z_k}(-2u)\right) + (N-1)E_{z_k}[\beta z_k\sin(z_k\beta u)]^2 \quad (4.40)
\end{aligned}
$$

The second moment of $Y'(u,\mathbf{z})$ is

$$\begin{aligned}
E[Y_z'^2] &= E_{z_k}\left[\left(\frac{1}{\sqrt{N}}\sum_{k=1}^{N}\beta z_k\cos(z_k\beta u)\right)^2\right] \\
&= E_{z_k}\left[\frac{1}{N}\sum_{k=1}^{N}\beta^2 z_k^2\cos^2(z_k\beta u)+\frac{1}{N}\sum_{k=1}^{N}\beta z_k\cos(z_k\beta u)\sum_{\substack{l=1\\l\neq k}}^{N}\beta z_l\cos(z_l\beta u)\right] \\
&= E_{z_k}\left[\beta^2 z_k^2\cos^2(z_k\beta u)\right]+(N-1)E_{z_k}[\beta z_k\cos(z_k\beta u)]^2 \\
&= \int_{B_0}^{B_1}\beta^2 f_{z_k}(z)z^2\cos^2(z\beta u)dz+(N-1)E_{z_k}[\beta z_k\cos(z_k\beta u)]^2 \\
&= \int_{B_0}^{B_1}\beta^2 f_{z_k}(z)z^2\left(\frac{1}{2}+\frac{\cos(2z\beta u)}{2}\right)dz+(N-1)E_{z_k}[\beta z_k\cos(z_k\beta u)]^2 \\
&= \int_{B_0}^{B_1}\frac{\beta^2}{2}f_{z_k}(z)z^2dz+\int_{B_0}^{B_1}\frac{\beta^2}{2}f_{z_k}(z)z^2\cos(2z\beta u)dz \\
&\quad +(N-1)E_{z_k}[\beta z_k\cos(z_k\beta u)]^2 \\
&= \frac{\beta^2 E_{z_k}[z_k^2]}{2}+\int_{B_0}^{B_1}\beta^2 f_{z_k}(z)z^2\frac{e^{j2z\beta u}+e^{-j2z\beta u}}{4}dz+(N-1)E_{z_k}[\beta z_k\cos(z_k\beta u)]^2 \\
&= \frac{\beta^2 E_{z_k}[z_k^2]}{2}+\frac{1}{4}\left(\frac{-4\int_{B_0}^{B_1}\beta^2 f_{z_k}(z)z^2e^{j2z\beta u}}{-4}-\frac{4\int_{B_0}^{B_1}\beta^2 f_{z_k}(z)z^2e^{-j2z\beta u}dz}{4}\right) \\
&\quad +(N-1)E_{z_k}[\beta z_k\cos(z_k\beta u)]^2 \\
&= \frac{\beta^2 E_{z_k}[z_k^2]}{2}+\frac{1}{4}\left(\frac{\hat{f_{z_k}}''(-2\beta u)}{-4}-\frac{\hat{f_{z_k}}''(2\beta u)}{4}\right)+(N-1)E_{z_k}[\beta z_k\cos(z_k\beta u)]^2 \\
&= \frac{\beta^2 E_{z_k}[z_k^2]}{2}-\frac{1}{16}\left(\hat{f_{z_k}}''(2\beta u)+\hat{f_{z_k}}''(-2\beta u)\right)+(N-1)E_{z_k}[\beta z_k\cos(z_k\beta u)]^2 \quad (4.41)
\end{aligned}$$

From the second moments in Eqs. (4.40) and (4.41), the quadrature component derivative variances, $\sigma^2_{X',z}(u)$ and $\sigma^2_{Y',z}(u)$, are

$$\sigma^2_{X',z}(u)=\frac{\beta^2 E_{z_k}[z_k^2]}{2}+\frac{1}{4}\left(\hat{f}''_{z_k}(2u)+\hat{f}''_{z_k}(-2u)\right)-\frac{m^2_{X',z}(u)}{N} \quad (4.42)$$

$$\sigma^2_{Y',z}(u)=\frac{\beta^2 E_{z_k}[z_k^2]}{2}-\frac{1}{4}\left(\hat{f}''_{z_k}(2u)+\hat{f}''_{z_k}(-2u)\right)-\frac{m^2_{Y',z}(u)}{N} \quad (4.43)$$

where $E_{z_k}[z_k^2]$ is the second moment of the array element location distribution.

With angle-independent statistics from Eqs. (4.29), (4.37), (4.39) and

$$\sigma^2_{X',z}(u) \approx \sigma^2_{Y',z}(u) \, \forall u \in \mathcal{S}, \tag{4.44}$$

Ref. [11] showed that the expected number of upward-crossings for some level P_0, provided $NP_0 > 1/2$, can be written in closed form as

$$E[\nu(P_0)] = \mu(\mathcal{S}_{nr}) \, \sigma_{X',z} \, \sqrt{NP_0} \, e^{-NP_0} \sqrt{\frac{2}{\pi}} \tag{4.45}$$

where $\sigma_{X',z}$ is $\sigma_{X',z}(u)$ independent of u. [6]

To obtain $\sigma^2_{X',z}(u) \approx \sigma^2_{Y',z}(u)$ along with Eqs. (4.29), (4.37), (4.39) and achieve approximate angle-independence, it is seen that

$$\left(\hat{f}''_{z_k}(2u) + \hat{f}''_{z_k}(-2u) \right) << 2\beta^2 E[z^2] \, \forall u \in \mathcal{S}. \tag{4.46}$$

Then,

$$\sigma^2_{X',z}(u) \approx \sigma^2_{Y',z}(u) \approx \frac{\beta^2 E[z^2]}{2} = \sigma^2_{X',z}. \tag{4.47}$$

By using this result, the expected number of upward-crossings can be given in terms of $E[z^2]$ as

$$E[\nu(P_0)] = \beta \mu(\mathcal{S}_{nr}) \, \sqrt{E[z^2]N} \, e^{-NP_0} \sqrt{\frac{P_0}{\pi}}. \tag{4.48}$$

It is shown in Appendix A that angle-independence applies when the element location distribution is shifted to have approximately zero mean. With approximately zero mean, the second moment of the element distribution, $E_{z_k}[z_k^2]$, is

$$E_{z_k}[z_k^2] \approx \sigma_z^2, \tag{4.49}$$

where σ_z^2 is the antenna location variance. Since shifting the element location distribution

[6] [1] ©2011 IEEE

does not change the far-field beampattern, the peak sidelobe level distribution is now

$$\begin{aligned}&\Pr\{P(u|\mathbf{z}) \geq \mathrm{P}_0 \,\forall\, \mathrm{u} \in \mathcal{S}\} \\ &\approx 1 - (1 - e^{-NP_0})\, e^{-\beta\mu(\mathcal{S}_{nr})\,\sigma_z\sqrt{N}\,e^{-NP_0}\sqrt{\frac{P_0}{\pi}}}. \end{aligned} \tag{4.50}$$

In Eq. (4.50), σ_z can be considered the effective length of the array [44]. In summary, Eq. (4.50) is the closed form expression for the peak sidelobe level distribution if the following conditions are valid for array elements with independent random positions on linear arrays or planar arrays that can be transformed into linear arrays:

- $\sqrt{N} \cdot \hat{f}_{z_k}(u)$ and $\sqrt{N} \cdot \hat{f}'_{z_k}(u)$ are close to zero in the sidelobe region with u.
- $\sigma^2_{X',z}(u) \approx \sigma^2_{Y',z}(u)\, \forall u \in \mathcal{S}$.[7]

It is interesting to note that Eq. (4.50) is a function of the second moment of $\mathbf{z}$. Further work needs to see if using higher-order moments can produce more accurate peak sidelobe level probability calculations.

4.5 Distribution Convergence with Increasing Array Elements[8]

If the antenna location variance, σ_z^2, is a function of the number of antennas, the peak sidelobe level distribution may not converge to zero as the number of array elements increases. In addition to this non-zero probability convergence, it will now be shown that the conditions to produce Eq. (4.50) hold if angle-independence of beampattern statistics also occurs asymptotically with the increase in elements.

[7] [1] ©2011 IEEE

[8] [1] ©2011 IEEE

If the conditions to produce Eq. (4.50) hold with increasing elements, the peak sidelobe level can converge between zero and one if

$$\lim_{N\to\infty} \mu(\mathcal{S}_{nr})\, \sigma_z(N)\, e^{-NP_0}\, \sqrt{N} = \kappa,\ 0 < \kappa < \infty \tag{4.51}$$

where $\sigma_z(N)$ is array effective length as a function of the number of elements. To produce the convergence in Eq. (4.51), one condition is that $\sigma_z(N)$ converges to infinity with N. Note that $\sigma_z(N)$ may not increase monotonically. However, to allow peak sidelobe level convergence between zero and one for arbitrarily large N, a monotonically increasing $\sigma_z(N)$ is desirable.

The effective array length must not converge to infinity faster or slower than $\mu(\mathcal{S}_{nr})e^{-NP_0}\sqrt{N}$ converges to zero. One general function that can be used to produce peak sidelobe level convergence to a constant between zero and one is

$$\sigma_z(N) = \frac{\kappa e^{NP_0}}{\sqrt{N}} + g(N) \tag{4.52}$$

where $g(N)$ is some function of N such that $\sigma_z(N)$ is positive and

$$\lim_{N\to\infty} g(N)\, e^{-NP_0}\, \sqrt{N}\, \mu(\mathcal{S}_{nr}) = 0. \tag{4.53}$$

Here, κ serves as a positive and finite proportionality constant for the effective length.

The maximum possible physical length of the array changes with the effective length. It is assumed the maximum possible physical length has a linear relationship with some function of the effective length, but this assumption is true for distributions encountered in this work. If elements are added to the array, the effective length increases, and the maximum possible physical length scales by some function $t(N)$ where N is the total number of elements. Since the array effective length converges to infinity with increasing number of elements by Eq. (4.52), $t(N)$ converges to infinity as well. To maintain a mean location of zero, the distances between element locations also scale by $t(N)$. If N_0 elements are added to the array, the

characteristic function of the new array element location distribution with $(N + N_0)$ nodes is

$$\hat{f}_{z_k}^{N_0}(u) \triangleq \int_{L_{\min}}^{L_{\max}} f_{z_k}(z) e^{-j\beta t(N+N_0)uz} dz \tag{4.54}$$

where $f_{z_k}(z)$ is the element location distribution before scaling the element locations by $t(N + N_0)$. By the Riemann-Lebesgue Lemma,

$$\lim_{N\to\infty} \int_{L_{\min}}^{L_{\max}} f_{z_k}(z) e^{-j\beta t(N)uz} dz = 0 \,\forall u \neq 0. \tag{4.55}$$

The means of the quadrature components are proportional to the square-root of the number of elements. By Eq. (4.52), $t(N)$ is increasing faster than $\sqrt{N}$. So from Eq. (4.55), the means of the quadrature components approach zero and the variances approach 1/2. The convergence of these statistics and the Central Limit Theorem allow the initial beampattern level distribution to converge to a Rayleigh distribution.

The length of the sidelobe region also approaches one. This convergence occurs because u_s is usually specified by the average beampattern or the average sidelobes being below some level as in Ref. [11]. Due to Eq. (4.55), the average beampattern outside of the main beam converges to zero.

The statistics of the quadrature component derivatives must also be shown to satisfy the angle-independent conditions that produce Eq. (4.50) if the effective array length grows large. The characteristic function derivative of a distribution with $N + N_0$ elements is

$$\hat{f}_{z_k}^{\prime N_0}(u) \triangleq -j \int_{L_{\min}}^{L_{\max}} \beta t(N + N_0) z f_{z_k}(z) e^{-j\beta t(N+N_0)uz} dz. \tag{4.56}$$

Eq. (4.56) will replace $\hat{f}'_{z_k}(u)$ in Eqs. (4.33) and (4.34) for the derivative means. The term $\hat{f}''_{z_k}(2u) + \hat{f}''_{z_k}(-2u)$ for the quadrature component derivative variances in Eqs. (4.42) and

(4.43) is replaced by

$$\begin{aligned}&\hat{f}''^{N_0}_{z_k}(2u) + \hat{f}''^{N_0}_{z_k}(-2u)\\ &= -\int_{L_{\min}}^{L_{\max}} \beta^2 t^2 (N+N_0) z^2 f_{z_k}(z) \cos(2z\beta t(N+N_0)u) dz. \end{aligned} \tag{4.57}$$

Eqs. (4.56) and (4.57) are not guaranteed to converge as N increases. The derivative means and Eq. (4.57) must converge to zero for beampattern statistics to become asymptotically angle-independent. If $m_{X',z}(u)$ and $m_{Y',z}(u)$ converge to zero but Eq. (4.57) does not, then $\sigma^2_{X',z}(u)$ and $\sigma^2_{Y',z}(u)$ can become approximately angle-independent for an arbitrarily large number of elements if $\sigma_z^2(N+N_0)$ is significantly larger than Eq. (4.57).

In summary, the closed form peak sidelobe level distribution in Eq. (4.50) is valid asymptotically as the number of elements increases if

- $\lim_{N\to\infty} \sigma_z(N) = \infty$
- $m_{X,z}(u)$, $m_{Y,z}(u)$, $m_{X',z}(u)$, $m_{Y',z}(u)$, and Eq. (4.57) converge to zero as the effective length of the array increases with the number of elements.

The normal element position distribution allows these conditions to be met. For any element position distribution, the means $m_{X,z}(u)$ and $m_{Y,z}(u)$ will converge to zero if the array aperture increases faster than $\sqrt{N+N_0}$. If $m_{X',z}(u)$ and $m_{Y',z}(u)$ converge to zero but Eq. (4.57) does not, then Eq. (4.50) is approximately valid for an arbitrarily large number of elements if Eq. (4.57) is much smaller than $\sigma_z^2(N)$. As examples, the triangle and semi-circle distributions do not allow Eq. (4.57) to converge to zero, but they keep it significantly smaller than the element variance for large N. These two distributions allow the means to converge to zero. Further work needs to show that, for an arbitrarily large number of elements, if $m_{X',z}(u)$, $m_{Y',z}(u)$, and Eq. (4.57) do not converge to zero but are smaller than $\sigma_z^2(N)$, then the closed form peak sidelobe level distribution is approximately valid.

If the statistics are asymptotically angle-independent, the probability of the beampattern

peak sidelobe level exceeding some value P_0 can converge between zero and one by

$$\lim_{N\to\infty} \Pr\{P(u|\mathbf{z}) \geq \mathrm{P_0}\,\forall\,\mathrm{u} \in \mathcal{S}\} = 1 - \mathrm{e}^{-\beta\kappa\sqrt{\frac{\mathrm{P_0}}{\pi}}}. \tag{4.58}$$

4.6 Examples[9]

To validate the peak sidelobe level distribution equations, this paper shows simulations of linear arrays with normal and triangle distributed elements. Simulations of planar arrays with uniform distributed elements from Ref. [11] are also given.

Table 4.1 shows Eq. (4.58) values for linear arrays and planar arrays that can be transformed into linear arrays as the constant κ changes. Here, the main beam is steered to $\phi_0 = 0$ degrees and $\lambda = 1$. As the number of antenna elements are increased for simulated antenna arrays, the peak sidelobe level distribution should converge to the values plotted in Table 4.1 for different effective length proportionality constants, κ. In the simulations, the standard deviation and effective length, σ_z, changes with the number of elements according to Eq. (4.52) with $g(N) = 0$. The probabilities shown in Table 4.1 are for a peak sidelobe level of $P_0 = -20$ dB. This level was chosen for simulation convenience, but any level could be used to test the validity of the peak sidelobe level distribution equations.

Table 4.1: *Peak Sidelobe Level Distribution Limit for Planar and Linear Arrays as Effective Length increases with Number of Elements,* $\Pr(max(P(u)) > P_0 = -20\,dB,\ \lambda = 1,$ *©2011 IEEE*

κ	5.00	4.33	3.67	3.00	2.33	1.67	1.00
Linear Pr	0.83	0.79	0.73	0.66	0.56	0.45	0.30
Planar Pr	0.97	0.95	0.93	0.88	0.81	0.69	0.51

Fig. 4.2 shows the simulated peak sidelobe level distribution convergence for a linear array with normal distributed elements. For the simulations, 10240 random beampatterns were generated for each pair of N and κ.

[9] [1] ©2011 IEEE

Similar peak sidelobe level distribution convergence is shown in Fig. 4.2 for a linear array of maximum length L with triangle distributed element locations. The pdf is given by

$$f_{z_k}(z) = \begin{cases} 4\frac{z+\frac{L}{2}}{L^2}, -\frac{L}{2} \leq z \leq 0 \\ \\ 4\frac{\frac{L}{2}-z}{L^2}, 0 \leq z \leq \frac{L}{2}. \end{cases} \tag{4.59}$$

Although this triangle distribution of antenna positions does not allow Eq. (4.57) to converge to zero with increasing position variance, Fig. 4.2 shows the peak sidelobe level probabilities are close to the values in Table 4.1 for linear arrays.

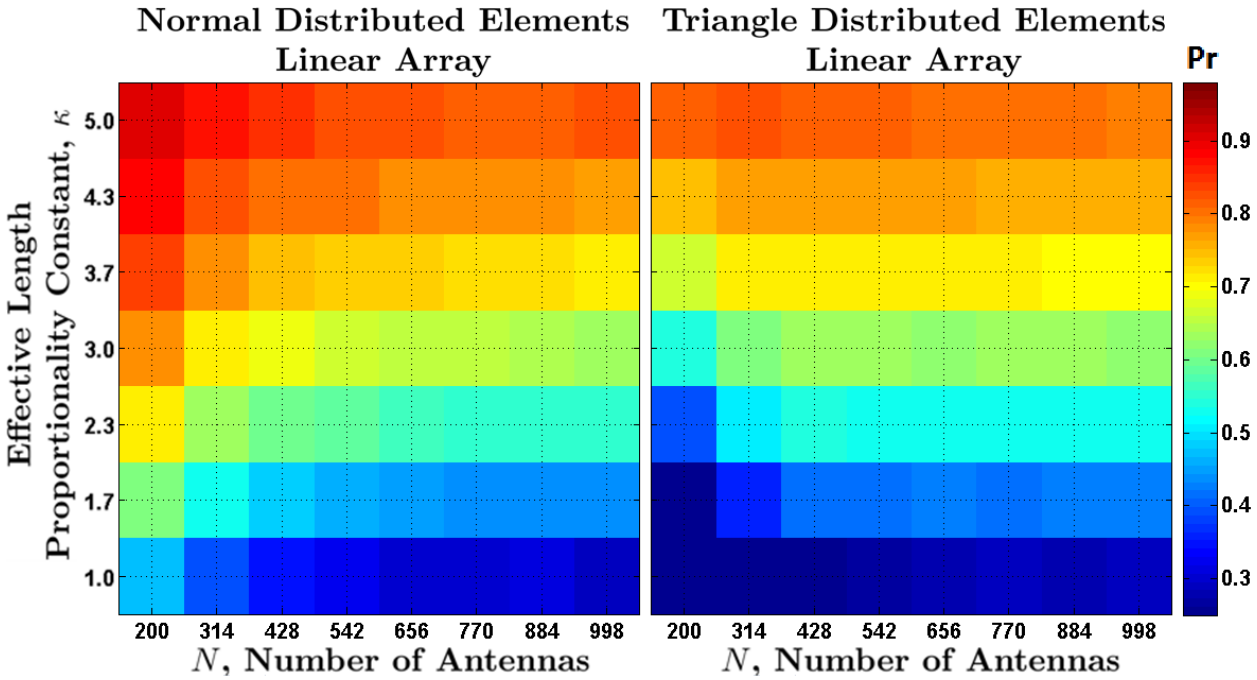

Figure 4.2: *Peak Sidelobe Level Distribution Convergence,* $\Pr\{P(u|\mathbf{z}) \geq -20\ dB \forall\, \mathrm{u} \in \mathcal{S}\}$*, for Linear Arrays with Zero-Mean Gaussian and Triangle Distributed Antenna Positions where* $\sigma_z(N) = \frac{\kappa e^{NP_0}}{\sqrt{N}}$*,* ©*2011 IEEE*

The peak sidelobe level distribution convergence is shown for a planar array with uniformly distributed elements in Fig. 4.3. The pdf for this element location distribution after

transforming into a linear array is

$$f_{z_k}(z) = \frac{2}{R^2\pi}\sqrt{R^2 - z^2},\ -R \leq z \leq R. \tag{4.60}$$

The physical length of the array, $2R$, changes with $\sigma_z(N)$. The simulation probabilities seem to converge to the theoretical values in Table 4.1.

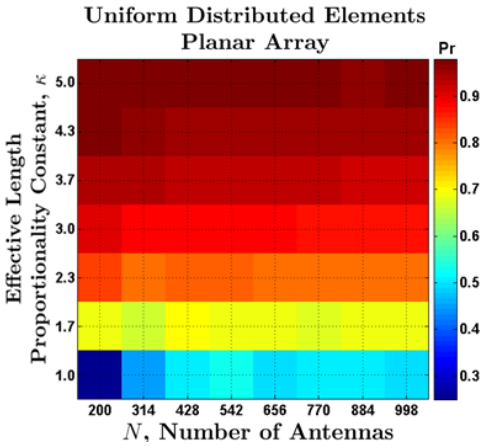

Figure 4.3: *Peak Sidelobe Level Distribution Convergence,* $\Pr\{P(u|\mathbf{z}) \geq -20\ dB \forall\, \mathrm{u} \in \mathcal{S}\}$*, for Uniformly Distributed Planar Array where* $\sigma_z(N) = \frac{\kappa e^{NP_0}}{\sqrt{N}}$*,* ©*2011 IEEE*

These results can help in designing an array. From $\sigma_z(N) = \frac{\kappa e^{NP_0}}{\sqrt{N}}$, $\sigma_z(N)$, κ, and N can be adjusted to produce an array with a desired peak sidelobe level probability for some given frequency. Once the number of elements and effective length that give the desired peak sidelobe level probability are determined, Monte Carlo methods may be used to determine element locations.

Eq. (4.51) suggests that there is a region of $\sigma_z(N)$ values where the sidelobe distribution does not converge to one or zero if the conditions for angle-independence with large effective aperture are met. This transition is shown in Fig. 4.4 with the simulated probabilities of the peak sidelobe level exceeding a beampattern level. The simulation is plotted with the closed form peak sidelobe level distribution of Eq. (4.50) for $N = 800$ triangle-distributed array element positions. There is good agreement between theory and simulation. Each simulation

point was found from generating 10240 random beampatterns. This curves can be useful in maximizing the length of an array while keeping peak sidelobe levels relatively low.

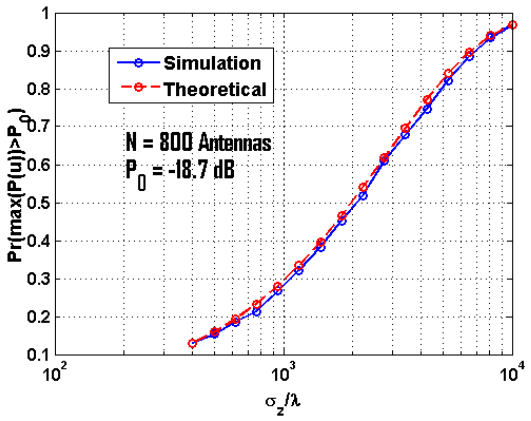

Figure 4.4: *Peak Sidelobe Level Distribution for Linear Array formed by Triangle Distributed Element Locations*

Chapter 5

Sidelobe Peak Distribution using Extreme Value Theory

5.1 Motivation: Inaccurate Probability Calculations with Upward-Crossing Method for Sparse Arrays

When $N \leq 200$, the method of upcrossings does not yield close results to simulation. The mismatch can be seen in Fig. 5.1. As the number of elements reduces to $N = 80$, the probability calculations begin to deviate from the simulation for large values of σ_z/λ. In Fig. 5.2, the cdf of the peak sidelobe level distribution is plotted for both the upcrossing and sample method with triangle distributed element locations. The cdf were generated using the method to numerically find the peak sidelobe levels explained in Appendix B. For both methods, we see that as the number of elements decreases, the theoretical cdf deviates further from the simulation for large σ_z/λ, or for sparse arrays. With the Gaussian distribution approximations made for the array factor quadrature components and their derivatives, it is difficult to correct the upward-crossing method for a smaller number of elements. Therefore, we turn to Extreme Value Theory (EVT) without making Gaussian approximations to deal

with smaller N.

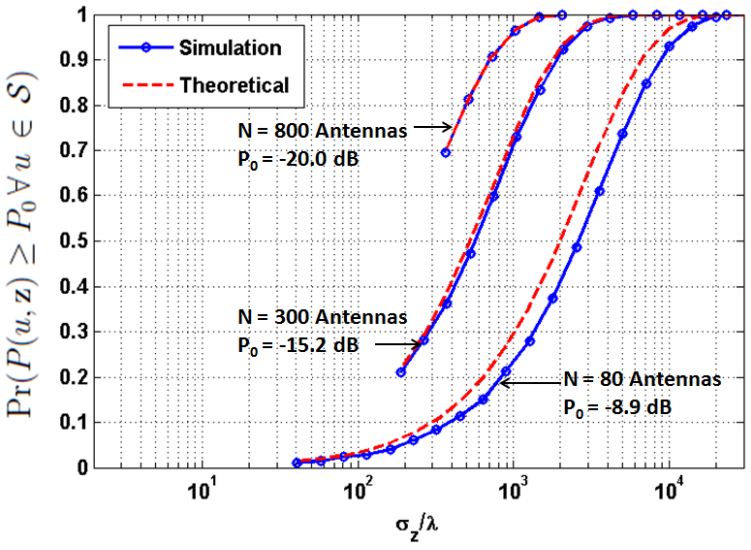

Figure 5.1: *Peak Sidelobe Level Distribution for Linear Array formed by Triangle Distributed Element Locations for different N and P_0*

5.2 Introduction to Extreme Value Theory

Researchers have long been interested in the properties of order statistics, especially the minimum and maximum of a sequence of random variables. This interest led to the area of Extreme Value Theory (EVT). One may look to other texts for deep historical surveys of EVT, but in this thesis, we condense the history described in Ref. [45].

One of the earliest recorded investigations into EVT was by Nicolas Bernoulli in 1709 who looked at the mean largest distance from the origin given n points lying at random on a straight line of fixed length t. Development of EVT was motivated from the need of astronomers to utilize or reject outlying observations. Refs. [46], [47], and [48] introduced and first investigated distributions of the largest value and looked at the exact cumulative distribution function and asymptotic distributions.

It was Ref. [49] who first claimed that the distribution of the maximum of a random

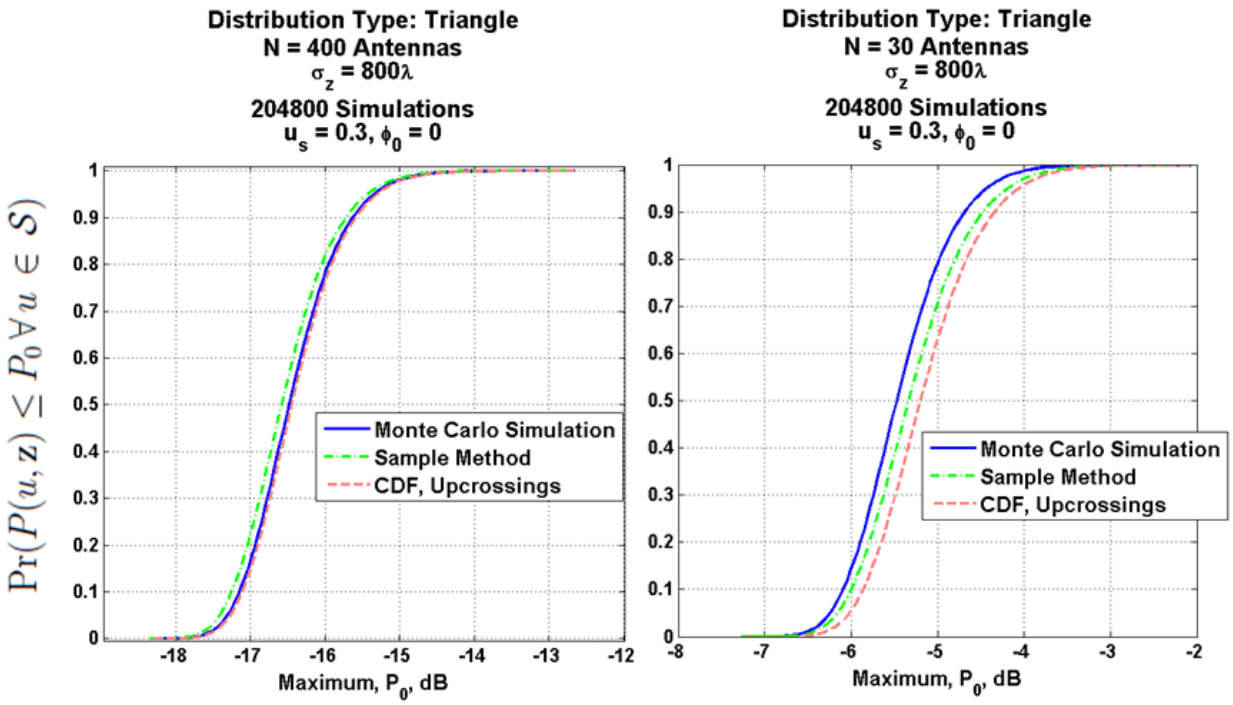

Figure 5.2: *Peak Sidelobe Level Distribution cdf for Linear Array formed by Triangle Distributed Element Locations for* $N = 400$ *and* $N = 30$*, Standard Deviation of Element Locations is* $\sigma_z = 800\lambda$.

variable can be only one of three types. Let there be iid random variables $\{X_1, X_2, \ldots, X_M\}$ with probability density function (pdf) $f_X(x)$ and cumulative density function (cdf) $F_X(x)$. Let

$$X_{\max} = \max\{X_1, X_2, \ldots, X_M\}.$$

The cdf of $X_{\max}$ can be given by

$$\begin{aligned} F_{\max}(x) &= \Pr(X_{\max} \leq x) \\ &= \Pr(X_1 \leq x) \Pr(X_2 \leq x) \cdots \Pr(X_M \leq x) \\ &= F_X^M(x). \end{aligned}$$

Ref. [49] gives that there can be for some a_M and b_M,

$$F_X^M(x) = F(b_M x + a_M). \tag{5.1}$$

Distributions that satisfy Eq. (5.1), which is called the stability postulate, are the following:

$$F(b_M x + a_M) = \begin{cases} e^{-x^{-\gamma}}, x \geq 0, \gamma > 0 \\ 0 \quad\quad , x < 0 \end{cases} \tag{5.2}$$

$$F(b_M x + a_M) = \begin{cases} 1 \quad\quad , x \geq 0 \\ e^{-(-x)^{\gamma}}, x < 0, \gamma > 0 \end{cases} \tag{5.3}$$

$$F(b_M x + a_M) = e^{-e^{-x}}, -\infty < x < \infty \tag{5.4}$$

E.J. Gumbel applied these distributions to human lifetimes, radioactive emissions, and flood analysis in Refs. [50], [51], [52], [53], and [54]. W. Weibull applied them to strength of materials in Ref. [55]. Ref. [56] applied them to earthquake magnitudes. Subsequently, Eq. (5.2) is the Frechet distribution, Eq. (5.3) is the Weibull distribution, and Eq. (5.4) is the Gumbel distribution.

Since

$$\lim_{M \to \infty} F^M(x) = \begin{cases} 0, F(x) < 1 \\ 1, F(x) = 1 \end{cases},$$

let there be parameters a_M and b_M that vary with M so that at each x, $F^M(b_M x + a_M)$ is constant for all M. The task is to determine a_M and b_M at each M and

$$\lim_{M \to \infty} F^M(b_M x + a_M).$$

It was B. Gnedenko in Ref. [57] who gave a rigorous proof that the three distributions that satisfy Eq. (5.1) are limiting distributions for the maximum of a sequence of random variables. He also gave sufficient and necessary conditions for the convergence of the distribution of the maximum of random variables to one of the three distributions.

Ref. [57] is interested in results of the form

$$\begin{aligned} \lim_{M\to\infty} X_{\max} - A_M &= 0 \\ \frac{X_{\max}}{B_M} &= 1 \end{aligned}$$

where A_M and B_M are constants and the convergence is in probability [58]. Let

$$x_F = \sup\{x : F_X(x) < 1\}.$$

The main problem addressed by Ref. [57] is to determine the conditions under which there exist constants $b_M > 0$ and a_M and a nondegenerate function $\Phi(x)$ such that

$$\lim_{M\to\infty} \Pr\left\{\frac{X_{\max} - a_M}{b_M} \le x\right\} = \lim_{M\to\infty} F^M(b_M x + a_M) = \Phi(x). \tag{5.5}$$

When Eq. (5.5) holds, then $\Phi(x)$ is said to be an extreme value limiting distribution function and $F_X(x)$ is in the domain of attraction of $\Phi(x)$.

5.2.1 Conditions for Domain of Attraction to Frechet Distribution

Following the symbols in Refs. [57] and [58],

$$\Phi(x) = \Phi_\gamma(x)$$

if $F_X(x)$ is in the domain of attraction of the Frechet distribution. The necessary and sufficient conditions for $F_X(x)$ to be in this domain of attraction, as given by Ref. [57] are

1. The function $1 - F_X(x)$ is regularly varying at infinity or

2. $$\lim_{x\to\infty} \frac{1 - F_X(x)}{1 - F_X(kx)} = k^\gamma,\ k > 0,\ \gamma > 0.$$

5.2.2 Conditions for Domain of Attraction to Weibull Distribution

When $F_X(x)$ is in the domain of attraction of the Weibull distribution,

$$\Phi(x) = \Psi_\gamma(x).$$

The necessary and sufficient condition is that there is some x_0 so that

$$\begin{aligned} F_X(x_0) &= 1 \\ F_X(x_0 - \epsilon) &< 1, \epsilon > 0 \end{aligned}$$

and

$$\lim_{x \to -0} \frac{1 - F_X(kx + x_0)}{1 - F_X(x + x_0)} = k^\gamma,\ k > 0,\ \gamma > 0.$$

Note that $x_F = x_0$. Ref. [59] gives the necessary and sufficient conditions in another form but also gives the condition that x_F be finite. If

$$\lim_{x \to \infty} \frac{1 - F_X\left(x_F - \frac{1}{kx}\right)}{1 - F_X\left(x_F - \frac{1}{x}\right)} = k^{-\gamma},\ k > 0,\ \gamma > 0,$$

then $F_X(x)$ is in the domain of attraction of the Weibull distribution.

5.2.3 Conditions for Domain of Attraction to Gumbel Distribution

$F_X(x)$ is in the domain of attraction of the Gumbel distribution if

$$\Phi(x) = \Lambda(x),$$

there exists a function $A(z)$ such that

$$\lim_{z \to x_F} A(z) = 0,$$

and

$$\lim_{z \to x_F} \frac{1 - F_X(z + zA(z)x)}{1 - F(z)} = e^{-x},\ -\infty < x < \infty \tag{5.6}$$

Formulations for $A(z)$ were given by Refs. [60], [61], [62], and [63]. Refs. [62] and [63] give $A(z)$ as

$$A(z) = \frac{\int_z^{x_F} (1 - F_X(t))\, dt}{z\,(1 - F_X(z))}.$$

Ref. [64] gives a sufficient but not necessary condition for $F_X(x)$ to be in the domain of attraction of the Gumbel distribution as

$$\lim_{x \to \infty} \frac{d}{dx} \frac{1 - F_X(x)}{F'_X(x)} = 0 \tag{5.7}$$

where

$$F'_X(x) = \frac{dF_X(x)}{dx}.$$

As mentioned in Ref. [58], Ref. [64] assumes $x_F = \infty$ but Ref. [57] showed that Eq. (5.7) also hold when $x_F < \infty$, and so a sufficient condition for $F_X(x)$ to be in the domain of attraction of the Gumbel distribution is

$$\lim_{x \to x_F} \frac{d}{dx} \frac{1 - F_X(x)}{F'_X(x)} = 0.$$

5.2.4 Maximum of Non-Identical Distributions

The limiting distributions from Refs. [49] and [57] assume that $X_{\max}$ is taken from a sequence of iid random variables, each with cdf $F_X(x)$. Ref. [65] extended the work in Ref. [57] to not necessarily iid random variables.

If the distributions of each sample are not identical, let the samples of the sequence $\{X_l\}$ have the CDFs $\{F_l(x)\}$. Then from Ref. [65], suppose

$$\lim_{M \to \infty} \sum_{l=1}^{M} F_l(b_M x + a_M) = K(x)$$

where $K(x)$ is a positive, non-decreasing function not identically a constant. Now, Ref. [65]

shows that the asymptotic limit of the distribution of the minimum of the sequence is

$$\lim_{M\to\infty}\prod_{l=1}(1-F_l(b_M x+a_M))=e^{-K(x)}. \tag{5.8}$$

To find the maximum of a sequence $\{X_l\}$, then the results from Ref. [65] will need to be applied to $\min\{-X_l\}$ since $\max\{X_l\}=-\min\{-X_l\}$.

Ref. [65] gives three forms to $K(x)$. Since we will show that beampattern samples may be assumed to be identically distributed, we will not discuss these forms and their verification further in this thesis. One may refer to Ref. [65] for more details.

5.2.5 EVT with Dependent Random Variables

Refs. [43] and [66] state that if r_n is the correlation of Gaussian variables X_i and X_{i+n}, then if

$$\lim_{n\to\infty} r_n \log n = 0$$

or

$$\sum_{n=1}^{\infty} r_n^2 < \infty$$

then the sequence of Gaussian random variables is in the domain of attraction of the Gumbel distribution.

Dealing with dependence in EVT can extend beyond Gaussian random variables. Let there be a sequence of random variables $\{X_1, X_2, \ldots, X_M\}$ where, for $1 \le i, j \le M$, X_i and X_j are independent only if $|i-j| > m$ where m is a positive integer. Ref. [67] shows that if

$$\lim_{c\to\infty}\frac{1}{\Pr(X_i>c)}\max_{|i-j|\le m}\Pr[(X_i>c),(X_j>c)]=0, \tag{5.9}$$

then the asymptotic distribution of $X_{\max}=\max\{X_1, X_2, \ldots, X_M\}$ will be the same as if all the random variables in the sequence $\{X_1, X_2, \ldots, X_M\}$ were independent.

If the random variables $\{X_1, X_2, \ldots, X_M\}$ for a mixing sequence such that terms in the

sequence are weakly dependent when, then Ref. [68] states that EVT may still be applied if

$$\lim_{i\to\infty} \Pr(X_1 < x, X_2 < x, X_i < x) = \Pr(X_1 < x, X_2 < x) \Pr(X_i < x). \tag{5.10}$$

So, if $F_X(x)$ is the cdf of each random variable in the sequence $\{X_1, X_2, \ldots, X_M\}$, then it is in the domain of attraction of on one of the three EVT distributions if Eq. (5.9) or Eq. (5.10) is satisfied.

5.2.6 EVT with Continuous Processes

In dealing with continuous processes, let there be a stationary stochastic process $X(t)$ whose maximum is

$$X_{\max}(T) = \sup\{X(t); 0 \le t \le T\}.$$

Let $F_X(x)$ be the cdf of $X(t)$ for all t. If $F_X(x)$ is in the domain of attraction of $\Phi(x)$ where $\Phi(x)$ is one of the three EVT distributions, then Ref. [43] showed that for some $b_T > 0$ and a_T,

$$\lim_{T\to\infty} \Pr\left(\frac{X_{\max}(T) - a_T}{b_T} \le x\right) = \Phi(x).$$

By letting

$$u_T = b_T x + a_T,$$

Ref. [43] gives that

$$\lim_{T\to\infty} \Pr\left(X_{\max} \le u_T\right) = e^{-\tau} \tag{5.11}$$

where the expression for τ depends on which EVT distribution has $F_X(x)$ in its domain of attraction.

Let the expected number of upcrossings of the process $X(t)$ of a level x_0 be $E[\nu(x_0)]$. See Eq. (4.21) for finding the expected number of upcrossings. Ref. [43] gives that τ in Eq. (5.11)

is

$$\lim_{T\to\infty} E[\nu(u_T)] = \tau.$$

5.3 Deriving Sidelobe Peak Distribution from Extreme Value Theory

5.3.1 Overview

Researchers have applied Extreme Value Theory (EVT) to many applications. Beyond the work by E.J. Gumbel, EVT has been applied to flood flows by Refs. [69] and [70]. Other applications include reliability analysis [71], glass fiber strength [72], wind speed [73], rainfall analysis [74], and the maximum height of water waves [75]. Ref. [45] lists references to many other applications.

We now apply EVT to finding the peak sidelobe level distribution of random beampatterns. We re-write the array factor and beampattern equations from Eqs. (2.6), (2.7), (2.8), and (2.9) here. The quadrature components of the array factor are

$$X(u,\mathbf{z}) = \frac{1}{\sqrt{N}}\sum_{k=1}^{N}\cos(z_k\beta u) \tag{5.12}$$

$$Y(u,\mathbf{z}) = \frac{1}{\sqrt{N}}\sum_{k=1}^{N}\sin(z_k\beta u). \tag{5.13}$$

The field pattern or array factor is

$$\begin{aligned} F(u,\mathbf{z}) &= \frac{1}{N}\sum_{k=1}^{N} e^{-j\beta u z_k} \\ &= \frac{1}{\sqrt{N}}\left(X(u,\mathbf{z}) - jY(u,\mathbf{z})\right). \end{aligned}$$

The beampattern of the antenna array is

$$\begin{aligned} P(u,\mathbf{z}) &= |F(u,\mathbf{z})|^2 \\ &= F(u,\mathbf{z})F^*(u,\mathbf{z}) \\ &= \frac{1}{N}(X^2(u,\mathbf{z}) + Y^2(u,\mathbf{z})). \end{aligned} \tag{5.14}$$

For a linear array, $\beta = 2\pi/\lambda$ and $u \in [0, 1 + |\sin[\phi_0]|$ where ϕ_0 is the steering angle. For a planar array, $\beta = 4\pi/\lambda$ and $u \in [0, 1]$.

The beampattern is a continuous process in u. From Ref. [43], calculating the expected number of upcrossings should give us the peak sidelobe level distribution. However, without making the Gaussian approximations of the quadrature components, calculating this expected number of upcrossings is difficult. So, we approach the problem by sampling the beampattern with M equally spaced samples. We need to give a bound to show how close the EVT distribution we get through sampling is to the true distribution of the peak sidelobe level.

Computing the peak sidelobe level distribution with EVT will use following steps:

1. Show that the beampattern is uniformly continuous so that there are no large fluctuations of the beampattern between samples.

2. Give an upper bound to the difference between the true maximum of a beampattern and the sampled maximum and show that the bound becomes smaller as the number of samples increases.

3. Show beampattern samples are approximately identically distributed in order to have the asymptotic distribution convergence of Refs. [49] and [57].

4. Show that dependent beampattern samples satisfy conditions from Refs. [43], [66], or [67] in order to use EVT as having independent samples

5. Find an expression for the distribution of the beampattern without approximating the

quadrature components of the array factor by Gaussian distributions

6. Show that for a large number of array elements, $N > 10$, the distribution of the beampattern can declared as being in the domain of attraction of the Gumbel distribution

7. For $N < 10$, show that simulations give that the domain of attraction is Weibull, but the analytical proof is non-trivial.

8. Find the parameters for Gumbel distribution for $N > 10$ case and the simulated parameters for the Weibull distribution for $N < 10$.

5.3.2 Uniform Continuity of Beampattern

Let u_n be some function of n so that

$$\lim_{n\to\infty} u_n = u \,\forall u \in [0, u_{\max}]$$

where

$$u_{\max} = \begin{cases} 1 + |\sin(\phi_0)|, \text{ linear array} \\ 1 \qquad\qquad\quad \text{, planar array} \end{cases}. \tag{5.15}$$

Then,

$$\lim_{n\to\infty} \cos(z_k \beta u_n) = \cos(z_k \beta u) \,\forall u \in [0, u_{\max}],\, \forall z_k \in \mathbf{z}$$

and

$$\lim_{n\to\infty} \sin(z_k \beta u_n) = \sin(z_k \beta u) \,\forall u \in [0, u_{\max}] \,\forall z_k \in \mathbf{z}.$$

Since $\cos(z_k \beta u)$ and $\sin(z_k \beta u)$ are continuous $\forall u \in [0, u_{\max}]$, $X(u, \mathbf{z})$ and $Y(u, \mathbf{z})$ are continuous since sums of continuous functions are also continuous [76]. Since products of continuous functions are continuous, $X^2(u, \mathbf{z})$ and $Y^2(u, \mathbf{z})$ are continuous [76]. Therefore, the beampattern in Eq. (5.14) is continuous $\forall u \in [0, u_{\max}]$.

Let u_n and v_n be sequences such that

$$\lim_{n\to\infty}[u_n - v_n] = 0.$$

If a function f has the property

$$\lim_{n\to\infty}[f(u_n) - f(v_n)] = 0,$$

then it is a uniformly continuous function [76].

Fig. 5.3 illustrates a uniformly continuous function. In a uniformly continuous function, for some δ, there is some ϵ such that

$$\left| f\left(u - \frac{\delta}{2}\right) - f\left(u + \frac{\delta}{2}\right) \right| < \epsilon \, \forall u \in D$$

where D is the domain of f.

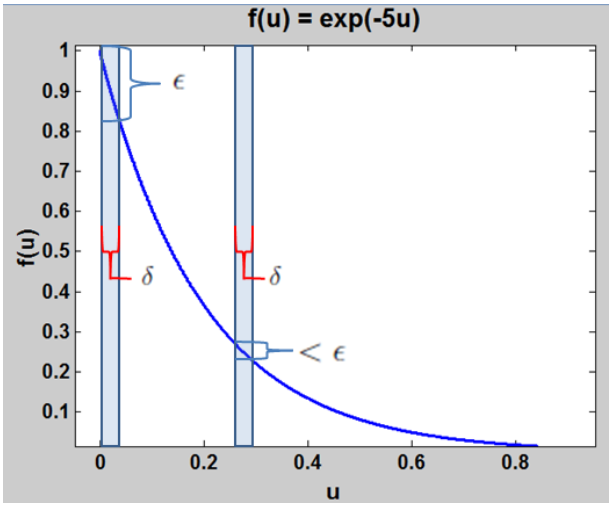

Figure 5.3: *Uniformly continuous function*

Further, if δ is part of a sequence δ_n with a corresponding sequence ϵ_n where

$$\left| f\left(u - \frac{\delta_n}{2}\right) - f\left(u + \frac{\delta_n}{2}\right) \right| < \epsilon_n \, \forall u \in D,$$

then as

$$\lim_{n\to\infty} \delta_n = 0, \tag{5.16}$$

then

$$\lim_{n\to\infty} \epsilon_n = 0. \tag{5.17}$$

From the Heine-Cantor theorem, a continuous function on a closed bounded interval is uniformly continuous [76].

Since the beampattern function in Eq. (5.14) is bounded on the interval $u \in [0, u_{\max}]$, it is uniformly continuous.

Let Eq. (5.14) be sampled uniformly with sampling interval δ starting at $u = u_s \in [0, u_{\max})$. Now, if the beampattern is sampled uniformly with sampling interval δ, then for the difference between beampattern samples,

$$|P(u_s + \delta i, \mathbf{z}) - P(u_s + \delta(i-1), \mathbf{z})| < \epsilon,\ i = \left\{1, 2, \ldots, \left\lfloor \frac{u_{\max} - u_s}{\delta} \right\rfloor \right\}.$$

Therefore, the beampattern value between any two sample points is guaranteed to be less than ϵ, and as the sampling interval reduces, the value of ϵ becomes smaller by Eqs. (5.16) and (5.17).

Let M be the number of samples taken of the beampattern with sampling interval δ starting at $u = u_s$. The value of M is

$$M = \left\lfloor \frac{u_{\max} - u_s}{\delta} \right\rfloor + 1$$

5.3.3 Upper Bound to Difference between True and Sampled Maxima of Beampattern

Ref. [77] showed how to find an upper bound to the difference between the true and sampled maxima of a complex polynomial. Ref. [78] used this result to bound the peak-to-mean

envelope power ratio. Although the beampattern in Eq. (5.14) is not a complex polynomial but a complex arithmetic expression, we can use a similar technique to bound the difference between the true peak sidelobe level and the maximum of the sidelobe region when using M samples.

Let the true maximum of $|F(u, \mathbf{z})|$ over u from the beginning of the sidelobe region, u_s, to $u = u_{\max}$ be attained at u_α so that

$$|F(u_\alpha, \mathbf{z})| = \max_{u_s \leq u \leq u_{\max}} |F(u, \mathbf{z})|.$$

As given in Eq. (5.15), $u_{\max} = 1 + |\sin(\phi_0)|$ for a linear array with ϕ_0 being the steering angle. For a planar array, $u_{\max} = 1$. Let the sample maximum of $|F(u, \mathbf{z})|$ when sampling with number of samples M be attained at u_ξ so that

$$|F(u_\xi, \mathbf{z})| = \max_{u=u_s, u_s+\frac{(u_{\max}-u_s)}{M-1}, u_s+\frac{2(u_{\max}-u_s)}{M-1}, \ldots, u_{\max}} |F(u, \mathbf{z})|$$

such that $\xi = i$ for some $i \in \{0, \ldots, M-1\}$ and

$$u_\xi = u_s + \xi \frac{(u_{\max} - u_s)}{M-1}, \xi \in \{0, \ldots, M-1\}.$$

Our goal is to find a bound to

$$\left| |F(u_\alpha, \mathbf{z})| - |F(u_\xi, \mathbf{z})| \right|.$$

First, let u_i be such that

$$|u_i - u_\alpha| \leq |u_l - u_\alpha|, \forall\, l = \{0, \ldots, M-1\} \tag{5.18}$$

where

$$\begin{aligned} u_i &= u_s + i\frac{u_{\max} - u_s}{M-1}, \forall i \in \{0, \ldots, M-1\} \\ u_l &= u_s + l\frac{u_{\max} - u_s}{M-1}, \forall l \in \{0, \ldots, M-1\}. \end{aligned}$$

In other words, out of M sample points, u_i is the closest sample point to u_α. Eq. (5.18) implies

$$|u_i - u_\alpha| \leq |u_\xi - u_\alpha|$$

but

$$|F(u_i, \mathbf{z})| \leq |F(u_\xi, \mathbf{z})|.$$

Now, using the triangle inequality,

$$\begin{aligned}
||F(u_\alpha, \mathbf{z})| - |F(u_\xi, \mathbf{z})|| &\leq ||F(u_\alpha, \mathbf{z})| - |F(u_i, \mathbf{z})|| \\
&\leq |F(u_\alpha, \mathbf{z}_s) - F(u_i, \mathbf{z}_s)| \\
&= \left| \frac{1}{N} \sum_{k=1}^{N} e^{-j\beta u_\alpha z_k} - \frac{1}{N} \sum_{k=1}^{N} e^{-j\beta u_i z_k} \right| \\
&= \frac{1}{N} \left| \sum_{k=1}^{N} e^{-j\beta u_\alpha z_k} - \sum_{k=1}^{N} e^{-j\beta u_i z_k} \right| \\
&= \frac{1}{N} \left| \sum_{k=1}^{N} \left(e^{-j\beta u_\alpha z_k} - e^{-j\beta u_i z_k} \right) \right| \\
&\leq \frac{1}{N} \sum_{k=1}^{N} \left| e^{-j\beta u_\alpha z_k} - e^{-j\beta u_i z_k} \right|.
\end{aligned}$$

Looking at at difference between the two complex exponentials, we have

$$\begin{aligned}
e^{-j\beta u_\alpha z_k} - e^{-j\beta u_i z_k} &= \cos(\beta u_\alpha z_k) - \cos(\beta u_i z_k) - j \sin(\beta u_\alpha z_k) + j \sin(\beta u_i z_k) \\
&= \cos(\beta u_\alpha z_k) - \cos(\beta u_i z_k) - j \left(\sin(\beta u_\alpha z_k) - \sin(\beta u_i z_k) \right) \\
&= \cos(\beta u_\alpha z_k) - \cos(\beta u_i z_k) - j \left(\sin(\beta u_\alpha z_k) - \sin(\beta u_i z_k) \right) \\
&= -2 \sin \left(\frac{\beta(u_\alpha + u_i) z_k}{2} \right) \sin \left(\frac{\beta(u_\alpha - u_i) z_k}{2} \right) \\
&\quad -j2 \cos \left(\frac{\beta(u_\alpha + u_i) z_k}{2} \right) \sin \left(\frac{\beta(u_\alpha - u_i) z_k}{2} \right).
\end{aligned}$$

Taking the absolute value, we have

$$\begin{aligned}
\left|e^{-j\beta u_\alpha z_k} - e^{-j\beta u_i z_k}\right|^2 &= 4\sin^2\left(\frac{\beta(u_\alpha + u_i)z_k}{2}\right)\sin^2\left(\frac{\beta(u_\alpha - u_i)z_k}{2}\right) \\
&\quad +4\cos^2\left(\frac{\beta(u_\alpha + u_i)z_k}{2}\right)\sin^2\left(\frac{\beta(u_\alpha - u_i)z_k}{2}\right) \\
&= 4\sin^2\left(\frac{\beta(u_\alpha - u_i)z_k}{2}\right)\left(\sin^2\left(\frac{\beta(u_\alpha + u_i)z_k}{2}\right)\right. \\
&\quad \left. +\cos^2\left(\frac{\beta(u_\alpha + u_i)z_k}{2}\right)\right) \\
&= 4\sin^2\left(\frac{\beta(u_\alpha - u_i)z_k}{2}\right) \\
\left|e^{-j\beta u_\alpha z_k} - e^{-j\beta u_i z_k}\right| &= 2\left|\sin\left(\frac{\beta(u_\alpha - u_i)z_k}{2}\right)\right|.
\end{aligned}$$

Now, the bound is

$$\begin{aligned}
||F(u_\alpha, \mathbf{z})| - |F(u_\xi, \mathbf{z})|| &\leq ||F(u_\alpha, \mathbf{z})| - |F(u_i, \mathbf{z})|| \\
&\leq |F(u_\alpha, \mathbf{z}_s) - F(u_i, \mathbf{z}_s)| \\
&\leq \frac{1}{N}\sum_{k=1}^{N} 2\left|\sin\left(\frac{\beta(u_\alpha - u_i)z_k}{2}\right)\right| \\
&= \frac{2}{N}\sum_{k=1}^{N}\left|\sin\left(\frac{\beta(\pm|u_\alpha - u_i|)z_k}{2}\right)\right| \\
&= \frac{2}{N}\sum_{k=1}^{N}\left|\pm\sin\left(\frac{\beta(|u_\alpha - u_i|)z_k}{2}\right)\right| \\
&= \frac{2}{N}\sum_{k=1}^{N}\left|\sin\left(\frac{\beta(|u_\alpha - u_i|)z_k}{2}\right)\right| \\
&= \frac{2}{N}\sum_{k=1}^{N}\left|\sin\left(\frac{\beta(|u_\alpha - u_i|)(\pm|z_k|)}{2}\right)\right| \\
&= \frac{2}{N}\sum_{k=1}^{N}\left|\pm\sin\left(\frac{\beta(|u_\alpha - u_i|)|z_k|}{2}\right)\right| \\
&= \frac{2}{N}\sum_{k=1}^{N}\left|\sin\left(\frac{\beta(|u_\alpha - u_i|)|z_k|}{2}\right)\right|.
\end{aligned}$$

Since $\beta = 2\pi/\lambda$ or $\beta = 4\pi/\lambda$ depending on whether the array is linear or planar, we write

$$\beta = \frac{2q}{\lambda},\ q = \{1, 2\}.$$

We now get

$$\frac{2}{N}\sum_{k=1}^{N}\left|\sin\left(\frac{\beta(|u_\alpha - u_i|)|z_k|}{2}\right)\right| = \frac{2}{N}\sum_{k=1}^{N}\left|\sin\left(\frac{2q\pi(|u_\alpha - u_i|)|z_k|}{2\lambda}\right)\right|. \tag{5.19}$$

Since the units of z_k can be in wavelengths, we may eliminate λ from Eq. (5.19) to get

$$\frac{2}{N}\sum_{k=1}^{N}\left|\sin\left(\frac{\beta(|u_\alpha - u_i|)|z_k|}{2}\right)\right| = \frac{2}{N}\sum_{k=1}^{N}\left|\sin\left(q\pi(|u_\alpha - u_i|)|z_k|\right)\right|$$

where z_k is in units of wavelength.

The difference between u_i and u_{i+1} for $i = \{0, \ldots, M-2\}$ is the sampling interval, which is

$$\frac{u_{\max} - u_s}{M-1}.$$

Therefore, the difference between u_i and the location of the true maximum is

$$|u_\alpha - u_i| \leq \frac{u_{\max} - u_s}{2(M-1)}.$$

For the following inequality to hold:

$$\left|\sin\left(q\pi(|u_\alpha - u_i|)|z_k|\right)\right| \leq \left|\sin\left(\frac{q(u_{\max} - u_s)\pi|z_k|}{2(M-1)}\right)\right|$$

$|z_k|$ must have the inequalities:

$$q\pi|z_k||u_\alpha - u_i| \geq 2\pi i,\ i = \{0, 1, 2, \ldots\}$$
$$\frac{q(u_{\max} - u_s)\pi|z_k|}{2(M-1)} \leq \frac{\pi}{2} + 2\pi i,\ i = \{0, 1, 2, \ldots\}$$

that give

$$\frac{2i}{q|u_\alpha - u_i|} \leq |z_k| \leq \frac{M - 1 + 4(M-1)i}{(u_{\max} - u_s)q},\ i = \{0, 1, 2, \ldots\}$$

or $|z_k|$ must have the inequalities:

$$q\pi|z_k||u_\alpha - u_i| \geq \pi + 2\pi i,\ i = \{0, 1, 2, \ldots\}$$
$$\frac{q(u_{\max} - u_s)\pi|z_k|}{2(M-1)} \leq \frac{3\pi}{2} + 2\pi i,\ i = \{0, 1, 2, \ldots\}$$

that give

$$\frac{1+2i}{q|u_\alpha - u_i|} \leq |z_k| \leq \frac{3(M-1) + 4(M-1)i}{(u_{\max} - u_s)q},\ i = \{0, 1, 2, \ldots\}.$$

Let

$$|z_k|_{\max} = \max\{|\mathbf{z}| = \{|z_1|, |z_2|, \ldots, |z_N|\}\}.$$

If

$$0 \leq |z_k| \leq \frac{M-1}{q},\ \forall z_k,\ k = \{1, 2, \ldots, N\},$$

then

$$\begin{aligned}
\frac{2}{N}\sum_{k=1}^{N} |\sin\left(q\pi(|u_\alpha - u_i|)|z_k|\right)| &\leq \frac{2}{N}\sum_{k=1}^{N} \left|\sin\left(\frac{q(u_{\max} - u_s)\pi|z_k|}{2(M-1)}\right)\right| \\
&\leq \frac{2}{N}\sum_{k=1}^{N} \left|\sin\left(\frac{q(u_{\max} - u_s)\pi|z_k|_{\max}}{2(M-1)}\right)\right| \\
&= 2\left|\sin\left(\frac{q(u_{\max} - u_s)\pi|z_k|_{\max}}{2(M-1)}\right)\right|, \\
&\quad 0 \leq |z_k|_{\max} \leq \frac{M-1}{q}.
\end{aligned}$$

So the bound is

$$\begin{aligned}
||F(u_\alpha, \mathbf{z})| - |F(u_\xi, \mathbf{z})|| &\leq ||F(u_\alpha, \mathbf{z})| - |F(u_i, \mathbf{z})|| \\
&\leq |F(u_\alpha, \mathbf{z}_s) - F(u_i, \mathbf{z}_s)| \\
&\leq \frac{2}{N} \sum_{k=1}^{N} |\sin\left(q\pi(|u_\alpha - u_i|)|z_k|\right)| \\
&\leq \frac{2}{N} \sum_{k=1}^{N} \left|\sin\left(\frac{q(u_{\max} - u_s)\pi|z_k|}{2(M-1)}\right)\right| \\
&\leq 2\left|\sin\left(\frac{q(u_{\max} - u_s)\pi|z_k|_{\max}}{2(M-1)}\right)\right|, \; 0 \leq |z_k|_{\max} \leq \frac{M-1}{q} \\
&= 2\sin\left(\frac{q(u_{\max} - u_s)\pi|z_k|_{\max}}{2(M-1)}\right), \; 0 \leq |z_k|_{\max} \leq \frac{M-1}{q} \quad (5.20)
\end{aligned}$$

For large M

$$\begin{aligned}
||F(u_\alpha, \mathbf{z})| - |F(u_\xi, \mathbf{z})|| &\leq 2\sin\left(\frac{q(u_{\max} - u_s)\pi|z_k|_{\max}}{2(M-1)}\right), \; 0 \leq |z_k|_{\max} \leq M \\
&\approx \frac{q(u_{\max} - u_s)\pi|z_k|_{\max}}{M-1}, \; 0 \leq |z_k|_{\max} \leq \frac{M-1}{q}, \\
& \quad q = \begin{cases} 1, \text{linear array} \\ 2, \text{planar array} \end{cases}. \quad (5.21)
\end{aligned}$$

As more samples are taken, the difference between the true and sampled maximums will reduce.

The average antenna array aperture size increases with the variance of the antenna position distribution. Since $|z_k|_{\max}$ is approximately directly proportional to aperture, the average value of $|z_k|_{\max}$ also increases with increasing variance. One may analyze an antenna position distribution to verify this claim. If we make the number of samples, M, to be proportional to the variance, then we also make M approximately proportional to to the average value $|z_k|_{\max}$ and approximately proportional to a random instance of $|z_k|_{\max}$. We let

$$M \approx K|z_k|_{\max} + 1, \; K > q$$

where K is some constant greater than q, then

$$\begin{aligned} ||F(u_\alpha, \mathbf{z})| - |F(u_\xi, \mathbf{z})|| &\leq 2\sin\left(\frac{q(u_{\max} - u_s)\pi|z_k|_{\max}}{2K|z_k|_{\max}}\right), 0 \leq |z_k|_{\max} \leq \frac{M-1}{q} \\ &\approx 2\sin\left(\frac{q(u_{\max} - u_s)\pi}{2K}\right), q = \begin{cases} 1, \text{linear array} \\ 2, \text{planar array} \end{cases} . \end{aligned} \quad (5.22)$$

Now, since both M and $|z_k|_{\max}$ are approximately proportional, increasing the number of samples will not reduce the bound unless the proportionality constant K also increases.

5.3.4 Identical Beampattern Samples

Since the value of the beampattern in Eq. (5.14) is a function of u, the distributions of beampattern samples will also be a function of u. The samples will not be identically distributed. Since iid samples are needed for the EVT results of Refs. [49] and [57], it needs to be shown that, approximately, the samples are identically distributed.

The distribution of the beampattern in Eq. (5.14) is found from the joint distribution of $X^2(u, \mathbf{z})$ and $Y^2(u, \mathbf{z})$. If the distributions of $X(u, \mathbf{z})$ and $Y(u, \mathbf{z})$ at each u are approximately identical, then $P(u, \mathbf{z})$ in Eq. (5.14) will have approximately the same distribution at each u. The distributions of $X(u, \mathbf{z})$ and $Y(u, \mathbf{z})$ can be found from their characteristic functions. Looking at Eq. (5.12) for $X(u, \mathbf{z})$ and Eq. (5.13) for $Y(u, \mathbf{z})$, they are formed from the sums independent random variables. Let

$$\begin{aligned} X_k(u, z_k) &= \frac{1}{\sqrt{N}}\cos(\beta u z_k) \\ Y_k(u, z_k) &= \frac{1}{\sqrt{N}}\sin(\beta u z_k) \end{aligned}$$

so that

$$\begin{aligned} X(u,\mathbf{z}) &= \sum_{k=1}^{N} X_k(u,z_k) \\ Y(u,\mathbf{z}) &= \sum_{k=1}^{N} Y_k(u,z_k) \end{aligned}$$

and

$$P(u,\mathbf{z}) = \frac{1}{N}\left(X^2(u,\mathbf{z}) + Y^2(u,\mathbf{z})\right).$$

Let the characteristic functions of the distributions of $X(u,\mathbf{z})$, $Y(u,\mathbf{z})$, $X_k(u,z_k)$, and $Y(u,z_k)$ be $\Phi_X(t,u)$, $\Phi_Y(t,u)$, $\Phi_{X_k}(t,u)$, and $\Phi_{Y_k}(t,u)$, respectively. We have

$$\begin{aligned} \Phi_X(t,u) &= \prod_{k=1}^{N} \Phi_{X_k}(t,u) \\ \Phi_Y(t,u) &= \prod_{k=1}^{N} \Phi_{Y_k}(t,u). \end{aligned}$$

We need to show that $\Phi_{X_k}(t,u)$ and $\Phi_{Y_k}(t,u)$ can be make approximately independent of u. Letting $E_{z_k}[X]$ be the expectation of random variable X over z_k, we have

$$\Phi_{X_k}(t,u) = \sum_{l=0}^{\infty} \frac{(jt)^l}{l} E_{z_k}[X_k^l(u,z_k)] \tag{5.23}$$

$$\Phi_{Y_k}(t,u) = \sum_{l=0}^{\infty} \frac{(jt)^l}{l} E_{z_k}[Y_k^l(u,z_k)]. \tag{5.24}$$

One may compute the characteristic functions in Eqs. (5.23) and (5.24) from the pdfs of $X_k(u,z_k)$ and $Y_k(u,z_k)$. Let the minimum and maximum values of z_k be L_{min} and L_{max}, respectively, so that for the pdf of z_k,

$$f_z(z_k) = 0,\ z_k < L_{min},\ z_k > L_{max}.$$

The pdfs of $X_k(u, z_k)$ and $Y_k(u, z_k)$ are given by

$$\begin{aligned} f_{X_k}(X_k(u,z_k)) &= \sum_{i=-\infty}^{\infty} \left(\left. \frac{\sqrt{N} f_z(z_k)}{\beta u |\sin(z_k \beta u)|} \right|_{\substack{z_k = \frac{\arccos(\sqrt{N}X_k)+2\pi i}{\beta u} \\ L_{min} \le z_k \le L_{max}}} \right. \\ &\quad \left. + \left. \frac{\sqrt{N} f_z(z_k)}{\beta u |\sin(z_k \beta u)|} \right|_{\substack{z_k = \frac{-\arccos(\sqrt{N}X_k)+2\pi i}{\beta u} \\ L_{min} \le z_k \le L_{max}}} \right) \\ &\quad , -\frac{1}{\sqrt{N}} \le X_k \le \frac{1}{\sqrt{N}} \\ &= 0, |X_k| > \frac{1}{\sqrt{N}} \end{aligned}$$

and

$$\begin{aligned} f_{Y_k}(Y_k(u,z_k)) &= \sum_{i=-\infty}^{\infty} \left(\left. \frac{\sqrt{N} f_z(z_k)}{\beta u |\cos(z_k \beta u)|} \right|_{\substack{z_k = \frac{\arcsin(\sqrt{N}Y_k)+2\pi i}{\beta u} \\ L_{min} \le z_k \le L_{max}}} \right. \\ &\quad \left. + \left. \frac{\sqrt{N} f_z(z_k)}{\beta u |\cos(z_k \beta u)|} \right|_{\substack{z_k = \frac{-\arcsin(\sqrt{N}Y_k)+\pi(1+2i)}{\beta u} \\ L_{min} \le z_k \le L_{max}}} \right) \\ &\quad , -\frac{1}{\sqrt{N}} \le Y_k \le \frac{1}{\sqrt{N}} \\ &= 0, |Y_k| > \frac{1}{\sqrt{N}}. \end{aligned}$$

Without knowing numerical values of L_{min} and L_{max}, it is difficult to evaluate how the characteristic function can be made approximately independent of u.

Instead, the characteristic functions in Eqs. (5.23) and (5.24) may be approximated by the first four moments of X_k and Y_k, respectively. We give examples with the uniform and Gaussian distributed antenna positions to see how the characteristic functions can be made independent of u.

Uniform Distribution:

If the positions are uniform distributed according to

$$f_z(z) = \frac{1}{L}, -\frac{L}{2} \leq z \leq \frac{L}{2},$$

then

$$\begin{aligned}
E_{z_k}[X_k(u, z_k)] &= \frac{1}{\sqrt{N}}\text{sinc}\left(\frac{Lu\beta}{2}\right) && (5.25)\\
E_{z_k}[X_k^2(u, z_k)] &= \frac{1}{2N} + \frac{1}{2N}\text{sinc}(Lu\beta) && (5.26)\\
E_{z_k}[X_k^3(u, z_k)] &= \frac{3}{4N\sqrt{N}}\text{sinc}\left(\frac{Lu\beta}{2}\right) + \frac{1}{4N\sqrt{N}}\text{sinc}\left(\frac{3Lu\beta}{2}\right)\\
E_{z_k}[X_k^4(u, z_k)] &= \frac{3}{8N^2} + \frac{1}{2N^2}\text{sinc}(Lu\beta) + \frac{1}{8N^2}\text{sinc}(2Lu\beta)
\end{aligned}$$

and

$$\begin{aligned}
E_{z_k}[Y_k(u, z_k)] &= 0 && (5.27)\\
E_{z_k}[Y_k^2(u, z_k)] &= \frac{1}{2N} - \frac{1}{2N}\text{sinc}(Lu\beta) && (5.28)\\
E_{z_k}[X_k^3(u, z_k)] &= 0\\
E_{z_k}[X_k^4(u, z_k)] &= \frac{3}{8N^2} - \frac{1}{2N^2}\text{sinc}(Lu\beta) + \frac{1}{8N^2}\text{sinc}(2Lu\beta)
\end{aligned}$$

where

$$\text{sinc}(x) = \frac{\sin(x)}{x}.$$

From these moments, we see that if the number of elements, N, or the maximum possible aperture of the antenna array, L, is large relative to βu, then the moments, and therefore, the characteristic functions of $X_k(u, z_k)$ and $Y_k(u, z_k)$ can be made approximately independent of u. We get approximately identically distributed beampattern samples. The same result is found for the triangle and semi-circle distributions where the range of z_k is limited.

Gaussian Distribution:

If the positions are Gaussian distributed according to

$$f_z(z) = \frac{1}{\sqrt{2\pi\sigma_z^2}} e^{-\frac{z^2}{2\sigma_z^2}},\ -\infty < z < \infty$$

then

$$\begin{aligned}
E_{z_k}[X_k(u,z_k)] &= \frac{1}{\sqrt{N}} e^{-\frac{1}{2}u^2\beta^2\sigma_z^2} && (5.29)\\
E_{z_k}[X_k^2(u,z_k)] &= \frac{1}{2N} + \frac{1}{2N} e^{-2u^2\beta^2\sigma_z^2} && (5.30)\\
E_{z_k}[X_k^3(u,z_k)] &= \frac{3}{4N\sqrt{N}} e^{-\frac{1}{2}u^2\beta^2\sigma_z^2} + \frac{1}{4N\sqrt{N}} e^{-\frac{9}{2}u^2\beta^2\sigma_z^2} &&\\
E_{z_k}[X_k^4(u,z_k)] &= \frac{3}{8N^2} + \frac{1}{2N^2} e^{-2u^2\beta^2\sigma_z^2} + \frac{1}{8N^2} e^{-8u^2\beta^2\sigma_z^2} &&
\end{aligned}$$

and

$$\begin{aligned}
E_{z_k}[Y_k(u,z_k)] &= 0 && (5.31)\\
E_{z_k}[Y_k^2(u,z_k)] &= \frac{1}{2N} - \frac{1}{2N} e^{-2u^2\beta^2\sigma_z^2} && (5.32)\\
E_{z_k}[X_k^3(u,z_k)] &= 0 &&\\
E_{z_k}[X_k^4(u,z_k)] &= \frac{3}{8N^2} - \frac{1}{2N^2} e^{-2u^2\beta^2\sigma_z^2} + \frac{1}{8N^2} e^{-8u^2\beta^2\sigma_z^2}. &&
\end{aligned}$$

From these moments, we see that if the number of elements, N, or the variance of the antenna positions, σ_z^2, is large relative to βu, then the moments, and therefore, the characteristic functions of $X_k(u,z_k)$ and $Y_k(u,z_k)$ can be made approximately independent of u. We get approximately identically distributed beampattern samples.

For $N > 8$ or $N > 10$, we may use the Central Limit Theorem to approximate the distributions of $X(u,\mathbf{z})$ and $Y(u,\mathbf{z})$ by Gaussian distributions. Since the Gaussian distribution can be completely described by the mean and variance, only the first and second moments can be seen to determine if the distributions of $X(u,\mathbf{z})$ and $Y(u,\mathbf{z})$ are approximately identical

at each u. From Eqs. (4.2), (4.5), (4.4), and (4.7), the means and variances of $X(u, \mathbf{z})$ and $Y(u, \mathbf{z})$ are

$$\begin{aligned} m_{X,z}(u) &= \sqrt{N}\left(\frac{\hat{f}_{z_k}(-u) + \hat{f}_{z_k}(u)}{2}\right) \\ m_{Y,z}(u) &= \sqrt{N}\left(\frac{\hat{f}_{z_k}(-u) - \hat{f}_{z_k}(u)}{j2}\right). \end{aligned}$$

and

$$\begin{aligned} \sigma^2_{X,z}(u) &= \frac{1}{2} + \frac{1}{2\sqrt{N}}\left(m_{X,z}(2u)\right) - \frac{m^2_{X_z}(u)}{N} \\ \sigma^2_{Y,z}(u) &= \frac{1}{2} - \frac{1}{2\sqrt{N}}\left(m_{X,z}(2u)\right) - \frac{m^2_{Y,z}(u)}{N}. \end{aligned}$$

As given in Eq. (4.28), if

$$\sqrt{N} \cdot \hat{f}_{z_k}(u) \approx 0 \, \forall u \in \mathcal{S}, \tag{5.33}$$

then the beampattern statistics may be considered angle-independent.

If angle-independence cannot be claimed, then the approaches mentioned by Ref. [65] must be used. We assume angle-independence in this thesis.

5.3.5 Independent Beampattern Samples

Let there be a beampattern sample at $u = u_1$ and $u = u_2$. For short notation,

$$\begin{aligned} X(u_1, \mathbf{z}) &\equiv X_1 \\ X(u_2, \mathbf{z}) &\equiv X_2 \\ Y(u_1, \mathbf{z}) &\equiv Y_1 \\ Y(u_2, \mathbf{z}) &\equiv Y_2. \end{aligned}$$

The covariances $COV(X_1, Y_1)$ and $COV(X_2, Y_2)$ were determined to be zero by Eqs. (4.8) and (4.9) when the antenna position probability density function (pdf), $f_{z_k}(z)$, is symmetric

about $z = 0$. The covariance of X_1 and Y_2, $COV(X_1, Y_2)$, and the covariance of X_2 and Y_1, $COV(X_2, Y_1)$, are given as follows. As before, $E_{\mathbf{z}}[X]$ is the expectation of X over the joint distribution of the elements of $\mathbf{z}$. $E_{z_k}[X]$ is the expectation of X over the distribution of element $z_k \in \mathbf{z}$. All the $z_k \in \mathbf{z}$ are assumed to have the same distribution.

$$
\begin{aligned}
COV(X_1, Y_2) &= E_{\mathbf{z}}[X_1 Y_2] - E_{\mathbf{z}}[X_1] E_{\mathbf{z}}[Y_2] \\
&= E_{\mathbf{z}}\left[\frac{1}{\sqrt{N}} \sum_{k=1}^{N} \cos(z_k \beta u_1) \frac{1}{\sqrt{N}} \sum_{l=1}^{N} \sin(z_l \beta u_2)\right] \\
&\quad - E_{\mathbf{z}}\left[\frac{1}{\sqrt{N}} \sum_{k=1}^{N} \cos(z_k \beta u_1)\right] E_{\mathbf{z}}\left[\frac{1}{\sqrt{N}} \sum_{l=1}^{N} \sin(z_l \beta u_2)\right] \\
&= \frac{1}{N} \sum_{k=1}^{N} E_{z_k}[\cos(z_k \beta u_1) \sin(z_k \beta u_2)] \\
&\quad + \frac{1}{N} \sum_{k=1}^{N} E_{z_k}[\cos(z_k \beta u_1)] \sum_{\substack{l=1 \\ l \neq i}}^{N} E_{z_k}[\sin(z_l \beta u_2)] \\
&\quad - \frac{1}{N} \sum_{k=1}^{N} E_{z_k}[\cos(z_k \beta u_1)] \sum_{l=1}^{N} E_{z_k}[\sin(z_l \beta u_2)] \\
&= E_{z_k}[\cos(z_k \beta u_1) \sin(z_k \beta u_2)] + (N-1) E_{z_k}[\cos(z_k \beta u_1)] E_{z_k}[\sin(z_l \beta u_2)] \\
&\quad - N E_{z_k}[\cos(z_k \beta u_1)] E_{z_k}[\sin(z_l \beta u_2)] \\
&= E_{z_k}[\cos(z_k \beta u_1) \sin(z_k \beta u_2)] - E_{z_k}[\cos(z_k \beta u_1)] E_{z_k}[\sin(z_l \beta u_2)] \\
&= \frac{1}{2} E_{z_k}[\sin(z_k \beta (u_1 + u_2)) - \sin(z_k \beta (u_1 - u_2))] \\
&\quad - E_{z_k}[\cos(z_k \beta u_1)] E_{z_k}[\sin(z_l \beta u_2)]. \qquad (5.34)
\end{aligned}
$$

$$
\begin{aligned}
COV(X_2, Y_1) &= \frac{1}{2} E_{z_k}[\sin(z_k \beta (u_2 + u_1)) - \sin(z_k \beta (u_2 - u_1))] \\
&\quad - E_{z_k}[\cos(z_k \beta u_2)] E_{z_k}[\sin(z_l \beta u_1)]. \qquad (5.35)
\end{aligned}
$$

Both covariances in Eqs. (5.34) and (5.35) are zero when the pdfs of the $z_k \in \mathbf{z}$ are even

functions, or are symmetric about $z = 0$.

The covariances of X_1 and X_2, $COV(X_1, X_2)$, and the covariances of Y_1 and Y_2, $COV(Y_1, Y_2)$, are given in Eqs. (4.10) and (4.11), respectively. We now compute these covariances for four different antenna position distributions: uniform, triangle, Gaussian, and semi-circle.

If the positions are uniform distributed according to

$$f_z(z) = \frac{1}{L}, -\frac{L}{2} \leq z \leq \frac{L}{2},$$

we have

$$E_{z_k}\left[\cos\left(z_k\beta x\right)\right] = \text{sinc}\left(\frac{L\beta x}{2}\right) \tag{5.36}$$

$$E_{z_k}\left[\sin\left(z_k\beta x\right)\right] = 0 \tag{5.37}$$

to give

$$\begin{aligned} COV(X_1, X_2) &= \frac{1}{2}E_{z_k}\left[\cos\left(z_k\beta(u_1 - u_2)\right) + \cos\left(z_k\beta(u_1 + u_2)\right)\right] \\ &\quad -E_{z_k}\left[\cos\left(z_k\beta u_1\right)\right]E_{z_k}\left[\cos\left(z_l\beta u_2\right)\right] \\ &= \frac{1}{2}\text{sinc}\left(\frac{L\beta(u_1 - u_2)}{2}\right) + \frac{1}{2}\text{sinc}\left(\frac{L\beta(u_1 + u_2)}{2}\right) \\ &\quad -\text{sinc}\left(\frac{L\beta u_1}{2}\right)\text{sinc}\left(\frac{L\beta u_2}{2}\right) \\ COV(Y_1, Y_2) &= \frac{1}{2}E_{z_k}\left[\cos\left(z_k\beta(u_1 - u_2)\right) - \cos\left(z_k\beta(u_1 + u_2)\right)\right] \\ &= \frac{1}{2}\text{sinc}\left(\frac{L\beta(u_1 - u_2)}{2}\right) - \frac{1}{2}\text{sinc}\left(\frac{L\beta(u_1 + u_2)}{2}\right) \end{aligned}$$

If the positions are triangle distributed according to

$$f_z(z) = \begin{cases} \frac{4\left(\frac{L}{2}+z\right)}{L^2}, -\frac{L}{2} \leq z \leq 0 \\ \frac{4\left(\frac{L}{2}-z\right)}{L^2}, 0 \leq z \leq \frac{L}{2} \end{cases}$$

we have

$$E_{z_k}\left[\cos\left(z_k\beta x\right)\right] = \mathrm{sinc}^2\left(\frac{L\beta x}{4}\right) \tag{5.38}$$

$$E_{z_k}\left[\sin\left(z_k\beta x\right)\right] = 0 \tag{5.39}$$

to give

$$\begin{aligned} COV(X_1,X_2) &= \frac{1}{2}E_{z_k}\left[\cos\left(z_k\beta(u_1-u_2)\right)+\cos\left(z_k\beta(u_1+u_2)\right)\right] \\ &\quad -E_{z_k}\left[\cos\left(z_k\beta u_1\right)\right]E_{z_k}\left[\cos\left(z_l\beta u_2\right)\right] \\ &= \frac{1}{2}\mathrm{sinc}^2\left(\frac{L\beta(u_1-u_2)}{4}\right)+\frac{1}{2}\mathrm{sinc}^2\left(\frac{L\beta(u_1+u_2)}{4}\right) \\ &\quad -\mathrm{sinc}^2\left(\frac{L\beta u_1}{4}\right)\mathrm{sinc}^2\left(\frac{L\beta u_2}{4}\right) \end{aligned} \tag{5.40}$$

$$\begin{aligned} COV(Y_1,Y_2) &= \frac{1}{2}E_{z_k}\left[\cos\left(z_k\beta(u_1-u_2)\right)-\cos\left(z_k\beta(u_1+u_2)\right)\right] \\ &= \frac{1}{2}\mathrm{sinc}^2\left(\frac{L\beta(u_1-u_2)}{4}\right)-\frac{1}{2}\mathrm{sinc}^2\left(\frac{L\beta(u_1+u_2)}{4}\right) \end{aligned} \tag{5.41}$$

If the positions are Gaussian distributed according to

$$f_z(z)=\frac{1}{\sqrt{2\pi\sigma_z^2}}e^{-\frac{z^2}{2\sigma_z^2}},\ -\infty<z<\infty$$

we have

$$E_{z_k}\left[\cos\left(z_k\beta x\right)\right] = e^{-\frac{1}{2}x^2\beta^2\sigma_z^2} \tag{5.42}$$

$$E_{z_k}\left[\sin\left(z_k\beta x\right)\right] = 0 \tag{5.43}$$

to give

$$\begin{aligned} COV(X_1, X_2) &= \frac{1}{2} E_{z_k} \left[\cos\left(z_k \beta (u_1 - u_2) \right) + \cos\left(z_k \beta (u_1 + u_2) \right) \right] \\ &\quad - E_{z_k} \left[\cos\left(z_k \beta u_1 \right) \right] E_{z_k} \left[\cos\left(z_l \beta u_2 \right) \right] \\ &= \frac{1}{2} e^{-\frac{1}{2}(u_1 - u_2)^2 \beta^2 \sigma_z^2} + \frac{1}{2} e^{-\frac{1}{2}(u_1 + u_2)^2 \beta^2 \sigma_z^2} - e^{-\frac{1}{2} u_1^2 \beta^2 \sigma_z^2} e^{-\frac{1}{2} u_2^2 \beta^2 \sigma_z^2} \quad (5.44) \\ COV(Y_1, Y_2) &= \frac{1}{2} E_{z_k} \left[\cos\left(z_k \beta (u_1 - u_2) \right) - \cos\left(z_k \beta (u_1 + u_2) \right) \right] \\ &= \frac{1}{2} e^{-\frac{1}{2}(u_1 - u_2)^2 \beta^2 \sigma_z^2} - \frac{1}{2} e^{-\frac{1}{2}(u_1 + u_2)^2 \beta^2 \sigma_z^2} \quad (5.45) \end{aligned}$$

If the positions are Semi-circle distributed according to

$$f_z(z) = \frac{8}{\pi L^2} \sqrt{\frac{L^2}{4} - z^2}, \; -\frac{L}{2} \leq z \leq \frac{L}{2}$$

we have

$$\begin{aligned} E_{z_k} \left[\cos\left(z_k \beta x \right) \right] &= \frac{4}{L \beta x} J_1 \left(\frac{L \beta x}{2} \right) \quad (5.46) \\ E_{z_k} \left[\sin\left(z_k \beta x \right) \right] &= 0 \quad (5.47) \end{aligned}$$

where ${}_0F_1(x)$ is the confluent hypergeometric function. We now give

$$\begin{aligned} COV(X_1, X_2) &= \frac{1}{2} E_{z_k} \left[\cos\left(z_k \beta (u_1 - u_2) \right) + \cos\left(z_k \beta (u_1 + u_2) \right) \right] \\ &\quad - E_{z_k} \left[\cos\left(z_k \beta u_1 \right) \right] E_{z_k} \left[\cos\left(z_l \beta u_2 \right) \right] \\ &= \frac{1}{2} \frac{4}{L\beta(u1 - u_2)} J_1 \left(\frac{L\beta(u_1 - u_2)}{2} \right) + \frac{1}{2} \frac{4}{L\beta(u_1 + u_2)} J_1 \left(\frac{L\beta(u_1 + u_2)}{2} \right) \\ &\quad - \frac{4}{L\beta u_1} J_1 \left(\frac{L\beta u_1}{2} \right) \frac{4}{L\beta u_2} J_1 \left(\frac{L\beta u_2}{2} \right) \\ COV(Y_1, Y_2) &= \frac{1}{2} E_{z_k} \left[\cos\left(z_k \beta (u_1 - u_2) \right) - \cos\left(z_k \beta (u_1 + u_2) \right) \right] \\ &= \frac{4}{L\beta(u_1 - u_2)} J_1 \left(\frac{L\beta(u_1 - u_2)}{2} \right) - \frac{4}{L\beta(u_1 + u_2)} J_1 \left(\frac{L\beta(u_1 + u_2)}{2} \right) \end{aligned}$$

For the four distributions given, we see that the covariances, $COV(X_1, X_2)$ and $COV(Y_1, Y_2)$, are a function of $u_1 - u_2$, the difference between beampattern samples.

The correlation between array factor values at $u = u_1$ and $u = u_2$ is given in Eq. (4.19) as

$$\begin{aligned} Corr[F(u_1, \mathbf{z}), F^*(u_2, \mathbf{z})] &= \frac{\frac{1}{N}[COV[X_1), X_2] + COV[Y_1, Y_2]]}{\frac{1}{N}\sqrt{VAR[X_1] + VAR[Y_1]}\sqrt{VAR[X_2] + VAR[Y_2]}} \\ &= \frac{[COV[X_1), X_2] + COV[Y_1, Y_2]]}{\sqrt{VAR[X_1] + VAR[Y_1]}\sqrt{VAR[X_2] + VAR[Y_2]}}. \end{aligned} \quad (5.48)$$

Equations for $VAR[X_1]$, $VAR[X_2]$, $VAR[Y_1]$, and $VAR[Y_2]$ can be found in Eqs. (4.4) and (4.7).

In Fig. 5.4, we plot a correlation matrix with discrete values of u_1 and u_2 for the triangle distributed case. We see that the matrix is symmetric about $u_1 = u_2$. We plot a slice, or diagonal, of the correlation matrix that is perpendicular to $u_1 = u_2$ against $u_1 - u_2$ to see how the correlation changes with distance between samples of the beampattern. We see that the correlation reduces as $u_1 - u_2$ increases.

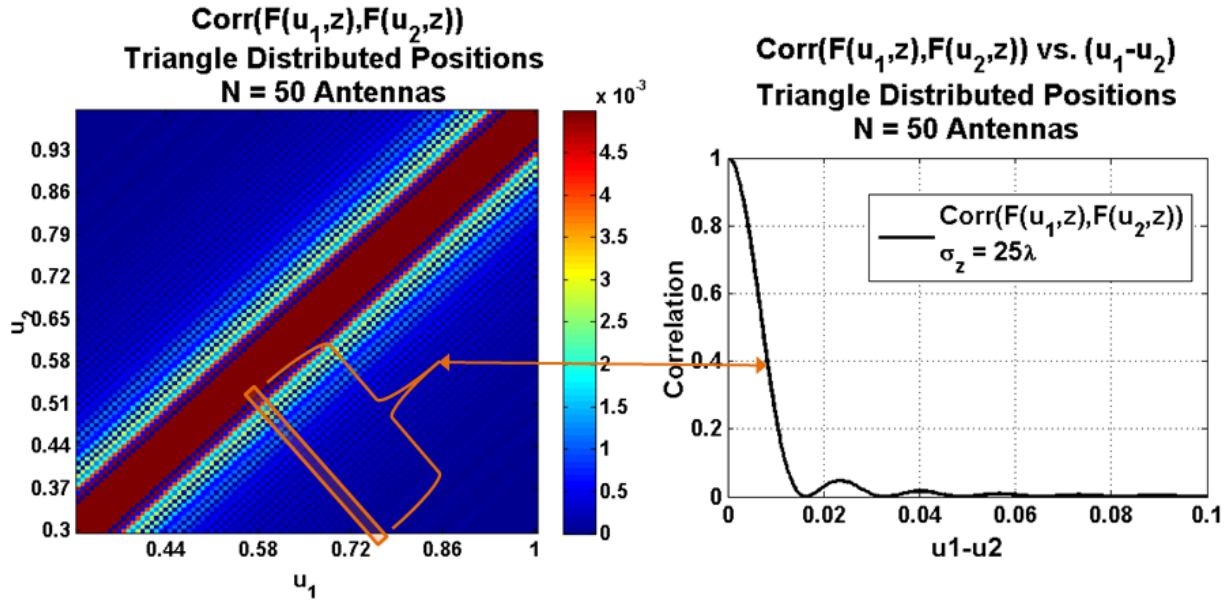

Figure 5.4: *Correlation of Eq.* (5.48) *for triangle antenna position distribution case. Partial diagonal of correlation matrix plotted against* $u_1 - u_2$

We plot the correlation vs. $u_1 - u_2$ in Eq. (5.48) for the uniform and Gaussian antenna position distribution cases in Fig. 5.5. Here, we see the correlation reduces as the variance of

the antenna positions, σ_z^2, increases. Similar behavior is found for the triangle and semi-circle (uniform planar) antenna position distribution cases.

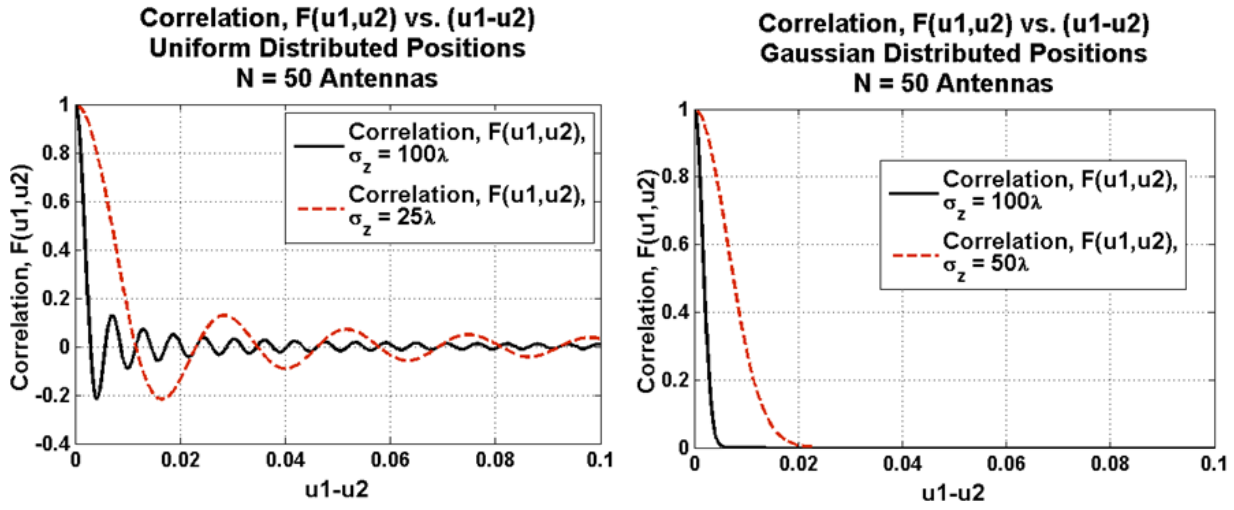

Figure 5.5: *Correlation of Eq.* (5.48) *for uniform and Gaussian antenna position distribution cases vs.* $u_1 - u_2$*, the distance between samples of the beampattern.*

For large N, we may assume that $X(u, \mathbf{z})$ and $Y(u, \mathbf{z})$ are approximately Gaussian distributed by the Central Limit Theorem. We claim that as the correlation between samples of the beampattern decreases, the samples become less dependent. Therefore, Eq. (5.10) from Ref. [68], which is stated here again as

$$\begin{aligned} &\lim_{i\to\infty} \Pr(P(u_1, \mathbf{z}) < P_0, P(u_2, \mathbf{z}) < P_0, P(u_i, \mathbf{z}) < P_0) \\ &= \Pr(P(u_1, \mathbf{z}) < P_0, P(u_2, \mathbf{z}) < P_0) \Pr(P(u_i, \mathbf{z}) < P_0), \end{aligned}$$

is satisfied. EVT analysis of the peak sidelobe level distribution can proceed in the same manner as with independent beampattern samples.

For small N, we claim that Eq. (5.10), is still satisfied for antenna array positions with large variance. As the antenna position variance increases, we know from Eq. (5.48) that the correlation between beampattern samples converges to zero. Since the dependence relationship between two widely separated points of the beampattern is non-trivial, we

can approximate the relationship as being independent if the correlation is small. So, the relationship is approximately independent when the variance of the antenna positions is large. This independence assumption is seen to be be satisfied in Figs. 5.6 and 5.7. As the variance of the antenna positions, σ_z/λ, increases, the conditional probability of the beampattern at $u = u_{\max}$ given $u = u_s$,

$$\frac{\Pr(P(u_{\max}, \mathbf{z}) > P_0, P(u_s, \mathbf{z}) > P_0)}{\Pr(P(u_s, \mathbf{z}) > P_0)},$$

is seen to become the probability of the beampattern at $u = u_{\max}$,

$$\Pr(P(u_{\max}, \mathbf{z}) > P_0)$$

meaning the joint probability

$$\Pr(P(u_{\max}, \mathbf{z}) > P_0, P(u_s, \mathbf{z}) > P_0),$$

is the joint probability of two independent random variables. As seen in Figs. 5.6 and 5.7, an increasing number of antenna elements causes the independence approximation to be met for smaller antenna position variance.

It must be noted that if the number of samples tends to infinity, then the number of samples with strong dependence will tend to infinity and Eq. (5.10) will not be satisfied.

5.3.6 Maximum Peak Sidelobe Level Distribution Simulations

Let $P_{\max}$ be defined as

$$\begin{aligned} P_{\max} &= \max\left\{P(u_s, \mathbf{z}), P\left(u_s + \frac{1}{M}, \mathbf{z}\right), P\left(u_s + \frac{2}{M}, \mathbf{z}\right), \ldots, \right. \\ &\quad \left. P\left(u_s + \frac{1}{M}\lfloor M(u_{\max} - u_s)\rfloor\right)\right\} \end{aligned} \tag{5.49}$$

or the maximum of M samples of the beampattern. The value of $u_{\max}$ is given in Eq. (5.15) depending on the steering angle and whether the array is linear or planar.

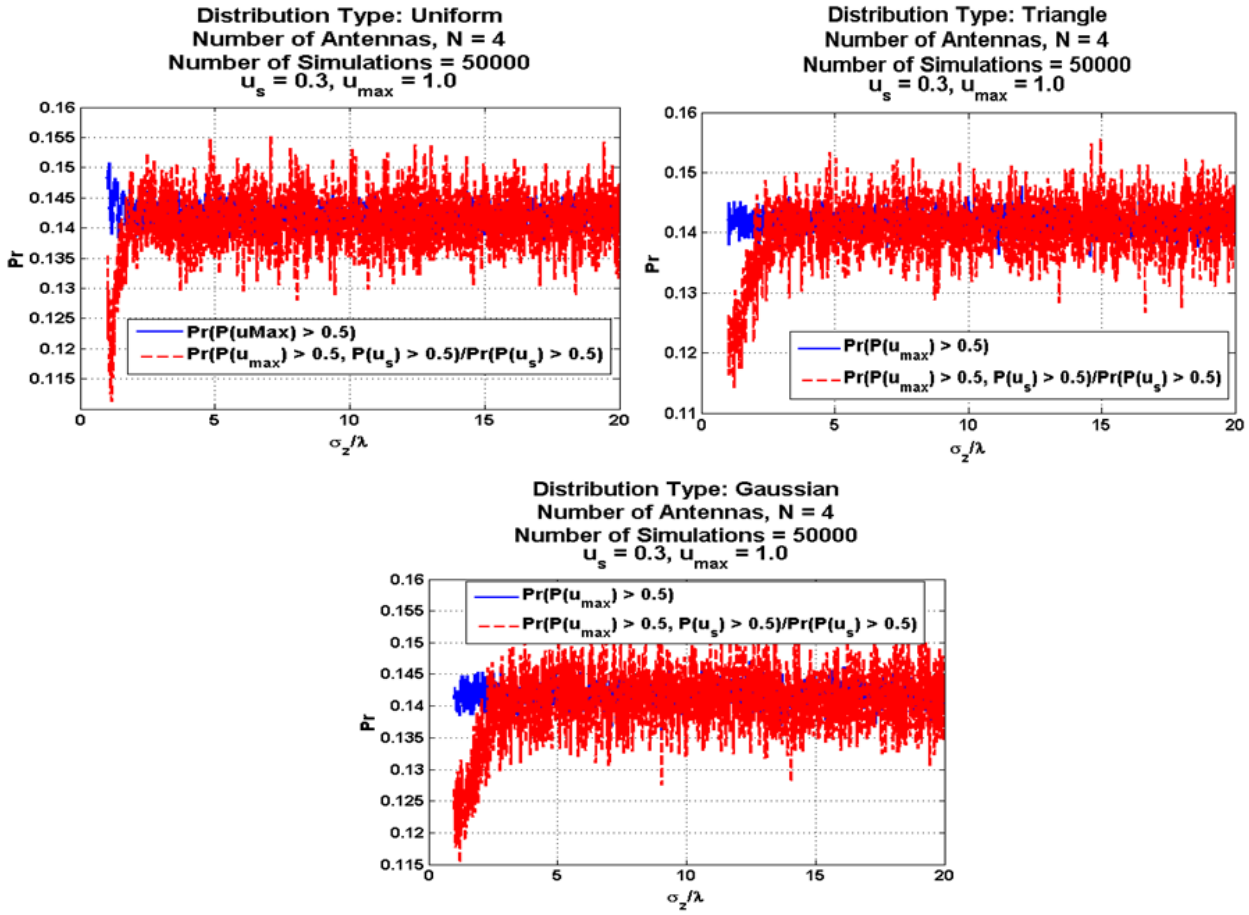

Figure 5.6: *Testing for independence between beampattern probabilities at $u = u_s$ and $u = u_{\max}$ for three different antenna position distributions, $N = 4$.*

Before determining the distribution of $P_{\max}$ analytically, we simulate the distribution of the true maximum of the beampattern. Since samples are being taken, $P_{\max}$ is an approximation of the true maximum for which the bound is given in Eqs. (5.20), (5.21), and (5.22).

In Figs. 5.8 and 5.9, the true peak sidelobe level distribution is plotted as a probability density function (pdf). Appendix B gives an explanation of how the true peak sidelobe levels are found. Linear arrays were used in both simulations. The beginning of the sidelobe region was arbitrarily set to $u_s = 0.3$ and the beampattern was not steered away from $\phi = 0$. Least squares estimates of Gumbel distribution parameters a and b are made. The pdf of the

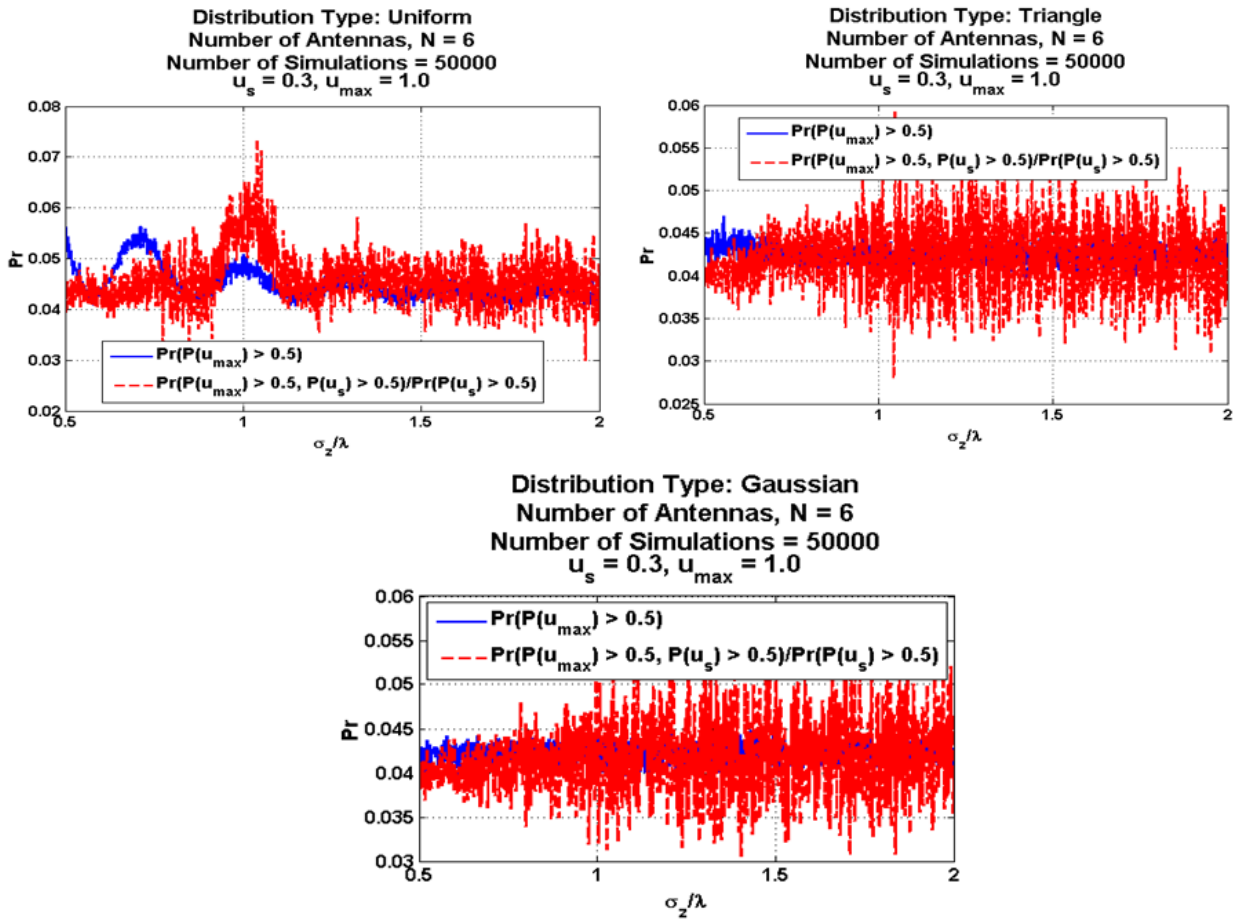

Figure 5.7: *Testing for independence between beampattern probabilities at $u = u_s$ and $u = u_{\max}$ for three different antenna position distributions, $N = 6$.*

beampattern maximum assuming it is Gumbel distributed is given as

$$f_{\max(P(u))}(P_0) = \frac{1}{b} e^{-\frac{P_0-a}{b} - e^{-\frac{P_0-a}{b}}}.$$

The pdf using the parameters is plotted against the simulated graph. Maximum Likelihood (ML) estimates of the Weibull distribution parameters a, b, and α are made. The pdf of the beampattern maximum assuming it is Weibull distributed is given as

$$f_{\max(P(u))}(P_0) = \frac{\alpha}{b}\left(\frac{-P_0+a}{b}\right)^{\alpha-1} e^{-(\frac{-P_0+a}{b})^{\alpha}}.$$

The pdf using the parameters is plotted against the simulated graph.

For both these antenna array geometries, the Gumbel and Weibull distribution estimates seem to match well. The estimated parameters do not seem to be dependent on the type of antenna position distribution.

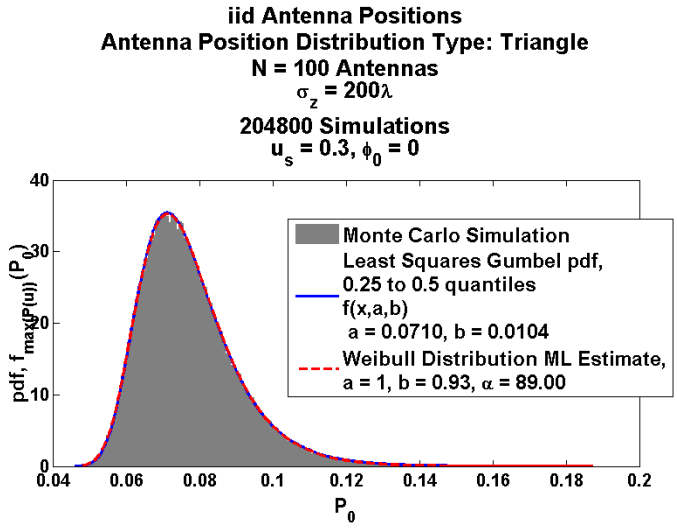

Figure 5.8: *The pdf of true maximum of beampattern, $N = 100$ Antennas, Triangle Antenna Position Distribution, Linear Arrays, Sidelobe starts at $u_s = 0.3$, Steering angle is $\phi_0 = 0$*

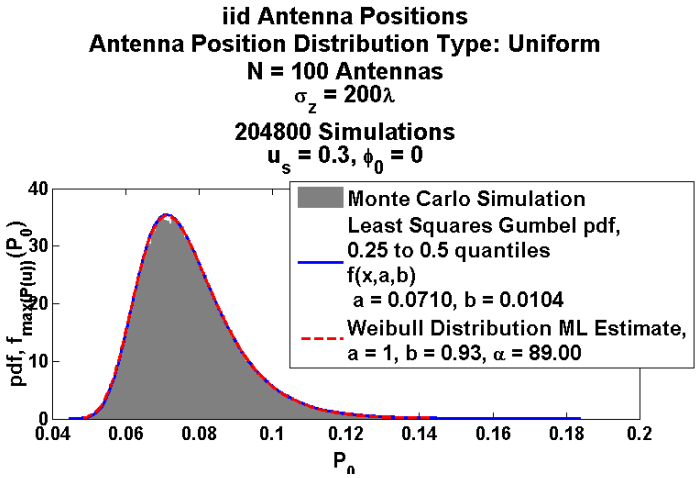

Figure 5.9: *The pdf of true maximum of beampattern, $N = 100$ Antennas, Uniform Antenna Position Distribution, Linear Arrays, Sidelobe starts at $u_s = 0.3$, Steering angle is $\phi_0 = 0$*

A similar good match occurs when the number of elements is increased to $N = 400$ and the variance is also increased as seen in Fig. 5.10.

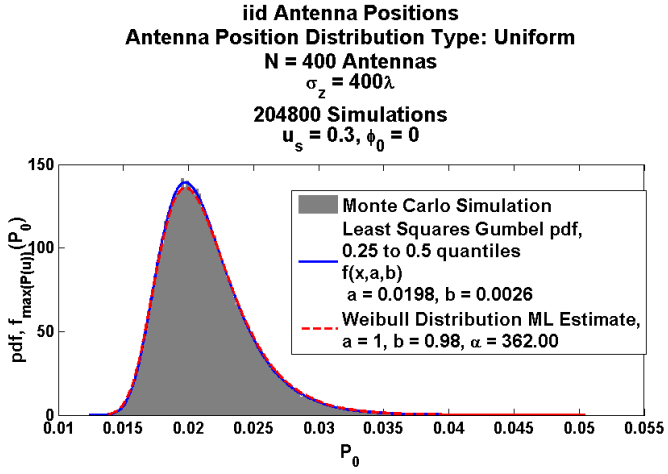

Figure 5.10: *The pdf of true maximum of beampattern, $N = 400$ Antennas, Uniform Antenna Position Distribution, Linear Arrays, Sidelobe starts at $u_s = 0.3$, Steering angle is $\phi_0 = 0$*

There still seems to be good agreement between the simulated pdf and the Gumbel and Weibull distribution fits for $N = 20$ in Fig. 5.11.

When $N = 10$, it is seen in Fig. 5.12 that the Weibull distribution begins to fit better to the simulated graph than the Gumbel distribution fit.

When the number of elements is reduces further to $N = 4$, Fig. 5.13 shows that the Weibull distribution estimate is better than the Gumbel distribution estimate. Therefore, we continue with calculating the distribution of $P_{\max}$ by seeing how the cumulative probability density function (cdf) of $P(u, \mathbf{z})$ at each angle is in the domain of attraction of the Weibull distribution and, when N is large, in the domain of attraction of the Gumbel distribution.

5.3.7 CDF of Beampattern at each Angle, u

We now see if the cumulative distribution function (cdf) at each beampattern sample is in the domain of attraction of one of the Extreme Value Theory (EVT) distributions. We now

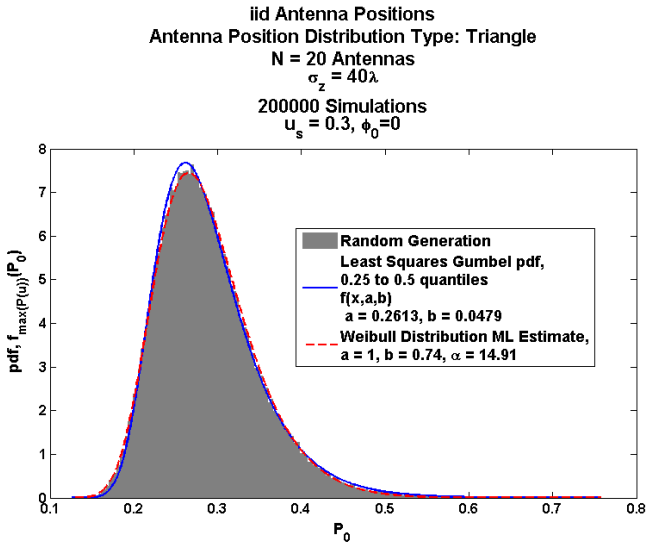

Figure 5.11: *The pdf of true maximum of beampattern, $N = 20$ Antennas, Triangle Antenna Position Distribution, Linear Arrays, Sidelobe starts at $u_s = 0.3$, Steering angle is $\phi_0 = 0$*

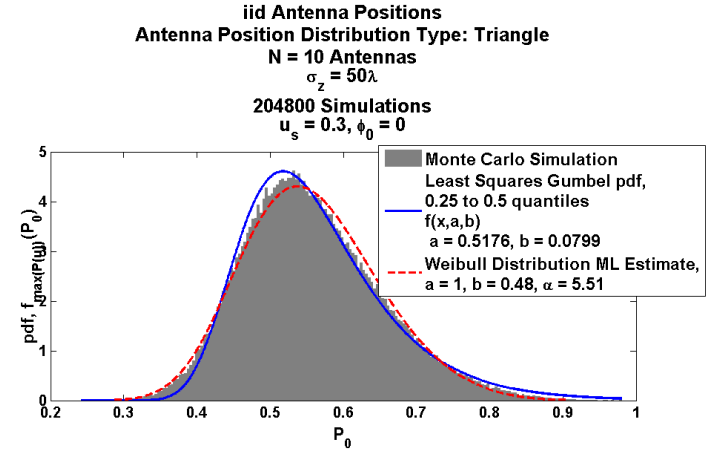

Figure 5.12: *The pdf of true maximum of beampattern, $N = 10$ Antennas, Triangle Antenna Position Distribution, Linear Arrays, Sidelobe starts at $u_s = 0.3$, Steering angle is $\phi_0 = 0$*

calculate the distribution of the beampattern at each angle u. No approximations such as the Gaussian approximation made for the sampling method used by Ref. [17] and the upcrossing method will be made here.

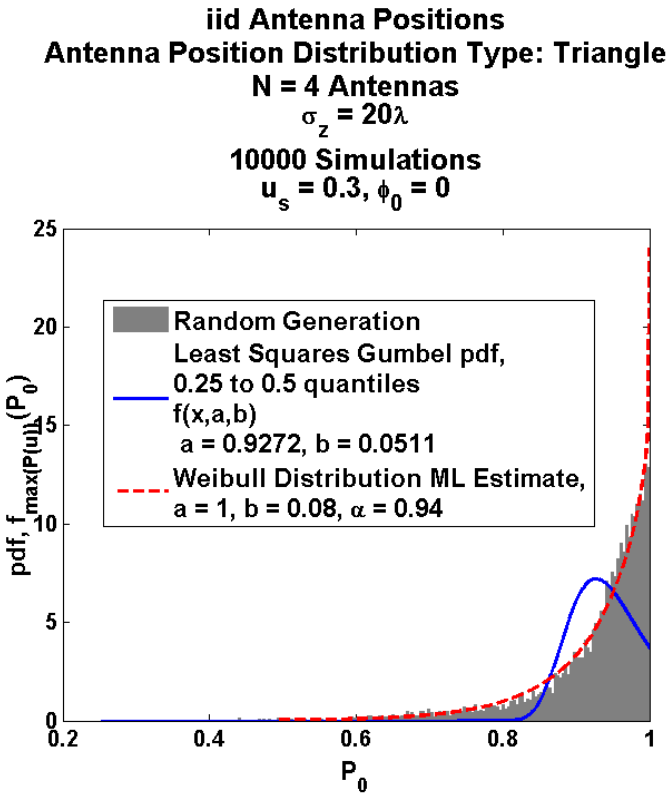

Figure 5.13: *The pdf of true maximum of beampattern, $N = 4$ Antennas, Triangle Antenna Position Distribution, Linear Arrays, Sidelobe starts at $u_s = 0.3$, Steering angle is $\phi_0 = 0$*

We re-write the equation of the field pattern, or array factor, of the beampattern as

$$\begin{aligned} F(u,\mathbf{z}) &= \frac{1}{N}\sum_{k=1}^{N} e^{-j\beta u z_k} \\ &= \sum_{k=1}^{N}\left(\frac{1}{N}\cos(\beta u z_k) - j\frac{1}{N}\sin(\beta u z_k)\right) \\ &= \sum_{k=1}^{N}\frac{1}{N}\cos(\beta u z_k) - j\sum_{k=1}^{N}\frac{1}{N}\sin(\beta u z_k) \\ &= \sum_{k=1}^{N} X_k(u,\mathbf{z}) - j\sum_{k=1}^{N} Y_k(u,\mathbf{z}) \end{aligned}$$

where

$$X_k(u,\mathbf{z}) = \frac{1}{N}\cos(\beta u z_k) \tag{5.50}$$

$$Y_k(u,\mathbf{z}) = \frac{1}{N}\sin(\beta u z_k). \tag{5.51}$$

To make reading equations easier, we rewrite $X_k(u,\mathbf{z})$ and $Y_k(u,\mathbf{z})$ as

$$X_k \equiv X_k(u,\mathbf{z})$$

$$Y_k \equiv Y_k(u,\mathbf{z})$$

where X_k and Y_k being a function of u and $\mathbf{z}$ is implied. It is seen from Eq. (5.50) and (5.51) that

$$-\frac{1}{N} \le X_k \le \frac{1}{N}$$
$$-\frac{1}{N} \le Y_k \le \frac{1}{N}.$$

Now,

$$F(u,\mathbf{z}) = \sum_{k=1}^{N} X_k - j\sum_{k=1}^{N} Y_k.$$

The beampattern is given by

$$\begin{aligned} P(u,\mathbf{z}) &= F(u,\mathbf{z})F^*(u,\mathbf{z}) \\ &= \frac{1}{N}\sum_{k=1}^{N} e^{-j\beta u z_k}\frac{1}{N}\sum_{k=1}^{N} e^{j\beta u z_k} \\ &= \left(\sum_{k=1}^{N} X_k - j\sum_{k=1}^{N} Y_k\right)\left(\sum_{k=1}^{N} X_k + j\sum_{k=1}^{N} Y_k\right) \\ &= \left(\sum_{k=1}^{N} X_k\right)^2 + \left(\sum_{k=1}^{N} Y_k\right)^2, -\frac{1}{N} \le X_k, Y_k \le \frac{1}{N}. \end{aligned} \tag{5.52}$$

Let $F_P(x)$ be the cumulative distribution function (cdf) of the the random variable $P(u,\mathbf{z})$ when the antenna positions, $\mathbf{z} = \{z_1, \ldots, z_N\}$, are independent and identically distributed

(iid). From Ref. [59], for a cdf, $F_X(x)$, to be in the domain of attraction of the Weibull distribution,

$$\lim_{t\to\infty} \frac{1 - F_X\left(\omega(F_X) - \frac{1}{tx}\right)}{1 - F_X\left(\omega(F_X) - \frac{1}{t}\right)} = x^{-\alpha},\ \alpha > 0,\ x > 0 \tag{5.53}$$

where

$$\omega(F_X) \equiv \sup\{x : F_X(x) < 1\}.$$

Since the power domain beampattern ranges from 0 to 1,

$$\omega(F_P) = \omega(F_P) = 1. \tag{5.54}$$

Now,

$$\begin{aligned}
\lim_{t\to\infty} \frac{1 - F_P\left(\omega(F_P) - \frac{1}{tx}\right)}{1 - F_P\left(\omega(F_P) - \frac{1}{t}\right)} &= \lim_{t\to\infty} \frac{1 - F_P\left(1 - \frac{1}{tx}\right)}{1 - F_P\left(1 - \frac{1}{t}\right)} \\
&= \frac{1 - F_P(1)}{1 - F_P(1)} \\
&= \frac{1-1}{1-1} \\
&= \frac{0}{0}.
\end{aligned}$$

Let

$$\begin{aligned}
v &= 1 - \frac{1}{tx} \\
w &= 1 - \frac{1}{t}
\end{aligned}$$

so that

$$\begin{aligned}
\frac{dv}{dt} &= \frac{1}{t^2 x} \\
\frac{dw}{dt} &= \frac{1}{t^2}.
\end{aligned}$$

Let $f_P(x)$ be the probability density function (pdf) of the beampattern in Eq. (5.52). Now,

$$\begin{aligned}
\lim_{t\to\infty}\frac{1-F_P\left(1-\frac{1}{tx}\right)}{1-F_P\left(1-\frac{1}{t}\right)} &= \lim_{t\to\infty}\frac{\frac{d}{dt}\left(1-F_P\left(1-\frac{1}{tx}\right)\right)}{\frac{d}{dt}\left(1-F_P\left(1-\frac{1}{t}\right)\right)} \\
&= \lim_{t\to\infty}\frac{-\frac{dF_P\left(1-\frac{1}{tx}\right)}{dt}}{-\frac{dF_P\left(1-\frac{1}{t}\right)}{dt}} \\
&= \lim_{t\to\infty}\frac{-\frac{dF_P(v)}{dv}\frac{dv}{dt}}{-\frac{dF_P(w)}{dw}\frac{dw}{dt}} \\
&= \lim_{t\to\infty}\frac{\frac{dF_P(v)}{dv}\frac{dv}{dt}}{\frac{dF_P(w)}{dw}\frac{dw}{dt}} \\
&= \lim_{t\to\infty}\frac{f_P(v)\frac{dv}{dt}}{f_P(w)\frac{dw}{dt}} \\
&= \lim_{t\to\infty}\frac{f_P(v)\frac{1}{t^2x}}{f_P(w)\frac{1}{t^2}} \\
&= \lim_{t\to\infty}\frac{f_P\left(1-\frac{1}{tx}\right)\frac{1}{t^2x}}{f_P\left(1-\frac{1}{t}\right)\frac{1}{t^2}} \\
&= \lim_{t\to\infty}\frac{f_P\left(1-\frac{1}{tx}\right)}{f_P\left(1-\frac{1}{t}\right)}\frac{1}{x} \\
&= \frac{f_P(1)}{f_P(1)}\frac{1}{x}. \qquad (5.55)
\end{aligned}$$

If the pdf of $P(u,\mathbf{z})$ is a finite non-zero constant at $P(u,\mathbf{z})=1$, then limit in Eq. (5.55) will be $1/x$. If the pdf is zero or not finite at $P(u,\mathbf{z})=1$, then the limit becomes

$$\begin{aligned}
\lim_{t\to\infty}\frac{\frac{d}{dt}f_P\left(1-\frac{1}{tx}\right)}{\frac{d}{dt}f_P\left(1-\frac{1}{t}\right)}\frac{1}{x} &= \lim_{t\to\infty}\frac{f'_P\left(1-\frac{1}{tx}\right)}{f'_P\left(1-\frac{1}{t}\right)}\frac{1}{x^2} \\
&= \frac{f'_P(1)}{f'_P(1)}\frac{1}{x^2}
\end{aligned}$$

where $f'_P(x)$ is the first derivative of the pdf $f_P(x)$.

If the nth derivative of $f_P(x)$,

$$f_P^{(n)}(x)$$

is a finite non-zero constant at $x = 1$ and all derivatives of $f_P(x)$

$$f_P^{(m)}(x),\ m < n$$

are zero or not finite at $x = 1$, then the limit in Eq. (5.55) is

$$\begin{aligned}\lim_{t\to\infty}\frac{1-F_P\left(1-\frac{1}{tx}\right)}{1-F_P\left(1-\frac{1}{t}\right)} &= \lim_{t\to\infty}\frac{f_P^{(n)}\left(1-\frac{1}{tx}\right)}{f_P^{(n)}\left(1-\frac{1}{t}\right)}\frac{1}{x^n}\\ &= \frac{f_P^{(n)}(1)}{f_P^{(n)}(1)}\frac{1}{x^{n+1}}\\ &= \frac{1}{x^{n+1}}.\end{aligned}$$

Finding expression for $f_P(x)$

We now focus on finding an expression for $f_P(x)$.

Let $f_{X_k,Y_k}(X_k, Y_k)$ be the joint distribution of X_k and Y_k. The characteristic function of this joint distribution is given by

$$\begin{aligned}\Phi_{X_k,Y_k}(t_1,t_2) &\equiv \int_{-\infty}^{\infty}\int_{-\infty}^{\infty} f_{X_k,Y_k}(X_k,Y_k)e^{j(t_1X_k+t_2Y_k)}d_{X_k}d_{Y_k}\\ &= \int_{-\frac{1}{N}}^{\frac{1}{N}}\int_{-\frac{1}{N}}^{\frac{1}{N}} f_{X_k,Y_k}(X_k,Y_k)e^{j(t_1X_k+t_2Y_k)}d_{X_k}d_{Y_k}.\end{aligned}$$

Define $\tilde{X}$ and $\tilde{Y}$ as

$$\begin{aligned}\tilde{X} &\equiv \textstyle\sum_{k=1}^{N} X_k\\ \tilde{Y} &\equiv \textstyle\sum_{k=1}^{N} Y_k.\end{aligned} \tag{5.56}$$

$\tilde{X}$ and $\tilde{Y}$ are implied functions of u and $\mathbf{z}$ so that

$$F(u,\mathbf{z}) = \tilde{X} - j\tilde{Y}$$

and

$$P(u,\mathbf{z}) = \tilde{X}^2 + \tilde{Y}^2.$$

Let $f_{\tilde{X},\tilde{Y}}(\tilde{X},\tilde{Y})$ be the joint probability density function of $\tilde{X}$ and $\tilde{Y}$. Although X_k and

Y_k are dependent, each $(X_k - jY_k)$, $k = \{1, \ldots, N\}$ is independent. So, the characteristic function of $f_{\tilde{X},\tilde{Y}}(\tilde{X}, \tilde{Y})$ can be written as

$$\begin{aligned} \Phi_{\tilde{X},\tilde{Y}}(t_1, t_2) &= \prod_{k=1}^{N} \Phi_{X_k,Y_k}(t_1, t_2) \\ &= \Phi^N_{X_k,Y_k}(t_1, t_2) \end{aligned}$$

Now, $f_{\tilde{X},\tilde{Y}}(\tilde{X}, \tilde{Y})$ can be found by an inverse 2D Fourier transform:

$$\begin{aligned} f_{\tilde{X},\tilde{Y}}(\tilde{X}, \tilde{Y}) &= \frac{1}{4\pi^2} \int_{-\infty}^{\infty} \int_{-\infty}^{\infty} \Phi_{\tilde{X},\tilde{Y}}(t_1, t_2) e^{-j(t_1\tilde{X}+t_2\tilde{Y})} dt_1 dt_2 \\ &= \frac{1}{4\pi^2} \int_{-\infty}^{\infty} \int_{-\infty}^{\infty} \Phi^N_{X_k,Y_k}(t_1, t_2) e^{-j(t_1\tilde{X}+t_2\tilde{Y})} dt_1 dt_2. \end{aligned} \tag{5.57}$$

Since our objective is to find a distribution for $P(u, \mathbf{z})$ and

$$\Pr(P(u, \mathbf{z}) \leq P_0) = \Pr(\sqrt{P(u, \mathbf{z})} \leq \sqrt{P_0}),$$

we re-write $\sqrt{P(u, \mathbf{z})}$ as

$$P = \sqrt{P(u, \mathbf{z})}$$

and find the pdf of P. We can write $\tilde{X}$ and $\tilde{Y}$ as

$$\begin{aligned} \tilde{X} &= P\cos(\psi) \\ \tilde{Y} &= P\sin(\psi) \end{aligned}$$

where ψ is a random variable with uniform distribution

$$f_\psi(\psi) = \frac{1}{2\pi},\ 0 \leq \psi \leq 2\pi.$$

We first find the joint pdf of P and ψ through the transformation:

$$\begin{aligned} f_{P,\psi}(P, \psi) &= |J(P, \psi)| f_{\tilde{X},\tilde{Y}}(\tilde{X}, \tilde{Y}) \\ &= |J(P, \psi)| f_{\tilde{X},\tilde{Y}}(P\cos(\psi), P\sin(\psi)) \end{aligned}$$

where

$$\begin{aligned}
|J(P,\psi)| &= \left|\det\begin{bmatrix} \frac{\partial \tilde{X}}{\partial P} & \frac{\partial \tilde{X}}{\partial \psi} \\ \frac{\partial \tilde{Y}}{\partial P} & \frac{\partial \tilde{Y}}{\partial \psi} \end{bmatrix}\right| \\
&= \left|\det\begin{bmatrix} \frac{\partial P\cos(\psi)}{\partial P} & \frac{\partial P\cos(\psi)}{\partial \psi} \\ \frac{\partial P\sin(\psi)}{\partial P} & \frac{\partial P\sin(\psi)}{\partial \psi} \end{bmatrix}\right| \\
&= |P\cos^2(\psi) + P\sin^2(\psi)| \\
&= |P| \\
&= P
\end{aligned}$$

We now have

$$\begin{aligned}
f_{P,\psi}(P,\psi) &= P f_{\tilde{X},\tilde{Y}}(P\cos(\psi), P\sin(\psi)) \\
&= \frac{P}{4\pi^2}\int_{-\infty}^{\infty}\int_{-\infty}^{\infty} \Phi^N_{X_k,Y_k}(t_1,t_2)e^{-j(t_1\tilde{X}+t_2\tilde{Y})}dt_1dt_2\Big|_{\substack{\tilde{X}=P\cos(\psi)\\ \tilde{Y}=P\sin(\psi)}} \\
&= \frac{P}{4\pi^2}\int_{-\infty}^{\infty}\int_{-\infty}^{\infty} \Phi^N_{X_k,Y_k}(t_1,t_2)e^{-j(t_1P\cos(\psi)+t_2P\sin(\psi))}dt_1dt_2. \qquad (5.58)
\end{aligned}$$

Since P and ψ are independent random variables, we can get the pdf of $\sqrt{P(u,\mathbf{z})}$ as

$$\begin{aligned}
f_P(P) &= \frac{P}{4\pi^2}\int_{-\infty}^{\infty}\int_{-\infty}^{\infty} \Phi^N_{X_k,Y_k}(t_1,t_2)\int_0^{2\pi} e^{-j(t_1P\cos(\psi)+t_2P\sin(\psi))}d\psi dt_1dt_2 \\
&= \frac{P_u}{4\pi^2}\int_{-\infty}^{\infty}\int_{-\infty}^{\infty} \Phi^N_{X_k,Y_k}(t_1,t_2)2\pi J_0\left(P\sqrt{t_1^2+t_2^2}\right)dt_1dt_2 \\
&= \frac{P}{2\pi}\int_{-\infty}^{\infty}\int_{-\infty}^{\infty} \Phi^N_{X_k,Y_k}(t_1,t_2)J_0\left(P\sqrt{t_1^2+t_2^2}\right)dt_1dt_2.
\end{aligned}$$

The function $J_m(x)$ is the bessel function of the first kind.

Fig. 5.14 shows what happens to the pdf, $f_P(P)$, as the number of elements increases. The pdf and its derivatives at $P = 1$ seem to become zero, and the pdf seems to approach a delta function at $P = 0$. We would like to see these effects analytically.

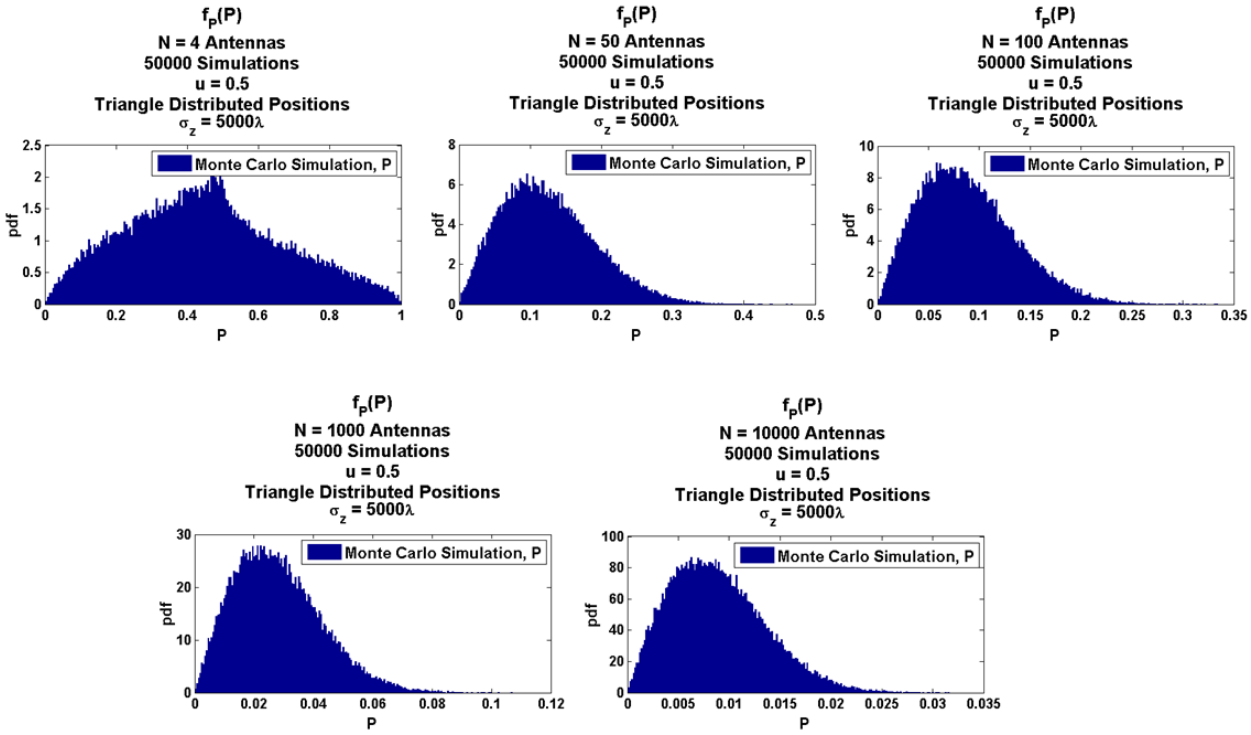

Figure 5.14: *The pdf of the beampattern at $u = 0.5$, $N = 4$ to $N = 10000$ Antennas, Triangle Antenna Position Distribution, Linear Arrays*

We re-write the pdf of $\sqrt{P(u, \mathbf{z})}$ at P as

$$
\begin{aligned}
f_P(P) &= \frac{1}{2\pi} \int_{-\infty}^{\infty} \int_{-\infty}^{\infty} \Phi^N_{X_k,Y_k}(t_1, t_2) P \cdot J_0 \left(P\sqrt{t_1^2 + t_2^2} \right) dt_1 dt_2 \\
&= \frac{1}{2\pi} \int_{-\infty}^{\infty} \int_{-\infty}^{\infty} \left(\int_{-\frac{1}{N}}^{\frac{1}{N}} \int_{-\frac{1}{N}}^{\frac{1}{N}} f_{X_k,Y_k}(X_k, Y_k) e^{j(t_1 X_k + t_2 Y_k)} d_{X_k} d_{Y_k} \right)^N \\
&\quad \times P \cdot J_0 \left(P\sqrt{t_1^2 + t_2^2} \right) dt_1 dt_2 \\
&= \frac{1}{2\pi} \int_{-\frac{1}{N}}^{\frac{1}{N}} \int_{-\frac{1}{N}}^{\frac{1}{N}} \cdots \int_{-\frac{1}{N}}^{\frac{1}{N}} \int_{-\frac{1}{N}}^{\frac{1}{N}} \left(\int_{-\infty}^{\infty} \int_{-\infty}^{\infty} \left(\prod_{k=1}^{N} f_{X_k,Y_k}(X_k, Y_k) \right) \right. \\
&\quad \times e^{jt_1 \sum_{k=1}^{N} X_k} e^{jt_2 \sum_{k=1}^{N} Y_k} \\
&\quad \left. \times P \cdot J_0 \left(P\sqrt{t_1^2 + t_2^2} \right) dt_1\, dt_2 \right) dX_1 \ldots dX_N\, dY_1 \ldots dY_N.
\end{aligned}
$$

We now focus on

$$\int_{-\frac{1}{N}}^{\frac{1}{N}}\int_{-\frac{1}{N}}^{\frac{1}{N}}\cdots\int_{-\frac{1}{N}}^{\frac{1}{N}}\int_{-\frac{1}{N}}^{\frac{1}{N}}\left(\prod_{k=1}^{N}f_{X_k,Y_k}(X_k,Y_k)\right)$$
$$\times\, e^{jt_1\sum_{k=1}^{N}X_k}e^{jt_2\sum_{k=1}^{N}Y_k}\,dX_1\,dY_1\ldots dX_N\,dY_N,\ -\frac{1}{N}\le X_k,Y_k\le\frac{1}{N}.$$

Let

$$\begin{aligned}V_k &\equiv \sqrt{N}X_k\\ W_k &\equiv \sqrt{N}Y_k\end{aligned}$$

so that

$$\begin{aligned}dX_k &= \frac{dV_k}{\sqrt{N}}\\ dY_k &= \frac{dW_k}{\sqrt{N}}\end{aligned}$$

and

$$\begin{aligned}f_{V_k,W_k}(V_k,W_k) &\equiv \left.\frac{f_{X_k,Y_k}(X_k,Y_k)}{|N|}\right|_{\substack{X_k=\frac{V_k}{\sqrt{N}}\\ Y_k=\frac{W_k}{\sqrt{N}}}}\\ &= \frac{f_{X_k,Y_k}\left(\frac{V_k}{\sqrt{N}},\frac{W_k}{\sqrt{N}}\right)}{N},\ -\frac{1}{\sqrt{N}}\le V_k,W_k\le\frac{1}{\sqrt{N}}.\end{aligned}$$

So,

$$f_{X_k,Y_k}\left(\frac{V_k}{\sqrt{N}},\frac{W_k}{\sqrt{N}}\right)=Nf_{V_k,W_k}(V_k,W_k),\ -\frac{1}{\sqrt{N}}\le V_k,W_k\le\frac{1}{\sqrt{N}}.$$

Now,

$$\begin{aligned}
&\int_{-\frac{1}{N}}^{\frac{1}{N}}\int_{-\frac{1}{N}}^{\frac{1}{N}}\cdots\int_{-\frac{1}{N}}^{\frac{1}{N}}\int_{-\frac{1}{N}}^{\frac{1}{N}}\left(\prod_{k=1}^{N}f_{X_k,Y_k}(X_k,Y_k)\right)\\
&\times e^{jt_1\sum_{k=1}^{N}X_k}e^{jt_2\sum_{k=1}^{N}Y_k}\,dX_1\,dY_1\ldots dX_N\,dY_N\\
&=\frac{1}{N^N}\int_{-\frac{1}{\sqrt{N}}}^{\frac{1}{\sqrt{N}}}\int_{-\frac{1}{\sqrt{N}}}^{\frac{1}{\sqrt{N}}}\cdots\int_{-\frac{1}{\sqrt{N}}}^{\frac{1}{\sqrt{N}}}\int_{-\frac{1}{\sqrt{N}}}^{\frac{1}{\sqrt{N}}}\left(\prod_{k=1}^{N}Nf_{V_k,W_k}(V_k,W_k)\right)\\
&\times e^{jt_1\sum_{k=1}^{N}\frac{V_k}{\sqrt{N}}}e^{jt_2\sum_{k=1}^{N}\frac{W_k}{\sqrt{N}}}\,dV_1\,dW_1\ldots dV_N\,dW_N\\
&=\int_{-\frac{1}{\sqrt{N}}}^{\frac{1}{\sqrt{N}}}\int_{-\frac{1}{\sqrt{N}}}^{\frac{1}{\sqrt{N}}}\cdots\int_{-\frac{1}{\sqrt{N}}}^{\frac{1}{\sqrt{N}}}\int_{-\frac{1}{\sqrt{N}}}^{\frac{1}{\sqrt{N}}}\left(\prod_{k=1}^{N}f_{V_k,W_k}(V_k,W_k)\right)\\
&\times e^{jt_1\sum_{k=1}^{N}\frac{V_k}{\sqrt{N}}}e^{jt_2\sum_{k=1}^{N}\frac{W_k}{\sqrt{N}}}\,dV_1\,dW_1\ldots dV_N\,dW_N.
\end{aligned}$$

We focus on

$$\int_{-\frac{1}{\sqrt{N}}}^{\frac{1}{\sqrt{N}}}\int_{-\frac{1}{\sqrt{N}}}^{\frac{1}{\sqrt{N}}}f_{V_k,W_k}(V_k,W_k)e^{jt_1\frac{V_k}{\sqrt{N}}}e^{jt_2\frac{W_k}{\sqrt{N}}}\,dV_k\,dW_k,\ k=\{1,\ldots,N\}$$

We would like to now do a Taylor Series expansion of

$$e^{jt_1\frac{V_k}{\sqrt{N}}}$$

$$e^{jt_2\frac{W_k}{\sqrt{N}}}$$

about $t_1=0$ and $t_2=0$, respectively. We are first interested in the case when N is large, so we only use the first three terms of the Taylor Series expansion.

The Taylor Series expansion of

$$e^{jt_1\frac{V_k}{\sqrt{N}}}$$

about $t_1=0$ is given by

$$e^{jt_1\frac{V_k}{\sqrt{N}}}=1+\frac{jt_1V_k}{\sqrt{N}}-\frac{t_1^2V_k^2}{2N}+O\left(\frac{t_1^3}{N}\right). \tag{5.59}$$

The Taylor Series expansion of

$$e^{jt_2\frac{W_k}{\sqrt{N}}}$$

about $t_2 = 0$ is given by

$$e^{jt_2\frac{V_k}{\sqrt{N}}} = 1 + \frac{jt_2W_k}{\sqrt{N}} - \frac{t_2^2W_k^2}{2N} + O\left(\frac{t_2^3}{N}\right). \tag{5.60}$$

Multiplying Eqs. (5.59) and (5.60), we get

$$\begin{aligned} e^{jt_1\frac{V_k}{\sqrt{N}}}e^{jt_2\frac{W_k}{\sqrt{N}}} &= \left(1 + \frac{jt_1V_k}{\sqrt{N}} - \frac{t_1^2V_k^2}{2N}\right)\left(1 + \frac{jt_2W_k}{\sqrt{N}} - \frac{t_2^2W_k^2}{2N}\right) \\ &= \frac{t_1^2t_2^2V_k^2W_k^2}{4N^2} - \frac{jt_1^2t_2V_k^2W_k}{2N^{\frac{3}{2}}} - \frac{jt_1t_2^2V_kW_k^2}{2N^{\frac{3}{2}}} - \frac{t_1^2V_k^2}{2N} \\ &\quad - \frac{t_1t_2V_kW_k}{N} - \frac{t_2^2W_k^2}{2N} + \frac{jt_1V_k}{\sqrt{N}} + \frac{jt_2W_k}{\sqrt{N}} + 1 \\ &\quad + O\left(\frac{t_1^3}{N^{\frac{3}{2}}}\right) + O\left(\frac{t_2^3}{N^{\frac{3}{2}}}\right). \end{aligned}$$

Now,

$$\begin{aligned} \int_{-\frac{1}{\sqrt{N}}}^{\frac{1}{\sqrt{N}}}\int_{-\frac{1}{\sqrt{N}}}^{\frac{1}{\sqrt{N}}} f_{V_k,W_k}(V_k,W_k)e^{jt_1\frac{V_k}{\sqrt{N}}}e^{jt_2\frac{W_k}{\sqrt{N}}}\,dV_k\,dW_k &= \int_{-\frac{1}{\sqrt{N}}}^{\frac{1}{\sqrt{N}}}\int_{-\frac{1}{\sqrt{N}}}^{\frac{1}{\sqrt{N}}} f_{V_k,W_k}(V_k,W_k)\left(\frac{t_1^2t_2^2V_k^2W_k^2}{4N^2}\right. \\ &\quad - \frac{jt_1^2t_2V_k^2W_k}{2N^{\frac{3}{2}}} - \frac{jt_1t_2^2V_kW_k^2}{2N^{\frac{3}{2}}} - \frac{t_1^2V_k^2}{2N} \\ &\quad - \frac{t_1t_2V_kW_k}{N} - \frac{t_2^2W_k^2}{2N} + \frac{jt_1V_k}{\sqrt{N}} + \frac{jt_2W_k}{\sqrt{N}} \\ &\quad \left. + 1 + O\left(\frac{t_1^3}{N^{\frac{3}{2}}}\right) + O\left(\frac{t_2^3}{N^{\frac{3}{2}}}\right)\right)\,dV_k\,dW_k \\ &\quad , k = \{1,\ldots,N\}. \end{aligned} \tag{5.61}$$

We now find the expectations of each term in Eq. (5.61) using the antenna position distributions. We use the relations

$$\begin{aligned} V_k &= \sqrt{N}X_k = \sqrt{N}\tfrac{1}{N}\cos(\beta uz) = \tfrac{1}{\sqrt{N}}\cos(\beta uz) \\ W_k &= \sqrt{N}Y_k = \sqrt{N}\tfrac{1}{N}\sin(\beta uz) = \tfrac{1}{\sqrt{N}}\sin(\beta uz). \end{aligned}$$

If the pdf of z is an even function, which it is in the cases of uniform, triangle, and Gaussian

distributions, then

$$\begin{aligned} E[V_k^2 W_k] &= 0 \\ E[V_k W_k] &= 0 \\ E[W_k] &= 0. \end{aligned}$$

Let $f_z(z)$ be the pdf of the antenna positions, and let $\hat{f}_z(u)$ be the characteristic function of $f_z(z)$. For the other terms in Eq. (5.61),

$$\begin{aligned} E[V_k] &= \frac{1}{\sqrt{N}} \int_z f_z(z) \cos(\beta u z)\, dz \\ &= \frac{1}{\sqrt{N}} \left(\frac{\hat{f}_z(u) + \hat{f}_z(-u)}{2} \right) \qquad (5.62) \\ E[V_k^2] &= \frac{1}{N} \int_z f_z(z) \cos^2(\beta u z)\, dz \\ &= \frac{1}{N} \left(\int_z f_z(z) \frac{1}{2}\, dz + \int_z f_z(z) \frac{\cos(2u)}{2}\, dz \right) \\ &= \frac{1}{2N} + \frac{1}{N} \left(\frac{\hat{f}_z(2u) + \hat{f}_z(-2u)}{2} \right) \qquad (5.63) \\ E[W_k^2] &= \frac{1}{N} \int_z f_z(z) \sin^2(\beta u z)\, dz \\ &= \frac{1}{N} \left(\int_z f_z(z) \frac{1}{2}\, dz - \int_z f_z(z) \frac{\cos(2u)}{2}\, dz \right) \\ &= \frac{1}{2N} - \frac{1}{N} \left(\frac{\hat{f}_z(2u) + \hat{f}_z(-2u)}{2} \right) \qquad (5.64) \\ E[V_k W_k^2] &= \frac{1}{N^{\frac{3}{2}}} \int_z f_z(z) \cos(\beta u z) \sin^2(\beta u z)\, dz \\ &= \frac{1}{8N^{\frac{3}{2}}} \left(\hat{f}_z(u) + \hat{f}_z(-u) - \hat{f}_z(3u) - \hat{f}_z(-3u) \right) \qquad (5.65) \\ E[V_k^2 W_k^2] &= \frac{1}{N^2} \int_z f_z(z) \cos^2(\beta u z) \sin^2(\beta u z)\, dz \\ &= \frac{1}{8N^2} - \frac{1}{16N^2} \left(\hat{f}_z(4u) + \hat{f}_z(-4u) \right) \qquad (5.66) \end{aligned}$$

The beampattern statistics need to be angle-independent for Extreme Value Theory to be

used, and it is seen in subsection 5.3.4 that this assumption approximately holds if the antenna position variance is large. For large antenna position variance, it was shown through examples in Eqs. (5.25), (5.26), (5.27), (5.28), (5.29), (5.30), (5.31), and (5.32) that

$$\begin{aligned}\int_z f_z(z)\cos(\beta u z) &\sim 0\\ \int_z f_z(z)\cos^2(\beta u z) &\sim \frac{1}{2}\\ \int_z f_z(z)\sin^2(\beta u z) &\sim \frac{1}{2}\end{aligned}$$

or

$$\begin{aligned}\lim_{\sigma_z^2\to\infty}\int_z f_z(z)\cos(\beta u z) &= 0\\ \lim_{\sigma_z^2\to\infty}\int_z f_z(z)\cos^2(\beta u z) &= \frac{1}{2}\\ \lim_{\sigma_z^2\to\infty}\int_z f_z(z)\sin^2(\beta u z) &= \frac{1}{2}\end{aligned} \tag{5.67}$$

where σ_z^2 is the antenna position variance. This angle-independence is also seen to be achieved for large antenna position variance when looking at the examples in Eqs. (5.36), (5.37), (5.38), (5.39), (5.42), (5.43), (5.46), and (5.47). So, the characteristic function with u dependence in Eqs. (5.62), (5.63), and (5.64), (5.65), and (5.66) may be dropped to get

$$\begin{aligned}E[V_k] &\approx 0\\ E[V_k^2] &\approx \frac{1}{2N}\\ E[W_k^2] &\approx \frac{1}{2N}\\ E[V_k W_k^2] &\approx 0\\ E[V_k^2 W_k^2] &\approx \frac{1}{8N^2}.\end{aligned}$$

Let $\sigma^2_{V_k}$ be the variance of V_k. Now,

$$\begin{aligned}
\sigma^2_{V_k} &= E[V_k^2] - E[V_k]^2 \\
&\approx \frac{1}{2N} \\
&\approx E[V_k^2] \\
&\approx E[W_k^2].
\end{aligned}$$

Now,

$$\begin{aligned}
\int_{-\frac{1}{\sqrt{N}}}^{\frac{1}{\sqrt{N}}} \int_{-\frac{1}{\sqrt{N}}}^{\frac{1}{\sqrt{N}}} f_{V_k,W_k}(V_k,W_k) e^{jt_1\frac{V_k}{\sqrt{N}}} e^{jt_2\frac{W_k}{\sqrt{N}}}\, dV_k\, dW_k &\approx \int_{-\frac{1}{\sqrt{N}}}^{\frac{1}{\sqrt{N}}} \int_{-\frac{1}{\sqrt{N}}}^{\frac{1}{\sqrt{N}}} f_{V_k,W_k}(V_k,W_k) \\
&\quad \left(\frac{t_1^2 t_2^2 V_k^2 W_k^2}{4N^2} \right. \\
&\quad -\frac{t_1^2 V_k^2}{2N} - \frac{t_2^2 W_k^2}{2N} + 1 \\
&\quad \left. +O\left(\frac{t_1^3}{N^{\frac{3}{2}}}\right) + O\left(\frac{t_2^3}{N^{\frac{3}{2}}}\right) \right) dV_k\, dW_k \\
&\quad , k = \{1, \ldots, N\} \\
&\approx \frac{t_1^2 t_2^2}{32N^4} - \frac{t_1^2 \sigma^2_{V_k}}{2N} - \frac{t_2^2 \sigma^2_{V_k}}{2N} + 1 \\
&\quad +O\left(\frac{t_1^3}{N^{\frac{3}{2}}}\right) + O\left(\frac{t_2^3}{N^{\frac{3}{2}}}\right) \\
&\quad , k = \{1, \ldots, N\}.
\end{aligned}$$

Now,

$$\begin{aligned}
f_P(P) &= \frac{1}{2\pi}\int_{-\frac{1}{N}}^{\frac{1}{N}}\int_{-\frac{1}{N}}^{\frac{1}{N}}\cdots\int_{-\frac{1}{N}}^{\frac{1}{N}}\int_{-\frac{1}{N}}^{\frac{1}{N}}\left(\int_{-\infty}^{\infty}\int_{-\infty}^{\infty}\left(\prod_{k=1}^{N}f_{X_k,Y_k}(X_k,Y_k)\right)\right.\\
&\quad\times e^{jt_1\sum_{k=1}^{N}X_k}e^{jt_2\sum_{k=1}^{N}Y_k}\\
&\quad\left.\times P\cdot J_0\left(P\sqrt{t_1^2+t_2^2}\right)\,dt_1\,dt_2\right)\,dX_1\ldots dX_N\,dY_1\ldots dY_N\\
&= \frac{1}{2\pi}\int_{-\infty}^{\infty}\int_{-\infty}^{\infty}\left(\int_{-\frac{1}{\sqrt{N}}}^{\frac{1}{\sqrt{N}}}\int_{-\frac{1}{\sqrt{N}}}^{\frac{1}{\sqrt{N}}}\cdots\int_{-\frac{1}{\sqrt{N}}}^{\frac{1}{\sqrt{N}}}\int_{-\frac{1}{\sqrt{N}}}^{\frac{1}{\sqrt{N}}}\left(\prod_{k=1}^{N}f_{V_k,W_k}(V_k,W_k)\right)\right.\\
&\quad\left.\times\, e^{jt_1\sum_{k=1}^{N}\frac{V_k}{\sqrt{N}}}e^{jt_2\sum_{k=1}^{N}\frac{W_k}{\sqrt{N}}}\times dV_1\,dW_1\ldots dV_N\,dW_N\right)\\
&\quad\times P\cdot J_0\left(P\sqrt{t_1^2+t_2^2}\right)\,dt_1\,dt_2\\
&\approx \frac{1}{2\pi}\int_{-\infty}^{\infty}\int_{-\infty}^{\infty}\left(\frac{t_1^2t_2^2}{32N^4}-\frac{t_1^2\sigma_{V_k}^2}{2N}-\frac{t_2^2\sigma_{V_k}^2}{2N}+1\right.\\
&\quad\left.+O\left(\frac{t_1^3}{N^{\frac{3}{2}}}\right)+O\left(\frac{t_2^3}{N^{\frac{3}{2}}}\right)\right)^N\times P\cdot J_0\left(P\sqrt{t_1^2+t_2^2}\right)\,dt_1\,dt_2\\
&\approx \frac{1}{2\pi}\int_{-\infty}^{\infty}\int_{-\infty}^{\infty}\left(1-\frac{(t_1^2+t_2^2)\sigma_{V_k}^2}{2N}+\frac{t_1^2t_2^2}{32N^4}+O\left(\frac{t_1^3}{N^{\frac{3}{2}}}\right)+O\left(\frac{t_2^3}{N^{\frac{3}{2}}}\right)\right)^N\\
&\quad\times P\cdot J_0\left(P\sqrt{t_1^2+t_2^2}\right)\,dt_1\,dt_2.
\end{aligned}$$

Let

$$q=\sqrt{t_1^2+t_2^2}$$

so that

$$\begin{aligned}
t_1 &= q\cos(\theta)\\
t_2 &= q\sin(\theta)
\end{aligned}$$

where

$$0\le\theta\le 2\pi.$$

We now have

$$\begin{aligned}
f_P(P) &\approx \frac{1}{2\pi}\int_{-\infty}^{\infty}\int_{-\infty}^{\infty}\left(1-\frac{(t_1^2+t_2^2)\sigma_{V_k}^2}{2N}+\frac{t_1^2t_2^2}{32N^4}+O\left(\frac{t_1^3}{N^{\frac{3}{2}}}\right)+O\left(\frac{t_2^3}{N^{\frac{3}{2}}}\right)\right)^N \\
&\quad \times P\cdot J_0\left(P\sqrt{t_1^2+t_2^2}\right)\,dt_1\,dt_2 \\
&\approx \frac{1}{2\pi}\int_0^{2\pi}\int_0^{\infty}\left(1-\frac{q^2\sigma_{V_k}^2}{2N}+\frac{q^4\cos^2(\theta)\sin^2(\theta)}{32N^4}+O\left(\frac{q^3\cos^3(\theta)}{N^{\frac{3}{2}}}\right)\right. \\
&\quad \left.+O\left(\frac{q^3\sin^3(\theta)}{N^{\frac{3}{2}}}\right)\right)^N \times Pq\cdot J_0\left(Pq\right)\,dq\,d\theta \\
&\approx \frac{1}{2\pi}\int_0^{2\pi}\int_0^{\infty}\left(1-\frac{q^2\sigma_{V_k}^2}{2N}+\frac{q^4\cos^2(\theta)\sin^2(\theta)}{32N^4}+O\left(\frac{q^3}{N^{\frac{3}{2}}}\right)\right)^N \\
&\quad \times Pq\cdot J_0\left(Pq\right)\,dq\,d\theta \\
&\approx \frac{1}{2\pi}\int_0^{2\pi}\int_0^{\infty}\left(1-\frac{q^2\sigma_{V_k}^2}{2N}+O\left(\frac{q^4}{N^2}\right)\right)^N \times Pq\cdot J_0\left(Pq\right)\,dq\,d\theta \\
&\approx \int_0^{\infty}\left(1-\frac{q^2\sigma_{V_k}^2}{2N}+O\left(\frac{q^4}{N^2}\right)\right)^N \times Pq\cdot J_0\left(Pq\right)\,dq
\end{aligned}$$

Pdf for Large N

Focusing on

$$\left(1-\frac{q^2\sigma_{V_k}^2}{2N}+O\left(\frac{q^4}{N^2}\right)\right)^N,$$

we have

$$\lim_{N\to\infty}\left(1-\frac{q^2\sigma_{V_k}^2}{2N}+O\left(\frac{q^4}{N^2}\right)\right)^N = e^{-\frac{q^2\sigma_{V_k}^2}{2}+O\left(\frac{q^4}{N}\right)}.$$

Now,

$$\begin{aligned}
f_P(P) &\approx \int_0^\infty e^{-\frac{q^2\sigma_{V_k}^2}{2}+O\left(\frac{q^4}{N}\right)} \times Pq \cdot J_0(Pq)\, dq \\
&\approx \int_0^\infty e^{-\frac{q^2\sigma_{V_k}^2}{2}} \times e^{O\left(\frac{q^4}{N}\right)} \times Pq \cdot J_0(Pq)\, dq \\
&\approx \int_0^\infty e^{-\frac{q^2\sigma_{V_k}^2}{2}} \times \left(1+O\left(\frac{q^4}{N}\right)\right) \times Pq \cdot J_0(Pq)\, dq \\
&\approx \int_0^\infty e^{-\frac{q^2\sigma_{V_k}^2}{2}} \times Pq \cdot J_0(Pq)\, dq \\
&\quad + \int_0^\infty e^{-\frac{q^2\sigma_{V_k}^2}{2}} O\left(\frac{q^4}{N}\right) Pq \cdot J_0(Pq)\, dq \\
&\approx \frac{P}{\sigma_{V_k}^2} e^{-\frac{P^2}{2\sigma_{V_k}^2}} + \int_0^\infty e^{-\frac{q^2\sigma_{V_k}^2}{2}} O\left(\frac{q^4}{N}\right) Pq \cdot J_0(Pq)\, dq. \qquad (5.68)
\end{aligned}$$

Since for $P > 0$,

$$\left| e^{-\frac{q^2\sigma_{V_k}^2}{2}} O\left(\frac{q^4}{N}\right) Pq \cdot J_0(Pq) \right| \leq e^{-\frac{q^2\sigma_{V_k}^2}{2}} Pq,\ \forall q \in [0,\infty),$$

and

$$\int_0^\infty e^{-\frac{q^2\sigma_{V_k}^2}{2}} Pq\, dq = \frac{P}{\sigma_{V_k}^2}$$

we have by Lebesgues' Dominated Convergence Theorem,

$$\begin{aligned}
\lim_{N\to\infty} \int_0^\infty e^{-\frac{q^2\sigma_{V_k}^2}{2}} O\left(\frac{q^4}{N}\right) Pq \cdot J_0(Pq) &= \int_0^\infty \lim_{N\to\infty} e^{-\frac{q^2\sigma_{V_k}^2}{2}} O\left(\frac{q^4}{N}\right) Pq \cdot J_0(Pq) \\
&= 0,\ \sigma_{V_k}^2 > 0,\ P > 0.
\end{aligned}$$

Therefore, for large N, we may ignore the term

$$\int_0^\infty e^{-\frac{q^2\sigma_{V_k}^2}{2}} O\left(\frac{q^4}{N}\right) Pq \cdot J_0(Pq)$$

in Eq. (5.68) to get

$$f_P(P) \approx \frac{P}{\sigma_{V_k}^2} e^{-\frac{P^2}{2\sigma_{V_k}^2}}. \qquad (5.69)$$

Since, for arbitrarily large antenna position variance so that there is no dependence on u,

$$\sigma_{V_k}^2 \approx \frac{1}{2N},$$

Now,

$$f_P(P) \approx 2PNe^{-P^2N}. \tag{5.70}$$

Eqs. (5.69) and (5.70) show that for arbitrarily large N, the pdf of the beampattern at each angle u in the sidelobe region is approximately Rayleigh distributed with parameter $\sigma_{V_k}^2 = 1/(2N)$.

We can also show that the distribution of the beampattern at each angle converges to the Rayleigh distribution as N tends to infinity by comparing the characteristic functions of the distributions. Let $f_R(P_0)$ be the pdf of the Rayleigh distribution, or

$$f_R(P_0) = 2P_0Ne^{-P_0^2N},\ 0 < P_0 < \infty. \tag{5.71}$$

Let $\Phi_R(t)$ be the characteristic function of $f_R(P_0)$, or

$$\Phi_R(t) \quad = \quad 1 - \frac{1}{\sqrt{2N}} te^{\frac{t^2}{4N}} \sqrt{\frac{\pi}{2}} \left(-j\text{erf}\left(\frac{jt}{2\sqrt{N}} \right) - j \right) \tag{5.72}$$

where $\text{erf}(x)$ is the error function.

Let $\Phi_P(t)$ be the characteristic function of $f_P(P_0)$, the beampattern distribution at angle u. It is given by

$$\Phi_P(t) \quad = \quad \sum_{l=0}^{\infty} \frac{(jt)^l}{l!} \mu_k' \tag{5.73}$$

where μ'_k is the kth moment of $f_P(P_0)$. The zeroth and first moments are

$$\begin{aligned}
\mu'_0 &= 1 \\
\mu'_1 &= E_{\mathbf{z}}\left[P(u,\mathbf{z})\right] \\
&= E_{\mathbf{z}}\left[F(u,\mathbf{z})F^*(u,\mathbf{z})\right] \\
&= E_{\mathbf{z}}\left[\frac{1}{N}\sum_{k=1}^{N} e^{-j\beta u z_k}\frac{1}{N}\sum_{l=1}^{N} e^{j\beta u z_l}\right] \\
&= \frac{1}{N^2}E_{\mathbf{z}}\left[\sum_{k=1}^{N} 1 + \sum_{k=1}^{N} e^{-j\beta u z_k}\sum_{\substack{l=1\\ l\neq k}}^{N} e^{j\beta u z_l}\right] \\
&= \frac{1}{N} + \frac{1}{N^2}E_{\mathbf{z}}\left[\sum_{k=1}^{N} e^{-j\beta u z_k}\sum_{\substack{l=1\\ l\neq k}}^{N} e^{j\beta u z_l}\right] \\
&= \frac{1}{N} + \frac{1}{N^2}\sum_{k=1}^{N} E_{z_k}\left[e^{-j\beta u z_k}\right]\sum_{\substack{l=1\\ l\neq k}}^{N} E_{z_k}\left[e^{j\beta u z_l}\right] \\
&= \frac{1}{N} + \frac{N(N-1)}{N^2}E_{z_k}\left[e^{-j\beta u z_k}\right] \\
&= \frac{1}{N} + \frac{N-1}{N}E_{z_k}\left[e^{-j\beta u z_k}\right] \\
&= \frac{1}{N} + \left(1-\frac{1}{N}\right)E_{z_k}\left[e^{-j\beta u z_k}\right]. \qquad (5.74)
\end{aligned}$$

In Eq. (5.74), $E_{z_k}\left[e^{-j\beta u z_k}\right]$ is the characteristic function of the antenna position distribution, $f_{z_k}(z_k)$, in u. Therefore,

$$E_{z_k}\left[e^{-j\beta u z_k}\right] < \infty \,\forall u.$$

The second moment is

$$
\begin{aligned}
\mu_2' &= E_{\mathbf{z}}\left[P^2(u,\mathbf{z})\right] \\
&= E_{\mathbf{z}}\left[F^2(u,\mathbf{z})\left(F^*(u,\mathbf{z})\right)^2\right] \\
&= \frac{1}{N^4}E_{\mathbf{z}}\left[\left(\sum_{k_1=1}^{N}1+\sum_{k_1=1}^{N}e^{-j\beta u z_{k_1}}\sum_{\substack{l_1=1\\ l_1\neq k_1}}^{N}e^{j\beta u z_{l_1}}\right)\right. \\
&\quad \left.\times\left(\sum_{k_2=1}^{N}1+\sum_{k_2=1}^{N}e^{-j\beta u z_{k_2}}\sum_{\substack{l_2=1\\ l_2\neq k_2}}^{N}e^{j\beta u z_{l_2}}\right)\right] \\
&= \frac{1}{N^4}\left(N^2+2NE_{\mathbf{z}}\left[\sum_{k_1=1}^{N}e^{-j\beta u z_{k_1}}\sum_{\substack{l_1=1\\ l_1\neq k_1}}^{N}e^{j\beta u z_{l_1}}\right]\right. \\
&\quad \left.+E_{\mathbf{z}}\left[\sum_{k_1=1}^{N}e^{-j\beta u z_{k_1}}\sum_{\substack{l_1=1\\ l_1\neq k_1}}^{N}e^{j\beta u z_{l_1}}\sum_{k_2=1}^{N}e^{-j\beta u z_{k_2}}\sum_{\substack{l_2=1\\ l_2\neq k_2}}^{N}e^{j\beta u z_{l_2}}\right]\right) \\
&= \frac{1}{N^2}+\frac{2N(N-1)}{N^3}E_{z_k}\left[e^{-j\beta u z_k}\right] \\
&\quad +\frac{1}{N^4}E_{\mathbf{z}}\left[\sum_{k_1=1}^{N}e^{-j\beta u z_{k_1}}\sum_{\substack{l_1=1\\ l_1\neq k_1}}^{N}e^{j\beta u z_{l_1}}\sum_{k_2=1}^{N}e^{-j\beta u z_{k_2}}\sum_{\substack{l_2=1\\ l_2\neq k_2}}^{N}e^{j\beta u z_{l_2}}\right] \\
&= \frac{1}{N^2}+\frac{2N(N-1)}{N^3}E_{z_k}\left[e^{-j\beta u z_k}\right]+\frac{1}{N^4}E_{\mathbf{z}}\left[\sum_{k=1}^{N-1}\sum_{l=k+1}^{N}\left(e^{-j\beta u(z_k-z_l)}+e^{j\beta u(z_k-z_l)}\right)\right. \\
&\quad \left.\times\sum_{k=1}^{N-1}\sum_{l=k+1}^{N}\left(e^{-j\beta u(z_k-z_l)}+e^{j\beta u(z_k-z_l)}\right)\right] \\
&= \frac{1}{N^2}+\frac{2N(N-1)}{N^3}E_{z_k}\left[e^{-j\beta u z_k}\right] \\
&\quad +\frac{1}{N^4}E_{\mathbf{z}}\left[N(N-1)+\sum_{k=1}^{N-1}\sum_{l=k+1}^{N}\left(e^{-j2\beta u(z_k-z_l)}+e^{j2\beta u(z_k-z_l)}\right)\right. \\
&\quad +\sum_{k_1=1}^{N-1}\sum_{l_1=k_1+1}^{N}\left(e^{-j\beta u(z_{k_1}-z_{l_1})}+e^{j\beta u(z_{k_1}-z_{l_1})}\right) \\
&\quad \left.\times\sum_{\substack{k_1,l_1\neq k_2,l_2}}^{\sum_{k_2=1}^{N-1}\sum_{l_2=k_2+1}^{N}}\left(e^{-j\beta u(z_{k_2}-z_{l_2})}+e^{j\beta u(z_{k_2}-z_{l_2})}\right)\right]. \qquad (5.75)
\end{aligned}
$$

Continuing from Eq. (5.75),

$$\begin{aligned}\mu_2' &= \frac{1}{N^2} + \frac{2N(N-1)}{N^3} E_{z_k}\left[e^{-j\beta u z_k}\right] + \frac{N(N-1)}{N^4} + \frac{2N(N-1)}{N^4} E_{z_k}[e^{-j2\beta u z_k}]^2 \\ &\quad + E_{\mathbf{z}}\left[\sum_{k_1=1}^{N-1}\sum_{l_1=k_1+1}^{N}\left(e^{-j\beta u(z_{k_1}-z_{l_1})} + e^{j\beta u(z_{k_1}-z_{l_1})}\right)\right. \\ &\quad \left.\times \sum_{\substack{k_1,l_1\neq k_2,l_2}}^{\sum_{k_2=1}^{N-1}\sum_{l_2=k_2+1}^{N}}\left(e^{-j\beta u(z_{k_2}-z_{l_2})} + e^{j\beta u(z_{k_2}-z_{l_2})}\right)\right]. \end{aligned} \tag{5.76}$$

Since $E_{z_k}\left[e^{-j\beta u z_k}\right]$ is the characteristic function of the antenna position distribution, in Eq. (5.76), for all u,

$$\begin{aligned}&E_{\mathbf{z}}\left[\sum_{k_1=1}^{N-1}\sum_{l_1=k_1+1}^{N}\left(e^{-j\beta u(z_{k_1}-z_{l_1})} + e^{j\beta u(z_{k_1}-z_{l_1})}\right)\right. \\ &\left.\times \sum_{\substack{k_1,l_1\neq k_2,l_2}}^{\sum_{k_2=1}^{N-1}\sum_{l_2=k_2+1}^{N}}\left(e^{-j\beta u(z_{k_2}-z_{l_2})} + e^{j\beta u(z_{k_2}-z_{l_2})}\right)\right] < \infty.\end{aligned}$$

As discussed in subsection 5.3.4 and in Eq. (5.67) of subsection 5.3.7, for large antenna position variance, the beampattern statistics become approximately angle-independent. The characteristic function of the antenna position distribution obtains the properties of Eq. (4.28) which is also given in Eq. (5.33) and here as

$$E_{z_k}\left[e^{-j\beta u z_k}\right] \approx 0 \,\forall u.$$

Now, the first three moments of the beampattern at each angle are given by

$$\mu_0' = 1 \tag{5.77}$$

$$\mu_1' \approx \frac{1}{N} \tag{5.78}$$

$$\begin{aligned}\mu_2' &\approx \frac{1}{N^2} + \frac{N(N-1)}{N^4} \\ &\approx \frac{2}{N^2} - \frac{1}{N^3}\end{aligned} \tag{5.79}$$

From Ref. [79],

$$|\Phi_P(t) - \mu_0' - j\mu_1' t| \leq \mu_2' \frac{|t|^2}{2}$$

and approximately

$$\left|\Phi_P(t) - 1 - \frac{jt}{N}\right| \leq \frac{|t|^2}{N^2} - \frac{|t|^2}{2N^3}. \tag{5.80}$$

The finite bound given in Eq. (5.80) implies that the higher moments of the beampattern at each angle are decreasing. Now, approximately,

$$\begin{aligned} \lim\sup_{N\to\infty} \left|\Phi_P(t) - 1 - \frac{jt}{N}\right| &\leq \lim\sup_{N\to\infty} \frac{|t|^2}{N^2} - \frac{|t|^2}{2N^3} \\ \left|\lim_{N\to\infty} \Phi_P(t) - 1\right| &\leq 0. \end{aligned} \tag{5.81}$$

Eq. (5.81) implies that all the moments other than the zeroth moment converge to zero as N, the number of elements, increases.

Taking the ratio of the Rayleigh distribution characteristic function in Eq. (5.72) to the true characteristic function of the beampattern at angle u, we have

$$\frac{\Phi_R(t)}{\Phi_P(t)} = \frac{1 - \frac{1}{\sqrt{2N}} t e^{\frac{t^2}{4N}} \sqrt{\frac{\pi}{2}} \left(-j\mathrm{erf}\left(\frac{jt}{2\sqrt{N}}\right) - j\right)}{\sum_{l=0}^{\infty} \frac{(jt)^l}{l!} \mu_k'}.$$

As the number of elements increases for a fixed number of beampattern samples,

$$\begin{aligned}
\lim_{N\to\infty} \frac{\Phi_R(t)}{\Phi_P(t)} &= \lim_{N\to\infty} \frac{1 - \frac{1}{\sqrt{2N}} t e^{\frac{t^2}{4N}} \sqrt{\frac{\pi}{2}} \left(-j\mathrm{erf}\left(\frac{jt}{2\sqrt{N}} \right) - j \right)}{\sum_{l=0}^{\infty} \frac{(jt)^l}{l!} \mu_k'} \\
&= \lim_{N\to\infty} \frac{1 - \frac{1}{\sqrt{2N}} t e^{\frac{t^2}{4N}} \sqrt{\frac{\pi}{2}} \left(-j\mathrm{erf}\left(\frac{jt}{2\sqrt{N}} \right) - j \right)}{\mu_0' + jt\mu_1' - \frac{1}{2}t^2\mu_2'} \\
&\approx \lim_{N\to\infty} \frac{1 - \frac{1}{\sqrt{2N}} t e^{\frac{t^2}{4N}} \sqrt{\frac{\pi}{2}} \left(-j\mathrm{erf}\left(\frac{jt}{2\sqrt{N}} \right) - j \right)}{1 + \frac{jt}{N} - \frac{t^2}{N^2} - \frac{t^2}{2N^3}} \\
&\approx \frac{1}{1} \\
&\approx 1. \qquad (5.82)
\end{aligned}$$

The reason why the ratio in Eq. (5.82) is approximate and not exact is because the characteristic function of the element position distribution is assumed to be approximately zero for all $u \neq 1$ which occurs for large antenna array apertures.

Eq. (5.82) also implies the following result when taking the difference of the characteristic functions:

$$\begin{aligned}
\left| \int_{-\infty}^{\infty} e^{jtP_0} (f_P(P_0) - f_R(P_0))\, dP_0 \right| &= \left| \int_{-\infty}^{\infty} e^{jtP_0} f_P(P_0)\, dP_0 - \int_{-\infty}^{\infty} e^{jtP_0} f_R(P_0)\, dP_0 \right| \\
&= \left| \int_{0}^{1} e^{jtP_0} f_P(P_0)\, dP_0 - \int_{-\infty}^{\infty} e^{jtP_0} f_R(P_0)\, dP_0 \right| \\
&= |\Phi_P(t) - \Phi_R(t)|\,.
\end{aligned}$$

From Eqs. (5.72) and (5.73), we have

$$|\Phi_P(t) - \Phi_R(t)| = \left| \sum_{l=0}^{\infty} \frac{(jt)^l}{l!} \mu_k' - 1 + \frac{1}{\sqrt{2N}} t e^{\frac{t^2}{4N}} \sqrt{\frac{\pi}{2}} \left(-j\mathrm{erf}\left(\frac{jt}{2\sqrt{N}} \right) - j \right) \right|.$$

From Eq. (5.80) the higher moments of the beampattern at each angle are reducing. Assuming the angle-dependency of the moments to be approximately zero, which is reasonable for large

array apertures, we have

$$\begin{aligned}
|\Phi_P(t) - \Phi_R(t)| &\approx \left|1 + (jt)\mu_1' - \frac{t^2}{2}\mu_2' - 1 + \frac{1}{\sqrt{2N}} t e^{\frac{t^2}{4N}} \sqrt{\frac{\pi}{2}} \left(-j\text{erf}\left(\frac{jt}{2\sqrt{N}}\right) - j\right)\right| \\
&\approx \left|1 + (jt)\frac{1}{N} - \frac{t^2}{2}\left(\frac{2}{N^2} - \frac{1}{N^3}\right) - 1 \right. \\
&\quad \left. + \frac{1}{\sqrt{2N}} t e^{\frac{t^2}{4N}} \sqrt{\frac{\pi}{2}} \left(-j\text{erf}\left(\frac{jt}{2\sqrt{N}}\right) - j\right)\right|.
\end{aligned}$$

Now, as the number of elements increases,

$$\begin{aligned}
\lim_{N\to\infty} |\Phi_P(t) - \Phi_R(t)| &\approx \lim_{N\to\infty} \left|1 + (jt)\frac{1}{N} - \frac{t^2}{2}\left(\frac{2}{N^2} - \frac{1}{N^3}\right) - 1 \right. \\
&\quad \left. + \frac{1}{\sqrt{2N}} t e^{\frac{t^2}{4N}} \sqrt{\frac{\pi}{2}} \left(-j\text{erf}\left(\frac{jt}{2\sqrt{N}}\right) - j\right)\right| \\
&\approx |1 - 1| \\
&\approx 0. \qquad (5.83)
\end{aligned}$$

Just as Eq. (5.82) shows the ratio of the characteristic functions of the Rayleigh distribution and the beampattern distribution at each angle converges to one, Eq. (5.83) shows that their difference converges to approximately zero. The approximation occurs because samples of the beampattern are assumed to be angle-independent. In real-world implementation, with increasing number of elements, the position variance of the elements will also have to increase. With the increasing position variance, the approximations of the moments in Eqs. (5.77), (5.78), and (5.79) become more exact, and the approximations in Eqs. (5.82) and (5.83) become more exact.

Eqs. (5.82) and (5.83) show that

$$\lim_{N\to\infty} \Phi_R(t) \approx 1 \qquad (5.84)$$

$$\lim_{N\to\infty} \Phi_P(t) \approx 1. \qquad (5.85)$$

Theorem 2.4 in Ref. [80] says, "for each $n \geq 1$, let $\phi_n(t)$ be the characteristic function of

a probability distribution α_n. Assume that $\lim_{n\to\infty}\phi_n(t) \equiv \phi(t)$ exists for each t and $\phi(t)$ is continuous at $t = 0$. Then $\phi(t)$ is the characteristic function of some probability distribution α and $\alpha_n \Rightarrow \alpha$." In Ref. [80], the notation "$\alpha_n \Rightarrow \alpha$" means that the probability distribution α_n converges weakly to a probability distribution α.

By Theorem 2.4 in Ref. [80] and Eqs. (5.84) and (5.85), the characteristic functions of the Rayleigh distribution and the true beampattern distribution converge approximately to a characteristic function that is 1. The pdf associated with such a characteristic function is given by

$$\begin{aligned}\frac{1}{2\pi}\int_{-\infty}^{\infty} e^{-jtx}\,dt &= \frac{1}{2\pi}\int_{-\infty}^{\infty} e^{-j2\pi\frac{t}{2\pi}x}\,dt \\ &= \int_{-\infty}^{\infty} e^{-j2\pi t'x}\,dt' \\ &= \delta(x). \end{aligned} \tag{5.86}$$

By Theorem 2.4 in Ref. [80],

$$\lim_{N\to\infty} f_P(x) \approx \delta(x) \tag{5.87}$$

$$\lim_{N\to\infty} f_R(x) \approx \delta(x) \tag{5.88}$$

with the convergence being a weak convergence. The result in Eq. (5.87) explains what is happening in the simulations of Fig. 5.14 where the beampattern distributions at each angle seem to become more like delta functions with increasing number of elements. From Eqs. (5.87) and (5.88), we have

$$\begin{aligned}\lim_{N\to\infty} f_P(x) &\approx \lim_{N\to\infty} f_R(x) \\ &\approx \lim_{N\to\infty} 2xNe^{-x^2N} \end{aligned} \tag{5.89}$$

and

$$\begin{aligned}\lim_{N\to\infty}|f_P(x)-f_R(x)| &\approx \lim_{N\to\infty}\left|f_P(x)-2xNe^{-x^2N}\right| \\ &\approx 0. \end{aligned} \tag{5.90}$$

From Eqs. (5.89) and (5.90), we again state

$$f_P(P_0)\approx 2P_0Ne^{-P_0^2N} \tag{5.91}$$

for large N but the convergence to the Rayleigh distribution as the number of elements, N, increases is a weak convergence.

Domain of Attraction of Weibull Distribution as Number of Elements Tends to Infinity

By Eq. (5.86), as the number of elements increases, we have the weak convergence

$$\begin{aligned}\lim_{N\to\infty} f_P(1) &\approx \delta(1) \\ &= 0 \end{aligned} \tag{5.92}$$

$$\begin{aligned}\lim_{N\to\infty} f_P^{(n)}(1) &\approx \lim_{N\to\infty}\frac{d^{(n)}\delta(x)}{dx^n}\, n>0 \\ &= 0\, n>0. \end{aligned} \tag{5.93}$$

Now, with $F_P(x)$ being the cdf of $P=\sqrt{P(u,\mathbf{z})}$, the condition for it to be in the domain of attraction of the Weibull distribution is

$$\begin{aligned}\lim_{t\to\infty}\frac{1-F_P\left(1-\frac{1}{tx}\right)}{1-F_P\left(1-\frac{1}{t}\right)} &= \lim_{t\to\infty}\frac{f_P^{(n)}\left(1-\frac{1}{tx}\right)}{f_P^{(n)}\left(1-\frac{1}{t}\right)}\frac{1}{x^n} \\ &= \frac{f_P^{(n)}(1)}{f_P^{(n)}(1)}\frac{1}{x^{n+1}} \\ &= \frac{1}{x^{n+1}} \end{aligned}$$

where $f_P^{(n)}(1)$ is the first finite non-zero derivative of $f_P(x)$ at $x = 1$. From Eqs. (5.92) and (5.93), $f_P(x)$ and all its derivatives at $x = 1$ converge weakly to approximately zero as N tends to infinity. Therefore, as N tends to infinity, the first non-zero derivative weakly converges to occur at an infinite derivative of $f_P(x)$, or

$$\lim_{N\to\infty} n = \infty.$$

From Ref. [59], if the cdf of the beampattern, $F_P(x)$, is in the domain of attraction of the Weibull distribution, then

$$\Pr(P_{\max} \leq P_0) = \begin{cases} 1 & \text{if } P_0 \geq a_M \\ e^{-\left(-\frac{P_0 - a_M}{b_M}\right)^{\alpha}} & \text{if } P_0 < a_M \end{cases}$$

where α is given in Eq. (5.53) and

$$\begin{aligned} a_M &= \sup\{x : F_P(x) < 1\} \\ b_M &= a_M - \inf\left\{x : 1 - F_P(x) \leq \frac{1}{M}\right\}. \end{aligned}$$

As N tends to infinity

$$\lim_{N\to\infty} F_P(x) = \lim_{N\to\infty} \int_0^x f_P(x)\, dx.$$

Since

$$|f_P(x)| \leq \max_x f_P(x)$$

and

$$\int_0^x \max_x f_P(x)\, dx = x \max_x f_P(x) < \infty,\ x < \infty,$$

we have by Lebesgue's Dominated Convergence Theorem,

$$\begin{aligned}\lim_{N\to\infty} F_P(x) &= \lim_{N\to\infty}\int_0^x f_P(x)\,dx \\ &= \int_0^x \lim_{N\to\infty} f_P(x)\,dx \\ &\approx \int_0^x \delta(x)\,dx \\ &\approx 1,\ x<\infty.\end{aligned}$$

Therefore, under weak convergence,

$$\begin{aligned}a_M &= 1 \\ \lim_{N\to\infty} b_M &\approx 1 \\ \lim_{N\to\infty}\alpha &= \lim_{N\to\infty}(n+1)=\infty.\end{aligned}$$

In the asymptotic limit of a large number of antennas, the distribution of the peak sidelobe level is with weak convergence approximately Weibull distributed with parameters $a_M = 1$, $b_M \approx 1$, and $\alpha = \infty$. In the asymptotic limit of a large antenna position variance, the approximation becomes exact with $b_M = 1$.

Pdf for arbitrary Number of Elements, N, including $N < 10$

For any arbitrary N, the Taylor Series approximation must be taken out to higher order terms, and the pdf of P is

$$\begin{aligned}f_P(P) \approx \frac{1}{2\pi}\int_{-\infty}^{\infty}\int_{-\infty}^{\infty}&\left(1+\frac{t_1^2t_2^2}{32N^4}-\frac{t_1^2\sigma_{V_k}^2}{2N}-\frac{t_2^2\sigma_{V_k}^2}{2N}+O\left(\frac{t_1^3}{N}\right)+O\left(\frac{t_2^3}{N}\right)+t_1O\left(\frac{t_2^3}{N}\right)\right. \\ &\left.+t_1^2O\left(\frac{t_2^3}{N}\right)\right)^N \times P\cdot J_0\left(P\sqrt{t_1^2+t_2^2}\right)\,dt_1\,dt_2.\end{aligned}$$

Since

$$\int_z f_z(z)\cos^n(\beta uz)\sin^{2m+1}(\beta uz) = 0,\ n=\{0,1,2,\ldots\},\ m=\{0,1,2,\ldots\}$$

and, for an arbitrarily large antenna position variance,

$$\int_z f_z(z)\cos^{2n+1}(\beta uz)\sin^m(\beta uz) \approx 0,\ n=\{0,1,2,\ldots\},\ m=\{0,1,2,\ldots\},$$

where $f_z(z)$ is an even antenna position distribution, only the terms with $t_1^{2n}t_2^{2m}$, $n=\{0,1,2,\ldots\}$, $m=\{0,1,2,\ldots\}$ will appear in the Taylor Series expansion of

$$\begin{aligned}\int_{-\frac{1}{\sqrt{N}}}^{\frac{1}{\sqrt{N}}}\int_{-\frac{1}{\sqrt{N}}}^{\frac{1}{\sqrt{N}}} f_{V_k,W_k}(V_k,W_k)e^{jt_1\frac{V_k}{\sqrt{N}}}e^{jt_2\frac{W_k}{\sqrt{N}}}\,dV_k\,dW_k &\approx \sum_{n=0}^{\infty}\sum_{m=0}^{\infty}\frac{j^{2n+2m}t_1^{2n}t_2^{2m}E\left[V_k^{2m}W_k^{2n}\right]}{(2n)!(2m)!N^{n+m}}\\ &\approx \sum_{n=0}^{\infty}\sum_{m=0}^{\infty}(-1)^{n+m}\frac{t_1^{2n}t_2^{2m}E\left[V_k^{2m}W_k^{2n}\right]}{(2n)!(2m)!N^{n+m}}\\ &\quad ,k=\{1,\ldots,N\}.\end{aligned}$$

So, the pdf becomes

$$\begin{aligned}f_P(P) &\approx \frac{1}{2\pi}\int_{-\infty}^{\infty}\int_{-\infty}^{\infty}\left(\sum_{n=0}^{\infty}\sum_{m=0}^{\infty}(-1)^{n+m}\frac{t_1^{2n}t_2^{2m}E\left[V_k^{2m}W_k^{2n}\right]}{(2n)!(2m)!N^{n+m}}\right)^N\\ &\quad\times P\cdot J_0\left(P\sqrt{t_1^2+t_2^2}\right)\,dt_1\,dt_2.\end{aligned}$$

Keeping

$$\begin{aligned}t_1 &= q\cos(\theta)\\ t_2 &= q\sin(\theta)\end{aligned}$$

where

$$0\le\theta\le 2\pi,$$

we have

$$\begin{aligned}f_P(P) &\approx \frac{1}{2\pi}\int_0^{2\pi}\int_0^{\infty}\left(\sum_{n=0}^{\infty}\sum_{m=0}^{\infty}(-1)^{n+m}\frac{q^{2(n+m)}\cos^{2n}(\theta)\sin^{2m}(\theta)E\left[V_k^{2m}W_k^{2n}\right]}{(2n)!(2m)!N^{n+m}}\right)^N\\ &\quad\times P\cdot J_0\left(Pq\right)q\,dq\,d\theta.\end{aligned}\tag{5.94}$$

We rewrite the approximate distribution as

$$f_P(P) \approx \sum_{k=1}^{\infty} \frac{1}{2\pi} \int_0^{2\pi} \int_0^{\infty} q^{2a_k} f_k(\theta) \times P \cdot J_0(Pq)\, q\, dq\, d\theta \tag{5.95}$$

In Eq. (5.95), each $f_k(\theta)$ is a function of θ. For each a_k, $a_k \in \mathbb{Z}^0$, the set of non-negative integers. Each term in the infinite sum of Eq. (5.95) is the Hankel transform of order 0 of q^{2a_k}. The Hankel transform of each q^{2a_k} will be valid if

$$\int_0^{\infty} |q^{2a_k}| q^{1/2}\, dq < \infty. \tag{5.96}$$

Eq. (5.96) does not hold for $a_k \in \mathbb{Z}^0$. Therefore, integrating over q is not the best way to proceed, and another method must be found to analytically show Weibull distribution convergence of the peak sidelobe level distribution. We finding another approach to subsequent research.

5.3.8 Domain of Attraction to Gumbel Distribution for $N \geq 10$

It was shown that cdf of Eq. (5.94) is with weak convergence in the domain of attraction of the Weibull distribution as N and the antenna position variance tend to infinity with parameters

$$\begin{aligned} a_M &= 1 \\ \lim_{\substack{\sigma_z^2 \to \infty \\ N \to \infty}} b_M &= 1 \\ \lim_{\substack{\sigma_z^2 \to \infty \\ N \to \infty}} \alpha_M &= \infty. \end{aligned} \tag{5.97}$$

For arbitrarily large antenna position variance, Eq. (5.94) is with weak convergence approximately in the Weibull domain of attraction with the parameters in Eq. (5.97). However, evaluating the Weibull distribution conditions for arbitrary N and σ_z^2 is not trivial.

With weak convergence as N becomes large, we use Eq. (5.91) or

$$f_P(P) \approx 2N \times P e^{-P^2 \times N}. \tag{5.98}$$

In Fig. 5.15, we plot Eq. (5.98) along with the simulated pdf of the beampattern. We see, that at least for large N, even for $N = 10$, the approximation in Eq. (5.98) seems accurate.

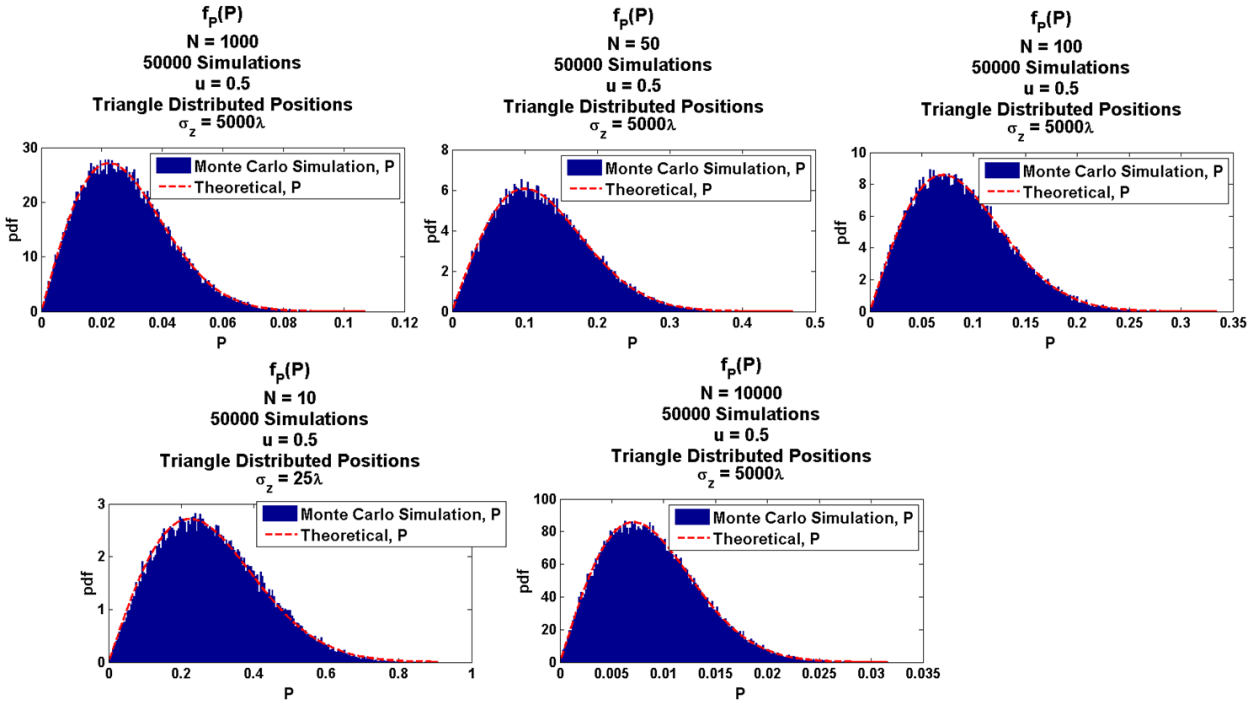

Figure 5.15: *Eq.* (5.98) *is fitted to simulated beampattern pdf.*

The cdf from Eq. (5.98) is given by

$$\begin{aligned} F_P(P) &\approx \int_0^P 2N \times P' e^{-P'^2 \times N} dP' \\ &\approx 1 - e^{-P^2 N}. \end{aligned} \tag{5.99}$$

We see that the cdf is one at $P = \infty$. Note that Eq. (5.99) is the same distribution one would get if the calculation proceeded by assuming the quadrature components of the beampattern are approximately Gaussian distributed. Due to the approximations made, Eq. (5.98) will not give the correct parameters when testing for domain of attraction to Weibull. However,

to see if it is in the domain of attraction of the Gumbel distribution, we have

$$\begin{aligned} A(z) &= \frac{P\int_z^\infty e^{-t^2N}dt}{ze^{-z^2N}} \\ &= \frac{\sqrt{\pi}e^{Nz^2}\text{erfc}\left(\sqrt{N}z\right)}{2\sqrt{N}z} \end{aligned}$$

and

$$\begin{aligned} \lim_{z\to\infty}\frac{1-F_P(z+zA(z)x)}{1-F(z)} &= \lim_{z\to\infty} e^{Nz^2-N\left(\frac{\sqrt{\pi}xe^{Nz^2}\text{erfc}(\sqrt{N}z)}{2\sqrt{N}}+z\right)^2} \\ &= e^{-x}. \end{aligned}$$

Therefore, when N, the number of antennas, is large, the distribution of the beampattern, $P=\sqrt{P(u,\mathbf{z})}$ is weakly in the domain of attraction of the Gumbel distribution. Therefore, the peak sidelobe level distribution weakly converges to the Gumbel distribution.

5.3.9 Domain of Attraction to Weibull Distribution for $N < 10$

Although it was shown that cdf of Eq. (5.94) is with weak convergence in the domain of attraction of the Weibull distribution as N and σ_z^2 tend to infinity with parameters

$$\begin{aligned} a_M &= 1 \\ \lim_{\substack{\sigma_z^2\to\infty \\ N\to\infty}} b_M &= 1 \\ \lim_{\substack{\sigma_z^2\to\infty \\ N\to\infty}} \alpha_M &= \infty, \end{aligned}$$

showing the domain of attraction for $N < 10$ is not trivial. When $N < 10$, the approximations made for large N will begin to cause significant error, especially if the array is sparse. We see through simulations that the Weibull distribution does seem to match well to the simulated peak sidelobe level pdf. Figs. 5.16, 5.17, 5.18, 5.19, 5.20, 5.21 show this match to the Weibull distribution for $N = 4$ to $N = 9$. Similar pdfs are given for each N if the antenna position variance, σ_z^2, is changed or a different antenna position distribution is used.

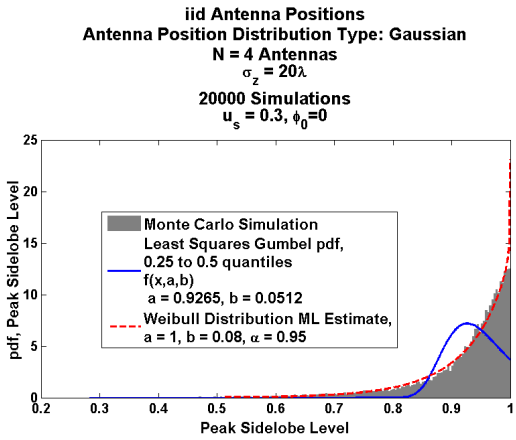

Figure 5.16: *Simulated pdf with $N = 4$ fitted to Weibull and Gumbel distribution estimates*

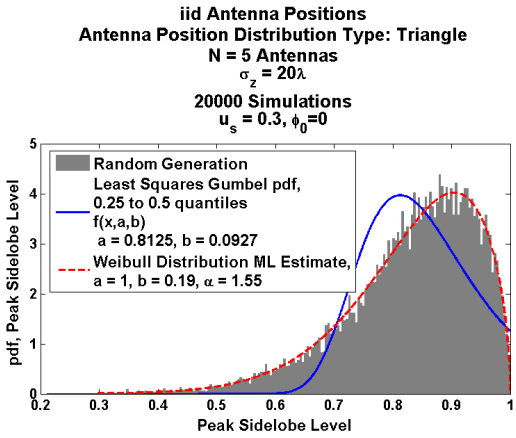

Figure 5.17: *Simulated pdf with $N = 5$ fitted to Weibull and Gumbel distribution estimates*

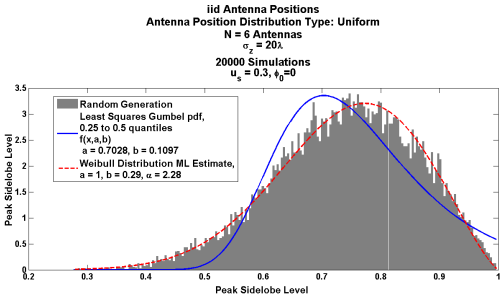

Figure 5.18: *Simulated pdf with $N = 6$ fitted to Weibull and Gumbel distribution estimates*

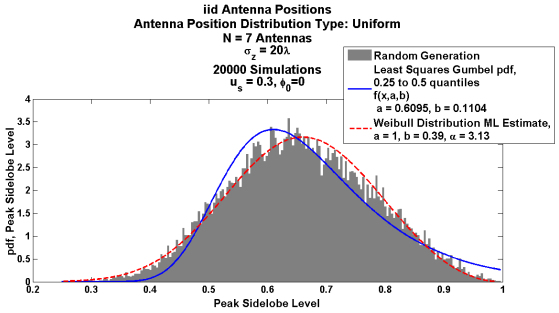

Figure 5.19: *Simulated pdf with $N = 7$ fitted to Weibull and Gumbel distribution estimates*

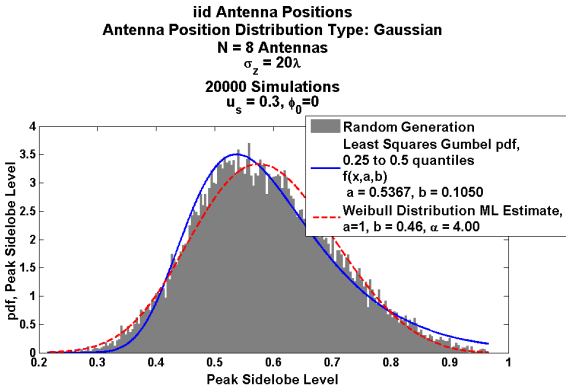

Figure 5.20: *Simulated pdf with $N = 8$ fitted to Weibull and Gumbel distribution estimates*

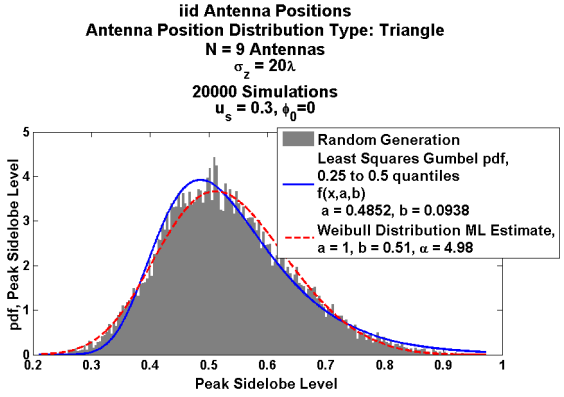

Figure 5.21: *Simulated pdf with $N = 9$ fitted to Weibull and Gumbel distribution estimates*

5.3.10 $N = 2$ and $N = 3$ Antenna Elements

If there are only two antenna elements, then grating lobes are guaranteed to occur if the distance between the antennas is greater than the wavelength, λ. If distances are to be kept

less than the wavelength, then the antenna position variances will need to be small. A small variance will cause the independent and identically distributed condition for Extreme Value Theory to not hold.

If $N = 3$, then there is still a high chance for grating lobes to occur with large antenna position variance. The samples of the beampattern taken with Extreme Value Theory do not account for an increase in grating lobes as aperture increases. Taking more samples will correct for this omission to some extent, but then there will be more samples with strong dependence and Extreme Value Theory will become less accurate.

5.3.11 Calculating Gumbel Distribution Parameters

From Eq. (5.4), the Gumbel distribution is given by

$$\Pr(P_{\max} \leq P_0) = e^{-e^{-\frac{P_0 - a_M}{b_M}}}, \; -\infty < P_0 < \infty.$$

From Ref. [59], the values of a_M and b_M are given by

$$a_M = \inf\left\{x : 1 - F(x) \leq \frac{1}{M}\right\}$$

and

$$b_M = a_M A(a_M).$$

From Ref. [81], these values for a_M and b_M gives the optimal rate of pointwise convergence to the Gumbel distribution. With the cdf in Eq. (5.99),

$$\begin{aligned} b_M &= \frac{1}{N} \\ a_M &= \frac{\log(M)}{N}. \end{aligned}$$

Comparing Simulated Values of b_M to Theoretical Values

Least squares estimates of b_M and a_M can be made from Monte Carlo simulations of the beampattern maximum in the sidelobe region. In Tables 5.1, 5.2, 5.3, 5.4, 5.5, and 5.6 we see that the least squares estimates for b_M are close to the theoretical $1/N$. The elements in the tables show the average b_M estimate taken from 20 Monte Carlo simulations with the particular antenna position distribution and standard deviation. The variances of the estimates are not shown because they were small. We see that the estimates begin to decrease and become less accurate as the position variance increases. However, for large N, the diminishing accuracy of the estimates seems to be less pronounced.

Table 5.1: *Least Squares Estimate for b_M for different antenna position distribution types (Triangle, Uniform, Gaussian); $N = 10$; $u_s = 0.3$, $\phi_0 = 0$; Theoretical $b_M = 0.1$; Each table element shows average b_M estimates averaged over 20 simulations*

σ_z	Triangle	Uniform	Gaussian
5λ	0.0961	0.0970	0.0959
15λ	0.0888	0.0885	0.0889
25λ	0.0847	0.0847	0.0850
50λ	0.0799	0.0802	0.0804
100λ	0.0757	0.0751	0.0761
200λ	0.0700	0.0696	0.0699
400λ	0.0631	0.0629	0.0636
800λ	0.0562	0.0559	0.0568

Simulated Number of Samples

Least squares estimates of a_M may also be given, but we are more interested in the value of M, the number of samples taken of the beampattern. Working with the simulations whose estimates of b_M are close to the theoretical $1/N$, we use the least squares estimates of a_M to

Table 5.2: *Least Squares Estimate for b_M for different antenna position distribution types (Triangle, Uniform, Gaussian); $N = 30$; $u_s = 0.3$, $\phi_0 = 0$; Theoretical $b_M = 0.0333$; Each table element shows average b_M estimates averaged over 20 simulations*

σ_z	Triangle	Uniform	Gaussian
15λ	0.0344	0.0348	0.0344
25λ	0.0338	0.0341	0.0339
50λ	0.0331	0.0333	0.0333
100λ	0.0325	0.0326	0.327
200λ	0.0318	0.0317	0.0318
400λ	0.0312	0.0312	0.0311
800λ	0.0307	0.0306	0.0306

Table 5.3: *Least Squares Estimate for b_M for different antenna position distribution types (Triangle, Uniform, Gaussian); $N = 50$; $u_s = 0.3$, $\phi_0 = 0$; Theoretical $b_M = 0.02$; Each table element shows average b_M estimates averaged over 20 simulations*

σ_z	Triangle	Uniform	Gaussian
25λ	0.0209	0.0211	0.0209
50λ	0.0206	0.0207	0.0205
100λ	0.0205	0.0203	0.0203
200λ	0.0200	0.0201	0.0201
400λ	0.0197	0.0198	0.0198
800λ	0.0195	0.0195	0.0194

Table 5.4: *Least Squares Estimate for b_M for different antenna position distribution types (Triangle, Uniform, Gaussian); $N = 100$; $u_s = 0.3$, $\phi_0 = 0$; Theoretical $b_M = 0.01$; Each table element shows average b_M estimates averaged over 20 simulations*

σ_z	Triangle	Uniform	Gaussian
50λ	0.0106	0.0106	0.0106
100λ	0.0105	0.0105	0.0104
200λ	0.0104	0.0104	0.0104
400λ	0.0103	0.0102	0.0103
800λ	0.0102	0.0102	0.0101

Table 5.5: *Least Squares Estimate for b_M for different antenna position distribution types (Triangle, Uniform, Gaussian); $N = 200$; $u_s = 0.3$, $\phi_0 = 0$; Theoretical $b_M = 0.005$; Each table element shows average b_M estimates averaged over 20 simulations*

σ_z	Triangle	Uniform	Gaussian
100λ	0.0053	0.0053	0.0053
200λ	0.0053	0.0053	0.0053
400λ	0.0052	0.0052	0.0052
800λ	0.0052	0.0052	0.0052

Table 5.6: *Least Squares Estimate for b_M for different antenna position distribution types (Triangle, Uniform, Gaussian); $N = 400$; $u_s = 0.3$, $\phi_0 = 0$; Theoretical $b_M = 0.0025$; Each table element shows average b_M estimates averaged over 20 simulations*

σ_z	Triangle	Uniform	Gaussian
200λ	0.0027	0.0027	0.0027
400λ	0.0026	0.0026	0.0026
800λ	0.0026	0.0026	0.0026

find estimates of M by

$$\hat{M} = e^{\hat{a}_M \cdot N}.$$

These estimates are given in Tables 5.7, 5.8, 5.9, 5.10, 5.11, and 5.12.

Table 5.7: *Estimate for M for different antenna position distribution types (Triangle, Uniform, Gaussian); $N = 10$; $u_s = 0.3$, $\phi_0 = 0$; Each table element shows average $\hat{M}$ averaged over 20 simulations plus/minus the standard deviation found from the sample variance of $\hat{M}$ from 20 simulations.*

σ_z	Triangle	Uniform	Gaussian
5λ	22.75± 0.30	22.68± 0.24	22.53± 0.23

Table 5.8: *Estimate for M for different antenna position distribution types (Triangle, Uniform, Gaussian); $N = 30$; $u_s = 0.3$, $\phi_0 = 0$; Each table element shows average $\hat{M}$ averaged over 20 simulations plus/minus the standard deviation found from the sample variance of $\hat{M}$ from 20 simulations.*

σ_z	Triangle	Uniform	Gaussian
15λ	74.67±0.94	73.46±1.01	74.34 ± 1.12
25λ	125.54 ± 1.11	124.49 ± 1.56	125.51 ± 1.78
50λ	253.72 ± 3.54	250.74 ± 2.36	251.94 ± 3.64
100λ	505.82 ± 6.08	500.75 ± 6.15	500.22 ± 5.45

Table 5.9: *Estimate for M for different antenna position distribution types (Triangle, Uniform, Gaussian); $N = 50$; $u_s = 0.3$, $\phi_0 = 0$; Each table element shows average $\hat{M}$ averaged over 20 simulations plus/minus the standard deviation found from the sample variance of $\hat{M}$ from 20 simulations.*

σ_z	Triangle	Uniform	Gaussian
25λ	131.43 ± 1.41	129.70 ± 1.74	131.43 ± 1.72
50λ	271.67 ± 4.38	268.61 ± 3.30	270.90 ± 2.34
100λ	552.78 ± 6.15	551.58 ± 5.98	549.15 ± 6.04
200λ	1117.58 ± 10.31	1110.39 ± 13.90	1108.61 ± 11.22
400λ	2231.18 ± 25.56	2232.85 ± 33.33	2214.24 ± 28.95
800λ	4441.58 ± 59.62	4434.81 ± 51.51	4412.94 ± 46.97

Table 5.10: *Estimate for M for different antenna position distribution types (Triangle, Uniform, Gaussian); $N = 100$; $u_s = 0.3$, $\phi_0 = 0$; Each table element shows average $\hat{M}$ averaged over 20 simulations plus/minus the standard deviation found from the sample variance of $\hat{M}$ from 20 simulations.*

σ_z	Triangle	Uniform	Gaussian
50λ	285.26 ± 3.00	282.76 ± 2.77	283.85 ± 3.68
100λ	589.92 ± 5.68	590.91 ± 6.02	591.20 ± 7.75
200λ	1217.43 ± 15.10	1215.45 ± 15.82	1214.21 ± 15.05
400λ	2494.99 ± 26.66	2505.04 ± 33.19	2494.22 ± 25.29
800λ	5074.41 ± 68.44	5119.35 ± 60.48	5076.33 ± 49.27

Table 5.11: *Estimate for M for different antenna position distribution types (Triangle, Uniform, Gaussian); $N = 200$; $u_s = 0.3$, $\phi_0 = 0$; Each table element shows average $\hat{M}$ averaged over 20 simulations plus/minus the standard deviation found from the sample variance of $\hat{M}$ from 20 simulations.*

σ_z	Triangle	Uniform	Gaussian
100λ	615.81 ± 7.56	606.36 ± 6.34	611.42 ± 6.31
200λ	1275.97 ± 16.80	1271.05 ± 18.23	1278.57 ± 13.73
400λ	2652.24 ± 35.55	2638.01 ± 26.87	2650.27 ± 33.44
800λ	5486.01 ± 75.24	5453.06 ± 57.05	5463.65 ± 86.44

Table 5.12: *Estimate for M for different antenna position distribution types (Triangle, Uniform, Gaussian); $N = 400$; $u_s = 0.3$, $\phi_0 = 0$; Each table element shows average $\hat{M}$ averaged over 20 simulations plus/minus the standard deviation found from the sample variance of $\hat{M}$ from 20 simulations.*

σ_z	Triangle	Uniform	Gaussian
200λ	1304.28 ± 14.67	1293.90 ± 19.27	1303.47 ± 15.01
400λ	2721.23 ± 37.00	2704.59 ± 35.62	2720.34 ± 43.62
800λ	5661.24 ± 88.36	5628.70 ± 70.61	5621.73 ± 64.63

Simulated Correlations Among Sampled Points

Each estimate of M in Tables 5.7, 5.8, 5.9, 5.10, 5.11, and 5.12 can give the estimated sampling interval as

$$\frac{u_{\max} - u_s}{\hat{M} - 1}. \tag{5.100}$$

For the estimates given in the tables, $u_{\max} = 1$ and $u_s = 0.3$.

We would now like to know if a specific correlation of two points of the beampattern separated by the sampling interval in Eq. (5.100) will require the number of samples M estimated by the previous tables. If a specific correlation is needed, then it can be used to determine M.

The radiation pattern correlation given by Eq. (5.48), which is repeated here:

$$Corr[F(u_1, \mathbf{z}), F^*(u_2, \mathbf{z})] = \frac{[COV[X_1), X_2] + COV[Y_1, Y_2]]}{\sqrt{VAR[X_1] + VAR[Y_1]}\sqrt{VAR[X_2] + VAR[Y_2]}},$$

can be expressed in terms of $u_1 - u_2$ by

$$\rho_F(u_1 - u_2) \equiv Corr[F(u_1, \mathbf{z}), F^*(u_2, \mathbf{z})].$$

Figs. 5.4 and 5.5 given previously plot $\rho_F(u_1 - u_2)$. We use these plots and determine the value of

$$\rho_F\left(\frac{u_{\max} - u_s}{\hat{\hat{M}} - 1}\right). \tag{5.101}$$

Here $\hat{\hat{M}}$ is the average estimate of M from 20 simulations. If $\sigma_{\hat{M}}$ is the sampled standard deviation of the estimate of M of, then

$$\hat{M} = \hat{\hat{M}} \pm \sigma_{\hat{M}}. \tag{5.102}$$

Eq. (5.102) is the value of each element in Tables 5.7, 5.8, 5.9, 5.10, 5.11, and 5.12.

In Fig. 5.22, we again plot $\rho_F(u_1 - u_2)$ and mark where it crosses Eq. (5.101), which for the case of $N = 50$ triangle distributed antenna positions with standard deviation $\sigma_z = 50\lambda$ is close to 0.7105.

In Tables 5.13, 5.14, 5.15, 5.16, 5.17, and 5.18, we see the correlations corresponding to Eq. (5.101) for the different antenna array geometries. The correlations seem close across antenna position distributions. As the standard deviation, σ_z, increases, the correlations seem to increase steadily. They also seem to increase with N, but $N = 200$ and $N = 400$ seem to have the same correlation values for given σ_z. These tables indicate that EVT chooses the sampling interval even if there is high correlation between samples. Also, these tables may be used a s guide in choosing M, but the tables do not seem to suggest an analytical way to find M.

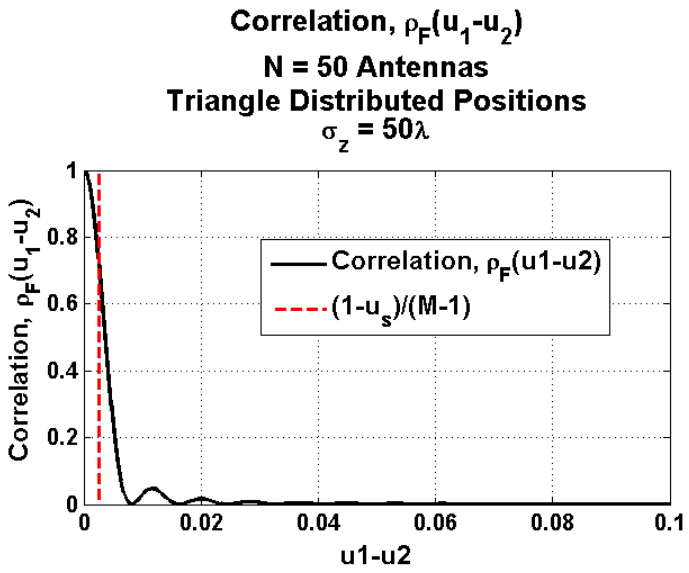

Figure 5.22: *Correlation among beampattern points at u_1 and u_2. Dashed red line indicates where correlation is equal to sampling interval from Eq.* (5.100).

Table 5.13: *Correlation with sampling interval given by Eq.* (5.101) *for different antenna position distribution types (Triangle, Uniform, Gaussian); $N = 10$*

σ_z	Triangle	Uniform	Gaussian
5λ	0.5827	0.5617	0.5998

Table 5.14: *Correlation with sampling interval given by Eq.* (5.101) *for different antenna position distribution types (Triangle, Uniform, Gaussian); $N = 30$*

σ_z	Triangle	Uniform	Gaussian
15λ	0.6581	0.6446	0.6697
25λ	0.6662	0.6534	0.6772
50λ	0.6743	0.6621	0.6848
100λ	0.6736	0.6614	0.6842

5.3.12 Upcrossing Method vs. Extreme Value Theory for Large Number of Elements

When $N > 200$, we may use the upcrossing method with Gaussian approximation of the beampattern quadrature components may be used to calculate the peak sidelobe level distri-

Table 5.15: *Correlation with sampling interval given by Eq.* (5.101) *for different antenna position distribution types (Triangle, Uniform, Gaussian);* $N = 50$

σ_z	Triangle	Uniform	Gaussian
25λ	0.6915	0.6807	0.7009
50λ	0.7106	0.7011	0.7189
100λ	0.7201	0.7113	0.7278
200λ	0.7257	0.7173	0.7332
400λ	0.7251	0.7166	0.7326
800λ	0.7230	0.7143	0.7306

Table 5.16: *Correlation with sampling interval given by Eq.* (5.101) *for different antenna position distribution types (Triangle, Uniform, Gaussian);* $N = 100$

σ_z	Triangle	Uniform	Gaussian
50λ	0.6841	0.6727	0.6939
100λ	0.7504	0.7435	0.7566
200λ	0.7644	0.7583	0.7699
400λ	0.7747	0.7691	0.7797
800λ	0.7815	0.7763	0.7862

Table 5.17: *Correlation with sampling interval given by Eq.* (5.101) *for different antenna position distribution types (Triangle, Uniform, Gaussian);* $N = 200$

σ_z	Triangle	Uniform	Gaussian
100λ	0.7689	0.7631	0.7742
200λ	0.7835	0.7784	0.7882
400λ	0.7983	0.7939	0.8024
800λ	0.8105	0.8066	0.8140

bution. Since this approach begins to break down when $N < 200$, the Gumbel distribution approximation with Extreme Value Theory may be used for $10 \leq N \leq 200$. The tables in Appendix C give a finer breakdown of the correlations for different N from $N = 10$ to $N = 200$. One may use these tables to estimate M and then estimate the Gumbel distribution

Table 5.18: *Correlation with sampling interval given by Eq.* (5.101) *for different antenna position distribution types (Triangle, Uniform, Gaussian);* $N = 400$

σ_z	Triangle	Uniform	Gaussian
200λ	0.7920	0.7873	0.7963
400λ	0.8076	0.8036	0.8113
800λ	0.8211	0.8177	0.8243

parameter a_M.

5.3.13 Calculating Weibull Distribution Parameters

From Ref. [59], if the cumulative distribution function of the beampattern, $F_P(P_0)$, is in the domain of attraction of the Weibull distribution, then

$$\Pr(P_{\max} \leq P_0) = \begin{cases} 1 & \text{if } P_0 \geq a_M \\ e^{-\left(-\frac{P_0 - a_M}{b_M}\right)^{\alpha}} & \text{if } P_0 < a_M \end{cases}$$

where

$$\begin{aligned} a_M &= \sup\{x : F_P(x) < 1\} \\ b_M &= a_M - \inf\left\{x : 1 - F_P(x) \leq \frac{1}{M}\right\}. \end{aligned}$$

and α is given by

$$\lim_{t\to\infty} \frac{1 - F_P\left(a_M - \frac{1}{tx}\right)}{1 - F_P\left(a_M - \frac{1}{t}\right)} = x^{-\alpha},\ \alpha > 0,\ x > 0$$

It is clear that

$$a_M = 1.$$

Since the distribution for the beampattern in terms of just P is not trivial to find for arbitrary N and σ_z^2, the following graphs show values of b_M and α for $N = 4$ to $N = 9$ over antenna position standard deviation, σ_z. Figs. 5.23, 5.24, 5.25, 5.26, 5.27, and 5.28 can be used to

estimate the Weibull distribution parameters for $N = 4$ to $N = 9$.

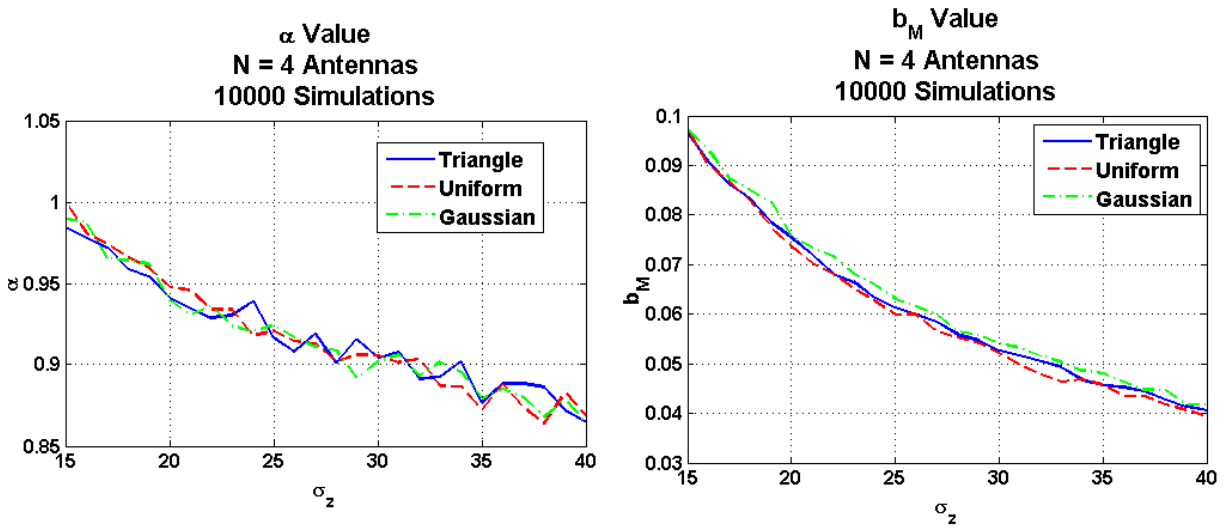

Figure 5.23: *Maximum Likelihood Estimates of α and b_M as a function of antenna position variance for Weibull distribution domain of attraction for $N = 4$ triangle, uniform, and Gaussian distributed antenna positions.*

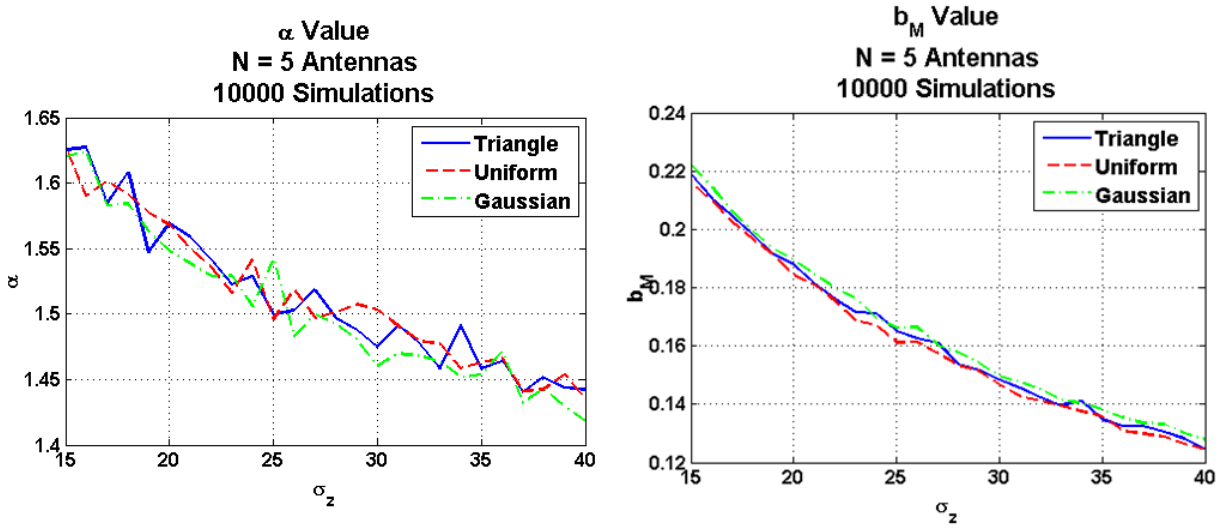

Figure 5.24: *Maximum Likelihood Estimates of α and b_M as a function of antenna position variance for Weibull distribution domain of attraction for $N = 5$ triangle, uniform, and Gaussian distributed antenna positions.*

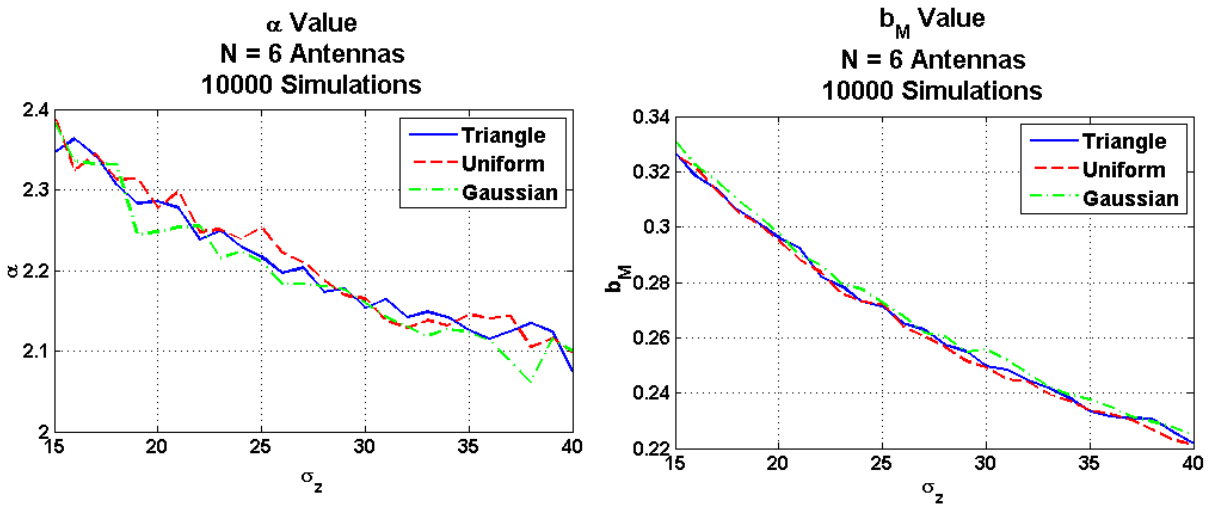

Figure 5.25: *Maximum Likelihood Estimates of α and b_M as a function of antenna position variance for Weibull distribution domain of attraction for $N = 6$ triangle, uniform, and Gaussian distributed antenna positions.*

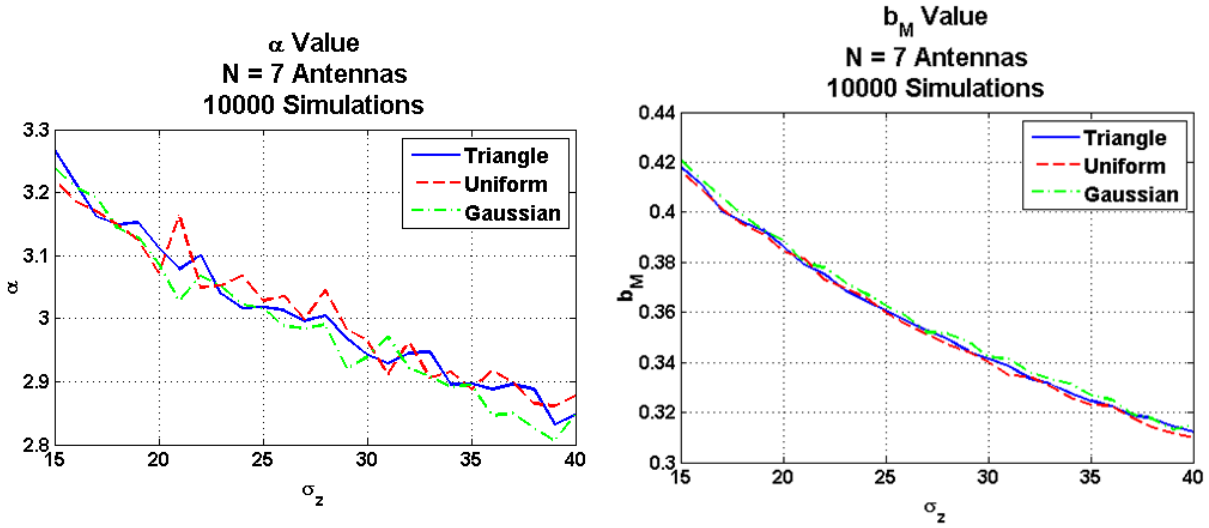

Figure 5.26: *Maximum Likelihood Estimates of α and b_M as a function of antenna position variance for Weibull distribution domain of attraction for $N = 7$ triangle, uniform, and Gaussian distributed antenna positions.*

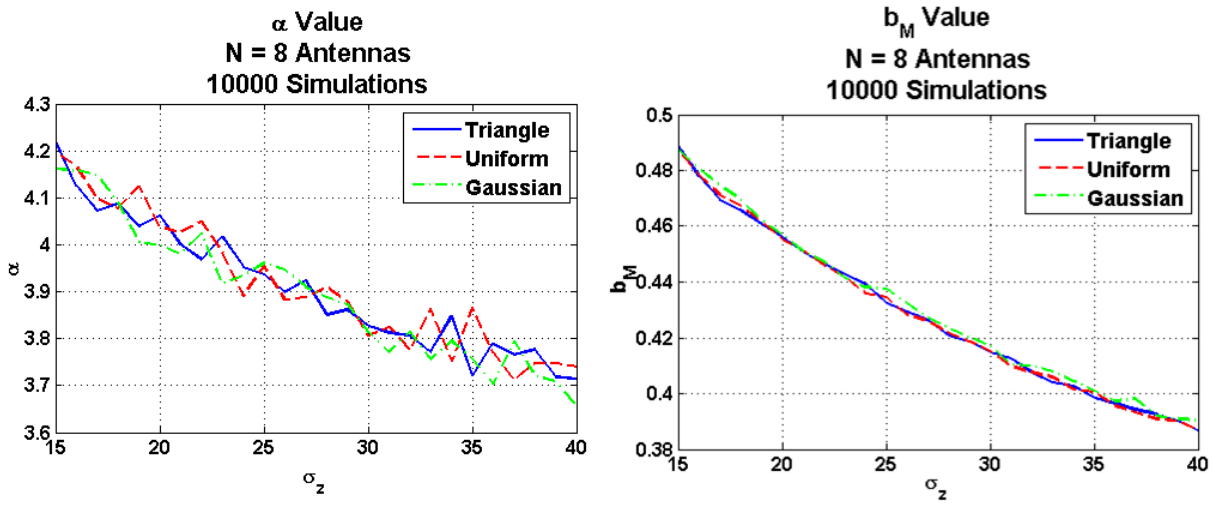

Figure 5.27: *Maximum Likelihood Estimates of α and b_M as a function of antenna position variance for Weibull distribution domain of attraction for $N = 8$ triangle, uniform, and Gaussian distributed antenna positions.*

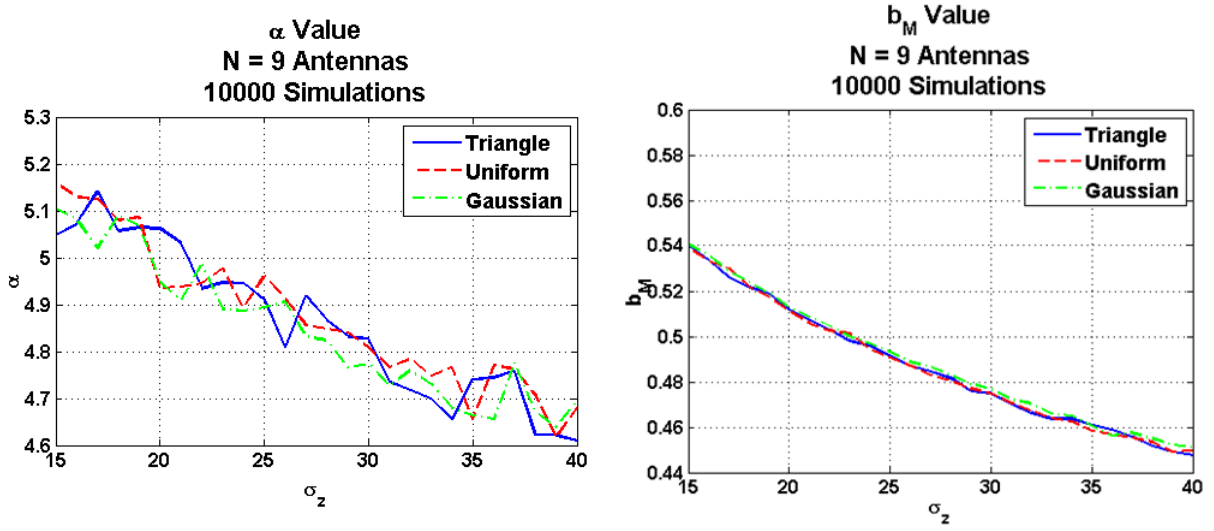

Figure 5.28: *Maximum Likelihood Estimates of α and b_M as a function of antenna position variance for Weibull distribution domain of attraction for $N = 9$ triangle, uniform, and Gaussian distributed antenna positions.*

Chapter 6

Dependent Antenna Positions/Radars

6.1 Correlated Antenna Positions with Radars

When the antenna positions in $\mathbf{z}$ are correlated, evaluating the peak sidelobe level distribution becomes more difficult. This situation arises when working with radars which have a transmit array and a receive array of elements.

Let there be a receive array with N_r antenna elements having location/phase center vector $\mathbf{r} = [r_1, r_2, \ldots, r_{N_r}]$ whose elements are independent and identically distributed (iid). Let there also be a transmit array with N_t antenna elements has location/phase center vector $\mathbf{t} = [t_1, t_2, \ldots, t_{N_t}]$ whose elements are also iid.

Transforming a transmitter array and receiver array pair into a system with one transmitter (or receiver) array and a single receiving (or transmitting) element simplifies finding the distribution of maximum sidelobe peaks for radar. This transformation occurs by convolving functions of the transmitter and receiver array positions[32]. The node locations of the resulting convolution produce a virtual transmitting (or receiving) array. Having the virtual array transmit to (or receive from) a single radiating element is equivalent to the operation of the transmitter array and receiver array pair. Fig. 6.1 illustrates the transformation to a

virtual array. The number of elements in the virtual array is $N_r \cdot N_t$.

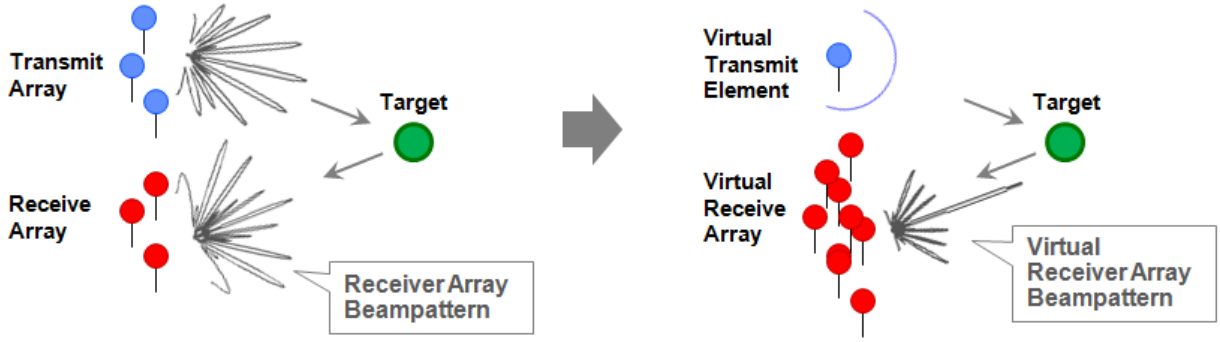

Figure 6.1: *Transformation of receive and transmit array radar pair to virtual receive array and single transmitting element.*

With the virtual antenna array elements having positions $\mathbf{z} = \{z_1, z_2, \ldots, z_{N_r \cdot N_t}\}$, the virtual antenna array factor is given by

$$\begin{aligned} F(u, \mathbf{z}) &= F(u, \mathbf{r}) F(u, \mathbf{t}) \\ &= \frac{1}{N_r \cdot N_t} \sum_{k_r=1}^{N_r} e^{-j\beta u \cdot r_{k_r}} \sum_{k_t=1}^{N_t} e^{-j\beta u \cdot t_{k_t}} \\ &= \frac{1}{N_r \cdot N_t} \sum_{k_r=1}^{N_r} \sum_{k_t=1}^{N_t} e^{-j\beta u \cdot r_{k_r}} e^{-j\beta u \cdot t_{k_t}} \\ &= \frac{1}{N_r \cdot N_t} \sum_{k_r=1}^{N_r} \sum_{k_t=1}^{N_t} e^{-j\beta u \cdot (r_{k_r} + t_{k_t})} \\ &= \frac{1}{N_r \cdot N_t} \sum_{k=1}^{N_r \cdot N_t} e^{-j\beta u \cdot z_k}. \end{aligned}$$

Here,

$$z_k = r_{k_r} + t_{k_t}$$

where $k_r = 1, 2, ..., K_r$, $k_t = 1, 2, ..., K_t$, and $k = 1, 2, ..., N_r \cdot N_t$. The probability density function (pdf) of each z_k is found by convolving the pdfs of r_{k_r} and t_{k_t}. Now, the z_k are correlated, and it is difficult to find the peak sidelobe level using the pdf of z_k.

We may write the beampattern of the virtual array as

$$\begin{aligned} P(u,\mathbf{z}) &= F(u,\mathbf{z})F^*(u,\mathbf{z}) \\ &= F(u,\mathbf{r})F(u,\mathbf{t})F^*(u,\mathbf{r})F^*(u,\mathbf{t}) \\ &= P(u,\mathbf{r})P(u,\mathbf{t}) \\ &= \frac{1}{N_r \cdot N_t}(X^2(u,\mathbf{r}) + Y^2(u,\mathbf{r}))(X^2(u,\mathbf{t}) + Y^2(u,\mathbf{t})) \end{aligned} \tag{6.1}$$

where

$$\begin{aligned} X(u,\mathbf{r}) &= \frac{1}{\sqrt{N}}\sum_{k=1}^{N_r}\cos(r_k\beta u) \\ Y(u,\mathbf{r}) &= \frac{1}{\sqrt{N}}\sum_{k=1}^{N_r}\sin(r_k\beta u) \\ X(u,\mathbf{r}) &= \frac{1}{\sqrt{N}}\sum_{k=1}^{N_t}\cos(t_k\beta u) \\ Y(u,\mathbf{r}) &= \frac{1}{\sqrt{N}}\sum_{k=1}^{N_t}\sin(t_k\beta u). \end{aligned}$$

Since

$$\begin{aligned} P(u,\mathbf{z}) &= \sqrt{P(u,\mathbf{z})} \\ P(u,\mathbf{r}) &= \sqrt{P(u,\mathbf{r})} \\ P(u,\mathbf{t}) &= \sqrt{P(u,\mathbf{t})}, \end{aligned}$$

We can find the probability distribution of

$$\sqrt{P(u,\mathbf{z})} = \sqrt{P(u,\mathbf{r})}\sqrt{P(u,\mathbf{t})}.$$

We may approximate, with weak convergence as N_r and N_t become large, the cumulative

distribution functions of $\sqrt{P(u,\mathbf{r})}$ and $\sqrt{P(u,\mathbf{t})}$ by Eq. (5.99), which is given again here as

$$\Pr[\sqrt{P(u,\mathbf{r})} \leq \sqrt{P_0}] \approx 1 - e^{-P_0 N_r} \tag{6.2}$$

$$\Pr[\sqrt{P(u,\mathbf{t})} \leq \sqrt{P_0}] \approx 1 - e^{-P_0 N_t}. \tag{6.3}$$

The pdfs of $\sqrt{P(u,\mathbf{r})}$ and $\sqrt{P(u,\mathbf{t})}$ are given by

$$\begin{aligned} f_{P(u,r)}(N_r P_0) &\approx e^{-N_r P_0} \\ f_{P(u,t)}(N_t P_0) &\approx e^{-N_t P_0}, \end{aligned}$$

respectively. Let

$$Z(u) = [\sqrt{P(u,\mathbf{r})}][\sqrt{P(u,\mathbf{t})}].$$

Using the fact that $\sqrt{P(u,\mathbf{r})}$ and $\sqrt{P(u,\mathbf{t})}$ are independent, the pdf of $Z(u)$ can be found as

$$\begin{aligned} f_{Z(u)}(y) &= \int_0^\infty \frac{1}{x} f_{P(u,r)}(x) f_{P(u,t)}\left(\frac{y}{x}\right) dx \\ &\approx \int_0^\infty \frac{1}{x} e^{-x} e^{-\frac{y}{x}} dx \\ &\approx 2K_0[2\sqrt{y}]. \end{aligned}$$

where $K_n(x)$ is the modified bessel function of the second kind. From Eq. (6.1),

$$\sqrt{P(u,\mathbf{z})} = \frac{Z(u)}{N_r \cdot N_t}.$$

The cdf of $P(u,\mathbf{z})$ can now be found as

$$\begin{aligned} \Pr[P(u,\mathbf{z}) \leq P_0] &= \Pr[\sqrt{P(u,\mathbf{z})}] \\ &= \Pr[Z(u) \leq N_t \cdot N_r P_0] \\ &\approx \int_0^{Nt \cdot N_r P_0} 2K_0[2\sqrt{y}] dy \\ &\approx 1 - 2\sqrt{Nr \cdot N_t P_0} K_1[2\sqrt{Nr \cdot N_t P_0}] \end{aligned} \tag{6.4}$$

When applying Eq. (6.4) to the EVT distributions, it is difficult to verify whether it is in

the domain of attraction of the Frechet or Gumbel distributions. The peak sidelobe level distribution may also be found by

$$\begin{aligned}\Pr(P(u,\mathbf{z}) \leq P_0 \forall u \in \mathcal{S}) &\approx \Pr(P_{\max} \leq P_0) \\ &\approx \left(1 - 2\sqrt{Nr \cdot N_t P_0} K_1[2\sqrt{Nr \cdot N_t P_0}]\right)^M\end{aligned}$$

where $P_{\max}$ is defined in Eq. (5.49) and M is the number of beampattern samples.

6.1.1 Co-located Tx/Rx Antennas

If the transmit and receive antennas are co-located so that $\mathbf{r} = \mathbf{t}$ and $N_r = N_t$, then

$$\begin{aligned}P(u,\mathbf{z}) &= P^2(u,\mathbf{r}) \\ &= \frac{1}{N_r^2}\left(X^2(u,\mathbf{r}) + Y^2(u,\mathbf{r})\right)^2\end{aligned}$$

and

$$\Pr(P(u,\mathbf{z}) \leq P_0) = \Pr(\left(X^2(u,\mathbf{r}) + Y^2(u,\mathbf{r})\right)^2 \leq N_r^2 P_0).$$

If we make the approximation that $X(u,\mathbf{z})$ and $Y(u,\mathbf{z})$ are approximately Gaussian distributed, then the distribution of $P(u,\mathbf{z})$ is the square of an exponential distribution. Letting

$$Z(u) = [X^2(u,\mathbf{r}) + Y^2(u,\mathbf{r})]^2.$$

The pdf of $Z(u)$ can be found as

$$\begin{aligned}f_{Z(u)}(y) &= \frac{1}{2x} f_{X^2(r)+Y^2(r)}(x)\Big|_{x=\sqrt{y}} \\ &= \frac{1}{2\sqrt{y}} f_{X^2(r)+Y^2(r)}(\sqrt{y}) \\ &\approx \frac{1}{2\sqrt{y}} e^{-\sqrt{y}}.\end{aligned}$$

The cdf of $P(u, \mathbf{z})$ can now be found as

$$\begin{aligned}
\Pr[P(u, \mathbf{z}) \leq P_0] &= \Pr[Z(u) \leq N_r^2 P_0] \\
&\approx \int_0^{N_r^2 P_0} \frac{1}{2\sqrt{y}} e^{-\sqrt{y}} dy \\
&\approx 1 - e^{-\sqrt{N_r^2 P_0}} \\
&\approx 1 - e^{-N_r \sqrt{P_0}}, \; 0 \leq P_0 < \infty. \qquad (6.5)
\end{aligned}$$

From the requirements for a cdf to be in the domain of attraction of the Gumbel distribution in Eq. (5.6) are met by Eq. (6.5) by

$$\begin{aligned}
x_F &= \sup\{x : 1 - e^{-N_r \sqrt{x}}\} \\
&= \infty
\end{aligned}$$

and

$$\begin{aligned}
A(z) &= \frac{\int_z^\infty \left(e^{-N_r \sqrt{t}} \right) dt}{z \left(e^{-N_r \sqrt{z}} \right)} \\
&= \frac{\frac{2e^{-N_r \sqrt{z}}(1 + N_r \sqrt{z})}{N_r^2}}{z \left(e^{-N_r \sqrt{z}} \right)} \\
&= \frac{2(1 + N_r \sqrt{z})}{N_r^2 z}
\end{aligned}$$

to get

$$\begin{aligned}
\lim_{z \to \infty} \frac{1 - \Pr[P(u, \mathbf{z}) \leq (z + zA(z)x)]}{1 - \Pr[P(u, \mathbf{z}) \leq z]} &\approx \lim_{z \to \infty} \frac{e^{-N_r \sqrt{z + zA(z)x}}}{e^{-N_r \sqrt{z}}} \\
&\approx \lim_{z \to \infty} \frac{e^{-N_r \sqrt{z + z \frac{2(1 + N_r \sqrt{z})}{N_r^2 z})x}}}{e^{-N_r \sqrt{z}}} \\
&\approx \lim_{z \to \infty} \frac{e^{-N_r \sqrt{z + \frac{2(1 + N_r \sqrt{z})}{N_r^2})x}}}{e^{-N_r \sqrt{z}}} \\
&\approx e^{-x}, \; -\infty < x < \infty.
\end{aligned}$$

Chapter 7

Concluding Remarks

7.1 Summary

When array element positions are randomly distributed, we found the resulting array beampattern and peak sidelobe levels for different number of array elements. Arrays were discussed in the context of antenna arrays using electromagnetic energy, but the computations in this thesis may be applied to any similar system of elements. The arrays were assumed to have independent and identically distributed element positions. Linear arrays were investigated, but the computations also apply to planar arrays with random elements that can be transformed into linear arrays. The peak sidelobe level distribution calculations for arrays with more than $N = 200$ elements were done using the number of times the beampattern crosses a threshold in an upward direction. For $N < 200$, Extreme Value Theory (EVT) was used to find the distribution of the peak sidelobe level in the limit of a large number of beampattern samples.

The method of upward-crossings of the beampattern was investigated to calculate the peak sidelobe level distribution. We contributed to this method by expressing the peak sidelobe level distribution as a function of the antenna position distribution. This closed-form expression in terms of the variance of the element position distribution is given by Eq. (4.50),

which is given here again as

$$\begin{aligned}&\Pr\{P(u|\mathbf{z}) \geq \mathrm{P}_0 \,\forall\, \mathrm{u} \in \mathcal{S}\} \\ &\approx 1 - (1 - e^{-NP_0})\, e^{-\beta\mu(\mathcal{S}_{nr})\,\sigma_z\sqrt{N}\, e^{-NP_0}\sqrt{\frac{P_0}{\pi}}}. \end{aligned} \tag{7.1}$$

In Eq. (7.1), P_0 is a beampattern threshold, $u \in \mathcal{S}$ means for all angles in the sidelobe region, $\mu(\mathcal{S}_{nr})$ is the length of the sidelobe region, β is the wave number, and σ_z is the array element position standard deviation. Eq. (7.1) holds for N array elements if

- $\sqrt{N} \cdot \hat{f}_{z_k}(u)$ and $\sqrt{N} \cdot \hat{f}'_{z_k}(u)$ are close to zero in the sidelobe region with angle u.
- $\sigma^2_{X',z}(u) \approx \sigma^2_{Y',z}(u)$ in the sidelobe region

where $\hat{f}_{z_k}(u)$ is the characteristic function of the antenna position distribution, $\hat{f}'_{z_k}(u)$ is its derivative with respect to u, and $\sigma^2_{X',z}(u)$ and $\sigma^2_{Y',z}(u)$ are the quadrature component derivative variances.

Another contribution to the upward-crossing method made in this thesis is the evaluation of the peak sidelobe level distribution in the asymptotic limit of a large number of antennas. We found that the closed form peak sidelobe level distribution in Eq. (7.1) is valid asymptotically as the number of elements increases if

- The element position standard deviation, or effective length, diverges as the number of elements increases.
- The means of the quadrature components and their derivatives with respect to angle u converge to zero as the effective length of the array increases with the number of elements.
- $\sigma^2_{X',z}(u)$ and $\sigma^2_{Y',z}(u)$ become angle-independent as the number of elements increases.

We let the effective array length, or array element position standard deviation, change with the number of elements by

$$\sigma_z(N) = \frac{\kappa e^{NP_0}}{\sqrt{N}} + g(N) \tag{7.2}$$

where P_0 is a beampattern threshold, $g(N)$ is some function of N such that $\sigma_z(N)$ is positive and

$$\lim_{N\to\infty} g(N)\, e^{-NP_0}\, \sqrt{N}\, \mu(\mathcal{S}_{nr}) = 0, \tag{7.3}$$

and κ serves as a positive and finite proportionality constant for the effective length. With the effective array length defined by Eq. (7.2), the probability of the peak sidelobe level exceeding some level can converge between zero and one with increasing number elements. Simulated examples were given that showed this convergence and how one can use the results in designing arrays with unequal element spacings.

It was also shown that for sparse arrays when the number of elements is approximately $N < 200$, the probability calculations using the upward-crossing method become inaccurate. We turned to EVT to calculate the peak sidelobe level distributions for $N < 200$. To avoid inaccuracies that occur for a smaller number of elements, we did not approximate the distributions of the beampattern quadrature components by Gaussian distributions. In using EVT, we first showed that the beampattern is uniformly continuous so that there are no large fluctuations of the beampattern between samples. We gave an upper bound to the difference between the true maximum of the beampattern and the sampled maximum to show that the bound becomes smaller as the number of samples increases. An expression for the beampattern distribution at each angle without assuming Gaussian distributed quadrature components was found and is given by Eq. (5.94) and is given here again as

$$\begin{aligned} f_P(P) \;\approx\; & \frac{1}{2\pi}\int_0^{2\pi}\int_0^{\infty}\left(\sum_{n=0}^{\infty}\sum_{m=0}^{\infty}(-1)^{n+m}\frac{q^{2(n+m)}\cos^{2n}(\theta)\sin^{2m}(\theta)E\left[V_k^{2m}W_k^{2n}\right]}{(2n)!(2m)!N^{n+m}}\right)^N \\ & \times P\cdot J_0\left(Pq\right) q\, dq\, d\theta \end{aligned} \tag{7.4}$$

where $E\left[V_k^{2m} W_k^{2n}\right]$ represents expectations over the array factor quadrature components and N is the number of elements in the array.

For an arbitrarily large number of elements, we showed that the cumulative distribution function of Eq. (7.4) was in the domain of attraction of the Gumbel distribution. However, it was also shown that being in this domain of attraction occurs under weak convergence with a large number of elements. The Gumbel distribution parameters for the peak sidelobe level were given in terms of the number of array elements and beampattern samples. Tables are given in subsection 5.3.11 and Appendix C to determine the number of samples given a certain number of array elements, element position variance, and the type of position distribution.

Showing that Eq. (7.4) was in the domain of attraction of the Weibull distribution proved non-trivial. However, it was shown that the distribution in the limit as the number of elements, N, tends to infinity is approximately in the domain of attraction of the Weibull distribution with parameters $a_M = 1$, $b_M \approx 1$, and $\alpha = \infty$. It was shown through simulations that the Weibull distribution seems to be in the domain of attraction of the beampattern distribution for any number of array elements. One may use the charts in subsection 5.3.13 to determine the Weibull distribution parameters for $N = 4$ array elements to $N = 9$ elements.

When array element positions become correlated, as in the case of radars, evaluating the peak sidelobe level distribution becomes more difficult. For radars with independently distributed transmit antennas and independently distributed receive antennas, an expression for the virtual beampattern distribution at a particular angle was found. It was not easily verified whether this distribution was in the domain of attraction of the Gumbel or Frechet EVT distributions. When radar transmit and receive antennas are co-located, then the expression for the virtual beampattern distribution at a particular angle was found to be in the domain of attraction of the Gumbel distribution.

7.2 Choosing Method to Calculate Peak Sidelobe Level Distributions Based on Number of Array Elements

Three methods to calculate the peak sidelobe level distribution were investigated in this thesis. They are:

1. Upward-Crossing Method
2. Gumbel distributed peak sidelobe level using Extreme Value Theory (EVT)
3. Weibull distributed peak sidelobe level using EVT

One may decide on the which method to use based on the number of elements, N, in the array.

- For $N > 200$ array elements, the peak sidelobe level distribution can be found using the method of upcrossings of the beampattern. It may also be used for smaller number of elements if the array is not sparse, meaning the variance of the element positions is relatively small.
- For $10 \leq N \leq 200$ array elements, especially if the array is sparse, we may use the Gumbel distribution from EVT. The number of samples can be found from the tables in subsection 5.3.11 and Appendix C.
- When $N < 10$, we may use the Weibull distribution from EVT. The charts in subsection 5.3.13 can be used to find the Weibull distribution parameters.

7.3 Future Work

An immediate concern is to analytically show Weibull distribution domain of attraction by manipulating the expression for the beampattern distribution at each angle. At least for a

small number of elements, $N < 10$, perhaps distributions that approximate the beampattern distribution at each angle can be used. The approximate distributions will need to be in the domain of attraction of the Weibull distribution.

Efforts can also be made in calculating the peak sidelobe level distribution using the exact equation for the expected number of upcrossings.

For radar, a method to determine the peak sidelobe level distribution using the method of upcrossings is desired. Also, it needs to be concluded that the virtual beampattern distribution when the transmit and receive arrays are not co-located is or is not in the domain of attraction of the Gumbel or Frechet distributions.

References

[1] S. Krishnamurthy, D. Bliss, and V. Tarokh, "Sidelobe level distribution computation for antenna arrays with arbitrary element distributions," in *Signals, Systems and Computers (ASILOMAR), 2011 Conference Record of the Forty Fifth Asilomar Conference on*, nov. 2011, pp. 2045 –2050.

[2] "Ieee standard definitions of terms for antennas." *IEEE Std 145-1993*, pp. i–, 1993.

[3] J. R. Freeman, H. E. Beere, and D. A. Ritchie, *Terahertz Spectroscopy and Imaging*. Springer-Verlag, 2013, ch. Generation and Detection of Terahertz Radiation.

[4] L. Novotny, "Optical antennas for enhanced light absorption and emission," in *Lasers and Electro-Optics (CLEO), 2011 Conference on*, 2011, pp. 1–1.

[5] E. Soliman, M. Sallam, and G. Vandenbosch, "Novel wire-grid nantenna array for optical communication systems," in *Antenna Technology (iWAT), 2013 International Workshop on*, 2013, pp. 109–112.

[6] S. Best, "Introduction to antennas," CD-ROM, 2004.

[7] W. L. Stutzman and G. A. Thiele, *Antenna Theory and Design*, 2nd ed. John Wiley & Sons, Inc., 1998.

[8] J. A. Kong, *Electromagnetic Wave Theory*. EMW Publishing, 2005.

[9] M. Eisenberg and R. Guy, "A proof of the hairy ball theorem," *Amer. Math. Monthly*, vol. 86, no. 7, pp. 572–574, 1979. [Online]. Available: http://dx.doi.org/10.2307/2320587

[10] B. Steinberg, "The peak sidelobe of the phased array having randomly located elements," *IEEE Transactions on Antennas and Propagation*, vol. 20, no. 2, pp. 129–136, Mar. 1972.

[11] H. Ochiai, P. Mitran, H. Poor, and V. Tarokh, "Collaborative beamforming for distributed wireless ad hoc sensor networks," *IEEE Transactions on Signal Processing*, vol. 53, no. 11, pp. 4110–4124, Nov. 2005.

[12] Y. Lo, "Sidelobe level in nonuniformly spaced antenna arrays," *Antennas and Propagation, IEEE Transactions on*, vol. 11, no. 4, pp. 511 – 512, jul 1963.

[13] ——, "A mathematical theory of antenna arrays with randomly spaced elements," *Antennas and Propagation, IEEE Transactions on*, vol. 12, no. 3, pp. 257 – 268, may 1964.

[14] L. Sodin, "Statistical analysis of nonequidistant linear antenna arrays," *Radio engineering & electronic physics*, vol. 11, no. 11, pp. 1715–1720, 1966.

[15] V. Sazonov, "Calculation of the level of side lobes in a random radiation pattern," *Radio engineering & electronic physics*, vol. 13, no. 3, pp. 339–345, 1968.

[16] A. Panicali and Y. Lo, "A probabilistic approach to large circular and spherical arrays," *Antennas and Propagation, IEEE Transactions on*, vol. 17, no. 4, pp. 514 – 522, jul 1969.

[17] V. Agrawal and Y. Lo, "Distribution of sidelobe level in random arrays," *Proceedings of the IEEE*, vol. 57, no. 10, pp. 1764–1765, 1969.

[18] V. D. Agrawal, "Mutual coupling in phased arrays of randomly spaced antennas," Ph.D. dissertation, University of Illinois at Urbana-Champaign, January 1971.

[19] V. Agrawal and Y. Lo, "Mutual coupling in phased arrays of randomly spaced antennas," *IEEE Transactions on Antennas and Propagation*, vol. 20, no. 3, pp. 288–295, May 1972.

[20] M. Alves and M. de Alencar, "Mutual coupling effects in a linear adaptive antenna array with random spacing," in *Personal, Indoor and Mobile Radio Communications, 2007. PIMRC 2007. IEEE 18th International Symposium on*, 2007, pp. 1–4.

[21] M. Skolnik, I. Sherman, J., and J. Ogg, F., "Statistically designed density-tapered arrays," *Antennas and Propagation, IEEE Transactions on*, vol. 12, no. 4, pp. 408–417, 1964.

[22] T. Maher and D. Cheng, "Random removal of radiators from large linear arrays," *Antennas and Propagation, IEEE Transactions on*, vol. 11, no. 2, pp. 106–112, 1963.

[23] G. Cook and D. A. H. Johnson, "Pseudo-random selection of elements in a multi-element array," *Radio and Electronic Engineer*, vol. 38, no. 2, pp. 82–88, 1969.

[24] M. Andreasen, "Linear arrays with variable interelement spacings," *Antennas and Propagation, IRE Transactions on*, vol. 10, no. 2, pp. 137–143, 1962.

[25] R. Harrington, "Sidelobe reduction by nonuniform element spacing," *Antennas and Propagation, IRE Transactions on*, vol. 9, no. 2, pp. 187–192, 1961.

[26] Y. Lo and S.-W. Lee, "A study of space-tapered arrays," *Antennas and Propagation, IEEE Transactions on*, vol. 14, no. 1, pp. 22–30, 1966.

[27] B. Basu and G. K. Mahanti, "Artificial bees colony optimization for synthesis of thinned mutually coupled linear array using inverse fast fourier transform," in *Devices and Communications (ICDeCom), 2011 International Conference on*, 2011, pp. 1–5.

[28] W. Du Plessis, "Sll, active elements and available elements of uniformly-excited linear thinned arrays," in *Electromagnetics in Advanced Applications (ICEAA), 2012 International Conference on*, 2012, pp. 558–561.

[29] S. Xianrong, Y. Huanqiang, and G. Yanchang, "A study of sidelobe level of large thinned phased array," in *Microwave Conference Proceedings, 1997. APMC '97, 1997 Asia-Pacific*, vol. 3, 1997, pp. 941–944 vol.3.

[30] B. Steinberg and E. Attia, "Sidelobe reduction of random arrays by element position and frequency diversity," *Antennas and Propagation, IEEE Transactions on*, vol. 31, no. 6, pp. 922–930, 1983.

[31] A. Vallecchi, M. Cerretelli, M. Linari, and G. Gentili, "Investigation of optimal array configurations for full azimuth scan hf skywave radars," in *Radar Conference, 2009. EuRAD 2009. European*, 2009, pp. 200–203.

[32] K. W. Forsythe and D. W. Bliss, *MIMO Radar: Concepts, Performance, Enhancements, and Applications*. John Wiley & Sons, 2009, ch. 2.

[33] E. Weinstein and A. Weiss, "Lower bounds on the mean square estimation error," *Proceedings of the IEEE*, vol. 73, no. 9, pp. 1433 – 1434, sept. 1985.

[34] T. Nohara and S. Haykin, "Application of the weiss-weinstein bound to a two-dimensional antenna array," *Acoustics, Speech and Signal Processing, IEEE Transactions on*, vol. 36, no. 9, pp. 1533 –1534, sep 1988.

[35] R. McAulay and E. Hofstetter, "Barankin bounds on parameter estimation," *Information Theory, IEEE Transactions on*, vol. 17, no. 6, pp. 669 – 676, nov 1971.

[36] C. Richmond, "Capon algorithm mean-squared error threshold snr prediction and probability of resolution," *Signal Processing, IEEE Transactions on*, vol. 53, no. 8, pp. 2748 – 2764, aug. 2005.

[37] ——, "Mean-squared error and threshold snr prediction of maximum-likelihood signal parameter estimation with estimated colored noise covariances," *Information Theory, IEEE Transactions on*, vol. 52, no. 5, pp. 2146 –2164, may 2006.

[38] ——, "Numerically efficient mean squared error threshold snr prediction for adaptive arrays," in *2010 IEEE Sensor Array and Multichannel Signal Processing Workshop (SAM)*, Oct. 2010, pp. 101–104.

[39] M. Donvito and S. Kassam, "Characterization of the random array peak sidelobe," *IEEE Transactions on Antennas and Propagation*, vol. 27, no. 3, pp. 379–385, May. 1979.

[40] M. Ahmed and S. Vorobyov, "Beampattern random behavior in wireless sensor networks with gaussian distributed sensor nodes," May. 2008, pp. 000 257–000 260.

[41] Y. Lo and R. Simcoe, "An experiment on antenna arrays with randomly spaced elements," *IEEE Transactions on Antennas and Propagation*, vol. 15, no. 2, pp. 231 – 235, Mar. 1967.

[42] S. Rice, "Mathematical analysis of random noise–part iii," *Bell Syst. Tech. J.*, vol. 24, pp. 46 – 156, 1945.

[43] H. R. M.R. Leadbetter, Georg Lindgren, *Extremes and Related Properties of Random Sequences and Processes*. Springer-Verlag, 1980.

[44] V. Agrawal, "Comments on "beamwidth of phased arrays"," *IEEE Transactions on Antennas and Propagation*, vol. 22, no. 6, pp. 841–842, Nov. 1974.

[45] S. Kotz and S. Nadarajah, *Extreme value distributions: theory and applications*. Imperial College Press, 2000.

[46] v. Bortkiewicz, L., "Variationsbreite und mittlerer fehler," *Sitzungsber. Berli. Math. Ges.*, vol. 22, pp. 3 – 11, 1922.

[47] L. Tippett, "On the extreme individuals and the range of samples taken from a normal population," *Biometrika*, vol. 17, pp. 364 – 387, 1925.

[48] M. Frechet, "Sur la loi de probabilite de l'ecart maximum," *Ann. Soc. Polon. Math. Cracovie*, vol. 6, pp. 93 – 116, 1927.

[49] R. A. Fisher and L. H. C. Tippett, "Limiting forms of the frequency distribution of the largest or smallest member of a sample," *Proceedings of the Cambridge Philosophical Society*, vol. 24, p. 180, 1928.

[50] E. Gumbel, "Les intervalles extremes entre les emissions radioactives," *J. Phys. Radium*, vol. 8, pp. 446 – 452, 1937.

[51] ——, "La duree extreme de la vie humaine," *Actualites Scientifique et Industrielles*, 1937.

[52] ——, "The return period of flood flows," *Ann. Math. Statist.*, vol. 12, pp. 163 – 190, 1941.

[53] ——, "On the plotting of flood discharges," *Trans. Amer. Geophys. Union*, vol. 25, pp. 699 – 719, 1944.

[54] ——, "Floods estimated by probability methods," *Engrg. News-Record*, vol. 134, pp. 97 – 101, 1945.

[55] W. Weibull, *A Statistical Theory of the Strength of Materials*, ser. Ingeniörsvetenskapsakademiens handlingar. Generalstabens litografiska anstalts förlag, 1939. [Online]. Available: http://books.google.com/books?id=otVRAQAAIAAJ

[56] J. M. Nordquist, "Theory of largest values applied to earthquake magnitudes," *Transactions, American Geophysical Union*, vol. 26, pp. 29–31, 1945.

[57] B. Gnedenko, "Sur la distribution limite du terme maximum d'une série aléatoire," *Ann. of Math. (2)*, vol. 44, pp. 423–453, 1943.

[58] R. L. Smith, *Breakthroughs in Statistics Valume I, Foundations and Basic Theory*. Springer-Verlag, 1991, ch. Introduction to Gnedenko (1943) On the Limiting Distribution of the Maximum Term in a Random Series, pp. 185–194.

[59] J. Galambos, *The Asymptotic Theory of Extreme Order Statistics*. Robert E. Krieger Publishing Company, 1987.

[60] D. Mejzler, "On a theorem of b.v. gndenko," *Sb. Trudov Inst. Mat. Akad. Nauk. Ukrain. RSR*, vol. 12, pp. 31 – 55, 1949.

[61] M. Marcus and M. Pinsky, "On the domain of attraction of $e^{-e^{-x}}$," *J. Math. Anal. Appl.*, vol. 28, pp. 440–449, 1969.

[62] L. de Haan, *On regular variation and its application to the weak convergence of sample extremes*, ser. Mathematical Centre Tracts. Amsterdam: Mathematisch Centrum, 1970, vol. 32.

[63] ——, "A form of regular variation and its application to the domain of attraction of the double exponential distribution," *Z. Wahrscheinlichkeitstheorie und Verw. Gebiete*, vol. 17, pp. 241–258, 1971.

[64] R. von Mises, "La disribution da la plus grande de n valeurs," *Revue de l'Union Interbalkanique*, vol. 1, pp. 1 – 20, 1936.

[65] M. L. Juncosa, "The asymptotic behavior of the minimum in a sequence of random variables," *Duke Math. J.*, vol. 16, pp. 609–618, 1949.

[66] S. M. Berman, "Limit theorems for the maximum term in stationary sequences," *Ann. Math. Statist.*, vol. 35, pp. 502–516, 1964.

[67] G. S. Watson, "Extreme values in samples from m-dependent stationary stochastic processes," *The Annals of Mathematical Statistics*, vol. 25, no. 4, pp. pp. 798–800, 1954. [Online]. Available: http://www.jstor.org/stable/2236668

[68] T. A. Buishand, "The effect of seasonal variation and serial correlation on the extreme value distribution of rainfall data," *J. Climate Appl. Meteor.*, vol. 24, p. 154Ű160, 1985.

[69] C. Cunnane and J. Nash, *Bayesian estimation of frequency of hydrological events*, 1974. [Online]. Available: http://books.google.com/books?id=6fxBygAACAAJ

[70] L. Pericchi and I. Rodriquez-Iturbe, *On the statistical analysis of floods*. Springer-Verlag, 1985, vol. A Celebration of Statistics: The I.S.I. Centenary Volume, pp. 511 – 541.

[71] J. King, "Summary of extreme-value theory and its relation to reliability analysis," in *Proc. 12th Annual Conference of the Americal Society for Quality Control*, vol. 13, 1959, pp. 163 – 167.

[72] A. Metcalfe and G. Smith, "Effects of length on the strength of glass fibres," in *Proc. Amer. Soc. Testing Materials*, vol. 64, 1964, pp. 1075 – 1093.

[73] E. Simiu and J. Filliben, "Probability distributions of extreme wind speeds," *Structural Div. National Bureau of Standards*, vol. 102, pp. 1861 – 1877, 1976.

[74] R. H., A. Aldabagh, and M. Ramamoorthy, "Rainfall analysis by power transformation," *J. Climate Appl. Meteor*, vol. 22, pp. 1411 – 1415, 1983.

[75] W. A. Silveria and D. R. Brillinger, "On maximum wave heights of severe seas." Houston, Texas: Offshore Technology Conference, May 1978.

[76] P. M. Fitzpatrick, *Advanced Calculus, 2nd ed.* American Mathematical Society, 2006.

[77] J. Beck, "Flat polynomials on the unit circleŮnote on a problem of littlewood," *Bulletin of the London Mathematical Society*, vol. 23, no. 3, pp. 269–277, 1991. [Online]. Available: http://blms.oxfordjournals.org/content/23/3/269.short

[78] K. Paterson and V. Tarokh, "On the existence and construction of good codes with low peak-to-average power ratios," *Information Theory, IEEE Transactions on*, vol. 46, no. 6, pp. 1974 –1987, sep 2000.

[79] B. Babadi and V. Tarokh, "Spectral distribution of random matrices from binary linear block codes," *Information Theory, IEEE Transactions on*, vol. 57, no. 6, pp. 3955–3962, 2011.

[80] S. Varadhan, *Probability Theory.* American Mathematical Society, 2001, ch. 2, Weak Convergence, pp. 19–35.

[81] D. Bai, P. Mitran, S. Ghassemzadeh, R. Miller, and V. Tarokh, "Rate of channel hardening of antenna selection diversity schemes and its implication on scheduling," *Information Theory, IEEE Transactions on*, vol. 55, no. 10, pp. 4353 –4365, oct. 2009.

[82] R. Brent, *Algorithms for Minimization without Derivatives.* Englewood Cliffs, NJ: Prentice Hall, 1973, ch. 5.

[83] M. Plotkin, "Beamwidth of phased arrays," *IEEE Transactions on Antennas and Propagation*, vol. 21, no. 5, pp. 695–697, Sep. 1973.

Appendix A

Second Moment of Element Positions Given by Variance

Eq. (4.48), which is repeated here,

$$E[\nu(P_0)] = \beta\mu(\mathcal{S}_{nr})\sqrt{E[z^2]N}\,e^{-NP_0}\sqrt{\frac{P_0}{\pi}},$$

seems to imply a different number of upward-crossings will appear in the far-field beampattern if the array element locations were shifted to have a different mean. It will now be shown that angle-independence applies when the element location distribution is shifted to have approximately zero mean. Assume that $\sqrt{N}\cdot\hat{f}_{z_k}(u)$ and $\sqrt{N}\cdot\hat{f}'_{z_k}(u)$ are close to zero in the sidelobe region with u for some arbitrary element location distribution. Also assume for the time being that the mean of the element distribution may be non-zero. Shift each element location, z_k, in the array by some real number, α, to produce a zero-mean location distribution. The new element location, $z_{k,0} = z_k + \alpha$, has the characteristic function

$$\hat{f}_{z_{k,0}}(u) \triangleq e^{-j\beta\alpha u}\hat{f}_{z_k}(u).$$

If

$$\hat{f}_{z_k}(u) \approx 0 \approx \hat{f}_{z_k}(-u),$$

then

$$\hat{f}_{z_{k,0}}(u) \approx 0 \approx \hat{f}_{z_{k,0}}(-u)$$

which implies

$$\begin{aligned} \hat{f}_{z_{k,0}}(-u) &= e^{j\beta\alpha u}\hat{f}_{z_k}(-u) \\ &\approx e^{j\beta\alpha u}\hat{f}_{z_k}(u) \\ &\approx e^{-j\beta\alpha u}\hat{f}_{z_k}(u). \end{aligned}$$

The equation

$$e^{j\beta\alpha u} \approx e^{-j\beta\alpha u}$$

can only hold for non-zero u if $\alpha \approx 0$. If there is approximately no shift, then the original element location must have had an approximately zero-mean distribution. When z_k has an approximately zero-mean distribution, the following equations show what happens to

angle-independent statistics when the shift α is much greater than zero:

$$\begin{aligned}
m_{X,z+\alpha}(u) &\approx \sqrt{N}\hat{f}_{z_k}(u)\cos(\beta\alpha u) \\
m_{Y,z+\alpha}(u) &\approx -\sqrt{N}\hat{f}_{z_k}(u)\sin(\beta\alpha u) \\
\sigma^2_{X,z+\alpha}(u) &\approx \tfrac{1}{2} + \tfrac{1}{2}\hat{f}_{z_k}(2u)\cos(2\beta\alpha u) \\
&\quad -\hat{f}^2_{z_k}(u)\cos^2(\beta\alpha u) \\
\sigma^2_{Y,z+\alpha}(u) &\approx \tfrac{1}{2} - \tfrac{1}{2}\hat{f}_{z_k}(2u)\cos(2\beta\alpha u) \\
&\quad -\hat{f}^2_{z_k}(u)\sin^2(\beta\alpha u) \\
m_{X',z+\alpha}(u) &\approx \sqrt{N}\alpha\beta\hat{f}_{z_k}(u)\sin(\beta\alpha u) \\
m_{Y',z+\alpha}(u) &\approx \sqrt{N}\alpha\beta\hat{f}_{z_k}(u)\cos(\beta\alpha u) \\
\sigma^2_{X',z+\alpha} &\approx \tfrac{\beta^2\sigma_z^2}{2} + \tfrac{1}{4}\Big(\hat{f}''_{z_k}(2u)e^{-j2\beta\alpha u} \\
&\quad +\hat{f}''_{z_k}(-2u)e^{j2\beta\alpha u} - j2\beta\alpha\hat{f}'_{z_k}(2u) \\
&\quad -\beta^2\alpha^2\hat{f}_{z_k}(2u)\cos(2\beta\alpha u)\Big) \\
&\quad -\tfrac{m^2_{X',z+\alpha}(u)}{N} \\
\sigma^2_{Y',z+\alpha} &\approx \tfrac{\beta^2\sigma_z^2}{2} - \tfrac{1}{4}\Big(\hat{f}''_{z_k}(2u)e^{-j2\beta\alpha u} \\
&\quad +\hat{f}''_{z_k}(-2u)e^{j2\beta\alpha u} - j2\beta\alpha\hat{f}'_{z_k}(2u) \\
&\quad -\beta^2\alpha^2\hat{f}_{z_k}(2u)\cos(2\beta\alpha u)\Big) \\
&\quad -\tfrac{m^2_{Y',z+\alpha}(u)}{N} \\
\sigma_{XX',z+\alpha} &\approx -\alpha\beta\hat{f}_{z_k}(2u)\sin(2\beta\alpha u) \\
&\quad -\tfrac{m_{X,z+\alpha}(u)m_{X',z+\alpha}(u)}{N} \\
\sigma_{YY',z+\alpha} &\approx \alpha\beta\hat{f}_{z_k}(2u)\sin(2\beta\alpha u) \\
&\quad -\tfrac{m_{Y,z+\alpha}(u)m_{Y',z+\alpha}(u)}{N}
\end{aligned}$$

For large α, it is seen that the statistics become angle-dependent. Therefore,

$$E_{z_k}[z_k^2] \approx \sigma_z^2$$

which is the antenna location variance.

Appendix B

Numerical Method for Finding Peak Sidelobe (Sidelobe Level) of Random Antenna Array Beampattern

This appendix describes the algorithm used to numerically find the peak sidelobe value or peak sidelobe level of a random beampattern.

Given an antenna array with N antenna elements at locations $\mathbf{z}$, $\mathbf{z} = \{z_1, z_2, \ldots, z_N\}$, a beampattern like the one in Fig. B.1 is produced. Here $u = \sin(\phi)$ where ϕ is the angular direction in the beampattern. Fig. B.1 is a normalized beampattern in the power domain. It is given by the beampattern equation in Eq. 2.9 which is

$$P(u, \mathbf{z}) \equiv \frac{1}{N^2} \left[\left(\sum_{k=1}^{N} \cos(u\beta z_k) \right)^2 + \left(\sum_{k=1}^{N} \sin(u\beta z_k) \right)^2 \right]$$

where $\beta = 2\pi/\lambda$ for linear arrays and $\beta = 4\pi/\lambda$ for planar arrays. λ is the wavelength.

For a random beampattern simulation for which the antenna positions are not known in advance and are randomly generated, we are interested in numerically computing the value

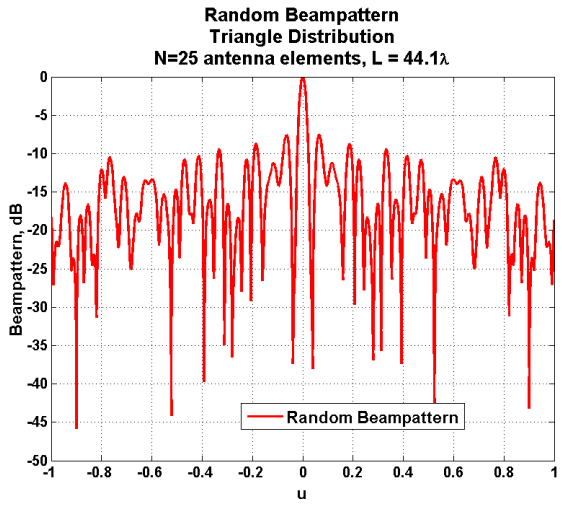

Figure B.1: *Beampattern,* $P(u, \mathbf{z})$

of the peak sidelobe or peak sidelobe level. Sampling the beampattern in u with smaller intervals will give more accurate values for sidelobe peaks. When our goal is to generate the peak sidelobe level distribution from a large number of simulations, reducing the sampling interval will cause long simulation run times. Also, the beampattern will need to be sampled at least twice with each consecutive sample run having smaller sampling intervals to make sure the global sidelobe maximum is being found. We can also use the first derivative of the beampattern with respect to u, $P'(u, \mathbf{z})$ to know how close to a maximum the estimated global maximum in the sidelobe region is.

The numerical approach taken in this paper is to sample the beampattern, use its first derivative, apply interpolation to find a set of local maximum sidelobe peaks, and then set the global peak sidelobe level to be the largest local maximum sidelobe peak. The method will avoid sampling heavily in regions of the beampattern that do not have sidelobe peaks, but not having enough samples may not find local maxima of sidelobes whose peaks are near the slopes of adjacent sidelobes.

B.1 Interpolation after Sampling

The algorithm in this paper uses the interpolation method from Ref. [82]. Samples of the beampattern are taken at evenly spaced intervals in u. Beampattern samples are shown as green circles in Fig. B.2.

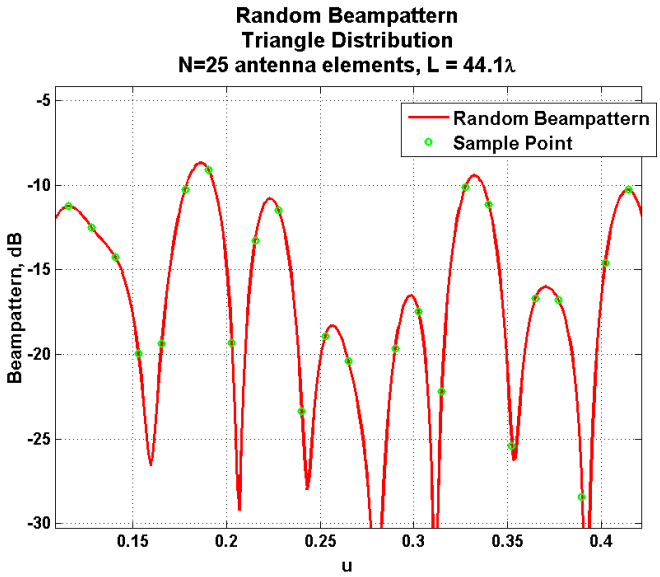

Figure B.2: *Beampattern with sample points*

The derivative of the beampattern with respect to u at each sample point, $P'(u_{sample}, \mathbf{z})$, is calculated where u_{sample} is the angle corresponding to the sample point. Two adjacent sample points are considered. One is at $u = u_a$, and the other is at $u = u_b$ where $u_a < u_b$. If for some $\epsilon > 0$,

$$P'(u_a, \mathbf{z}) > 0 \tag{B.1}$$

and

$$|P'(u_b, \mathbf{z})| < \epsilon, \tag{B.2}$$

then $P(u_b, \mathbf{z})$ is considered a local maximum and its value and the value of u_b are stored. We choose ϵ to be small and close to 0. In these examples, $\epsilon = 10e - 4$.

If $P(u_b, \mathbf{z})$ is not considered a local maximum, then if

$$P'(u_a, \mathbf{z}) > 0 \tag{B.3}$$

and

$$P'(u_b, \mathbf{z}) < 0, \tag{B.4}$$

then there is a local peak at some $u, u_a < u < u_b$. If Eqs. (B.3) and (B.4) are not true, then the next sample point is considered. When moving to the next sample point, u_b becomes u_a and the new sample point location is designated u_b. If Eqs. (B.3) and (B.4) are true, then the interpolation method from Ref. [82] is used to find the local maximum. First, the midpoint of line segment u_a and u_b is found:

$$u_c \equiv \frac{u_a + u_b}{2}. \tag{B.5}$$

If

$$|P'(u_c, \mathbf{z})| < \epsilon \tag{B.6}$$

then $P(u_c, \mathbf{z})$ is declared a local maximum at u_c and the next sample point at $u > u_b$ is analyzed. Otherwise, with the points

$$\begin{gathered}(u_a, P(u_a, \mathbf{z})) \\ (u_b, P(u_b, \mathbf{z})) \\ (u_c, P(u_c, \mathbf{z})),\end{gathered} \tag{B.7}$$

a parabola is found. These points and the parabola connecting them are shown in Fig. B.3. Now, the maximum of the parabola is found at some $u = u_d$ where $u_a \leq u_d \leq u_b$.

If

$$|P'(u_d, \mathbf{z})| < \epsilon, \tag{B.8}$$

then $P(u_d, \mathbf{z})$ is declared a local maximum at u_d and the next sample point at $u > u_b$ is

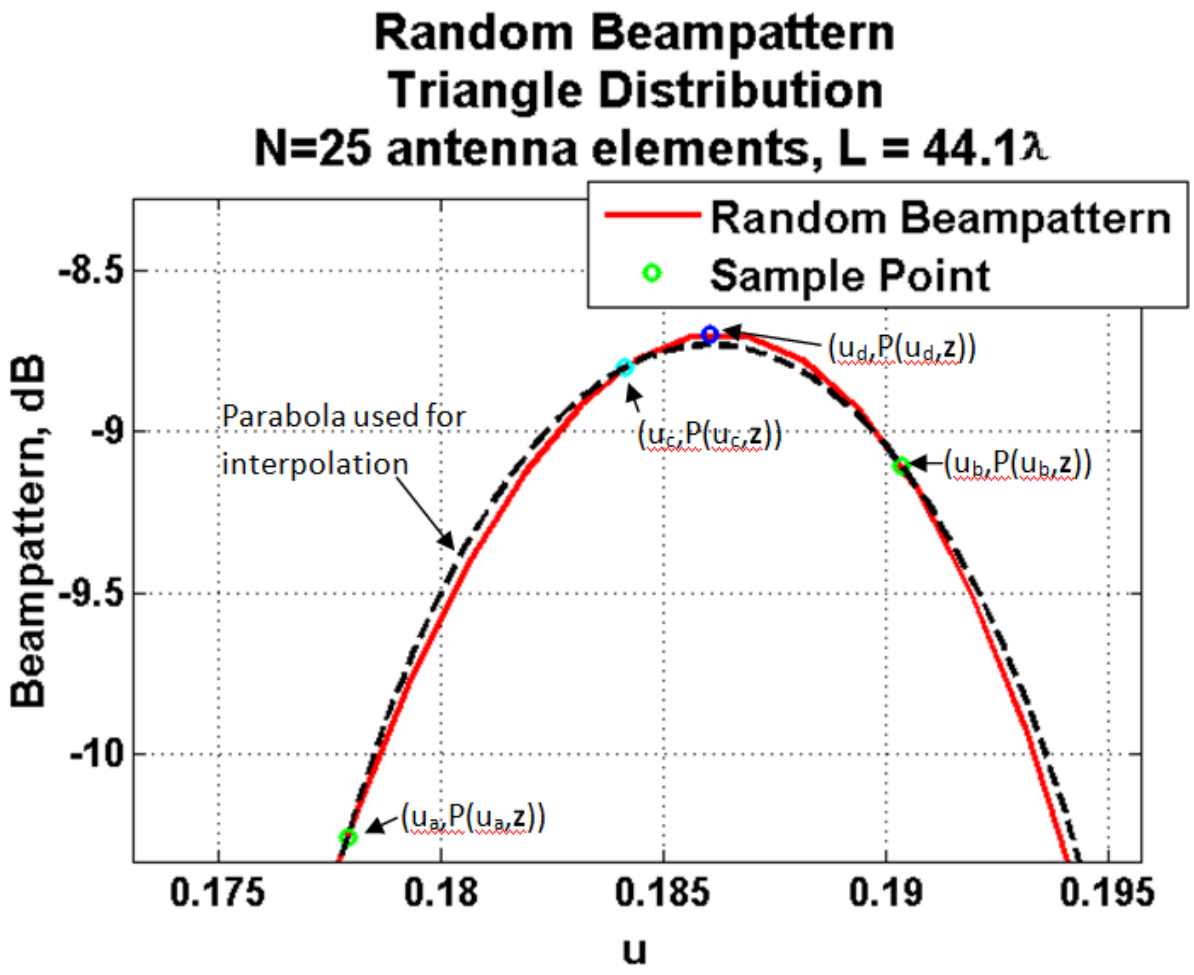

Figure B.3: *Interpolating parabola through points in Eq.* (B.7) *to get maximum of parabola at* $u = u_d$ *from which point* $(u_d, P(u_d, \mathbf{z}))$ *is determined*

analyzed. Otherwise, the process of interpolation is repeated with a smaller bracket between u_a and u_b. The smaller bracket is obtained by redefining u_a and u_b to be from two adjacent

points among

$$\begin{aligned}(u_a, P(u_a, \mathbf{z}))\\ (u_b, P(u_b, \mathbf{z}))\\ (u_c, P(u_c, \mathbf{z}))\\ (u_d, P(u_d, \mathbf{z}))\end{aligned} \tag{B.9}$$

so that

$$P'(u_a, \mathbf{z}) > 0$$

and

$$P'(u_b, \mathbf{z}) < 0.$$

In the example in Fig. B.3,

$$\begin{aligned}P'(u_c, \mathbf{z}) > 0\\ P'(u_d, \mathbf{z}) > 0,\end{aligned} \tag{B.10}$$

and so

$$u_a = u_d, \tag{B.11}$$

and u_b retains the same value since $P'(u_b, \mathbf{z}) < 0$.

As seen in Fig. B.4, a new point

$$(u_c, P(u_c, \mathbf{z})) \tag{B.12}$$

is found from

$$u_c = \frac{u_a + u_b}{2}.$$

A parabola is used to find the point

$$(u_d, P(u_d, \mathbf{z})) \tag{B.13}$$

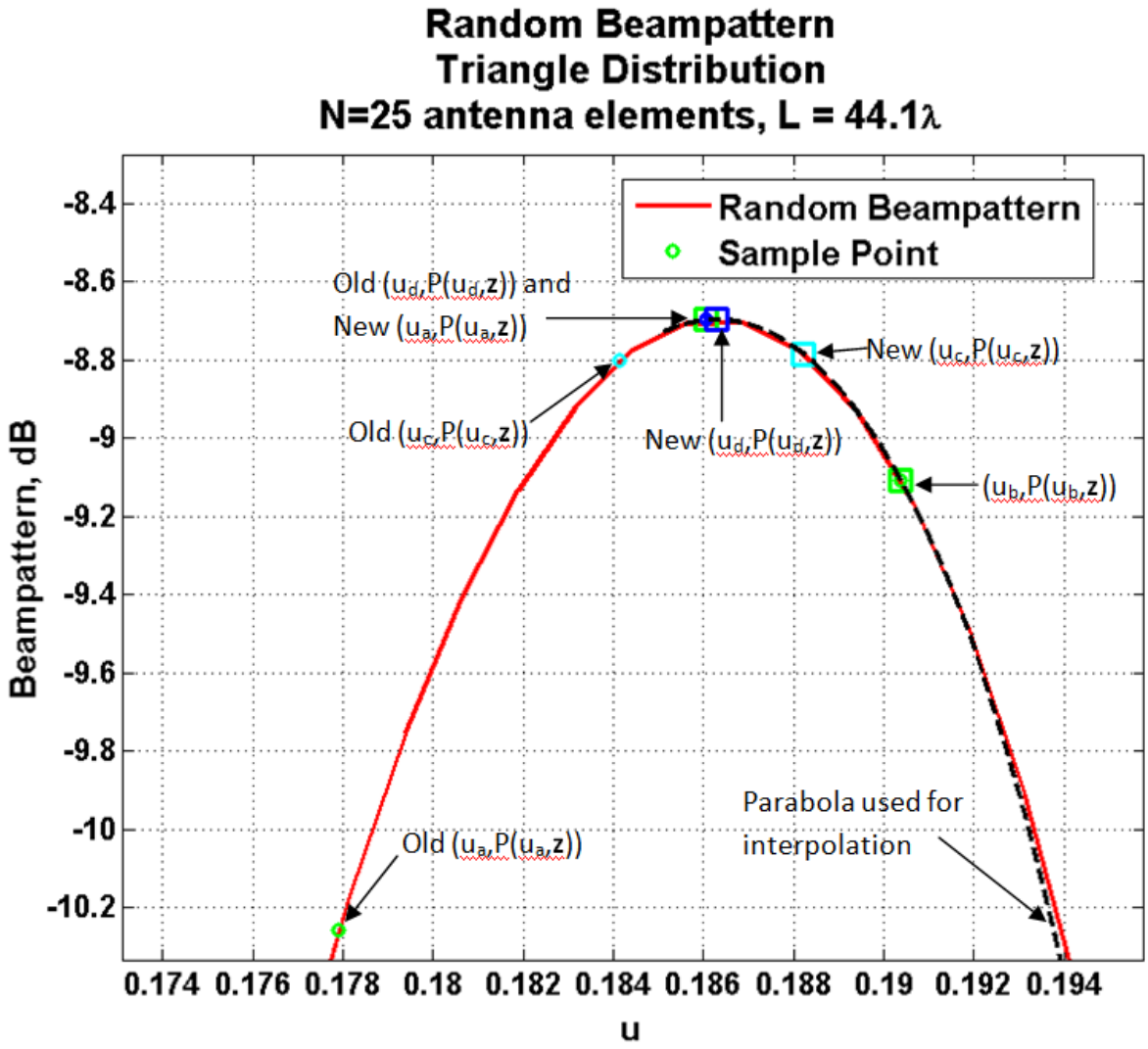

Figure B.4: *Interpolating parabola through next iteration of points to get closer to local maximum*

as shown in Fig. B.4. A new interpolation bracket is created and the process repeats until

$$|P'(u_c, \mathbf{z})| < \epsilon$$

or

$$|P'(u_d, \mathbf{z})| < \epsilon$$

which sets the local maximum. The process is repeated for all sets of adjacent sample points that indicate a local maximum between them from their derivatives with respect to u.

This interpolation method cannot work if the points corresponding to u_a, u_b, and u_c are on a horizontal line, but it will not happen with beampatterns.

B.2 Interpolation Results

Fig. B.5 shows the results of the algorithm in determining the local maxima. The global maximum, and the peak sidelobe or peak sidelobe level, is the largest beampattern value of the set of local maxima. Zooming into Fig. B.5 shows that sidelobes with peaks that are near slopes of adjacent sidelobes do not get their local maxima determined. The height of these sidelobes before the beginning of the adjacent sidelobe is 1 to 2 dB. The sampling interval must be reduced to determine the local maxima of these smaller sidelobes.

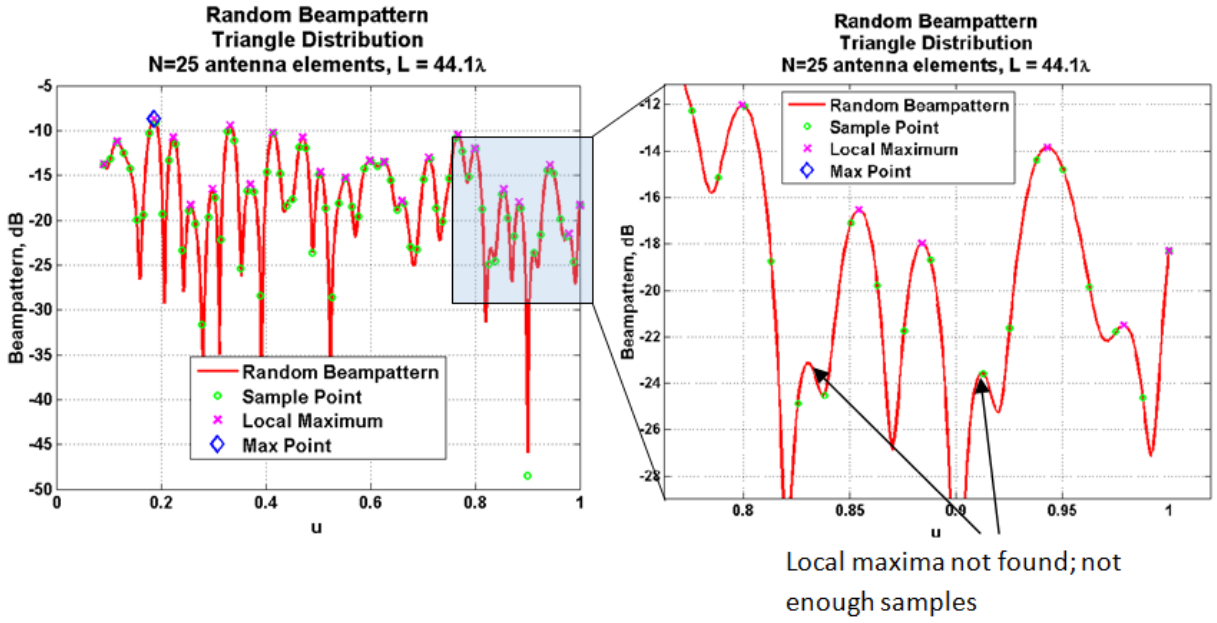

Figure B.5: *Beampattern with global and most local maxima found; not enough samples to find some local maxima*

The algorithm outlined in this paper accounts for a global maximum occuring at the beginning of the sidelobe region at $u = u_s$ or at the end of the sidelobe region at $u = 1$. The

sidelobe values at these extremes may not be peaks, but they may still be the maximum values. Therefore, the values at these extremes are included in the set of local maxima even if they are not near-peak values. The case where $u = 1$ will not be included in the set of local maxima is if another local maxima was found between it and the preceding sample point.

B.3 Choosing Sampling Rate

To set a reasonable sampling interval to take simulated beampattern measurements, we use knowledge of the main beam width. In Fig. B.6, zooming into the main beam of the beampattern at $u = 0$ shows that the shape main beam lobe above at least -3 dB is close to the shape of the sidelobes around the sidelobe peaks.

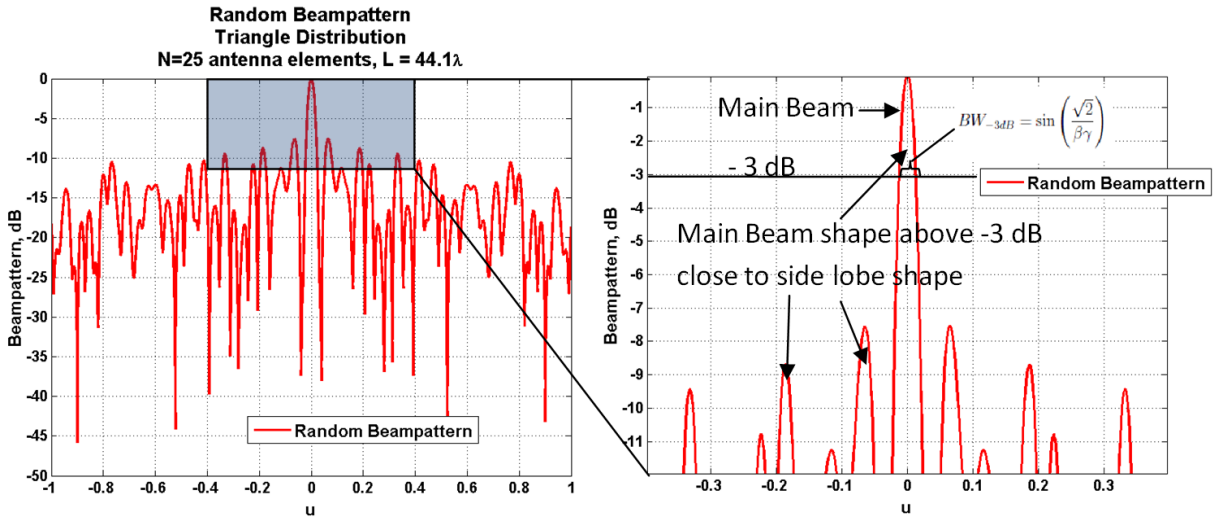

Figure B.6: *Beampattern sidelobe shapes compared to main beam*

The width of the main beam at the -3 dB level or half power beamwidth is given by Ref. [83] as

$$BW_{-3dB} \equiv \sin\left(\frac{\sqrt{2}}{\beta\gamma}\right). \tag{B.14}$$

Here, γ is

$$\gamma \equiv \sqrt{\frac{1}{N}\left(\sum_{k=1}^{N} z_k^2\right) - \frac{1}{N^2}\left(\sum_{k=1}^{N} z_k\right)^2}. \tag{B.15}$$

If the antenna positions, $\mathbf{z}$, are independent, then by the Laws of Large Numbers,

$$\lim_{N\to\infty} \gamma = \sigma_z \tag{B.16}$$

where σ_z is the standard deviation of the antenna array element positions.

If the antenna positions have some correlation among themselves, then the half-power beamwidth will be larger as seen in Fig. B.7 for correlated virtual antenna positions formed by convolving the positions of iid transmit and receive antenna positions. In Fig. B.7 also, the main beam lobe shape above -3 dB is close to the shape of the side lobe peaks.

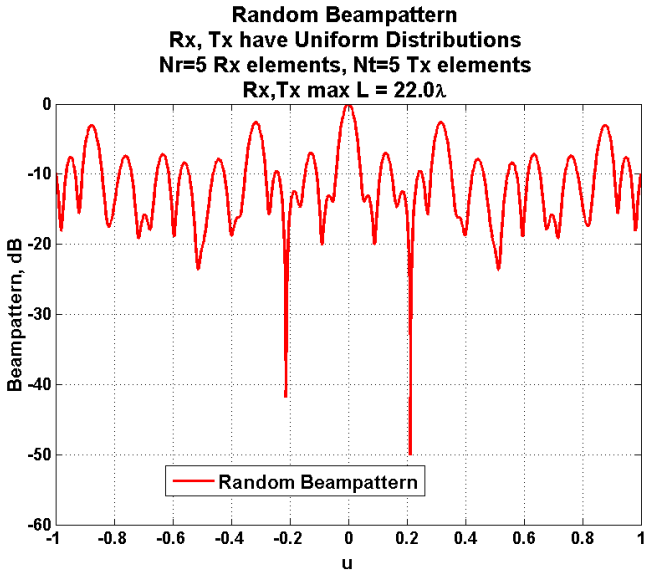

Figure B.7: *Beampattern formed from virtual antenna array with correlated element positions*

The sampling interval in Fig. B.5 was set to

$$\frac{(1-u_s)}{\left\lceil \frac{2(1-u_s)}{BW_{-3dB}} \right\rceil} \tag{B.17}$$

where $u = u_s$ is where the sidelobe region starts and $u_s > 0$. To find local maxima of sidelobes

whose peaks are near the slopes of adjacent sidelobes, reducing the sampling interval to

$$\frac{(1-u_s)}{\lceil \frac{4(1-u_s)}{BW_{-3dB}} \rceil} \tag{B.18}$$

seems to allow local maxima to be found for the smaller sidelobes as seen in Fig. B.8. It is also seen that the global maxima was chosen at the same sidelobe as when a longer sampling interval was used.

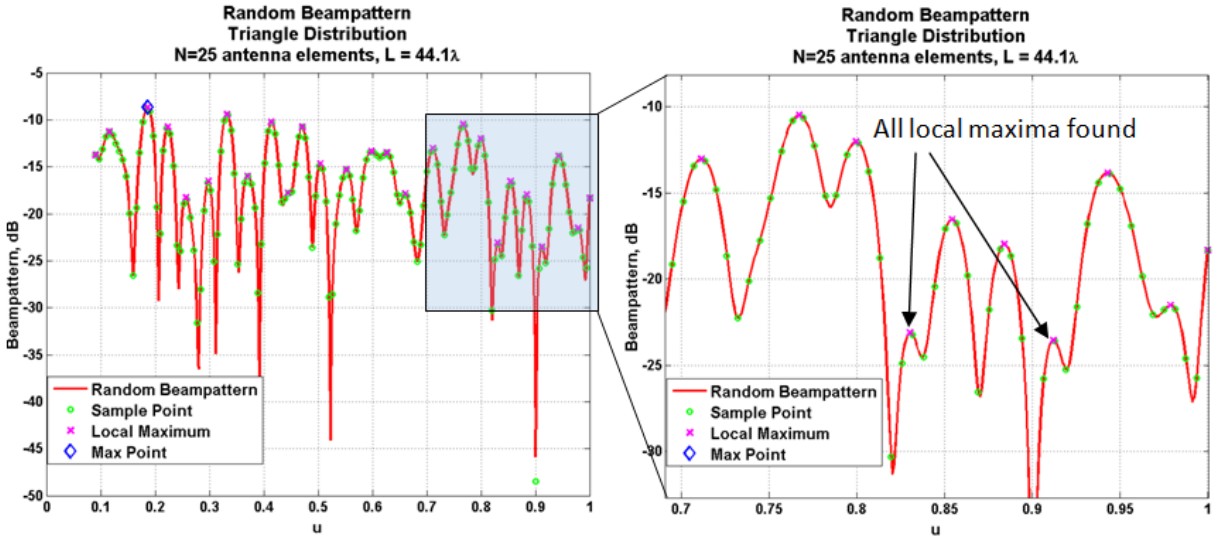

Figure B.8: *Beampattern with global and local maxima found; reduced sampling interval to* $\frac{(1-u_s)}{\lceil \frac{4(1-u_s)}{BW_{-3dB}} \rceil}$

When dealing with antenna arrays with correlated antenna positions, it is better to choose the sampling interval as though the random antenna positions are independent to ensure enough sample points will be used.

B.4 Additional Simulations

The following simulations in Figs. B.9, B.10, B.11, and B.12 were able to correctly find the maximum peak sidelobe or sidelobe level.

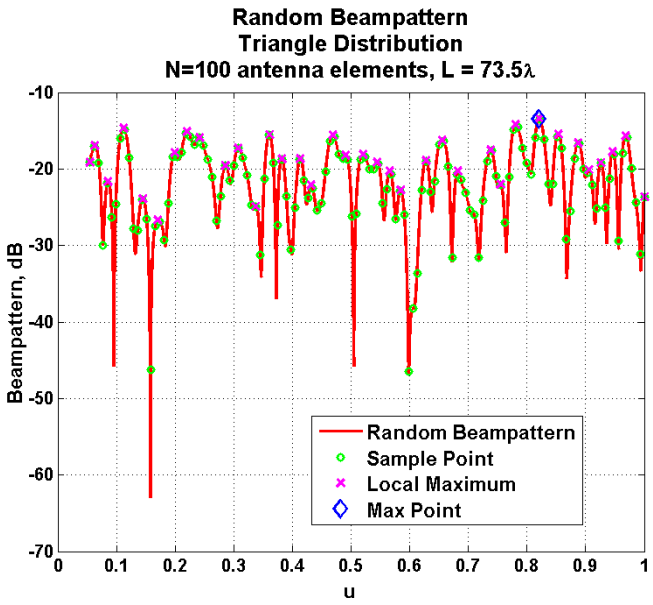

Figure B.9: *Beampattern with $N = 100$ independently distributed antenna elements*

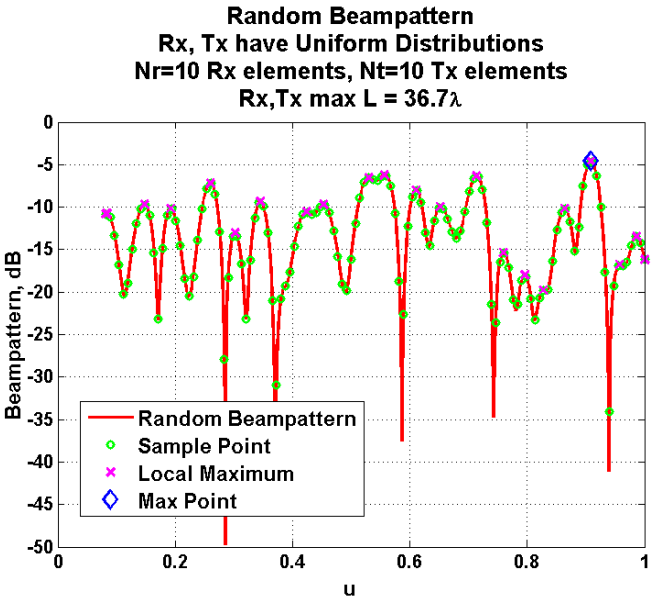

Figure B.10: *Beampattern with $N = 100$ random virtual antenna elements with some correlation among each other. Transmit and receive antennas are iid*

B.5 Problems with Algorithm

If the sampling interval is too long, then sidelobes with peaks near the slopes of adjacent sidelobes may not have their local minima determined. One of these undetected local minima

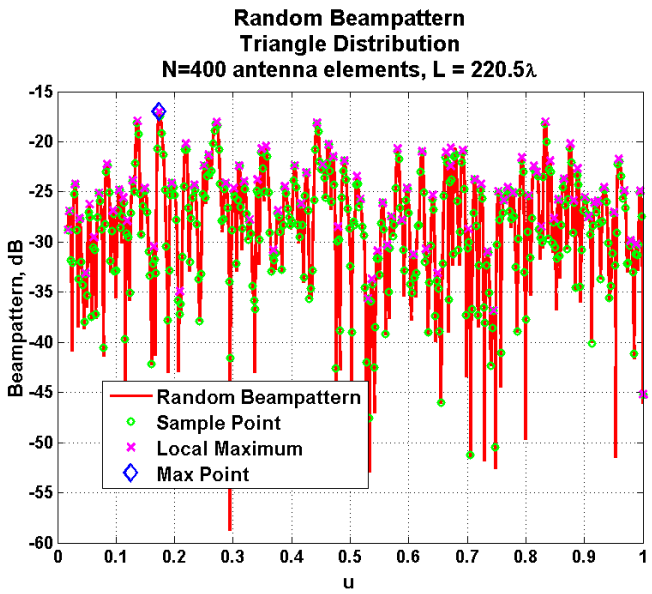

Figure B.11: *Beampattern with $N = 400$ independently distributed antenna elements*

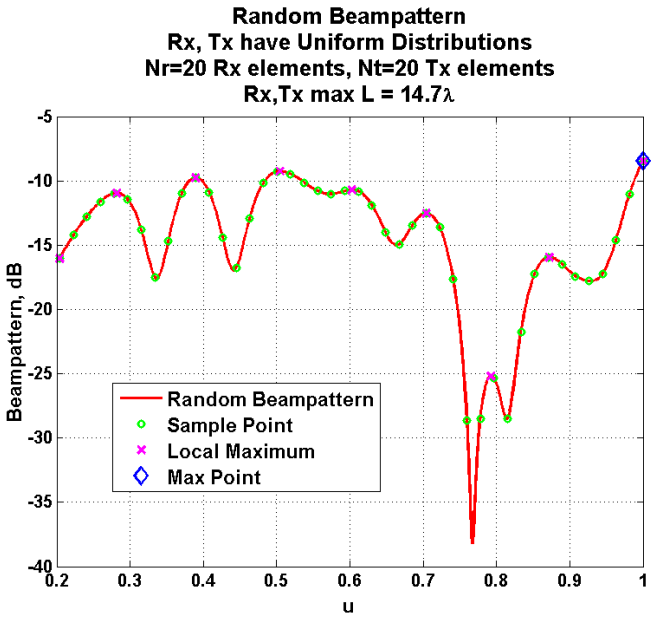

Figure B.12: *Beampattern with $N = 400$ random virtual antenna elements with some correlation among each other. Transmit and receive antennas are iid*

could be a local maximum.

Appendix C

Correlations of Beampattern Samples, $10 \leq N \leq 200$

These tables give the correlation with the sampling interval given by

$$\rho_F \left(\frac{u_{\max} - u_s}{\hat{\hat{M}} - 1} \right) \tag{C.1}$$

for different N, σ_z, and antenna position distribution type. One may use these tables to estimate $\hat{\hat{M}}$, given $u_{\max}$ and u_s, so the Gumbel distribution parameter,

$$a_M = \frac{\log M}{N}$$

may be estimated.

Table C.1: *Correlation with Sampling Interval given in Eq.* (C.1) *for different antenna position distribution types (Triangle, Uniform, Gaussian); correlation given for antenna position variances of* $\sigma_z = 1/2N$, $\sigma_z = N$, *and* $\sigma_z = 2N$; $N = 10$

σ_z	Triangle	Uniform	Gaussian
5λ	0.5799	0.5554	0.5956
10λ	0.5726	0.5392	0.5786
20λ	0.5316	0.4989	0.5375

Table C.2: *Correlation with Sampling Interval given in Eq.* (C.1) *for different antenna position distribution types (Triangle, Uniform, Gaussian); correlation given for antenna position variances of* $\sigma_z = 1/2N$, $\sigma_z = N$, *and* $\sigma_z = 2N$; $N = 20$

σ_z	Triangle	Uniform	Gaussian
10λ	0.6302	0.6043	0.6319
20λ	0.6397	0.6072	0.6388
40λ	0.6349	0.5970	0.6400

Table C.3: *Correlation with Sampling Interval given in Eq.* (C.1) *for different antenna position distribution types (Triangle, Uniform, Gaussian); correlation given for antenna position variances of* $\sigma_z = 1/2N$, $\sigma_z = N$, *and* $\sigma_z = 2N$; $N = 30$

σ_z	Triangle	Uniform	Gaussian
15λ	0.6624	0.6457	0.6628
30λ	0.6709	0.6572	0.6766
60λ	0.6737	0.6615	0.6765

Table C.4: *Correlation with Sampling Interval given in Eq.* (C.1) *for different antenna position distribution types (Triangle, Uniform, Gaussian); correlation given for antenna position variances of* $\sigma_z = 1/2N$, $\sigma_z = N$, *and* $\sigma_z = 2N$; $N = 40$

σ_z	Triangle	Uniform	Gaussian
20λ	0.6781	0.6538	0.6840
40λ	0.6881	0.6811	0.7003
80λ	0.6919	0.6912	0.7093

Table C.5: *Correlation with Sampling Interval given in Eq.* (C.1) *for different antenna position distribution types (Triangle, Uniform, Gaussian); correlation given for antenna position variances of* $\sigma_z = 1/2N$, $\sigma_z = N$, *and* $\sigma_z = 2N$; $N = 50$

σ_z	Triangle	Uniform	Gaussian
25λ	0.6902	0.6768	0.7045
50λ	0.7163	0.6985	0.7190
100λ	0.7178	0.7132	0.7188

Table C.6: *Correlation with Sampling Interval given in Eq.* (C.1) *for different antenna position distribution types (Triangle, Uniform, Gaussian); correlation given for antenna position variances of* $\sigma_z = 1/2N$, $\sigma_z = N$, *and* $\sigma_z = 2N$; $N = 60$

σ_z	Triangle	Uniform	Gaussian
30λ	0.7016	0.6876	0.7105
60λ	0.7253	0.7038	0.7297
120λ	0.7249	0.7207	0.7435

Table C.7: *Correlation with Sampling Interval given in Eq.* (C.1) *for different antenna position distribution types (Triangle, Uniform, Gaussian); correlation given for antenna position variances of* $\sigma_z = 1/2N$, $\sigma_z = N$, *and* $\sigma_z = 2N$; $N = 70$

σ_z	Triangle	Uniform	Gaussian
35λ	0.7136	0.6929	0.7215
70λ	0.7292	0.7167	0.7372
140λ	0.7408	0.7403	0.7529

Table C.8: *Correlation with Sampling Interval given in Eq.* (C.1) *for different antenna position distribution types (Triangle, Uniform, Gaussian); correlation given for antenna position variances of* $\sigma_z = 1/2N$, $\sigma_z = N$, *and* $\sigma_z = 2N$; $N = 80$

σ_z	Triangle	Uniform	Gaussian
40λ	0.7235	0.7039	0.7311
80λ	0.7366	0.7262	0.7350
160λ	0.7512	0.7378	0.7625

Table C.9: *Correlation with Sampling Interval given in Eq.* (C.1) *for different antenna position distribution types (Triangle, Uniform, Gaussian); correlation given for antenna position variances of* $\sigma_z = 1/2N$, $\sigma_z = N$, *and* $\sigma_z = 2N$; $N = 90$

σ_z	Triangle	Uniform	Gaussian
45λ	0.7231	0.7068	0.7349
90λ	0.7437	0.7440	0.7554
180λ	0.7559	0.7540	0.7636

Table C.10: *Correlation with Sampling Interval given in Eq.* (C.1) *for different antenna position distribution types (Triangle, Uniform, Gaussian); correlation given for antenna position variances of* $\sigma_z = 1/2N$, $\sigma_z = N$, *and* $\sigma_z = 2N$; $N = 100$

σ_z	Triangle	Uniform	Gaussian
50λ	0.7283	0.7189	0.7427
100λ	0.7465	0.7441	0.7561
200λ	0.7644	0.7600	0.7722

Table C.11: $N = 110$

σ_z	Triangle	Uniform	Gaussian
55λ	0.7423	0.7263	0.7456
110λ	0.7536	0.7429	0.7594
220λ	0.7694	0.7682	0.7700

Table C.12: *Correlation with Sampling Interval given in Eq.* (C.1) *for different antenna position distribution types (Triangle, Uniform, Gaussian); correlation given for antenna position variances of* $\sigma_z = 1/2N$, $\sigma_z = N$, *and* $\sigma_z = 2N$; $N = 120$

σ_z	Triangle	Uniform	Gaussian
60λ	0.7426	0.7283	0.7558
120λ	0.7631	0.7481	0.7680
240λ	0.7730	0.7716	0.7863

Table C.13: *Correlation with Sampling Interval given in Eq.* (C.1) *for different antenna position distribution types (Triangle, Uniform, Gaussian); correlation given for antenna position variances of* $\sigma_z = 1/2N$, $\sigma_z = N$, *and* $\sigma_z = 2N$; $N = 130$

σ_z	Triangle	Uniform	Gaussian
65λ	0.7491	0.7370	0.7508
130λ	0.7636	0.7554	0.7683
260λ	0.7769	0.7709	0.7852

Table C.14: *Correlation with Sampling Interval given in Eq.* (C.1) *for different antenna position distribution types (Triangle, Uniform, Gaussian); correlation given for antenna position variances of* $\sigma_z = 1/2N$, $\sigma_z = N$, *and* $\sigma_z = 2N$; $N = 140$

σ_z	Triangle	Uniform	Gaussian
70λ	0.7526	0.7401	0.7535
140λ	0.7705	0.7584	0.7762
280λ	0.7789	0.7783	0.7888

Table C.15: *Correlation with Sampling Interval given in Eq.* (C.1) *for different antenna position distribution types (Triangle, Uniform, Gaussian); correlation given for antenna position variances of* $\sigma_z = 1/2N$, $\sigma_z = N$, *and* $\sigma_z = 2N$; $N = 150$

σ_z	Triangle	Uniform	Gaussian
75λ	0.7552	0.7444	0.7506
150λ	0.7678	0.7659	0.7765
300λ	0.7779	0.7861	0.7942

Table C.16: *Correlation with Sampling Interval given in Eq.* (C.1) *for different antenna position distribution types (Triangle, Uniform, Gaussian); correlation given for antenna position variances of* $\sigma_z = 1/2N$, $\sigma_z = N$, *and* $\sigma_z = 2N$; $N = 160$

σ_z	Triangle	Uniform	Gaussian
80λ	0.7563	0.7501	0.7621
160λ	0.7778	0.7706	0.7790
320λ	0.7869	0.7909	0.7962

Table C.17: *Correlation with Sampling Interval given in Eq.* (C.1) *for different antenna position distribution types (Triangle, Uniform, Gaussian); correlation given for antenna position variances of* $\sigma_z = 1/2N$, $\sigma_z = N$, *and* $\sigma_z = 2N$; $N = 170$

σ_z	Triangle	Uniform	Gaussian
85λ	0.7589	0.7545	0.7670
170λ	0.7704	0.7767	0.7807
340λ	0.7806	0.7892	0.7956

Table C.18: *Correlation with Sampling Interval given in Eq.* (C.1) *for different antenna position distribution types (Triangle, Uniform, Gaussian); correlation given for antenna position variances of* $\sigma_z = 1/2N$, $\sigma_z = N$, *and* $\sigma_z = 2N$; $N = 180$

σ_z	Triangle	Uniform	Gaussian
90λ	0.7601	0.7570	0.7692
180λ	0.7826	0.7772	0.7881
360λ	0.7964	0.7890	0.8021

Table C.19: *Correlation with Sampling Interval given in Eq.* (C.1) *for different antenna position distribution types (Triangle, Uniform, Gaussian); correlation given for antenna position variances of* $\sigma_z = 1/2N$, $\sigma_z = N$, *and* $\sigma_z = 2N$; $N = 190$

σ_z	Triangle	Uniform	Gaussian
95λ	0.7632	0.7556	0.7647
190λ	0.7825	0.7748	0.7879
380λ	0.7943	0.7891	0.8013

Table C.20: *Correlation with Sampling Interval given in Eq.* (C.1) *for different antenna position distribution types (Triangle, Uniform, Gaussian); correlation given for antenna position variances of* $\sigma_z = 1/2N$, $\sigma_z = N$, *and* $\sigma_z = 2N$; $N = 200$

σ_z	Triangle	Uniform	Gaussian
100λ	0.7739	0.7581	0.7741
200λ	0.7849	0.7747	0.7856
400λ	0.8035	0.7941	0.8046